CONDUCTING ORGANIC SALT ENZYME ELECTRODES

by

Lindy Jane Murphy B.Sc. A.R.C.S.

A thesis submitted for the degree of Doctor of Philosophy of the University of London and for the Diploma of Membership of Imperial College.

Department of Chemistry
Imperial College
London SW7 2AY

October 1989

ABSTRACT

It has been found that electrodes composed of conducting organic salts can oxidize flavoenzyme oxidases that are reduced during the catalytic oxidation of their substrate. In this thesis, a number of oxidoreductase enzymes are tested for electroactivity at a conducting organic salt electrode composed of either TTF TCNQ or NMP TCNQ, in the configuration of a membrane electrode. These enzymes have a variety of cofactors. The responses of the membrane electrodes to increasing concentrations of substrate for the enzyme are analysed according to the membrane electrode theory proposed by W.J. Albery and P.N. Bartlett. This theory allows the rate controlling process of both the unsaturated and the saturated electrode responses to be determined. Electron micrographs are presented of electrodes prepared by a variety of methods.

The mechanism of electron transfer between a reduced enzyme and a conducting organic salt electrode is controversial. Two theories, based on previous experimental observations, are presented for the mechanism: the homogeneous mediation theory and the heterogeneous redox catalysis theory. These theories predict the dependence of the current of a rotating TTF TCNQ disc electrode, in the presence of reduced glucose oxidase, on the bulk substrate and enzyme concentrations, the rotation speed of the electrode and the electrode potential. Results are presented and analysed according to the two theories. A platinum ring-TTF TCNQ disc electrode study is made with reduced glucose oxidase to detect any possible mediator species lost from the TTF TCNQ disc. These results strongly support the homogeneous mediation theory.

For my parents

"I have no data yet. It is a capital mistake to theorize before one has data. Insensibly one begins to twist facts to suit theories, instead of theories to suit facts."

Sherlock Holmes to Dr Watson
A Scandal in Bohemia
by Sir Arthur Conan Doyle

ACKNOWLEDGMENTS

I would like to thank:

John Albery for his supervision and the production of numerous screeds

Derek Craston and Bruce Lennox for their supervision

Yogi, Girish, Edmund and Wendy for proof reading parts of this thesis

Hugh for introducing me to the electron microscope

Justin for all his encouragement (and nagging) and Tessa for listening

Mike Pritchard for the electrodes and John Hooper for an excellent box of electronics

Bill and Drs Michael Spiro and Russ Edgell for the loan of Macintoshes

The WJA group for making life so interesting over the past few years, especially Derek, Bryan, Mark, Gamini, Bruce, Anne, Paul, Shu, Sim, Bill and any one else who knows me

CONTENTS

Chapter 1:	Introduction	22
1.1	Applications of enzyme electrodes	23
1.2	Types of enzyme electrodes	26
1.2.2	Mode of operation	28
1.3	Classical enzyme electrodes	29
1.3.1	The use of whole cells and organisms	30
1.3.2	Multiple enzyme electrodes	30
1.3.3	Enzyme immunoassays	31
1.3.4	Using artificial enzymes	32
1.3.5	Immobilization of the enzyme	33
1.4	Mediated electrodes	35
1.4.1	Organic mediators	37
1.4.2	Inorganic mediators	39
1.5	Direct electron transfer	40
1.5.1	Use of a modified electrode	41
1.5.2	Direct electron transfer at a bare electrode (or thin layer electrode)	42
1.5.3	Covalent attachment of mediator to the enzyme	44
1.5.4	Conducting organic salt electrodes	44
1.6	Conducting organic salts	47
1.6.1	Synthesis of the salts	49
1.6.2	Conductivity of the salts	49
1.6.3	Crystallographic structure of the salts	50
1.6.4	Band structure of the salts	54
1.6.5	Temperature dependence of the conductivity	58

1.6.6 Electrochemistry of the salts 59
1.7 Flavoproteins 59
1.8 The rest of this thesis 64

Chapter 2: Experimental 66
2.1 Chemicals and solutions 66
2.1.1 Enzyme preparations 66
2.2 Electrode preparation 69
2.2.1 Preparation of salts 69
2.2.2 Preparation of electrodes 70
2.2.3 Membrane electrodes 72
2.3 Apparatus 73
2.3.1 The cell 73
2.3.2 Deoxygenating solution 75
2.3.3 Electrochemical measurements 76
2.4 Experimental procedures 77
2.4.1 Cyclic voltammograms 77
2.4.2 Membrane electrode experiments 77
2.4.3 Mechanistic experiments 78
2.4.4 Ring-disc experiments 79
2.4.4.1 Collection efficiency 79
2.4.4.2 Ring-disc electrode experiments 79
2.4.5 Potential step experiments 80
2.4.5.1 Mechanistic potential step experiments 80
2.4.5.2 Bilirubin oxidase potential step experiment 81
2.5 Scanning electron micrography 81
2.6 UV/ visible spectroscopy 81

Chapter 3: Conducting organic salt membrane electrodes

	prepared with novel enzymes	82
3.1	Introduction	82
3.2	Membrane electrode theory	83
	3.2.1 The steady state equation	85
	3.2.2 No product inhibition	86
	3.2.3 Application of the analysis	87
	3.2.4 Product inhibition	94
	3.2.5 Effect of half order dependence on e' by the electrode flux	97
3.3	Experimental	100
3.4	Membrane electrode results	103
	3.4.1.1 Sarcosine oxidase	103
	3.4.1.2 Sarcosine oxidase results	105
	3.4.2.1 Glycolate oxidase	113
	3.4.2.2 Glycolate oxidase results	115
	3.4.3.1 L-lactate-2-monooxygenase	120
	3.4.3.2 L-lactate-2-monooxygenase results	120
	3.4.4.1 Pyruvate oxidase	125
	3.4.4.2 Pyruvate oxidase results	126
	3.4.5.1 Oxalate oxidase	133
	3.4.5.2 Oxalate oxidase results	135
	3.4.6.1 Bilirubin oxidase	140
	3.4.6.2 Bilirubin oxidase results	142
3.5	Problems encountered	146
	3.5.1 The oxygen effect	146
	3.5.2 Reproducibility	148
	3.5.3 Scanning electron microscopy	149
	3.5.4 The mediated reaction layer thickness	156
3.6	Conclusions	158

Chapter 4: The mechanism of electron transfer between an enzyme and a conducting organic salt electrode 166
4.1 Introduction 166
4.2 Current understanding of the mechanism 167
4.3 Introduction to the two theories 169
4.3.1 Introducing the homogeneous mediation mechanism 169
4.3.1.1 The case V - VI boundary 176
4.3.1.2 The case VI - I boundary 180
4.3.1.3 The case V - II boundary 182
4.3.1.4 The case II - I boundary 183
4.3.2 Introducing the heterogeneous redox catalysis mechanism 184
4.3.2.1 Heterogeneous plot for data at constant [E] 191
4.3.2.2 Heterogeneous plot for data at constant [S] 192
4.4 Choice of experimental conditions 192
4.4.1 Glucose oxidase 195
4.5 Preliminary analysis of results 196
4.5.1 Dependence of current on $[E]^1$ 196
4.5.2 Dependence of current on $[E]^{1/2}$ 201
4.5.3 Dependence of current on $[S]^1$ 206
4.5.4 Dependence of current on $[S]^{1/2}$ 211
4.5.5 Dependence of current on $[S]^0$ 216
4.5.6 Dependence of current on ω 217
4.5.7 Dependence of current on potential 220
4.5.8 Summary of the preliminary analysis 220
4.5.8.1 Concentration polarization of substrate 223
4.6 Fitting experimental data to theoretical plots:

the homogeneous mediation theory 225
4.6.1 Cases V and VI: varying [E] 226
4.6.2 Cases I and II 231
4.6.3 Cases V and VI: varying [S] 238
4.6.4 Cases VI and I 242
4.6.5 Cases V and II 247
4.6.6 Summary of the homogeneous mediation fit 252
4.7 Fitting experimental data to theoretical plots: the heterogeneous redox catalysis theory 255
4.7.1 Varying [E] 255
4.7.2 Varying [S] 260
4.7.3 Conclusion of the heterogeneous redox catalysis fit 265
4.8 Conclusions 266

Chapter 5: Further investigations of the mechanism of electron transfer 270
5.1 Potential dependence of the electrode 271
5.1.1 The homogeneous case 271
5.1.2 The heterogeneous case 274
5.1.3 The potential dependence results 276
5.1.4 Conclusion of the potential step experiment 281
5.2 Ring-disc electrode studies 283
5.2.1 Collection efficiency 284
5.2.2 Potential dependence of the ring current 286
5.2.3 Identification of the redox species 289
5.2.4 The dependence of the ring and disc currents on the concentration of substrate 295

5.2.5 Analysis of the collection efficiency 303
5.2.6 Conclusion of the ring-disc electrode study 308
5.3 Conclusions 309

Chapter 6: Conclusions 311

Appendix A: The homogeneous mediation theory 315
A.1 The basic theory 315
A.2 Differential equations and boundary conditions 317
A.3 The physical significance of the dimensionless variables 321
A.4 Derivation of the cases 322
A.4.1 Cases I and II 323
A.4.2 Cases II and III 326
A.4.3 Cases I and IV 330
A.4.4 Cases III and IV 332
A.4.5 Cases III and V 335
A.4.6 Cases V and VI 337
A.4.7 Cases IV and VII 341
A.4.8 Cases VI and VII 344
A.4.9 Cases I and VII 345
A.5 The complete case diagram 346
A.6 New coordinates for the case diagram 352
A.6.1 Cases V and II 357
A.6.2 Cases VI and I 358
A.6.3 The complete case diagram with the new coordinates 359
A.6.4 The $\phi \approx 1$ plane 361
A.7 Experimental variables 361

Appendix B: The heterogeneous redox catalysis theory 365

B.1 Theoretical description of the theory 365

B.2.1 Kinetics at the electrode surface 368

B.2.2 Enzyme kinetics 370

B.2.3 Flux of electrons 371

B.3 The physical significance of the dimensionless variables 372

B.4 Derivation of the cases 373

B.4.1 The $\theta >> 1$ plane 374

B.4.2 The complete case diagram 376

B.4.3 The $\theta << 1$ plane 378

B.5 The experimental variables 380

References 381

LIST OF FIGURES

Figure 1.1	Chemical structures of TTF, NMP^+ and TCNQ	48
Figure 1.2	Temperature dependence of the conductivity of TTF TCNQ	51
Figure 1.3	The structures of TTF TCNQ and NMP TCNQ determined by x-ray crystallography	52
Figure 1.4	The lateral displacement of molecules in the stack	53
Figure 1.5	Formation of band structure in a solid	55
Figure 1.6	Typical cyclic voltammograms of TTF TCNQ and NMP TCNQ	60
Figure 1.7	Formulae for the flavin nucleotide sequence	62
Figure 2.1	The cavity electrode	71
Figure 2.2	The electrochemical cell	74
Figure 3.1	The mechanistic scheme for the membrane electrode theory	84
Figure 3.2	The interplay of the three possible rate determining steps	89
Figure 3.3	Plots of flux against substrate concentration, Hanes and y vs. ρ	91
Figure 3.4	The case diagram for product inhibition	96
Figure 3.5.1	Plots of flux vs. substrate concentration for sarcosine oxidase membrane electrodes	106
Figure 3.5.2	Data from fig(3.5.1) plotted as Hanes plots	107
Figure 3.5.3	Data from fig(3.5.1) plotted as ρ-plots	111
Figure 3.5.4	Data from fig(3.5.1) plotted as y^2 vs. ρ	112
Figure 3.6.1	Plots of flux vs. substrate concentration for glycolate oxidase membrane electrodes	116

Figure 3.6.2	Data from fig(3.6.1) plotted as Hanes plots	117
Figure 3.6.3	Data from fig(3.6.1) plotted as ρ-plots	118
Figure 3.7.1	Plots of flux vs. substrate concentration for L-lactate-2-monooxygenase membrane electrodes	121
Figure 3.7.2	Data from fig(3.7.1) plotted as Hanes plots	122
Figure 3.7.3	Data from fig(3.7.1) plotted as ρ-plots	123
Figure 3.8.1	Plot of flux vs. [TPP] for a pyruvate oxidase membrane electrode	127
Figure 3.8.2	Plots of flux vs. substrate concentration for glycolate oxidase membrane electrodes	128
Figure 3.8.3	Data from fig(3.8.2) plotted as Hanes plots	129
Figure 3.8.4	Data from fig(3.8.3) plotted as ρ-plots	130
Figure 3.9.1	Plot of flux vs. substrate concentration for an oxalate oxidase membrane electrode	136
Figure 3.9.2	Data from fig(3.9.1) plotted as a Hanes plot	137
Figure 3.9.3	Data from fig(3.9.1) plotted as a ρ-plot	138
Figure 3.10.1	Response of a TTF TCNQ electrode to bilirubin	143
Figure 3.10.2	Tafel plot for the oxidation of bilirubin oxidase on TTF TCNQ	145
Figure 3.11	Effect of dissolved oxygen on the response profile and the Hanes plot for a membrane electrode	147
Figure 3.12.1	Electron micrograph of a "good" TTF TCNQ electrode	150
Figure 3.12.2	Electron micrograph of a "poor" TTF TCNQ electrode	151
Figure 3.12.3	Electron micrograph of a "good" NMP TCNQ electrode	153

Figure 3.12.4	Electron micrograph of a Si oil : TTF TCNQ electrode	154
Figure 3.12.5	Electron micrograph of an NMP TCNQ pressed pellet electrode	155
Figure 4.1	Scheme for the homogeneous mediation theory	171
Figure 4.2	The case diagram for the homogeneous mediation theory drawn with the new coordinates: the $\phi > 1$ plane	173
Figure 4.3	The predicted plot for the case V - VI boundary	179
Figure 4.4	The fit of the theoretical plot to the experimental data for the case VI - I boundary	181
Figure 4.5	Scheme for the heterogeneous redox catalysis theory	185
Figure 4.6	The case diagram for the heterogeneous redox catalysis theory: the $\theta > 1$ plane	188
Figure 4.7(a-f)	Current response of a TTF TCNQ electrode with glucose oxidase plotted vs. $[E]^1$	197
Figure 4.8(a-f)	Current response of a TTF TCNQ electrode with glucose oxidase plotted vs. $[E]^{1/2}$	202
Figure 4.9(a-f)	Current response of a TTF TCNQ electrode with glucose oxidase plotted vs. $[S]^1$	207
Figure 4.10(a-f)	Current response of a TTF TCNQ electrode with glucose oxidase plotted vs. $[S]^{1/2}$	212
Figure 4.11(a-b)	Plots of ω dependence of a TTF TCNQ electrode with glucose oxidase vs. log [E]	218
Figure 4.11(c-d)	Plots of ω dependence of a TTF TCNQ electrode with glucose oxidase vs. log [S]	219

Figure 4.12(a-f) Plots of experimental data for the case V - VI boundary: varying [E] 227

Figure 4.13(a-f) Plots of experimental data with the theoretical plot superimposed for the case II - I boundary 232

Figure 4.13.g Data from 4.13 replotted for the case II - I boundary using the true [E] 235

Figure 4.14(a-f) Plots of experimental data for the case V - VI boundary: varying [E] 239

Figure 4.15(a-f) Plots of experimental data with the theoretical plot superimposed for the case IV - I boundary 243

Figure 4.16(a-f) Plots of experimental data with the theoretical plot superimposed for the case V - II boundary 248

Figure 4.17 Placing the experimental data on the case diagram for the homogeneous mediation theory 253

Figure 4.18(a-f) Plots of experimental data according to the Eθ - Sθ case boundary: varying [E] 256

Figure 4.19(a-f) Plots of experimental data according to the Eθ - Sθ case boundary: varying [S] 261

Figure 5.1 Effect of a decrease in potential on the $\phi >> 1$ plane for the homogeneous theory 273

Figure 5.2 Effect of a decrease in potential on the $\theta >> 1$ plane for the heterogeneous theory 275

Figure 5.3(a-c) Tafel plots for the potential dependence of the disc electrode 277

Figure 5.4	The Levich plot for the ring-disc electrode measured with $K_3Fe(CN)_6$	285
Figure 5.5	Koutecky-Levich plot for the data in fig(5.4)	287
Figure 5.6	The potential dependence of the ring current in the absence of E and S, in the presence of E and in the presence of E and S	290
Figure 5.7	The effect on the ring current of switching the disc electrode to open circuit potential	291
Figure 5.8	The response of the ring and the disc electrode to successive injections of S	297
Figure 5.9	Plot of the rotation speed dependence of the ring current vs. log [S]	298
Figure 5.10(a-b)	Plots of the disc current vs. $[S]^1$ and $[S]^{1/2}$ respectively	299
Figure 5.11	Plot of the rotation speed dependence of the disc electrode vs. [S]	301
Figure 5.12(a-b)	Plots of experimental data for the disc electrode with the theoretical plot superimposed for the case V - II boundary and the case VI - I boundary respectively	302
Figure 5.13	Plot of the collection efficiency vs. log [S]	304
Figure A.1	Scheme for the mechanism for the homogeneous mediation theory	316
Figure A.2	The $\gamma > 1$ plane: cases I and II	325
Figure A.3	The $\gamma > 1$ plane: cases II and III	329
Figure A.4	The $\gamma > 1$ plane: cases I and IV	331
Figure A.5	The $\gamma > 1$ plane: cases III and IV	334
Figure A.6	The $\gamma > 1$ plane: cases III and V	336
Figure A.7	The $\gamma > 1$ plane: cases V and VI	339

Figure A.8	The $\gamma > 1$ plane: cases IV and VII	343
Figure A.9	The complete $\gamma > 1$ plane	347
Figure A.10	The complete $\gamma > 1$ plane showing the concentration profiles of oxidized and reduced mediator species	350
Figure A.11	The complete $\gamma > 1$ plane showing the concentration profiles of oxidized and reduced enzyme species	351
Figure A.12	The incomplete $\phi > 1$ plane	356
Figure A.13	The complete $\phi > 1$ plane	360
Figure A.14	The $\phi \approx 1$ plane	362
Figure B.1	Scheme for the heterogeneous redox catalysis mechanism	366
Figure B.2	The $\gamma > 1$ plane showing the concentration profiles for the oxidized and reduced species of the enzyme	377
Figure B.3	The $\gamma < 1$ plane	379

LIST OF TABLES

Table 2.1	Enzyme preparations as commercially supplied	67
Table 2.2	Buffers	68
Table 3.1	Possible cases for different values of ρ_o and K_{ME} for a membrane electrode	93
Table 3.2	Experimental conditions for the membrane electrode experiments	101
Table 3.3	Physical data for the enzymes	102
Table 3.4	Kinetic data for sarcosine oxidase membrane electrodes	110
Table 3.5	Kinetic data for glycolate oxidase membrane electrodes	119
Table 3.6	Kinetic data for L-lactate-2-monooxygenase membrane electrodes	124
Table 3.7	Kinetic data for pyruvate oxidase membrane electrodes	131
Table 3.8	Kinetic data for oxalate oxidase membrane electrode	139
Table 3.9	k'_S values for enzymes electroactive on conducting organic salt electrodes	160
Table 3.10	k' values for enzymes electroactive on conducting organic salt electrodes	162
Table 3.11	Active sites of the enzymes tested on conducting organic salt electrodes	164
Table 4.1	Values of D for various species	174
Table 4.2	Values of k_M for various mediator species	174
Table 4.3	Dependence of current on [E] , [S] and ω according to the homogeneous mediation theory	177

Table 4.4	Dependence of current on [E] , [S] and ω according to the heterogeneous redox catalysis theory	190
Table 4.5	Experimental conditions for the series of mechanistic experiments	194
Table 4.6	Analysis of the plots of i vs. $[E]^1$	200
Table 4.7	Analysis of the plots of i vs. $[E]^{1/2}$	205
Table 4.8	Analysis of the plots of i vs. $[S]^1$	210
Table 4.9	Analysis of the plots of i vs. $[S]^{1/2}$	215
Table 4.10	Analysis of the plots of i vs. $[S]^0$	216
Table 4.11	The linear portion of the i vs. $[S]^1$ plots	224
Table 4.12	Data from the case V - VI boundary analysis: varying [E]	230
Table 4.13	Data from the case II - I boundary analysis	236
Table 4.14	Data from the case VI - I boundary analysis	246
Table 4.15	Data from the case V - II boundary analysis	251
Table 4.16	Data from the heterogeneous analysis at constant [S]	259
Table 4.17	Data from the heterogeneous analysis at constant [E]	264
Table 5.1	nα values from the potential dependence of the electrode	279
Table 5.2	N and N' for the ring-disc electrode measured with $K_3Fe(CN)_6$	288
Table 5.3	The potentials for the oxidation of various redox species existing on a TTF TCNQ electrode within its stable range	294
Table A.1	Expressions for $(\delta u'/\delta \chi)_o$ on the case boundaries for the homogeneous mediation theory	348

Table A.2 Converting the case boundaries into the new coordinates for the homogeneous mediation case diagram 354

Chapter 1

Introduction

An enzyme electrode is an analytical device containing an immobilized enzyme in close contact with a suitable electrode which converts the biochemical signal into a quantifiable electrical signal. The enzyme may be either physically or chemically immobilized, while the electrode may measure the change in concentration of a reactant or product of the enzyme reaction, respond to a mediator species, or allow direct electron transfer between the enzyme and the electrode.

The usefulness of an enzyme electrode arises from the specificity of the enzyme and, in some cases, from the selectivity of the electrode system. An enzyme is a highly specific biological catalyst, capable of reacting with only a particular substrate or group of substrates. By combining an immobilized enzyme with a suitable electrode probe, highly sensitive and selective measurements of substrate and enzyme can be made. The wide range of enzymes available makes possible the construction of a large number of enzyme electrodes, in some cases measuring substances not previously analysed routinely.

Enzyme electrodes are a type of biosensor. A biosensor utilizes biological material such as tissue slices, whole cells, enzymes or antigen/antibody reactions with a variety of transducers such as electrodes, gravimetric sensors, fibre optic sensors, solid state devices such as ISFETS, or piezoelectric sensors. The overall aim of

developing any biosensor is to measure a particular target molecule selectively. This work is concerned only with enzyme electrodes, and a discussion of biosensors is beyond the scope of this introduction. For further information on biosensors, readers are referred to a selection of excellent review articles [1-5].

1.1 Applications of enzyme electrodes

There is a variety of applications for enzyme electrodes in medicine, industry, pollution and environmental monitoring, and the military arena [4]. Similarly there is a variety of substances it would be desirable to measure simply and cheaply, such as metabolites, fertilizers and pesticides, flavourings, toxic vapours and gases, heavy metals, drugs, explosives, nerve gases and contaminants in general. It is hoped that by choosing an appropriate enzyme, an enzyme electrode could be devised for any particular substrate. For example, TNT can be monitored using TNT oxidoreductase [6].

There are certain attributes desirable for a sensor irrespective of use: cheapness; reliability; robustness; fast response time; ease of comprehension of results, such as a digital readout; and adequate lifetime. Also for an in vitro sensor, mass transport should be the rate limiting process of the electrode response, as this will minimize the sensitivity of the device to changes in condition such as temperature, pH and enzyme activity [7]. For an in vivo sensor, mass transport control is not desirable since it is erratic and unknown. The rate limiting process in this case should be the enzyme-substrate reaction or the enzyme-electrode reaction.

The medical profession is the largest user of analytical services in the Western world [8]. Thus it is not surprising that the majority of enzyme electrodes developed are intended for medical use. In vivo sensors would be useful for the controlled administration of drugs, especially those with a narrow therapeutic range, also anaesthetics and analgesics e.g. certain drugs are inhibitors for acetyl cholinesterase [9]. Thus this enzyme could be used in a sensor for monitoring drugs by following the inhibition of the enzyme. They could be particularly invaluable in intensive care to indicate any critical change in metabolite levels. The most common metabolite measured at present is glucose, in the monitoring of diabetics. Consequently a large proportion of the work on biosensors so far has been directed towards measuring glucose. Knowledge of the glucose levels in a diabetic is necessary in order to administer the correct dosage of insulin [10]. A continuous monitor of glucose levels could alert a patient to low levels of glucose, a condition called hypoglycaemia, which results in unconsciousness and eventually death if not recognised and treated in time [10,11]. A continuous monitoring system could also be used to control the dosage of insulin in response to the transient glucose level, thus eliminating under- or over- dosage, and allowing normoglycaemia to result.

The ideal in vivo biosensor, in addition to all the desirable properties of a biosensor mentioned above, should also be biocompatible and sufficiently small for intravenous or transcutaneous use. Problems arise with in vivo biosensors because the protective mechanisms of the body may result in the deposition of fibrinous proteins or the formation of blood clots, limiting the response of the sensor [9].

Ex vivo, biosensors can be used for routine analyses where changes in metabolite levels are non-critical i.e. to monitor the levels of drugs and thereby adjust the dosage e.g. anti-epileptic drugs [9]. They could be used in a medical laboratory, a hospital ward, a doctor's surgery or at home by a patient. Ex vivo sensors can be used in industry also. In particular flow through analysers are used for the on-line monitoring of continuous processes such as those in the fermentation industry, the food industry and effluent streams. Industrial sensors must be particularly robust and stable at extremes of conditions, such as pH and temperature.

There are few commercial analysers utilizing biosensors available. Yellow Springs Instruments Co. introduced a glucose analyser based on the Clark oxygen electrode in the 1970's [3]. The detector has two platinum electrodes, one to measure the enzyme reaction by following the rate of oxygen uptake, and the other to measure any other redox active species such as ascorbate. Yellow Springs market similar sensors for disaccharides and alcohol. Other companies have market ed analysers for other substrates, all of which utilise the Clark oxygen electrode. Recently Medisense have introduced a portable glucose analyser, in the form of a pen; this uses a derivative of ferrocene as a mediator for the electron transfer between the enzyme and the electrode.

Another application of enzyme electrodes is in biochemical research. It is desirable to understand the movement of charge in biological redox systems, in order to interpret biological phenomena. There are three classes of molecules of interest [12]:

(1) small, non-proteinaceous molecules such as quinones and ascorbate;

(2) redox proteins not directly involved in redox catalysis, such as ferrodoxins and cytochromes;

(3) redox proteins involved in catalysis, such as oxido-reductases, especially flavoproteins and metalloproteins.

Because it is difficult to achieve direct electron transfer between an enzyme and an electrode, this type of investigation has relied on the use of modified electrodes or mediated electrode systems to measure the standard potentials of the molecules of interest. It should be noted that the environment of the electroactive species can affect its $E^{o'}$ [12]. For example, the $E^{o'}$ of a cofactor in solution is different from the cofactor bound to the protein [13].

1.2 Types of enzyme electrodes

Enzyme electrodes can be classified into three types depending on the electroactive species:

(1) Measurement of reactant or product of the enzyme reaction.

Here the loss of a reactant (R) or the formation of a product (P) due to the enzyme (E) - substrate (S) reaction is followed electrochemically:

$$E_{ox} + S + \underline{\mathbf{R}} \longrightarrow E_{red} + \underline{\mathbf{P}}.$$

The species in bold and underlined denotes the one being followed electrochemically. The reactant is usually a gaseous species taking part in the reaction, such as oxygen.

If the species is a gas molecule in solution, then a gas sensing probe can be used e.g. the depletion of oxygen by oxidases can be followed amperometrically using a Clark oxygen electrode. Alternatively if the species is ionic, then an ion-selective electrode (ISE) can be used - this is less common.

(2) Use of a mediator.

A mediator (M) shuttles between the redox centre of the enzyme and the electrode:

$$E_{ox} + S \longrightarrow E_{red} + P$$

$$E_{red} + M_{ox} \longrightarrow E_{ox} + \underline{M_{red}}$$

$$\underline{M_{red}} \longrightarrow M_{ox} + e^- \qquad \text{at electrode}$$

where ox denotes oxidised and red denotes reduced.

Besides acting as an electron shuttle, the mediator may also serve as an oxidant or reductant, or to accelerate the rate of attainment of equilibrium between the enzyme and the electrode.

(3) Direct electron transfer.

This is most commonly observed at some electrode composed of or modified with an organic material, although other examples are known:

$$\underline{E_{red}} \longrightarrow E_{ox} + e^- \qquad \text{at modified electrode.}$$

It is thought that the surface of the electrode contains a chemical functional group capable of binding with the enzyme, thus enabling the redox centre of the enzyme to closely approach the electrode and direct electron transfer to occur (the rate of electron transfer is exponentially dependent on the distance between the enzyme and the electrode) [14]. The binding process is thought to mimic the interaction of the enzyme with its physiological partners i.e. the surface groups on the electrode bind to the enzyme in such a manner as to permit facile electron transfer. The enzyme can be reversibly or irreversibly bound to the electrode surface.

1.2.1 Mode of operation

There are two modes of operation of enzyme electrodes. In the potentiometric mode, the potential of the electrode is measured under equilibrium conditions i.e. no current flow. These enzyme electrodes commonly use gas sensing electrodes as the transducer, such as an ammonia or CO_2 electrode; the enzyme is immobilized in a layer on the probe. The electrode responds to a change in gas tension in the sample caused by the enzyme - substrate reaction. There is a subsequent change in the electrode potential, given by the Nernst equation [15] :

$$E = E^{\ominus} + RT/nF \ln(a_{ox}/a_{red}) \qquad (1.1)$$

where $E^{\ominus}$ is the standard electrode potential, n is the number of electrons transferred per electrode reaction, and a is the activity of the electroactive species. Thus if n = 1, a change in potential of 59 mV would indicate a ten fold change in activity or concentration. Some classical enzyme electrodes and some mediated electrodes are potentiometric, the latter being used predominantly by biochemists to determine the redox potentials of redox active biochemical species such as proteins.

In the amperometric mode, the electrode is held at a constant potential with respect to a reference electrode. Electroactive species such as mediator or redox enzyme transfer electrons to the electrode, giving rise to a current. The magnitude of the current is determined by the concentration gradient of the electroactive species at the electrode, which in turn is governed ultimately by the substrate concentration. All enzyme electrodes exhibiting direct electron transfer between the enzyme and the electrode are amperometric; some mediated enzyme electrodes are also amperometric. Experiments carried out in this thesis all use electrodes in the amperometric mode.

1.3 Classical enzyme electrodes

The first enzyme electrode was developed by Clark in 1962 [16]; it measured the oxygen depletion caused by the reaction of glucose with glucose oxidase immobilized by a membrane next to a platinum electrode. Subsequently a great many sensors using this configuration have been developed, using different enzymes and sometimes different electrodes such as NH_3 or CO_2 electrodes [17].

The main limitation of this type of electrode is the interference caused by changes in the background gas level. Consequently much research has been directed at finding sensors independent of gas level, such as mediated electrode systems. These are discussed more fully in the next section. In the remainder of this section, variations on the classical enzyme electrode are discussed.

1.3.1 The use of whole cells and organisms

Some electrodes have used whole cells and organisms as the source of the enzyme(s) [3]. The loss of a reactant e.g. O_2 [18] or the formation of a product e.g. CO_2 [19] is measured. For example, a microbial sensor for nitriloacetic acid (NTA) has been reported [20]. The immobilized bacterial cells carry out a four step reaction sequence converting the NTA to ammonia.

Enzyme electrodes prepared with whole cells or microorganisms have the advantage of readily available cofactors, the enzyme(s) need not be isolated or purified, the cell is stable for several days if supplied with nutrients, and multiple-reaction sequences involving several enzymes contained in the cell are possible. However response times are slower and sensitivity is poorer due to lower enzyme activity. There may also be interferences to the probe.

1.3.2 Multiple enzyme electrodes

Not all enzyme-substrate reactions produce electroactive substances; however reacting the analyte with an enzyme can produce a product which will react with one or more other enzymes

to produce an electroactive product. Many other multiple enzyme electrodes have been reported.

For example, a sucrose sensor has been reported that utilizes three enzymes [21]. Sucrose is hydrolysed by invertase to give α-D-glucose. However glucose oxidase is specific for β-D-glucose. Thus the α form must first be converted to the β form by mutarotase before reaction with glucose oxidase can occur. The depletion of dissolved oxygen caused by the glucose oxidase reaction is then followed with an oxygen electrode.

1.3.3 Enzyme immunoassays

Another application of classical enzyme electrodes has been in enzyme immunoassays (EIAs). The determination of antigens (e.g. drugs, viruses) is presently achieved by exploiting the high selectivity of immunochemical reactions, thus minimising interferences. However the nature of the antibody-antigen reaction is such that no easily measurable change in reactant or product occurs. The labelling of antigen overcomes this problem, allowing free antigen to be distinguished from bound antigen.

A common method is to label the antigen with radioactive ^{125}I : this is called a radioimmunoassay (RIA). However the use of radioactive material is undesirable due to the problems of disposal. An alternative procedure is to label the antigen with enzyme, and to use electrochemical detection to determine the amount of free enzyme: this is known as an enzyme immunoassay (EIA) [22].

There are two types of EIA: homogeneous, which does not require separation of the free and bound enzyme-labelled antigen;

and heterogeneous, in which the antibody is chemically immobilized to a surface thus permitting rapid and convenient separation of the free and bound enzyme label. Electrochemical detection of the activity of the free enzyme-labelled antigen is possible because the antigen is a small molecule relative to the enzyme and so it does not inhibit the enzyme active site in the free enzyme-antigen complex. However on binding to an antibody, which is a relatively much larger molecule, the close proximity of the antibody to the enzyme active site results in a much reduced activity. Thus changes in enzyme activity can be followed electrochemically and this allows a measure of the antigens to be made. The enzyme activity may be measured by classical methods i.e. gas sensing probes [23] or by the use of mediators, such as ferrocene [24]. For example, insulin can be measured by immobilizing the antigen on a HPLC column [25]. A platinum electrode is placed at the end of the column to measure H_2O_2 , a product of the enzyme reaction. The use of a column allows the amount of antigen used in the assay to be increased and thus increases the sensitivity of the sensor.

The biggest problem with EIAs is the adsorption of labelled and free antigens at non-specific sites, particularly if the number of antibody sites is small. The main requirement of the enzyme is that it is highly active, thus reducing interferences and assay times.

1.3.4 Using artificial enzymes

An interesting variation on the classical enzyme electrode utilizes an artificial enzyme, known as a synzyme. A synzyme is a synthetic polymer chain with functional groups that mimic the biocatalytic

activity of natural enzymes. An oxalacetate sensor has been described which utilizes the synzyme PEIQ-NH_2 with a CO_2 electrode [26]. PEIQ-NH_2 synzyme catalyses the decarboxylation of oxalacetate:

$$HOOCC(=O)CH_2CO_2^- + H^+ \xrightarrow{\text{PEIQ-NH}_2\ \text{synzyme}} HOOCC(=O)CH_3 + CO_2$$

The synzyme enzyme electrode was found to have many advantages over an identical electrode using natural enzyme, most notably a significant increase in electrode lifetime from one week for natural enzyme to six months for the artificial counterpart. In addition no cofactor was required, and the lifetime of the sensor could be significantly increased compared to the natural enzyme electrode - the sample of synzyme used in the study was ≈ 10 years old.

1.3.5 Immobilization of the enzyme

One problem common to all types of enzyme electrodes is the short lifetime of the electrode. This may vary from a few hours to as much as a year. The limiting component in an enzyme electrode is usually the loss of enzyme activity. Deterioration in the electrode response is usually characterised by a loss of response e.g. for a potentiometric electrode from 59 mV per 10 fold change in concentration to 20 - 30 mV, an increase in response time and a decrease in the upper limit of the electrode [17]. Immobilization of the enzyme can increase the lifetime of the enzyme and has other advantages:

(1) : the sensor may be reused;

(2) : it may prevent the enzyme from adsorbing on the electrode surface and thus poisoning it;

(3) : the selectivity of the enzyme may be enhanced, in particular towards inhibitors;

(4) : the pH range of the enzyme may be increased;

(5) : the enzyme may exhibit increased stability towards organic solvents, and conformational changes .

Immobilization can be achieved either physically, such as entrappment by a membrane or in an inert matrix such as starch or polyacrylamide gel [27], or chemically by binding to an insoluble molecule or support [28]. Physical immobilization is easiest to achieve and often gives faster response times, but the enzyme usually attains much greater stability and lifetime by chemical immobilization e.g. 3 weeks or 100 assays compared to 1 year or several thousand assays [17].

The enzyme can be immobilized to dialysis membranes, pig intestines, nylon nets [29] which confer great mechanical strength and to collagen which, although quite fragile, enjoys commercial success [17] using a chemical bridge between the protein and the support such as glutaraldehyde. Also, different enzymes may be immobilized to each side of the nylon net: this often achieved the best results. For example, an enzyme specific for a disaccharide, such as β-galactosidase is immobilized on the side of a nylon net exposed to the bulk solution containing galactose; on the side of the net next to the electrode, glucose oxidase is immobilized [30]. However chemical immobilization can be difficult to achieve in practice as the

enzyme active site may be chemically modified, resulting in a loss of the enzyme activity.

It should be noted that a membrane will increase the linear range of the electrode since the bulk substrate concentration is greater than the internal concentration behind the membrane due to partitioning [31]. Choosing a membrane of greater thickness will result in a slower response time but a larger linear range. The pore size of the membrane can be selected to keep interferents from the enzyme or, alternatively, to keep a cofactor behind the membrane.

Recently attempts have been made to immobilize enzymes in conducting polymers grown on a base electrode such as platinum or glassy carbon. For example, poly-*N*-methyl pyrrole has been grown on platinum, entrapping glucose oxidase [32]. Similar experiments for entrapping GOD have used polyindole [33] and polypyrrole [34]. In all these entrappment experiments the observed current is due to H_2O_2 oxidation and not to direct electron transfer between the conducting polymer and the enzyme. The denaturation of the enzyme is a problem with this technique.

1.4 Mediated electrodes

Redox proteins, some of which are redox enzymes, tend to be very large, with a typical molecular weight of $\approx 10^4 - 10^5$. Close approach to the electrode can be impossible; direct electron transfer then occurs at a rate which is too low to give faradaic currents. Applying a large overpotential may give rise to a faradaic current, although this can denature the protein and is also prone to interferences. A

mediator overcomes the need for an overpotential by shuttling between the redox centre of the protein and the electrode.

Many studies have been made on the electrochemical properties of mediators [35-38] and their viability as good mediators. Fulst and Durst [38] give a comprehensive list of organic mediators and Szentrimay et al [35] list in particular inorganic mediators.

There are many desirable properties of a good mediator:

(1) : well defined n value;

(2) : known standard potential ($E^{o'}$) under experimental conditions;

(3) : fast heterogeneous and homogeneous electron transfer;

(4) : soluble in aqueous media at or near the experimental pH;

(5) : stable redox species;

(6) : good optical window;

(7) : does not inhibit or interact with the enzyme.

All of these properties can rarely be met, but fortunately some properties are more important than others, depending on the particular conditions of the system and so compromises can be successfully made. It is imperative that experimental conditions i.e. pH and potential, are chosen so that insolubility or adsorption of the mediator on the electrode do not occur.

Mediators are in common use in experiments determining the oxidation/reduction potential of biological compounds. One standard method used is the potentiometric titration. Aliquots of reductant (usually $Na_2S_2O_4$) are added successively to achieve reduction of the protein, while aliquots of oxidant (usually $K_3Fe(CN)_6$) are added in the reverse direction. Mediators enable quick equilibr ation between the oxidant/reductant and proteins [39]. Alternatively a three-

electrode potentiostat can be used to poise the solution at a particular potential [40]. Again the mediator serves to achieve fast equilibration, in this case between the electrode and the protein.

Mediators are used in a variety of electrochemical techniques: cyclic voltammetry, spectroelectrochemistry, chronoamperometry, potentiometric titrations and polarography. In all cases mediators enable fast rates of electron transfer and quicker analysis times. Note that for spectroelectrochemistry the mediator may be either colourless so as not to interfere [40], or may be involved in the spectroscopic measurements [41].

1.4.1 Organic mediators

Most commonly used organic mediators can be grouped in terms of class of compound:

(1) : Viologens.

Viologens are substituted bipyridinium salts. The most commonly used is methyl viologen. Viologens have two, one electron oxidation/reduction steps, the first of which is usually reversible. Only the first reduction potential is important in terms of the use of the mediator. The neutral form of viologen is sparingly soluble in water and adsorbs strongly on electrodes. However the separation of the $E^{o'}$ values of the two oxidation/reduction steps is usually sufficient for most viologens to permit the generation of the radical cation without interference from the neutral viologen. The radical

cation can also be sparingly soluble depending on the particular viologen and the counter ion present.

(2) : Quinones.

These are mostly two electron acceptors e.g. benzoquinones, naphthoquinones and anthraquinones [38], although some are one electron acceptors i.e. tetracyanoquinodimethane (TCNQ) and its anion ($TCNQ^-$) [42]. The use of TCNQ supports the possibility that an electrode composed of NMP TCNQ (N-methyl phenazinium tetracyanoquinodimethane) would allow the direct electron transfer to an enzyme to occur.

(3) : Phenazines.

The most widely used is phenazine methosulphate (N-methyl phenazinium or NMP). Phenazines are commonly used as mediators in biological redox systems. Near pH 7.0 their redox reactions involve two electrons and one proton, but outside this pH complex behavior is observed, and phenazines become unsuitable for use as mediators. Again, the use of NMP as a mediator supports the possibility that an electrode composed of NMP TCNQ would enable direct electron transfer to an enzyme to occur [38].

(4) : Phenylenediamines.

The most commonly used is N,N,N',N'-tetramethyl-ρ-phenylenediamine (TMPD). TMPD is thought to be a one electron,

no proton redox reagent, although at pH < 6.5 it is thought that some proton transfer may also occur [36].

1.4.2 Inorganic mediators

Inorganic metal complexes are also used as mediators, being particularly useful at higher potentials [35]. $K_3Fe(CN)_6$ is often used as both a mediator and an oxidant in potentiometric titrations in conjunction with $Na_2S_2O_4$ as reductant [29].

Derivatives of ferrocene offer significant advantages over other mediators [43]. They have a wide range of $E^{o'}$ values (-50 to + 450 mV wrt SCE); they are electrochemically reversible one electron redox species; and the reduced form is non-auto xidisable. In addition, varying the substituents on the cyclopentadienyl ring shifts the redox potential. They also exhibit poor solubility, so that if the mediator has been evaporated onto the electrode, there is insignificant loss of mediator to the bulk. The oxidized form is more soluble, thus enhancing the oxidation of the reduced enzyme.

A number of substituted ferrocenes have been found to be effective mediators for the flavoenzyme glucose oxidase chemically immobilized on a graphite electrode [43]. 1,1'-dimethyl ferrocene was found to be the best mediator: the electrode was linear in the range 1 - 30 mM glucose, pH independent and relatively oxygen independent. Ferrocene monocarboxylic acid has been found to be an effective mediator with a number of other flavin oxidoreductases [44].

Of particular interest are carbon monoxide: acceptor oxidoreductase [45], which may be used as a sensor for CO gas, and

PQQ-linked glucose dehydrogenase [46]. The former contains flavin, iron, acid-labile sulfide and possibly molybdenum and is possibly of the same class of enzyme as xanthine oxidase; it is uncertain in this case which is the redox active group on the enzyme. The latter is a quinoprotein, so called because its prosthetic group is pyrrolo-quinolinium quinone (PQQ) [47]. PQQ-linked enzymes are oxidoreductases which are oxygen independent, and also FMN (flavin adenine mononucleotide), FAD (flavin adenine dinucleotide), NAD (β-nicotinamide-adenine dinucleotide) and NADP (NAD phosphate) independent. Glucose dehydrogenase has a turnover number thirty times greater than for flavoprotein glucose oxidase (320,000 min^{-1}) and a very high specific activity (3000 u/mg protein) [46]. The second order rate constant for electron transfer between the enzyme and 1,1'-dimethyl ferrocene is forty times faster for the PQQ-linked enzyme compared to the flavoenzyme [46]. Thus it is expected that PQQ-linked glucose dehydrogenase could offer many advantages over its flavoprotein counterpart.

1.5 Direct electron transfer

The reversible, direct electron transfer between an enzyme and an electrode is difficult to achieve: the redox site of an enzyme is hidden deep inside the enzyme and cannot closely approach an electrode surface and since the rate of electron transfer between an enzyme and an electrode depends exponentially on the distance between them [14], the rate of electron transfer is low. If a large overpotential is applied the enzyme molecule may flatten out onto the electrode surface in the strong electric field. The enzyme may be

denatured or adsorb on the electrode surface, and interferences from other electroactive substances at such a high overpotential may occur.

1.5.1 Use of a modified electrode

One approach to solving this problem is to modify an electrode with a known mediator for the enzyme. It is thought that the modifier contains a group capable of binding with the enzyme, enabling the redox active site of the enzyme to closely approach the electrode and electron transfer to occur. The binding process is thought to mimic the action of the enzyme with its biological counterparts.

Covalent bonding may occur between the enzyme and the electrode. For example, glucose oxidase [48], xanthine oxidase and L-amino acid oxidase [49] give low currents observed by differential pulse polarography (DPP) at graphite electrodes modified with cyanuric chloride. Dipping the modified electrode into a solution of the enzyme results in covalent attachment of the enzyme to the electrode via a cyanuric chloride linkage. Similar behaviour is observed with glucose oxidase at a (3-aminophenyl)- boronic acid modified glassy carbon electrode [50].

Alternatively the protein may be reversibly adsorbed on the modified electrode surface; for example, cytochrome c at a 4,4'-bipyridyl modified gold electrode [51]. Cytochrome c is a redox active protein involved in electron transfer in the mitochondrial respiratory chain. A further 54 bifunctional modifiers have been studied to assess the necessary requirements for an efficient

modifier for direct electron transfer between cytochrome c and a modified gold electrode [52]. The modifiers contain two functional groups, one of which, X, covalently binds to the gold electrode, while the other, Y, binds to the cytochrome c. X was found to be a Lewis base i.e. nitrogen, phosphorous or sulphur; Y was found to be an anionic group such as carboxylate, phosphate or sulphonate which can bind to the positively charged lysine residues ($-NH_3^+$) on cytochrome c. The modifier can be flexible or rigid (provided the Y group is projected out from the electrode surface), and delocalization between the functional groups is not necessary.

Another approach to achieving direct electron transfer is to modify the electrode so that a cofactor for the enzyme may turn over at the electrode. Graphite electrodes modified with phenazine methosulphate (PMS or NMP) or phenazine ethosulphate (PES) are capable of the oxidation of NADH, reducing the overpotential for the oxidation by 550 mV compared to the bare graphite electrode [53]. Similarly the overpotential for the NADH oxidation was reduced by $\approx$ 200 mV at electrodes modified with 3,4-dihydroxybenzylamine or 3-hydroxytyramine [54].

1.5.2 Direct electron transfer at a bare electrode (or thin layer electrode)

In some cases, the direct electrochemistry of an enzyme at a bare electrode has been possible, without applying a large overpotential. For example, the electron transfer of a number of redox active proteins of varying surface charge is possible at a RuO_2 thin layer electrode [55]. The electrode surface has hydroxyl groups which may

protonate or deprotonate to give positive or negative sites, the ratio of positive to negative sites being dependent on the pH of the solution. It is found that the overall surface charge of the electrode determines whether direct electrochemistry is observed. For instance, ferredoxin and rubredoxin (negatively charged proteins) exhibit cation-promoted direct electrochemistry at pH 8.0. The cations are thought to shield the electrostatic repulsion between the negatively charged electrode and the proteins. For positively charged cytochrome c, a current is observed which decreases as pH decreases, at pH > 6.5 . This is thought due to the electrode surface becoming more positive, and so decreasing the interaction between the positively charged protein and the electrode. Azurin, a relatively neutral protein, shows the least dependence of current on pH.

Glucose oxidase [56] and other large biological molecules [57] have undergone direct electrochemistry at a platinum electrode in a thin layer cell. A fast continuous linear potential sweep had to be applied to the electrode for several hours for any current to be observed. Repeated scanning in the presence of the enzyme improved the quality of the cyclic voltammogram. The reason for the effectiveness of the pretreatment of the electrode is unknown.

Electron transfer between a protein containing negatively charged binding sites and an electrode is possible by the introduction of positively charged groups. For example, ferredoxin, a small redox active protein, can turn over at a pyrolytic graphite electrode in the presence of divalent cations, in particular Mg^{2+} [58]. It is believed that Mg^{2+} shields the electrostatic repulsion between the highly charged protein and the carboxylate groups on the electrode surface.

1.5.3 Covalent attatchment of mediator to the enzyme

A recent development attacks the problem from a new angle: electron relays are covalently attatched to the enzyme which enhance the rate of electron transfer between the enzyme and the electrode. Glucose oxidase has been modified with a derivative of ferrocene, such as the monocarboxylic acid [59] or acetic or butanoic acid [60] derivatives. These electron mediators are covalently attatched to the enzyme without grossly perturbing the enzyme conformational structure, although there is some loss in enzyme activity compared to the native enzyme. The FAD/$FADH_2$ redox couple can transfer electrons via the ferrocene relays to the electrode surface. By the introduction of more redox groups into the enzyme, it is thought that the distance between redox active groups is decreased, and the rate of electron transfer within the enzyme itself and between the enzyme and the electrode is increased [59].

1.5.4 Conducting organic salt electrodes

Conducting organic salt electrodes are another class of electrode which enable direct electron transfer between the enzyme and the electrode. The work in this thesis is concerned solely with these electrodes; the proposed mechanism of conductivity in these materials is described in the next section. The remainder of this section gives a summary of work carried out with these electrodes to date.

Kulys et al first used conducting organic salts as electrode materials in 1980 [61]. Cytochrome b_2, reduced by its substrate L-lactate, was electrooxidized by an electrode composed of a pressed disc of NMP TCNQ. Similarly glucose oxidase was oxidised at NMP TCNQ in the presence of glucose.

Subsequent work has concentrated on either trying different salts or different enzymes. To date, a number of enzymes have been found to be electroactive. They fall into two classes: either flavin oxidoreductases [62-64] or NADH dependent dehydrogenases [65]. PQQ-linked alcohol dehydrogenase has also been found to be electroactive [66]. It is believed that the reduced cofactor can be oxidized at the electrode surface. Thus in theory any enzyme containing the flavin, NAD(P) or PQQ prosthetic groups can be electrooxidized at these electrodes. As there are approximately 200 NADH dependent enzymes known, there is a large number of potential sensors available.

A variety of salts have been tested for their ability to turn over glucose oxidase [62]. The best electrode materials were found to be the NMP^+, TTF^+ (tetrathiofulvalinium) and Q^+ (quinolinium) salts of $TCNQ^-$. For most subsequent work, TTF TCNQ was the material of choice, since it exhibited the lowest background current.

A TTF TCNQ/ glucose oxidase electrode has been successfully operated for one month [67]. The enzyme was immobilized next to the electrode with a membrane. Transport of the substrate through the membrane was always rate limiting for the unsaturated electrode and therefore any loss in enzyme activity did not affect the electrode response. It was concluded that conducting organic salt electrodes exhibit great stability.

It should be noted that glucose oxidase adsorbs strongly and irreversibly on the electrode surface. This allowed an in vivo electrode to be prepared in order to monitor the glucose levels in rat brains without the need for a membrane to retain the enzyme [68].

Further studies on the adsorbed enzyme have been made using radiolabelled enzyme [69]. It was concluded that ≈ 25 monolayers of enzyme adsorb onto the electrode surface; the layers closest to the electrode are irreversibly adsorbed and redox inactive, while the outermost layers are reversibly adsorbed and redox active. It was concluded that it was necessary to have layers of irreversibly adsorbed inactive enzyme for electron transfer to occur. However it should be noted that the number of monolayers could have been overestimated, since the authors assume the area of the electrode is equal to its geometric area. That this is clearly not the case has been confirmed by electron micrographs of the electrode surface [69]. The surface is polycrystalline and consists of a wide range of crystal sizes and orientations. The surface coverage would be larger for the true surface area compared to the geometric surface area, with a concomitant reduction in the number of monolayers.

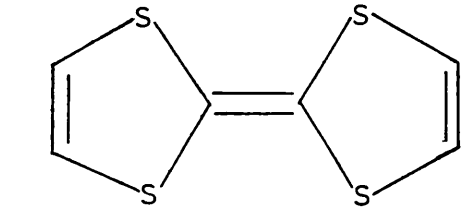
The mechanism of electron transfer between the redox active enzyme and the electrode is controversial. Kulys considers the electron transfer to be mediated by species dissolving from the electrode surface [70], in the so-called homogeneous mediation mechanism [71]. Albery proposes heterogeneous redox catalysis occurs [72]: in this theory the electrode material dissolves to a small extent on the electrode surface, enabling electron transfer to occur. Alternatively the electron transfer could be direct and be independent of any dissolved species [62]. The mechanisms are discussed in more detail in Chapters 4 & 5, where the experimental evidence for and against each theory is assessed.

An understanding of the mechanism is important in terms of the potential medical and industrial uses of an enzyme electrode prepared with a conducting organic salt. If the salt is soluble and the electrode effectively dissolves away under continuous use, then techniques must be employed which will limit the amount of salt lost to an acceptable minimum. This is necessary in terms of the lifetime of the sensor, and also in terms of any potential health hazard posed to any person working with the electrodes [73].

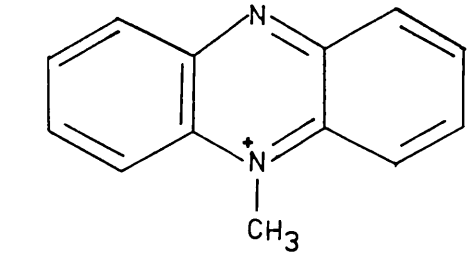
1.6 Conducting organic salts

Conducting organic salts have excited much interest over recent years due to their high room temperature conductivities. Research into these materials has had two purposes: to synthesize new, more highly conductive salts and to understand the mechanism by which these materials conduct.

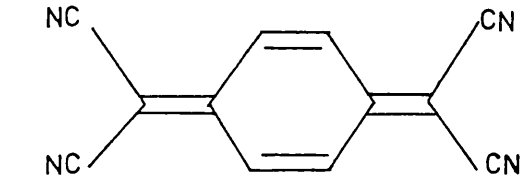
This thesis is concerned with two of the most highly conducting of these salts, TTF TCNQ (tetrathiofulvalinium tetracyanoquinodimethane) and NMP TCNQ (N-methyl phenazinium tetracyanoquinodimethane), shown in fig(1.1). Semiconducting salts of TCNQ were first prepared in the 1960s primarily as a result of work carried out by Melby and coworkers at DuPont [74]. This led to the preparation of NMP TCNQ, the most highly conductive organic material known at that time [75]. The room temperature conductivity of NMP TCNQ is 200 $\Omega^{-1}cm^{-1}$ [75]. In 1973, TTF TCNQ was first synthesized by Ferraris et al; this salt has an even higher room temperature conductivity of 500 $\Omega^{-1}cm^{-1}$ [76].



TTF^{o}



NMP^{+}



$TCNQ^{o}$

Fig(1.1) The chemical structures of TTF^{o}, NMP^{+} and $TCNQ^{o}$.

1.6.1 Synthesis of the salts

Conducting organic salts are made up of an electron donor species and an electron acceptor species. Work on the synthesis of these salts has concentrated on the preparation of novel donors and acceptors with various substituents [77,78]. The method of synthesis is simple and follows one of two routes: either direct combination of donor and acceptor in solution, as in the preparation of TTF TCNQ, or by metathesis between donor and acceptor salts, as in the case of NMP TCNQ:

$$TTF^{o} + TCNQ^{o} \longrightarrow TTF\ TCNQ$$

$$NMP^{+}MeSO_4^{-} + Li^{+}TCNQ^{-} \longrightarrow NMP\ TCNQ + Li^{+}MeSO_4^{-}.$$

The direct mixing of the reactant solutions results in instant precipitation of small crystals. Large crystals can be produced by the slow diffusion of the individual reactant solutions into a reaction vessel. This process can take many weeks. Alternatively crystals can be electrochemically grown, although there is difficulty in producing large, even crystals [79].

1.6.2 Conductivity of the salts

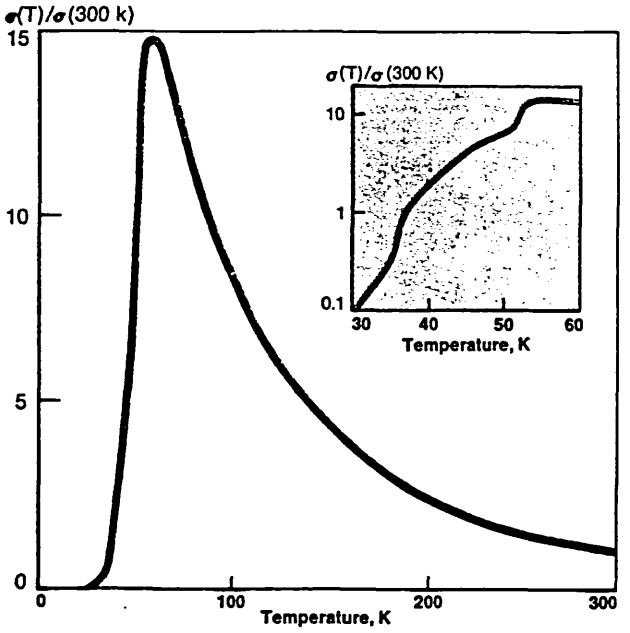
The conductivity of TTF TCNQ is highly anisotropic, varying along the crystal axes in the three principle directions in the ratio 500 : 5 : 1 [80], giving rise to the term 'quasi one-dimensional' to describe its conductivity. The conductivity is strongly temperature dependent,

as shown in fig(1.2). Maximum conductivity is observed at roughly 59 K [80]. Above this temperature, the salt conducts like a metal, and conductivity decreases with temperature. Below 59 K, the salt behaves like an insulator, with conductivity decreasing as temperature decreases; the conductivity approaches zero as 0 K is approached. Thus TTF TCNQ goes through an insulator-metal transition around 59 K. The above behaviour is typical of highly conducting organic salts and is also observed in NMP TCNQ.

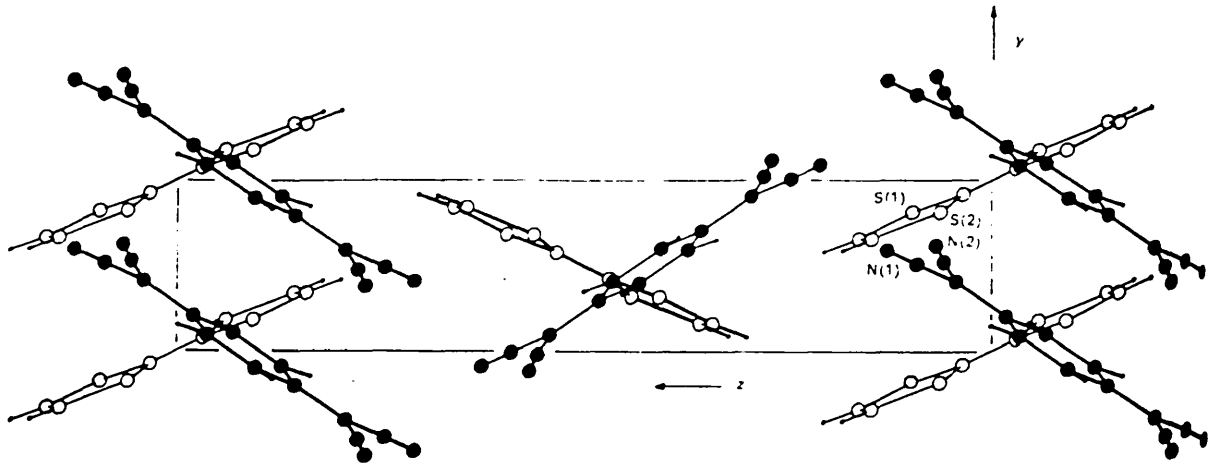
1.6.3 Crystallographic structure of the salts

The crystal structures of these salts give a good deal of insight into how they conduct. The structures of NMP TCNQ and TTF TCNQ have been determined by x-ray crystallography [81,82], shown in fig(1.3). The crystals consist of stacks of molecules, each stack containing either donor or acceptor, but never a mixture of the two. This gives rise to the term "segregated stacking" to describe the structure of the salts and other similarly packed highly conducting organic salts. Within a stack, both donor and acceptor molecules are planar and equally spaced, and pack in a direction perpendicular to their molecular plane.

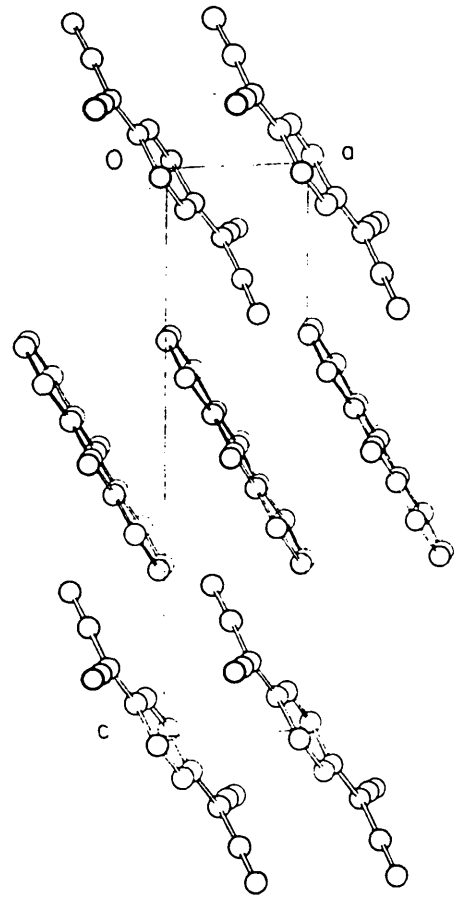
The interplanar distance within a stack serves as an indication of any bonding between molecules in the stack direction. In the TCNQ stacks of both NMP TCNQ and TTF TCNQ, the interplanar distance is very short compared to the Van der Waals spacing in neutral TCNQ. It is concluded that some bonding between the TCNQ molecules has occurred, and it is likely that conductivity will take place in these stacks in the direction perpendicular to the plane of the molecules



Fig(1.2) The temperature dependence of the conductivity of TTF TCNQ
(reproduced from [80]).

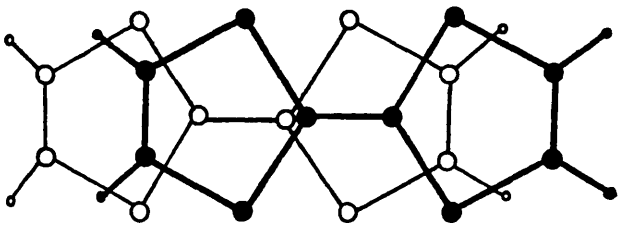


(a) A view down [100] of the crystal packing in TTF–TCNQ. The shaded molecules have their centroids at $x=\frac{1}{2}$.

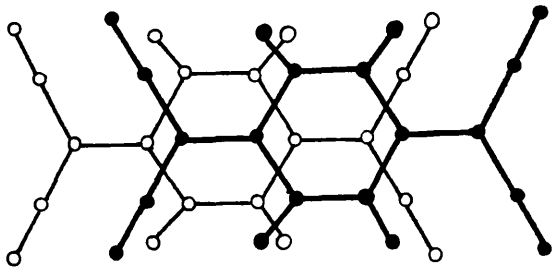


(b) (010] projection.

Fig(1.3) The crystal structures of (a) TTF TCNQ and (b) NMP TCNQ determined from x-ray crystallography (reproduced from [82] and [81] respectively).



TTF



TCNQ

Fig(1.4) The molecular overlap in the columnar stacking of (a) TTF and (b) TCNQ ions respectively. The view direction is normal to the plane of the molecules.

[81,82]. Similarly in the TTF stacks of TTF TCNQ, the interplanar distance is smaller than in the neutral TTF^{o} crystal [82]; thus TTF stacks can also take part in conduction. However in NMP TCNQ, the interplanar distance in NMP stacks is approximately the same as the Van der Waals spacing, and it is thought unlikely that NMP stacks can support conduction [81].

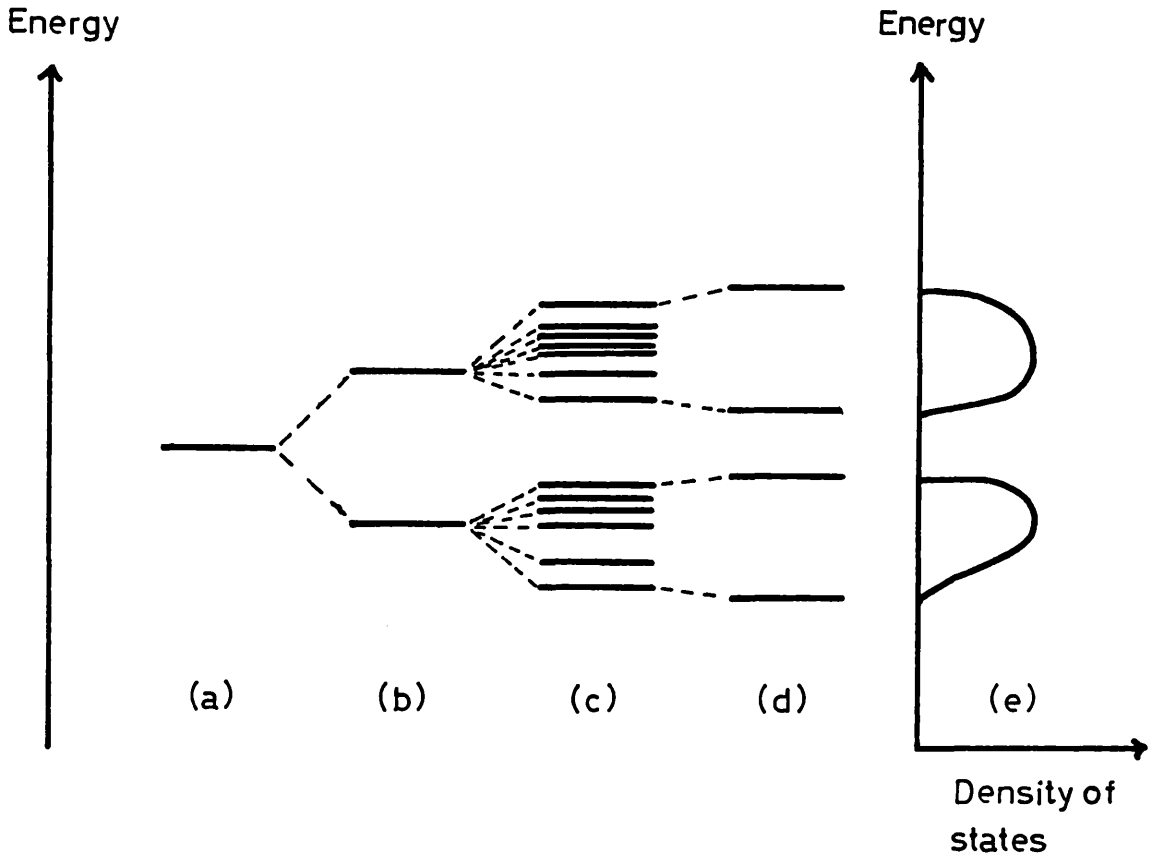
The inter-stack distance is 10-15 Å and is too great for any bonding between adjacent molecules to occur in the non-stacking direction. Hence the anisotropy observed in the TTF TCNQ conductivity can be understood: conductivity only occurs in the stack direction.

Within a stack, the molecules do not lie directly on top of one another: there is a lateral displacement giving ring-over-bond overlap. The exocyclic C=C double bond lies over the ring of the molecule adjacent to it in the stack shown in fig(1.4). The short interplanar distance between adjacent molecules allows significant interaction between π-molecular orbitals of neighbours, leading to the formation of a band of allowed energies in the solid.

1.6.4. Band structure of the salts

The formation of band structure in a solid is shown in fig(1.5). The precise solid state description of band formation is not given here and readers are referred to a standard text [144].

The filling of the band with electrons follows the Aufbau principle in atomic orbital theory: electrons are placed in pairs in the lowest energy state available. A band based on a single π-molecular orbital from each of n molecules in a uniform stack will contain n states into



Fig(1.5) The formation of band structure in a solid. The diagram shows the orbital energies of (a) an atom (b) a small molecule (c) a large molecule (d) a solid and (e) the density of states corresponding to (d).
(Reproduced from [144]).

which can be placed 2n electrons. The band may be full as for an insulator, or it may be incomplete as for a conductor. Above the highest occupied state will be unoccupied states into which an energetically excited electron can hop. There is a threshold energy level above which this can occur, known as the Fermi level. In a conductor, this is infinitesimally higher in energy than the highest occupied state, while in an insulator, it is within the band gap between the highest occupied state in the full band and the lowest unoccupied state in the empty band.

The number of electrons transferred from donor to acceptor molecules is known as the degree of charge transfer, ρ. The magnitude of ρ determines the conductivity of the salt. If each donor molecule transferred one electron to each acceptor molecule i.e. $\rho = 1$, then the acceptor band would be half full and one would expect conduction to occur by promotion of an electron to an empty state which is infinitesimally higher in energy than the Fermi level. However this situation would result in one electron on each TCNQ molecule. Then in order for conduction to occur, an electron would have to hop onto a neighbouring molecule, resulting in two electrons on the same molecule. There would be a large coulombic repulsion between the two electrons, and so transfer of an electron would be energetically unfavourable. This results in a Mott-Hubbard energy gap opening up between the filled and empty bands. The material cannot support conduction and is an insulator, known as a Mott-Hubbard insulator.

If $\rho < 1$, i.e. there is incomplete electron transfer, for each n donor molecules and n acceptor molecules, less than n electrons will be transferred. In a physical sense this corresponds to some acceptor

molecules being in a neutral state and some carrying charge. An electron could hop from a charged molecule to a neutral molecule and so conduction can occur.

In TTF TCNQ, $\rho = 0.59$ [83] i.e. per 100 TTF molecules there are 59 electrons transferred to the TCNQ stack. The acceptor band is only partially filled and conduction can take place since there is little coulombic repulsion between electrons i.e. an electron can hop from one molecule to another without putting two electrons on one TCNQ molecule. Similarly, in NMP TCNQ, $\rho = 0.91$ [83]; incomplete charge transfer occurs and conduction results.

The ability of an electron to migrate from one molecule to another is closely related to the presence of an aromatic sextet which can migrate from one molecule to the next [84]. If both the oxidized and reduced form of the acceptor and donor are aromatic, then their stability to electron transfer will be enhanced and electron transfer will be energetically favourable. TTF, NMP and TCNQ all have aromatic sextets for both oxidized and reduced forms.

From the above discussion, a summary of the desirable features of a donor/acceptor combination capable of supporting conduction can be made:

(1) : the molecules should be planar to allow a high degree of overlap with π-delocalization throughout the whole molecule, and formation of a new aromatic sextet on charge transfer.

(2) : the donor and acceptor molecules should be approximately the same length to allow close packing of the molecules [77].

(3) : the donor and acceptor should be of moderate strength i.e. moderate ionization energy and electron affinity respectively, so that complete charge transfer does not occur [83].

(4) : the donor and the acceptor should have the same high degree of symmetry.

1.6.5 Temperature dependence of the conductivity

The band theory given above can be used to explain the temperature dependence of the conductivity of these salts. Taking TTF TCNQ as an example, it has been noted above that the material goes through an insulator-metal transition at 59 K. Loss of conductivity is seen above this temperature because of scattering of the conducting electrons by lattice vibrations, known as phonons. As the temperature is decreased, there are less lattice vibrations, the electrons are decreasingly scattered and conductivity increases.

As temperature is further decreased and 59 K approached, the stacks can no longer maintain long range order, and lattice distortions occur i.e. the stack is contracted in one region and stretched in another, so that there is a variation in charge density on going through the solid from molecule to molecule. This variation in charge density through the stack is known as a charge density wave (CDW). The electrons become localized on certain molecules since they have insufficient energy to hop to another. This causes an energy gap to open up between the filled electron band at lower energy and the empty electron band at higher energy. This energy gap, known as the Peierls instability gap, results in an insulating solid. On increasing the temperature once more, electrons are allowed to jump into the higher energy state; thus the electronic energy advantage from the distorted lattice is lost, and increased vibrational motions favour a uniform lattice. The material will then

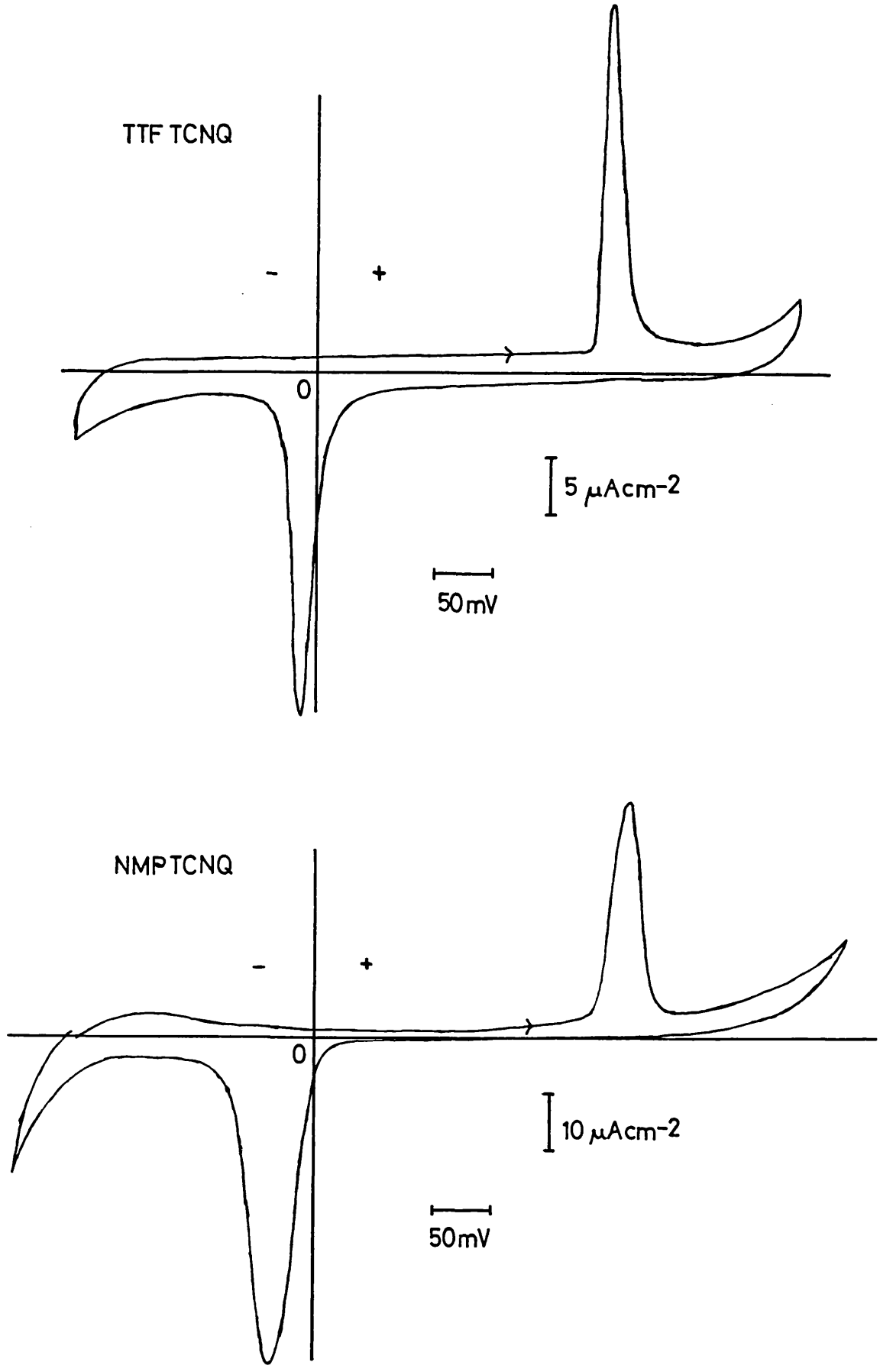
undergo an insulator-metal transition and gain a uniform lattice structure.

1.6.6 Electrochemistry of the salts

The electrochemical behaviour of TTF TCNQ and NMP TCNQ has been well characterised in a number of aqueous electrolytes [85-87]. Typical cyclic voltammograms of these materials are shown in fig(1.6). The salts have a wide stable range. The oxidation peak observed at +250 mV for TTF TCNQ and + 270 mV for NMP TCNQ is assigned to the oxidation of $TCNQ^-$ to insoluble $TCNQ^0$. The reduction peak observed at - 15 mV for TTF TCNQ and - 40 mV for NMP TCNQ is assigned to the reduction of $TCNQ^0$ to $TCNQ^-$ [85]. The wide peak separation indicates the irreversiblity of the electron transfer. It should be noted that these peaks are only observed if the material has been taken outside its stable range. They are not essential for the electrode to facilitate electron transfer to an enzyme. Peaks for the oxidation/reduction of TTF and NMP redox couples are not observed due to the high solubility of the oxidized and reduced species in this media.

1.7 Flavoproteins

Flavoenzymes were employed for the majority of work in this thesis. Flavoproteins are commonly found in nature. Many act directly on a substrate, while others act as intermediates in the respiratory chain by bridging the electron-transport gap between pyridine nucleotides, which they dehydrogenate and the



Fig(1.6) Typical cyclic voltammograms of TTF TCNQ and NMP TCNQ in pH 7.4 phosphate buffer, 0.15 M in NaCl. Scan rate 10 mV s^{-1}

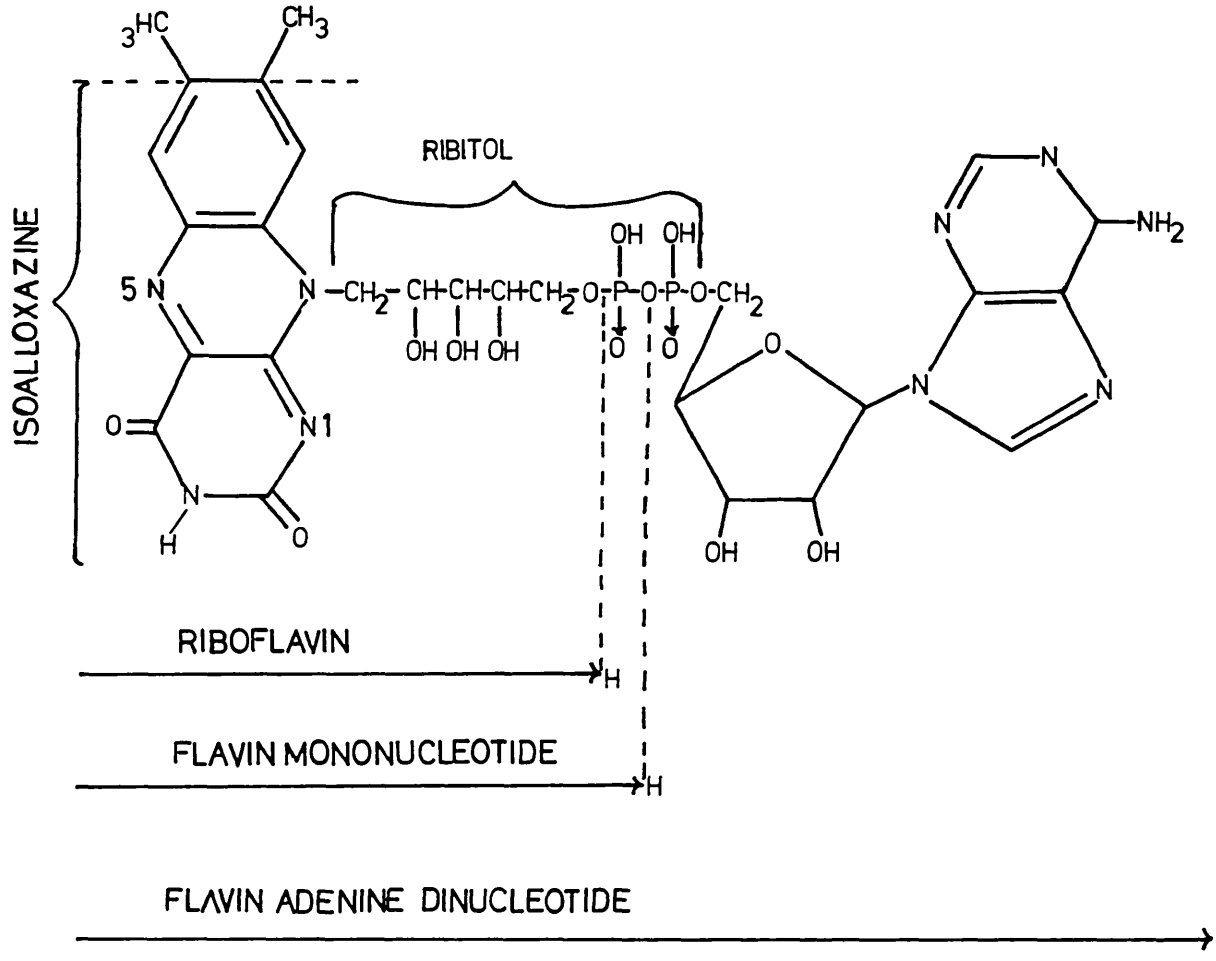
cytochromes, to which they transfer electrons. They are particularly amenable to study because the oxidation and reduction reactions of the enzyme can be studied separately, the flavin can be monitored spectroscopically, and, using an oxygen electrode, good kinetic data can be obtained [89].

Flavoproteins contain the flavin cofactor. This is yellow and fluorescent and is responsible for the characteristic yellow colour of flavoproteins. The flavin may be either FMN or FAD. The structure of these flavins are shown in fig(1.7). There is a three ring structure containing a benzene ring, a pyrazine ring and a pyrimidine ring which forms the isoalloxazine ring system. The tricyclic flavin can undergo both one and two electron reductions, through the binding of two hydrogen atoms to N atoms N(1) and N(5).

The semiquinone form is a radical anion, and is formed on one electron reduction of the quinone (oxidized) form. The radical is centred on the N(5) position. The product of the two electron reduction is the hydroquinone form, 1,5-dihydroflavin. Depending on the pH, one cationic, one neutral and one anionic species can be distinguished for each redox state [88]. Irrespective of whether one or two electrons are transferred per flavin molecule, flavins are thermodynamically reversible redox systems.

The physiological electron acceptors for flavins are, in general, iron-containing prosthetic groups and molecular oxygen which become reduced on flavin oxidation. The reaction of dihydroflavin with oxygen catalyses the two electron reduction of oxygen to hydrogen peroxide:

$$E\text{-}FADH_2 + O_2 \longrightarrow E\text{-}FAD + H_2O_2 .$$



Fig(1.7) The chemical structure of the flavin cofactor.

The central dihydro-pyrazine ring reacts with oxygen, yielding a superoxide anion and semiquinone radical as metastable species. Thus flavins are very amen able for use in classical enzyme electrodes since the consumption of oxygen or the formation of hydrogen peroxide can easily be measured. Alternatively small redox proteins can act as an electron shuttle between other flavoproteins e.g. in photosynthesis, flavodoxins transfer electrons between hydrogenases and other flavoproteins [90]. These simple flavoproteins have a molecular weight of ≈15,000 - 21,000 and contain a single FMN group.

Flavoproteins can be divided into two main types: those containing a trace of metal ions, such as iron, molybdenum, copper or manganese, and those not containing any metal. The role of metal ions in enzymatic catalysis probably consists in binding apoenzyme, substrate and coenzyme through the formation of various chelates. The presence of metals may facilitate the interaction of flavoproteins with one electron acceptors by stabilization of intermediates which are functionally important in the catalytic process.

The redox potential of the flavin group varies widely depending on the flavoenzyme with which it is associated. In addition to redox potential, the rate constants of biochemical electron-transfer reactions are strongly influenced by the exposure of the prosthetic groups at the protein surface, the steric accessibility of the exposed redox centre and the electrostatic interactions involving charged groups principally at or near the site of reaction [91].

The electrochemical behaviour of free flavins is characterised by strong adsorption and two superimposed reversible one electron

processes [90]. Because flavins have rapid electrode kinetics, they have been used as mediators i.e. FMN has been used to mediate the reduction of methemoglobin at a platinum electrode, lowering the overpotential required [92]. When bound to an enzyme as a prosthetic group, the rate of electron exchange is generally decreased due to the additional distance and the extra steric hindrance involved[90].

It should be noted that flavins are very sensitive to light. On absorption of light, hydrogen is transferred from the hydroxylic side chain to the isoalloxazine ring with the side chain being subsequently split off. This irreversible photolysis can be prevented by adding external electron donors that themselves are more easily dehydrogenated by the light activated flavin in its triplet state. Then only a photoreduction of the flavin occurs, which is reversible on the addition of oxygen [88].

1.8 The rest of this thesis

A number of enzymes have been found to be electroactive on the conducting organic salts TTF TCNQ and NMP TCNQ [63-65]. To date, nearly all these enzymes have contained the cofactor FAD. It was thought interesting to discover whether enzymes with other cofactors could also be electroactive. Thus a number of other types of oxidase enzymes were tested for electroactivity using a membrane electrode. These are reported in Chapter 3. The enzymes contained either FAD, FMN or copper at the active site. In addition, scanning electron microscopy was used to determine how the surface of an

electrode was related to its method of preparation and its saturated response in the presence of reduced enzyme.

As stated above, the actual mechanism of electron transfer between a reduced flavoenzyme and a conducting organic salt electrode is unknown. Thus in Chapter 4, the two mechanisms thought most likely to occur are outlined, namely heterogeneous redox catalysis and homogeneous mediation. The two theories are outlined in full in the Appendices A and B. Preliminary data are presented and analysed according to the two theories. In Chapter 5, further experiments are reported for the potential dependence of the electrode and a rotating ring-disc electrode study is made. Again these results are analysed in terms of the two theories. At the end of Chapter 5, all the mechanistic data is summarised and an attempt is made to conclude which of the theories is most strongly supported. A summary of the conclusions from Chapters 3, 4 and 5 is given in Chapter 6.

Chapter Two

Experimental

2.1 Chemicals and solutions

All chemicals and enzymes were commercially supplied and used without further purification. All chemicals were Analar grade where possible. Electrode materials were prepared following the methods given in section 2.2.

All solutions were made up using doubly deionized water (DDW) that had been purified using a MilliQ (Millipore) system, with a minimum resistivity of 18 MΩ cm. D-glucose and D-galactose solutions were prepared at least 24 hours prior to use to allow equilibriation of the anomers.

2.1.1 Enzyme preparations

Details of the enzymes used are given in table 2.1. All enzymes were supplied as lyophilized powders and stored at -10°C or 4°C as recommended.

Enzyme solutions were prepared as needed and stored at 4°C. Each enzyme and its corresponding substrate were prepared in the appropriate buffer for that enzyme. Details of the buffers used are given in table 2.2. Buffers were balanced using a Kent EIL 7020 pH meter, and stored at 4°C.

Enzyme	EC number	Supplier	Activity	Source
Glucose Oxidase	1.1.3.4	Boehringer	457 mg ≡100,000u	Aspergillus niger
Sarcosine Oxidase	1.5.3.1	Boehringer	309 mg ≡ 500u	Pseudomonas sp.
Glycolate Oxidase	1.1.3.15	Sigma	0.9 u/mg	Spinach
Lactate Oxidase	1.13.12.4	Sigma	20.8 u/mg	Mycobacterium smegmatis
Pyruvate Oxidase	1.2.3.3	Boehringer	9.9 mg ≡ 100 u	bacterial origins
Oxalate Oxidase	1.2.3.4	Boehringer	10 u ≈ 40 mg	barley seedlings
Bilirubin Oxidase	1.3.3.5	Sigma	1700u/mg	Myrothecium sp.

Table 2.1 Commercial preparations of the enzymes

pH	buffer	enzyme(s) used with
7.4	0.1M Na_2HPO_4 0.15M NaCl balanced with conc. HCl	glucose oxidase sarcosine oxidase glycolate oxidase
7.4	0.1M Na_2HPO_4 0.15M KBr balanced with conc. H_2SO_4	bilirubin oxidase
7.0	0.1M Na_2HPO_4 0.15M NaCl balanced with conc. HCl	lactate oxidase
6.0	0.1M Na_2HPO_4 0.15M NaCl balanced with conc. HCl	pyruvate oxidase
3.8	0.1M sodium succinic acid 0.1M sodium acetate balanced with Na_2HPO_4	oxalate oxidase

Table 2.2 Buffer solutions

2.2 Electrode preparation

2.2.1 Preparation of salts

TTF TCNQ was prepared following the method of Ferraris et al [78]. To a boiling solution of TTF (0.5g , 2.45 $x10^{-3}$ mol) in acetonitrile (75 cm^3) was added a boiling solution of TCNQ (0.5g , 2.45 $x10^{-3}$ mol) in acetonitrile (75 cm^3). Crystals formed immediately. The reaction vessel was allowed to cool slowly to room temperature and left for 24 hours prior to collecting the crystals and washing with copious amounts of acetonitrile. The solid was recrystallized from acetonitrile (150 cm^3) and again cooled slowly to room temperature and left overnight for 24 hours. The crystals were collected and washed with acetonitrile, and then diethylether and dried overnight in vacuo. The resultant crystals were small, black, shiny and needle shaped.

NMP TCNQ was prepared following the method of Melby [75]. This is a two stage synthesis: firstly LiTCNQ is prepared, which is then reacted with commercially supplied NMP $MeSO_4$ to give NMP TCNQ.

LiTCNQ was prepared by adding a boiling solution of TCNQ (1g , 0.005 mol) in acetonitrile (100 cm^3) to a boiling solution of LiI (2g , 0.015 mol) in acetonitrile (5 cm^3). Purple crystals immediately formed; the mixture was left overnight to cool. The solid was collected and washed with acetonitrile, and then diethylether. The crystals were dried in vacuo overnight.

NMP TCNQ was prepared by adding a boiling solution of LiTCNQ (0.96g , 0.005 mol) in absolute ethanol (100 cm^3) to a boiling

solution of NMP $MeSO_4$ (1g , 0.005 mol) in absolute ethanol (50 cm^3). Black crystals formed immediately; the solution was allowed to cool down slowly to room temperature and left for 24 hours. The solid was collected and and washed with ethanol, then recrystallized in acetonitrile (100 cm^3). The solution was left overnight , and the solid collected, washed with acetonitrile and dried in vacuo overnight. The crystals formed were black/purple, shiny and of mixed size.

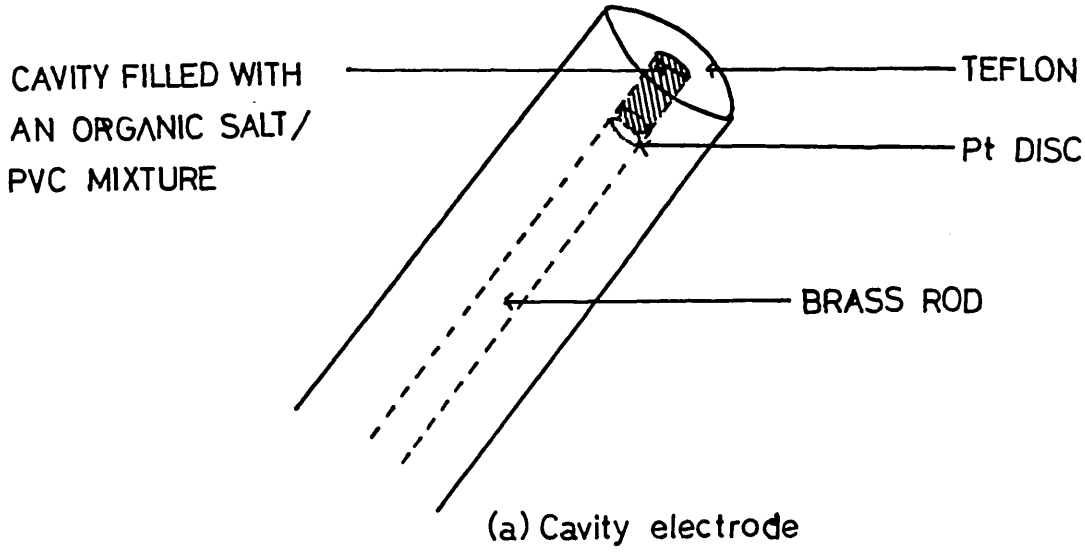
All salts were sent for microanalysis and good purity was found (within 0.1% for each element).

2.2.2 Preparation of electrodes

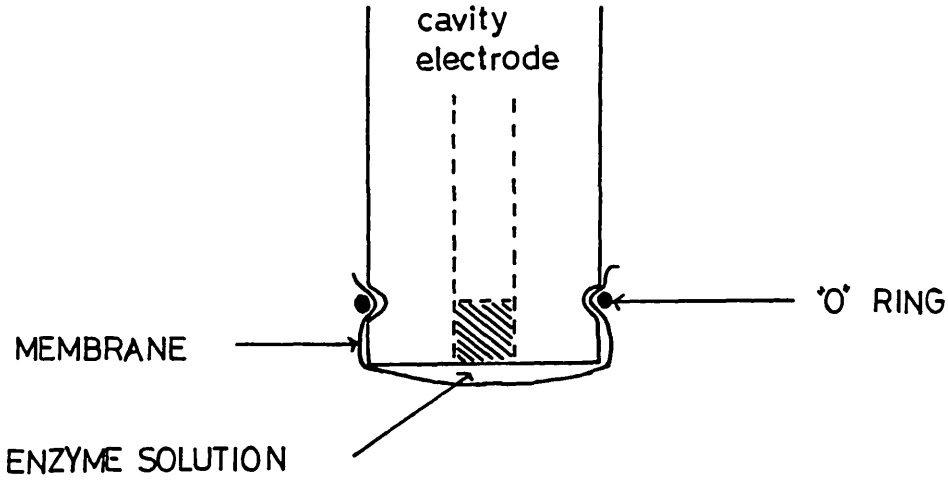
Electrodes were made in house. Cavity electrodes consisted of a platinum disc (diameter 1, 2 or 7 mm) press fitted into teflon to a depth of ≈ 1mm. Contact was made to the platinum via a brass rod inside the teflon. The overall diameter of the cavity electrodes was 1 cm. A cavity electrode is shown in fig(2.1).

Cavity electrodes were prepared initially by cleaning the platinum contact with 0.3 μm alumina and followed by copious washing with DDW and drying with a tissue. The cavity was then filled with either a PVC : salt slurry or a Si^oil (Silicone) : salt paste.

The PVC : salt slurry was prepared by weighing out a mixture 9 : 1 by weight of salt : PVC. PVC was high molecular weight supplied by Sigma. THF (Aldrich gold label) was added dropwise to give a thick slurry. The slurry was left for ≈ 10 minutes to allow the PVC to dissolve. The cavity was filled with the slurry and left for at



(a) Cavity electrode



(b) Membrane electrode

Fig(2.1) Schematic representation of (a) a cavity electrode and (b) a membrane electrode.

least one hour for the solvent to evaporate. The electrode was then trimmed using a scalpel.

The Si oil : salt paste was prepared by mixing one microspatula of salt with approximately one drop of Si oil (high temperature, Aldrich) to give a very thick, almost dry paste. This paste could then be placed inside the cavity, and the top of the electrode cleaned and smoothed by polishing on filter paper. The paste could be stored for several weeks without any deterioration. Because of the low adhesive properties of the paste, it was best used in a cavity electrode with a 1 mm diameter cavity; larger cavities resulted in the paste falling out.

The ring-disc electrode consisted of a 3 mm diameter TTF TCNQ pressed pellet surrounded by a concentric platinum ring, of thickness 0.25 mm, set in epoxy resin. The overall diameter of the electrode was 1 cm. Contact was made to the ring through the brass sleeve of the electrode; contact was made to the disc through the central brass rod. The TTF TCNQ pressed pellet was made using a Specac 15011 pellet press machine, applying a constant pressure of 3 tons for 3 minutes. No binder was used. The face to face pellet resistance was less than 1 KΩ.

2.2.3 Membrane electrodes

Membrane electrodes were prepared using cavity electrodes. Spectra/Por (spec) cellulose dialysis membranes were supplied by Pierce Warriner (UK) Ltd. Either Spectra/Por 2 (molecular weight cutoff ≈ 12,000 - 14,000 , dry thickness 0.00254 cm) or Spectra/Por 4 (molecular weight cutoff ≈12,000 - 14,000, dry thickness 0.00229

cm) were used. It should be noted that the dialysis time of Spectra/Por 2 membrane is half that of Spectra/Por 4 membrane (supplier's literature).

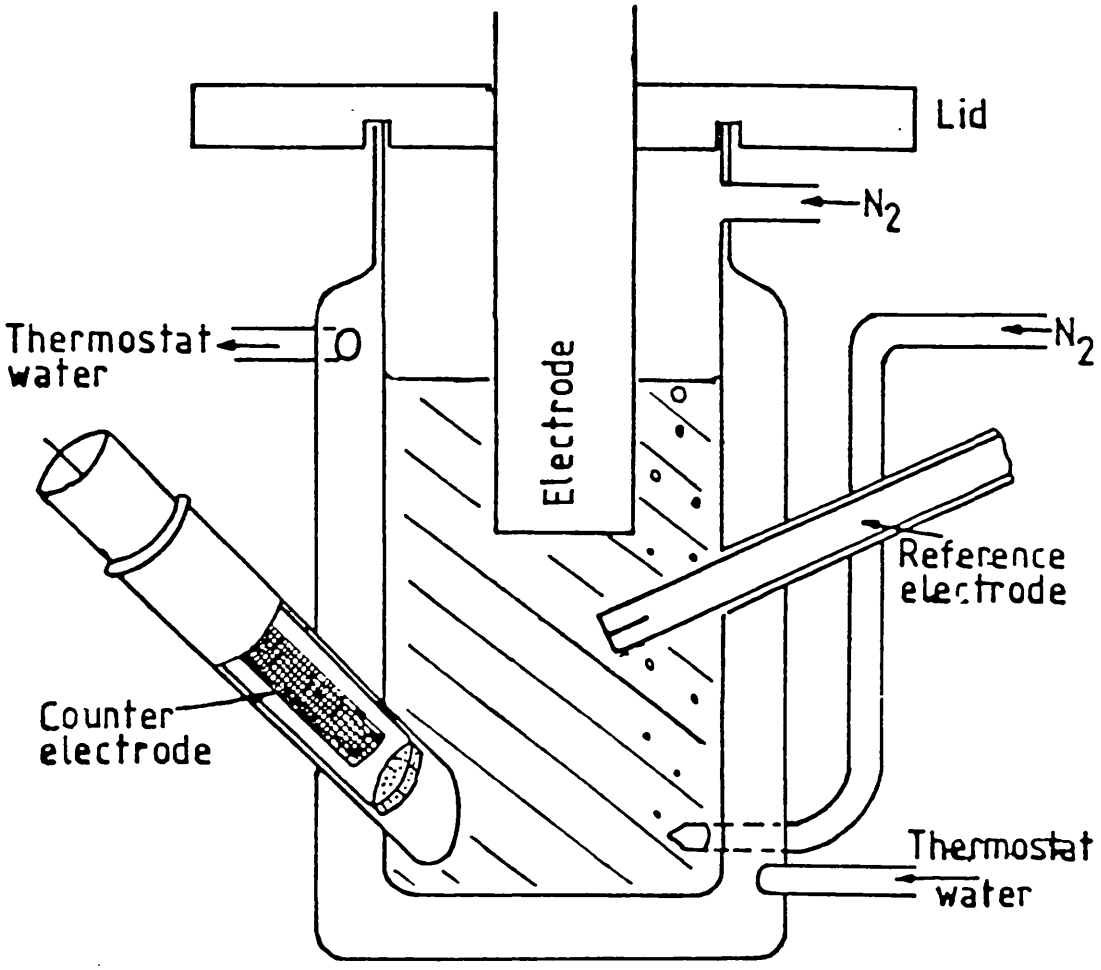
Membranes were prepared by boiling in a 1% weight/volume Na_2CO_3 solution for 10 minutes. This improves the quality of the membrane by removing impurities and softening it. When cool, the membranes were washed with copious amounts of DDW. The membranes were stored at 4°C in a solution of 10 mM Tris and 1 mM EDTA. A freshly cut square of membrane was used in the preparation of each membrane electrode. The membrane was washed with copious amounts of DDW prior to placing on the electrode.

The electrode was assembled by covering the electrode surface with enzyme solution, checking no air bubbles were trapped at the electrode surface. The membrane was then placed over the electrode surface and secured with a rubber 'O' ring. The membrane was trimmed and excess enzyme solution was removed by copious washing with DDW. When not in use, membrane electrodes were stored by dipping the membrane end of the electrode into the appropriate buffer solution.

2.3 Apparatus

2.3.1 The cell

A glass cell with two side arms was used for all experiments (fig(2.2)). The cell was stored in Decon 90 (BDH) solution when not in use. Prior to an experiment, it was thoroughly washed with



Fig(2.2) Schematic representation of the electrochemical cell.

distilled water, then DDW and dried at 100°C in an oven. The cell was left to cool to room temperature before use. The cell was thermostatted at 25°C for all experiments using a home made water bath.

The counter electrode was a platinum gauze prepared in house; this was placed in a side arm of the cell. The electrode was stored with the cell when not in use, and cleaned in the same manner as the cell.

The reference electrode was a saturated calomel electrode (SCE), prepared in the laboratory. The potential was frequently checked against other calomel electrodes. When in use the reference electrode was placed in the second side arm of the cell and when not in use it was stored in saturated KCl.

The solution in the cell was deoxygenated prior to use for 15 minutes with BOC oxygen free nitrogen. This was passed through a deoxygenating solution before reaching the cell. The deoxygenating solution consisted of a reduced anthraquinone-2-sulphonate and zinc amalgam. The gas line was connected to the cell either by means of a ground glass joint on the cell, or by dipping teflon tubing just below the surface of the solution. For membrane electrode experiments, solutions were stirred using a magnetic stirrer and stirrer bead. For mechanistic and ring-disc experiments, the electrode was rotated using an Oxford Electrodes rotator and motor controller.

2.3.2 Deoxygenating solution

Zinc (70g, 1.07 mol) was added to 3 M HCl (30 cm^3). After 30 sec, a 2% by weight $HgCl_2$ solution (30 cm^3) was added, with

stirring. The solution was stirred until hydrogen evolution ceased. This coated the zinc with a mercury wash. Sodium anthraquinone-2-sulphonate (1.2g) was added to 1 M NaOH solution (600 cm^3) (note the anthraquinone is not soluble). This solution was added to the Zn/Hg amalgam with stirring. This produced the red hydroquinone, which reacts with oxygen rapidly. It is converted to the colourless quinone if not regenerated by zinc.

Three dreschel bottles were filled with the mixture, ensuring some Zn/Hg amalgam was placed inside each bottle. The bottles were connected by tubing to the nitrogen gas line on one side and to a dreschel bottle filled with DDW on the other side, from which tubing led to the cell. The dreschel bottle of DDW was used to wash any volatile species from the nitrogen.

2.3.3 Electrochemical measurements

All measurements were made using modular electronics designed and made in the laboratories by Mr John Hooper. Typical experiments used a triangular wave generator, followers, a potentiostat, a subtractor and sometimes a sallen and key filter. The triangular wave generator was sometimes used as a constant potential source. Potentials were checked with a Fluke 8000A digital voltmeter. For ring-disc experiments, the voltage source for the ring was a modular voltage source, supplied by a 9V battery. All voltages were followed before and after leaving the potentiostat.

For all measurements, the saturated calomel reference electrode was earthed and all potentials measured relative to this. All membrane electrode experiments were carried out at +50mV vs SCE,

with the exception of oxalate oxidase, which were carried out at +100mV vs SCE.

Currents were recorded on a Gould BS 273 yy'y"t recorder or a Bryan 60000 xyt recorder.

2.4 Experimental procedures

2.4.1 Cyclic voltammograms

All new polymer paste electrodes were checked by cyclic voltammetry (CV) prior to use, to test whether good electrical contact had been made between the salt and the platinum base. Electrodes were cycled between their stable limits. For TTF TCNQ this was -160 mV to +330 mV vs SCE, and for NMP TCNQ this was -175 mV to +250 mV vs SCE. The scan rate commonly used was 50 mV s^{-1}. The solution was neither degassed nor stirred.

Si oil : salt paste electrodes were found to be consistently very good and exhibited excellent voltammograms. Consequently it was not necessary to inspect these by CV prior to use.

2.4.2 Membrane electrode experiments

After switching on, membrane electrodes were left for at least 30 minutes to allow the background current to fall to a steady value. An injection of a known volume of substrate solution was made to the bulk solution, using Hamilton Microliter gastight syringes or Gilson Pipetman syringes. When a new steady state current had

been reached, another injection was made. Injections were made until no further change in current was observed on injection.

The current response to an injection of current was measured relative to the background current (the current at zero substrate concentration in the cell).

2.4.3 Mechanistic experiments

A Si oil : salt paste electrode was prepared immediately prior to each experiment. Enzyme solutions were prepared on the day of the experiment, and made up to 1000 u/ml. D-glucose solutions were either 0.1 or 1 M.

The background current was allowed to fall to a steady level for 1 hour, degassing the bulk solution throughout. The electrode was rotated at 9 Hz: this was taken as the baseline rotation speed.

After 1 hour, the initial substrate or enzyme solution (which was kept constant throughout the whole experiment) was injected, and the current observed at 9 Hz, then 1 Hz, then returned to 9 Hz. Injection of enzyme or substrate solution was then made, and the current allowed to reach a steady value. The current at 1 Hz was measured and the electrode returned to 9 Hz. Further injections were made following this procedure for the rotation speed. The current response to an injection was measured relative to the background current at the appropriate rotation speed.

2.4.4 Ring-disc experiments

The dimensions of the ring-disc electrode are as follows:

disc radius	1.505 mm
inner ring radius	1.618 mm
outer ring radius	1.790 mm.

Prior to all experiments, the platinum ring electrode was cleaned by repeated scanning for several hours between - 1.0 V and + 1.2 V vs SCE at 100 mV s^{-1} in pH 7.4 phosphate buffer. The TTF TCNQ disc electrode was also checked by CV, following the method given in section 2.4.1.

2.4.4.1 Collection efficiency

The collection efficiency, N, of the ring was measured using 10 mM $K_3Fe(CN)_6$, made up with pH 7.4 phosphate buffer. The solution was degassed to prevent air oxidation of the ferro cyanide ion. The ring and disc electrodes were held at +400 mV and -100 mV respectively. The electrode was rotated at 1, 4 , 9, 16, 25 and 36 Hz and current measurements were made at each rotation speed for both the ring and disc electrodes.

2.4.4.2 Ring-disc electrode experiments

Experiments were performed in an Argon atmosphere using a polyethylene Atmos bag (supplied by Aldrich). The bag was filled with Argon (BOC) and evacuated three times before sealing and

refilling with argon. A slow flow of argon into the bag was maintained throughout the experiment. The solution was degassed with argon for at least two hours before injection of substrate. The solution was also degassed with nitrogen as before, and the same experimental procedure for mechanistic experiments in section 2.4.3 was followed, with the exception that the currents were recorded at three rotation speeds: 1, 4 and 9 Hz.

2.4.5 Potential step experiments

Potential steps were made by dialling the required voltage on a modular voltage source supplied by a 9v battery. The applied potential was followed on a digital voltmeter.

2.4.5.1 Mechanistic potential step experiments

The mechanistic potential step experiment was carried out under argon in an Atmos bag, following the procedure given in section 2.4.4.2 above. The electrode was a 1 mm diameter cavity electrode, packed with a Si oil : salt paste of TTF TCNQ. The electrode was rotated at 4 Hz throughout. The initial potential was 0 mV vs SCE, and potential steps of + 50 mV were made up to + 300 mV vs SCE. The current was allowed to settle to its previous level when switched from + 300 mV back to 0 mV. Otherwise measurements at each potential were taken 15 minutes after the potential step was made.

After injection of enzyme solution, the background current at each potential was measured. Injections of substrate were made at 0 V once the current had settled to its previous value. When the

steady state response of the electrode had been reached, potential steps were then made. The current response to an injection was measured relative to the background current at the appropriate rotation speed and potential.

2.4.5.2 Bilirubin oxidase potential step experiment

Potential steps were carried out with 46 u/ml bilirubin oxidase in bulk solution, rotating the electrode at 4 Hz throughout. The solution was degassed with nitrogen.

2.5 Scanning electron micrography

Samples were inspected with a Jeol JSM T200 scanning electron microscope. Machine settings were a working distance of 20 mm and an accelerating voltage of 25 KV. Photographs were taken with Ilford FP4 film.

Samples were prepared using a screw-top cavity electrode, of which the top 1 mm of the electrode screwed off to reveal the platinum base. The packed cavity was in the removeable top. The sample was mounted on an aluminium stub using silver epoxy, and gold sputtered to a depth of ≈ 40 nm.

2.6 UV/visible spectroscopy

Spectra were taken using a Hewlett Packard 8450A diode array spectrophotometer.

Chapter 3

Conducting organic salt membrane electrodes prepared with novel enzymes

3.1 Introduction

This chapter describes the behaviour of a number of enzyme electrodes, using the conducting organic salts TTF TCNQ or NMP TCNQ as the electrode material. As stated in section 1.5.4, a number of flavoenzymes have been found to be electroactive on TTF TCNQ [62-65]. In this chapter a further selection of flavoenzymes are tested for electroactivity in order to confirm the general nature of the electron transfer between the flavin cofactor and a conducting organic salt electrode. In addition, the work has been extended to include the enzyme bilirubin oxidase, which has an active site containing copper and no flavin moieties, to see whether other cofactors are capable of direct electron transfer at these electrodes.

The response of the electrodes to increasing concentrations of substrate is analysed according to the membrane electrode theory developed by W.J. Albery and P.N. Bartlett for conducting organic salt electrodes [93]. This theory is summarised below. The theory is considered for the cases when the electrode rate constant has either first order or half order dependence on the reduced enzyme. The analysis allows the assignment of the rate controlling process or processes for both the unsaturated and the saturated electrode response.

Problems encountered in the use of these electrodes are discussed, and use is made of scanning electron microscopy to suggest the factors required for a good electrode and to draw some conclusions about the nature of the electron transfer process at these electrodes.

3.2 Membrane electrode theory

The steady state theory for a conducting organic salt membrane electrode is given by W.J. Albery and P.N. Bartlett in [93]. A summary of it is given here.

The mechanistic scheme is shown in fig(3.1). Substrate in the bulk diffuses through the membrane with diffusion rate constant $k'_S = K_S D_S / L_M$, where K_S is the partition coefficient for S in the membrane (no units), D_S is the diffusion coefficient for S through the membrane (in cm s^{-1}), and L_M is the thickness of the membrane (in cm). The substrate then reacts with enzyme, E, in the electrolyte layer,thickness L, behind the membrane, according to the scheme:

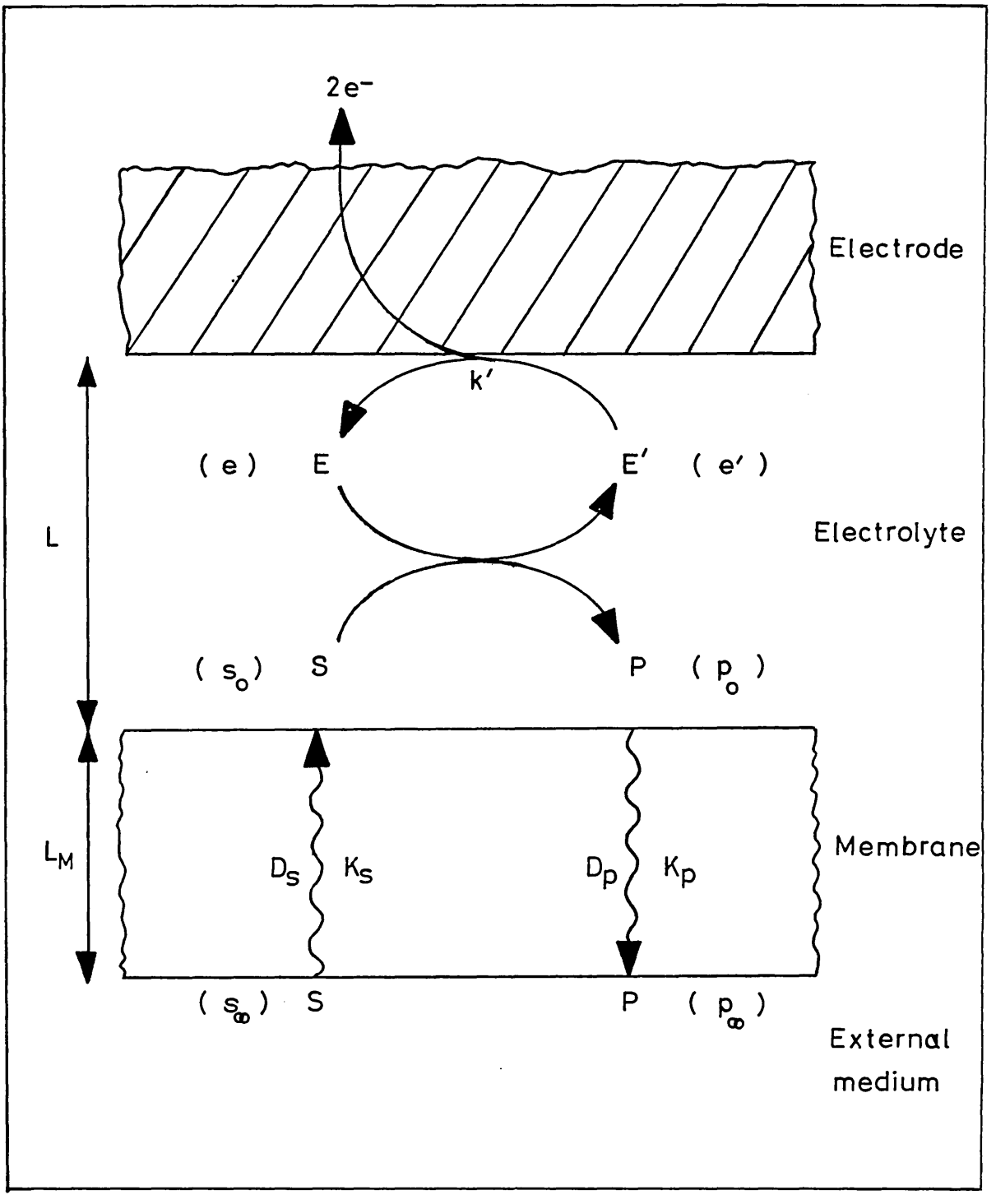
$$E + S \underset{}{\overset{K_1}{\rightleftharpoons}} ES \overset{K_2}{\rightleftharpoons} E'P \overset{K_3}{\rightleftharpoons} E' + P$$

where E denotes enzyme,

S denotes substrate,

ES denotes enzyme-substrate complex,

E'P denotes reduced enzyme-product complex,



Fig(3.1) Mechanistic scheme for the membrane electrode.

E' denotes reduced enzyme,

P denotes product,

and $K_n = k_n / k_{-n}$ for each step in the above scheme, and $K_{TD} = K_1K_2K_3$, where K_{TD} describes the overall equilibrium between E + S and E' + P.

Finally the reduced enzyme is oxidized at the electrode surface, described by the rate constant k'. This is assumed to be irreversible.

All primed rate constants are heterogeneous, measured in cm s^{-1}. The subscripts S and P refer to the substrate and product. The subscripts ∞ and o refer to the concentration of species in the bulk or in the electrolyte layer. It is assumed that the electrolyte layer is so thin ($\approx 10\mu m$) that there is no concentration polarization in the layer. It should be noted L has been calculated to be 2 μm for the choline oxidase membrane electrode [79], thus agreeing with this assumption.

3.2.1 The steady state equation

In the steady state we can write for the flux , j, measured in mol cm^{-2} s^{-1} :

$$j = k'_S(s_\infty - s_o) \quad (3.1)$$

$$j = L (k_1 s_o e - k_{-1} es) \quad (3.2)$$

$$j = L (k_2 es - k_{-2} e'p) \quad (3.3)$$

$$j = L (k_3 e'p - k_{-3} p_\infty e') \quad (3.4)$$

$$j = k'_P (p_o - p_\infty) \quad (3.5)$$

$$j = k' e' \ . \quad (3.6)$$

The total concentration of enzyme, e_Σ , is given by:

$$e_\Sigma = e + e' + es + e'p \ . \qquad (3.7)$$

Elimination of the six unknowns, s_o , p_o , es , e'p , e' and e between eqn.s (3.1) and (3.7) gives:

$$e_\Sigma /j = \{ 1- j/k'_s\, s_\infty \}\{ 1/Lk_{cat} + 1/k' + K_3^{-1}(1+K_2^{-1})/k' [p_\infty + j/k'_P]\}$$

$$+1/s_\infty \{ K_M/Lk_{cat} + K_1^{-1}K_2^{-1}K_3^{-1}/k' [p_\infty + j/k'_P] \} + e_\Sigma /k'_s\, s_\infty \qquad (3.8)$$

where $$1/k_{cat} = 1/k_2 + 1/K_2k_3 + 1/k_3 \qquad (3.9)$$

and $$K_M/k_{cat} = 1/k_1 + 1/K_1k_2 + 1/K_1K_2k_3 \ . \qquad (3.10)$$

3.2.2 No product inhibition

If we assume no product inhibition, then $p_o \approx 0$ i.e. $[p_\infty + j/k'_P] \approx 0$, and eqn. (3.8) reduces to:

$$e_\Sigma /j = \{1- j/k'_s\, s_\infty \}(1/Lk_{cat} + 1/k') + 1/s_\infty\, (K_M/Lk_{cat}) + e_\Sigma /k'_s\, s_\infty \ . \qquad (3.11)$$

This is rearranged to give a form similar to a Hanes plot [94] for the analysis of Michaelis-Menten kinetics:

$$s_\infty/j = 1/k'_{ME} \{ 1+ (s_\infty/ K_{ME})(1- j/k'_s\, s_\infty)\} \qquad (3.12)$$

where $$1/k'_{ME} = K_M/Lk_{cat}e_\Sigma + 1/k'_s \qquad (3.13)$$

and $$K_{ME} = [\, K_M/Lk_{cat} + e_\Sigma/k'_s \,] \;/\; [\, 1/Lk_{cat} + 1/k' \,] \quad . \qquad (3.14)$$

k'_{ME} is the effective electrochemical rate constant for the enzyme electrode at low substrate concentrations. Depending on which term in eqn. (3.13) is larger, the effective electrochemical rate constant will be determined either by the transport of substrate through the membrane (the k'_s term) or the enzyme kinetics (the $Lk_{cat}e_\Sigma / K_M$ term).

K_{ME} is the equivalent of the Michaelis constant for an enzyme electrode. Thus at concentrations of substrate below K_{ME} , the enzyme electrode is unsaturated, and the response of the electrode is governed by k'_{ME} and is proportional to the concentration of substrate. At concentrations greater than K_{ME} , the electrode becomes saturated and the response of the electrode is governed by $k'_{cat,E}$, the electrochemical equivalent of k_{cat} in Michaelis-Menten kinetics.

$k'_{cat,E}$ is obtained from eqn. (3.11), putting $j/k'_s\, s_\infty$ and $1/s_\infty$ equal to zero since at saturation, s_∞ is very large:

$$1/k'_{cat,E} = 1/Lk_{cat} + 1/k' = e_\Sigma / j_{max} \quad . \qquad (3.15)$$

Thus the saturated electrode response will be determined by the saturated enzyme kinetics, given by Lk_{cat} , or by the electrode rate constant, given by k'.

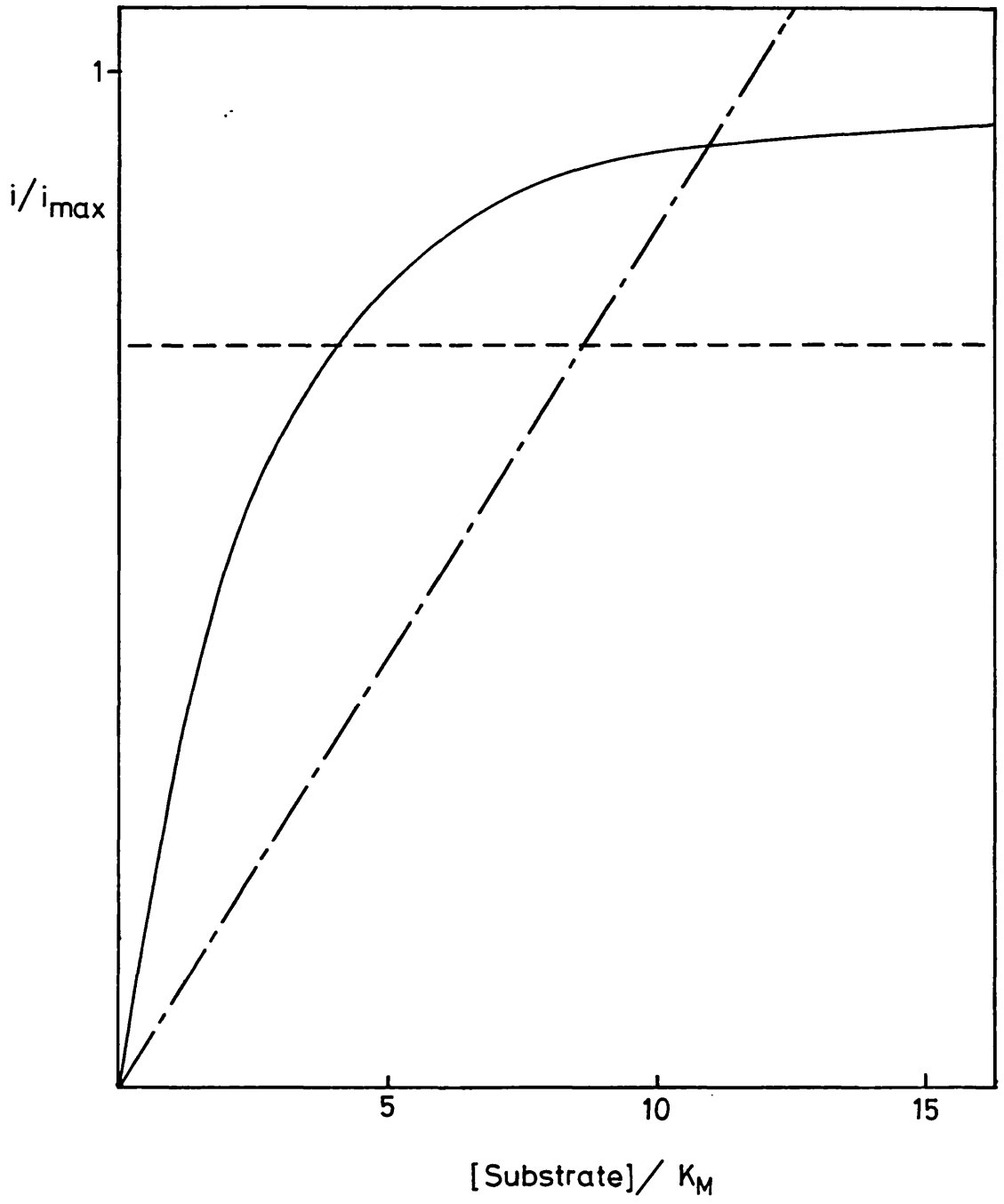
From eqn.s (3.13) - (3.15) , it is found that:

$$k'_{cat,E} = K_{ME}\, k'_{ME} / e_{\Sigma} \quad . \qquad (3.16)$$

Thus $k'_{cat,E}$ can be calculated from eqn. (3.16), and also from eqn. (3.15) using $k'_{cat,E} = j_{max} / e_{\Sigma}$. Both methods should give the same answer. The saturated enzyme rate constant, Lk_{cat} , can also be calculated, assuming a value of L of $\approx 10\mu m$. Comparison of the values obtained for $k'_{cat,E}$ and Lk_{cat} allows determination of the rate controlling process for the saturated electrode kinetics.

3.2.3 Application of the analysis

The response of a membrane electrode is limited by one of three possible kinetic steps: the diffusion of substrate through the membrane, the enzyme kinetics and the rate of oxidation of E' at the electrode. The rates for the first two processes are dependent on the substrate concentration. The interplay of the three steps is shown in fig(3.2). The slowest step will be rate determining. The rates for the various processes can be varied by altering the experimental conditions i.e. increasing the thickness of the membrane will decrease the membrane transport rate constant, increasing the concentration of enzyme behind the membrane will increase the enzyme rate constant and increasing the potential of the electrode will increase the electrode rate constant. Using the steady state theory for the membrane electrode, the rate controlling process for both the unsaturated and the saturated membrane electrode can be identified and the electrode response optimized.



Fig(3.2) Theoretical plots of current vs. [substrate] when the electrode response is controlled by the rate of substrate diffusion through the membrane (— • —), the enzyme kinetics (——) and the electrode kinetics (— — —) respectively.

Typical responses for a membrane electrode are shown in fig(3.3.a) for different values of k'_{ME}/k'_s. This ratio can vary from 1 to 0 and corresponds to total membrane control to total enzyme kinetics control respectively of the unsaturated electrode response (this is seen from eqn. (3.13)). Intermediate values of k'_{ME}/k'_s indicates that the membrane and enzyme rate constants are of a similar size and so each contributes significantly to the unsaturated electrode response.

In the first stage of the analysis, a Hanes plot of s_∞/j vs. s_∞ is made according to eqn. (3.12). The limiting value of $[\ s_\infty/j\ ]_0$ as $s_\infty \rightarrow 0$ gives $1/k'_{ME}$. If membrane kinetics are rate limiting, then $j \approx k'_s\ s_\infty$, so that eqn. (3.12) simplifies to:

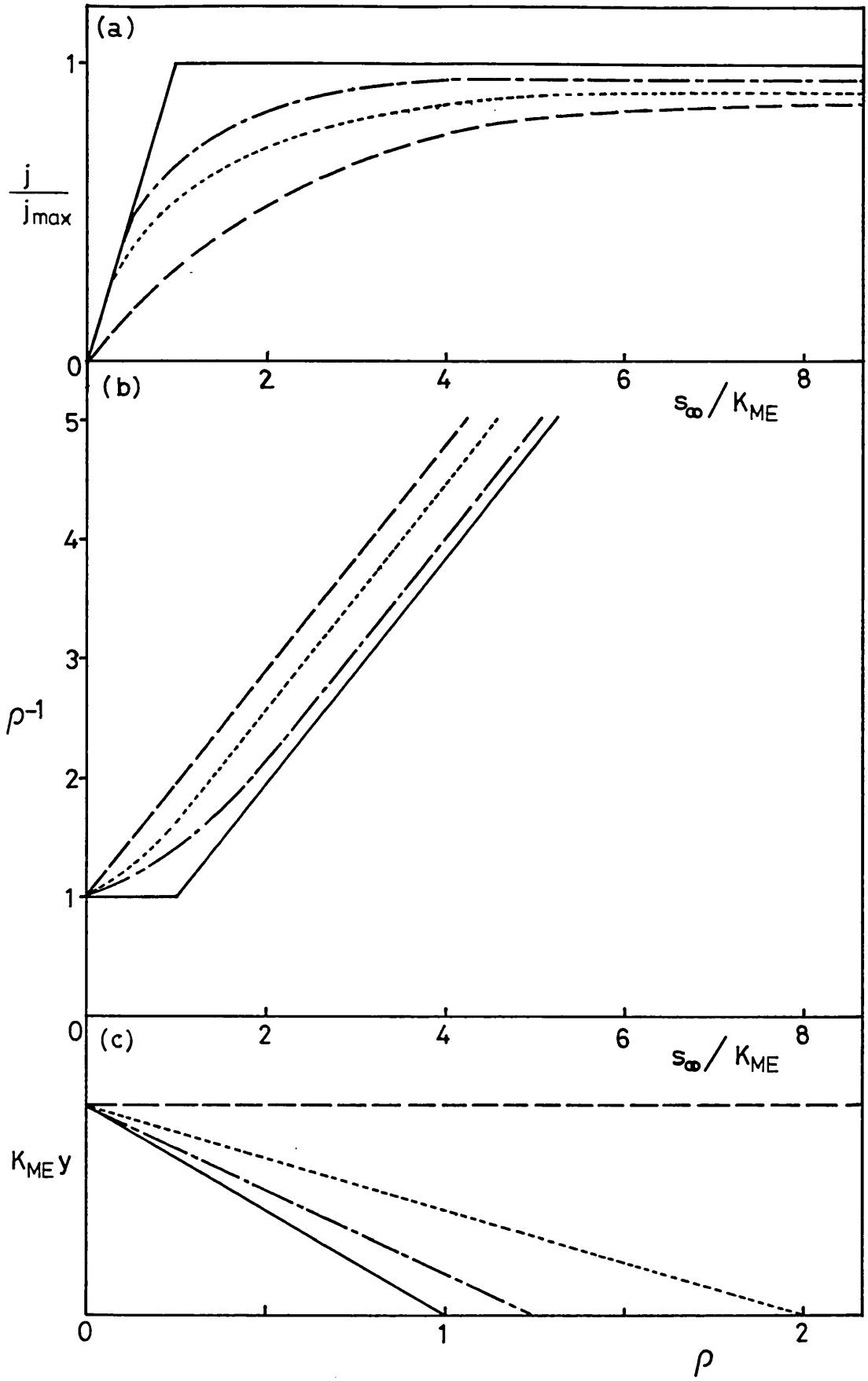
$$s_\infty/j = 1/k'_{ME} \ . \qquad (3.17)$$

Thus the gradient of the line obtained is zero, and the intercept on the s_∞/j axis is $1/k'_{ME}$. If enzyme or electrode kinetics are rate limiting, $j << k'_s\ s_\infty$, so that eqn. (3.12) simplifies to:

$$s_\infty/j = 1/k'_{ME}\ \{\ 1 + s_\infty/K_{ME}\ \} \ . \qquad (3.18)$$

A straight line of positive gradient is obtained, and the intercept on the s_∞/j axis is given by$1/k'_{ME}$.

In practice, for the unsaturated electrode, both membrane kinetics and either enzyme or electrode kinetics may be observed on increasing s_∞. Ideally, the switch over between the two processes will be clearly observed, resulting in the plot changing from a line of zero gradient to one of gradient $1/k'_{ME}K_{ME}$. This is shown in



Fig(3.3) (a) Typical plots of flux vs. substrate concentration for different values of k'_{ME}/ k'_S for the case where there is no product inhibition. Plots (b) and (c) show the corresponding Hanes and ρ-plots. The values of k'_{ME} are as follows:

—— 1.0; — • — 0.8; ····· 0.5; — — — 0.0.

fig(3.3.b) as a solid line. However if the switch over is not clean, then a curve may result, also shown in fig(3.3.b).

In the next stage of the analysis, a ρ-plot is made for values of s_∞/j significantly greater than $[\ s_\infty/j\ ]_0$. Values of ρ are calculated, where:

$$\rho = [\ j/s_\infty\ ] / [\ j/s_\infty\ ]_0 < 1 \ . \qquad (3.19)$$

Substitution in eqn. (3.12) gives:

$$y = (\rho^{-1} - 1)/\ s_\infty = 1/K_{ME}\ [\ 1 - \rho\ k'_{ME}/k'_s\ ] \ . \qquad (3.20)$$

The intercept on the y-axis is $1/K_{ME}$ and so K_{ME} can be calculated. The intercept on the ρ-axis gives $\rho_0 = k'_s/k'_{ME}$. If $\rho_0 = 1$, then $k'_{ME} = k'_s$ i.e. at low substrate concentrations, transport through the membrane is rate limiting. If $\rho_0 > 1$, then enzyme kinetics are comparable to membrane kinetics and each contributes to k'_{ME} , as seen from eqn. (3.13). If y is independent of ρ and constant, then $k'_{ME} << k'_s$, and k'_{ME} is determined by enzyme kinetics only. Thus the ρ-plot is a diagnostic tool that can be used to discover the rate limiting process at low substrate concentrations. Possible cases for the ρ-plot are shown in fig(3.3.c).

The values of ρ_0 and K_{ME} calculated from the ρ-plot allows the rate limiting step of both the unsaturated and saturated electrode, provided K_M for the enzyme is known. In table 3.1, a summary is made of the possible cases for different values of ρ_0 and K_{ME} . These give information about the unsaturated and the saturated electrode kinetics respectively. Note that for $K_{ME} > K_M$ to occur, the only

	$K_{ME} < K_M$	$K_{ME} = K_M$	$K_{ME} > K_M$	Electrode response
$\rho_o = 1$	Transport	Transport	Transport	Unsaturated
	Electrode	Electrode or enzyme	Electrode or enzyme	Saturated
$\rho_o = \infty$	Enzyme	Enzyme	Enzyme	Unsaturated
	Electrode	Electrode	?????	Saturated

Table 3.1 Summary of the mechanistic deductions from K_{ME} and ρ.

possible explanation is that the linear range of the electrode has been extended by the membrane. This is possible if $\rho_0 = 1$, since the unsaturated electrode kinetics are governed by the membrane kinetics, while the saturated electrode kinetics are governed either by the saturated enzyme kinetics or the electrode kinetics. However if $\rho_0 = \infty$, this indicates that enzyme control occurs in the unsaturated region and is in direct contradiction with $K_{ME} > K_M$. Thus this situation is physically impossible.

3.2.4 Product inhibition

Let us now return to the case where product inhibition is important. The Hanes plot can be derived as before from eqn. (3.8) by assuming $j/ k'_P \rightarrow 0$ as $s_\infty \rightarrow 0$. Eqn. (3.8) then reduces to the familiar form for the Hanes plot of eqn. (3.12), allowing $[j/s_\infty]_0$ to be found from the plot as before.

To obtain a ρ-plot for product inhibition, we assume firstly that transport of s through the membrane is not rate limiting, and hence ignore all terms in k'_s in eqn. (3.8) . Secondly we assume that p_∞ is negligible and that it escapes easily into the bulk solution by passing through the membrane.

Then eqn. (3.8) reduces to:

$$e_\Sigma/j = 1/Lk_{cat} + 1/k' + [K_3^{-1}(1 + K_2^{-1})/k'] (j/k'_P) + K_M/Lk_{cat}s_\infty + [K_{TD}^{-1}/s_\infty k'] (j/k'_P) . \qquad (3.21)$$

This can be rearranged to give:

$$y = 1/K_{ME} + \rho Q + QK_1(1 + K_2)(1- \rho)/y \qquad (3.22)$$

where

$$Q = k'^{2}_{ME} / k' k'_P K_{TD} e_\Sigma \ . \qquad (3.23)$$

The relative sizes of the three terms in eqn. (3.22) give different cases of product inhibition. Suppose we rewrite eqn. (3.22) as:

$$K_{ME}y = 1 + K_{ME} \rho Q + K_{ME} Q K_1(1 + K_2)(1- \rho)/y \ . \qquad (3.24)$$

Then the sizes of $K_{ME} Q$ and $K_{ME} Q K_1(1 + K_2)$ relative to unity will determine the different solutions for $K_{ME}y$.

Fig(3.4) shows the different cases. If $K_{ME} Q$ and $K_{ME} Q K_1(1 + K_2)$ are less than unity, then eqn. (3.24) reduces to $K_{ME}y \approx 1$; this is shown in the bottom left hand quadrant of the diagram. This case is the same as that given in eqn. (3.20) where $k'_{ME} << k'_s$, and implies no product inhibition is occuring; the kinetics are those of the saturated enzyme.

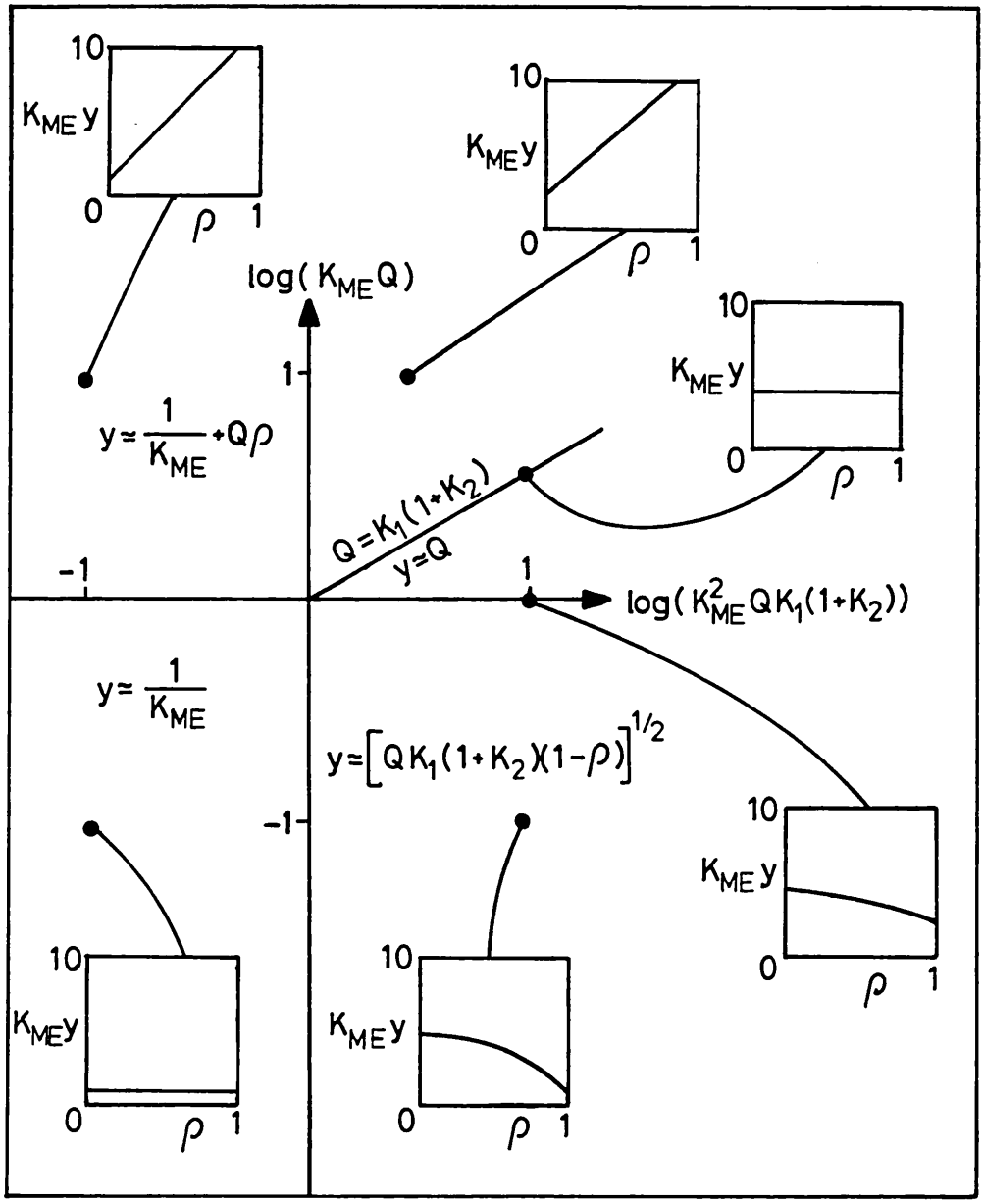
The remaining cases all describe some form of product inhibition. If $K_{ME} Q >> 1$ and $K_{ME} Q K_1(1 + K_2) << 1$, then eqn. (3.24) reduces to:

$$K_{ME}y \approx 1 + K_{ME} \rho Q \ .$$

This is shown in the top left hand quadrant of fig(3.4). A plot of y vs. ρ is linear, with positive gradient, and the most stable form of the enzyme is free enzyme.

If $K_{ME} Q << 1$ and $K_{ME} Q K_1(1 + K_2) >> 1$, then eqn. (3.24) reduces to:

$$y \approx [Q K_1(1 + K_2)(1- \rho)]^{1/2} \ .$$



Fig(3.4) Case diagram for product inhibition. Inset are shown the diagnostic plots for y vs. ρ.

This is in the bottom right hand quadrant of fig(3.4). A plot of y vs. ρ will be curved with negative gradient, and may appear to be quite similar to the case given in eqn. (3.20) for no product inhibition. However a plot of y^2 vs. ρ should be linear and thus the two cases can be distinguished. Note that in this case the most stable form of the enzyme is either ES or E'P.

In the case where $K_{ME}\, Q >> 1$ and $K_{ME}\, Q\, K_1(1 + K_2) >> 1$, the most complicated kinetics arise. This occurs in the top right hand quadrant of fig(3.4). A further case occurs in this quadrant when $Q = K_1(1 + K_2)$; eqn. (3.24) simplifies to $y \approx Q$ and a plot similar to that in the bottom left hand quadrant is obtained. However in the $y \approx Q$ case there is a dependence on e_Σ and experiments at different e_Σ will allow the two cases to be distinguished.

3.2.5 Effect of half order dependence on e' by the electrode flux

In the above theory (sections 3.2.1 -3.2.4) it has been assumed that the flux of E' turning over at the electrode has first order dependence on e' ; this is given by eqn. (3.6). However it is noted in section 4.2 that half order dependence on e_Σ has been observed by P.N. Bartlett. This is also observed for experiments involving glucose oxidase with a rotating disc electrode, reported in section 4.5.2 of this thesis. Thus the effect of half order dependence must be considered for the membrane electrode theory.

The electrode flux is now given by:

$$j = k' (e')^{1/2} \quad . \tag{3.25}$$

This replaces eqn. (3.6) in the previous analysis (section 3.2.1). Following the method given before, we obtain:

$$e_\Sigma /j = \{1- j/k'_s\, s_\infty\}\{1/Lk_{cat} + j/(k')^2 + j\, K_3^{-1}(1+K_2^{-1})/(k')^2 [\, p_\infty + j/k'_P \,]\}$$

$$+1/s_\infty \{\, K_M/Lk_{cat} + j\, K_1^{-1}K_2^{-1}K_3^{-1}/(k')^2 [\, p_\infty + j/k'_P \,]\} + e_\Sigma /k'_s\, s_\infty \quad . \tag{3.26}$$

This equation should be compared with eqn. (3.8). Assuming there is no product inhibition, eqn. (3.26) becomes:

$$s_\infty/j = 1/k'_{ME} \{\, 1+ k'_{ME}\, s_\infty [\, 1/Lk_{cat}e_\Sigma + j / (k')^2 e_\Sigma \,](1- j/k'_s\, s_\infty)\}. \tag{3.27}$$

Now if membrane control is occuring, i.e. $j \approx k'_s\, s_\infty$, eqn. (3.27) becomes:

$$s_\infty/j \approx 1/k'_{ME} \quad .$$

This is the same expression obtained before (eqn. (3.17)). If the unsaturated enzyme kinetics are rate controlling, i.e. $j << k'_s\, s_\infty$, eqn. (3.27) becomes:

$$s_\infty/j \approx 1/k'_{ME} \{\, 1+ k'_{ME}\, s_\infty [\, 1/Lk_{cat}e_\Sigma + j/(k')^2 e_\Sigma \,] \quad .$$

Now when $s_\infty \longrightarrow 0$, $s_\infty/j \approx 1/k'_{ME}$ as before. However plotting s_∞/j vs. s_∞ will no longer give a straight line because of the extra term in j compared to eqn. (3.18). Thus for the Hanes plot, the same analysis applies for finding $1/k'_{ME}$ from the intercept on the s_∞/j axis regardless of whether the electrode flux depends on e' or $(e')^{1/2}$.

Now we must consider the effect of $(e')^{1/2}$ dependence on the ρ-plot. Rearranging eqn. (3.27) into the form of the ρ-plot gives:

$$y = (\rho^{-1} -1)/s_\infty = k'_{ME} [\ 1/Lk_{cat}e_\Sigma + j/(k')^2e_\Sigma] [\ 1 - \rho \ k'_{ME}/k'_s \ ]. \quad (3.28)$$

The first bracket on the right hand side of eqn. (3.28) can be rewritten as:

$$1/j_{max} = 1/Lk_{cat}e_\Sigma + j_{max}/(k')^2e_\Sigma \quad (3.29)$$

where j_{max} has replaced j in the term for the electrode kinetics since we are concerned with the saturated electrode response. $Lk_{cat}e_\Sigma$ describes the saturated enzyme kinetics as before. $j_{max}/(k')^2e_\Sigma$ describes the electrode kinetics. If the electrode kinetics are rate controlling, then $Lk_{cat}e_\Sigma >> k' (e')^{1/2}$ and eqn. (3.25) becomes $j_{max} \approx k' (e')^{1/2}$. Also from eqn. (3.29), $j_{max} \approx k' (e_\Sigma)^{1/2}$. Thus $e' \approx e_\Sigma$ i.e. the reduced form of the enzyme is predominant. Eqn. (3.28) can be rewritten as:

$$y = 1/K'_{ME} [\ 1 - \rho \ k'_{ME}/k'_s \ ] \quad (3.30)$$

where

$$K'_{ME} = [\ K_M/Lk_{cat}e_\Sigma + 1/k'_s \ ] / [\ 1/Lk_{cat}e_\Sigma + 1/k'(e_\Sigma)^{1/2} \ ] . \quad (3.31)$$

K'_{ME} is the equivalent of K_{ME} for the electrode flux having half order dependence on e' . Plotting y vs. ρ will give a straight line as before, with $\rho_o = k'_s / k'_{ME}$ and the intercept on the y axis given by $1/K'_{ME}$.

Thus in conclusion, the Hanes plot and the ρ-plot analyses are identical regardless of whether the electrode rate constant has first order or half order dependence on e'. Minor differences occur in the shape of the Hanes plot if unsaturated enzyme kinetics are rate controlling, and in the ρ-plot, the value of the y-intercept is no longer $1/K_{ME}$ but $1/K'_{ME}$.

The effect of $(e')^{1/2}$ dependence must also must also be considered for product inhibition. Terms in k' become $j/(k')^2 e_\Sigma = 1/ k'(e_\Sigma)^{1/2}$ as above, since the ρ-plot is applied to the saturated electrode response. Then eqn. (3.22) is obtained as before except K_{ME} becomes K'_{ME} and Q becomes Q' where $Q' = Q/(e_\Sigma)^{1/2}$. The plots for the different cases of product inhibition apply as before. Thus it is concluded that the half order dependence on e' by the electrode flux does not alter the membrane electrode analysis.

3.3 Experimental

Membrane electrodes were prepared as described in Chapter 2, and the experimental procedure described therein was followed.

The experimental conditions for each enzyme are given in table 3.2. In addition, pyruvate oxidase experiments were carried out with 500 μM thiamin pyrophosphate (TPP) in the bulk solution, and oxalate oxidase experiments were carried out with 4 μM FMN in the

Enzyme	Substrate molarity in M	Membrane	Electrode binder	Electrode material	Enzyme solution in u/ml
Sarcosine oxidase	0.1	spec 2	PVC	TTF TCNQ	215
	0.1	spec 2	PVC	NMP TCNQ	444
Glycolate oxidase	0.1	spec 4	PVC	TTF TCNQ	22.1
	0.1	spec 4	PVC	NMP TCNQ	23.4
Lactate Oxidase	1.0	spec 4	Si oil	TTF TCNQ	220
	1.0	spec 4	Si oil	NMP TCNQ	236
Pyruvate oxidase	1.0	spec 4	Si oil	TTF TCNQ	231
	1.0	spec 4	Si oil	NMP TCNQ	237
Oxalate Oxidase	0.1	spec 2	Si oil	NMP TCNQ	2.5
Bilirubin oxidase	8.5×10^{-3}	/	PVC	TTF TCNQ	3910

Table 3.2 Experimental conditions

Enzyme	K_M / mM	k_{cat} / s^{-1}	optimum pH	molecular weight / g
Sarcosine oxidase	3.4 mM sarcosine[a]	5.8[a]	7.7 [95] in KH_2PO_4	174,000 [96]
Glycolate oxidase	0.38 mM glycollic acid[b]	35[b,c]	8.3 [97] in glycine	296,000 [98]
Lactate oxidase	17 mM L-lactic acid[d]	27[d,e]	5.6 - 6.0 [101]	260,000 [99]
Pyruvate oxidase	10 mM sodium pyruvate[f]	9000[f]	5.8 [102]	265,000 [102]
Oxalate oxidase	0.42 mM sodium oxalate[g]	—	3.5 in succinate [103]	150,000 [104]
Bilirubin oxidase	50 μM[h] or 190 μM[i]	—	8.0 [106]	52,000 [106]

Table 3.3 Physical data for the enzymes

a) at pH 8.3 and 37°C [95].
b) at pH 8.0 and 25°C [97].
c) 720 moles glycolic acid per min per 100,000g of enzyme [97]
d) at pH 7.0 and 37°C [99].
e) 470 moles lactate per mole enzyme per min in O_2 , assuming M_r = 75,000 [100]
f) at pH 6.0 and 31°C [102].
g) at pH 3.5 and 22°C [103].
h) at pH 7.4 and 37°C [105]
i) at pH 8.4 and 37°C [120]

bulk solution. Physical data, where known, for each enzyme, are given in table 3.3.

All substrates were tested for electroactivity. With the exception of bilirubin, none were found to be electroactive.

Bilirubin solutions were prepared by placing bilirubin (4.4 mg, 7.5 $x10^{-6}$ mol) in 1 ml buffer, then adding 0.1 ml of 2 M NaOH to dissolve. Fresh bilirubin solutions were bright orange. After ≈ 24 hours, the solution was pale yellow/ green, characteristic of biliverdin. The presence of biliverdin was confirmed by UV/ VIS spectroscopy at 440 nm (ε = 6,400 $M^{-1}cm^{-1}$ [107]), (ε, bilirubin = 50,000 $M^{-1}cm^{-1}$ [107]).

3.4 Membrane electrode results

A short description of each enzyme is given before the results are presented and analysed according to the membrane electrode theory.

3.4.1.1 Sarcosine oxidase

Sarcosine oxidase (EC 1.5.3.1) catalyses the oxidative demethylation of sarcosine:

$$\text{sarcosine} + H_2O + O_2 \longrightarrow \text{glycine} + H_2O_2 + HCHO\,.$$

The enzyme also reacts with N-methyl-l-alanine and N-ethyl-glycine, but no other N-methyl amino acids [95]. It should be noted that formaldehyde, a product of the reaction, inhibits the enzyme activity by approximately 50% at 20 mM [95].

The cofactor for the enzyme is FAD. There are two molecules of FAD per molecule of enzyme, one of which is covalently bound, while the other one is non-covalently bound: this distinguishes sarcosine oxidase from all other known flavoenzymes [95].

The non-covalently bound FAD can be released quite easily by heat, treatment with 10% trichloroacetic acid or with 80% ammonium sulphate (at pH 4.0) [96]. The loss of the non-covalently bound flavin causes practically no alteration in the polypeptide backbone structure, but there is a complete loss of enzyme activity. This could be due to a localized modification in the flavin-binding region [96]; else it could be that the non-covalently bound FAD is responsible for the demethylation of sarcosine, while the covalently bound FAD is responsible for the electron transfer, resulting in the reduction of both FAD moieties [108].

The measurement of sarcosine is not clinically important at present. There is a disorder called sarcosinemia, which is caused by a defect in sarcosine dehydrogenase activity in liver and kidney. A person suffering from this disorder is characterised by abnormal increases in blood and urine sarcosine and mild mental retardation. Thus it is envisaged that a quick direct measure of sarcosine could be useful in a study of sarcosinemia.

More important could be the use of sarcosine in a multiple enzymatic determination of creatine and/or creatinine. Both creatine and creatinine are routinely determined clinically. The enzyme creatininase converts creatinine to creatine, while the enzyme creatinase converts creatine to sarcosine. Thus a multiple enzyme system coupled with a conducting organic salt electrode should allow creatinine and/or creatine to be determined directly. Conventional

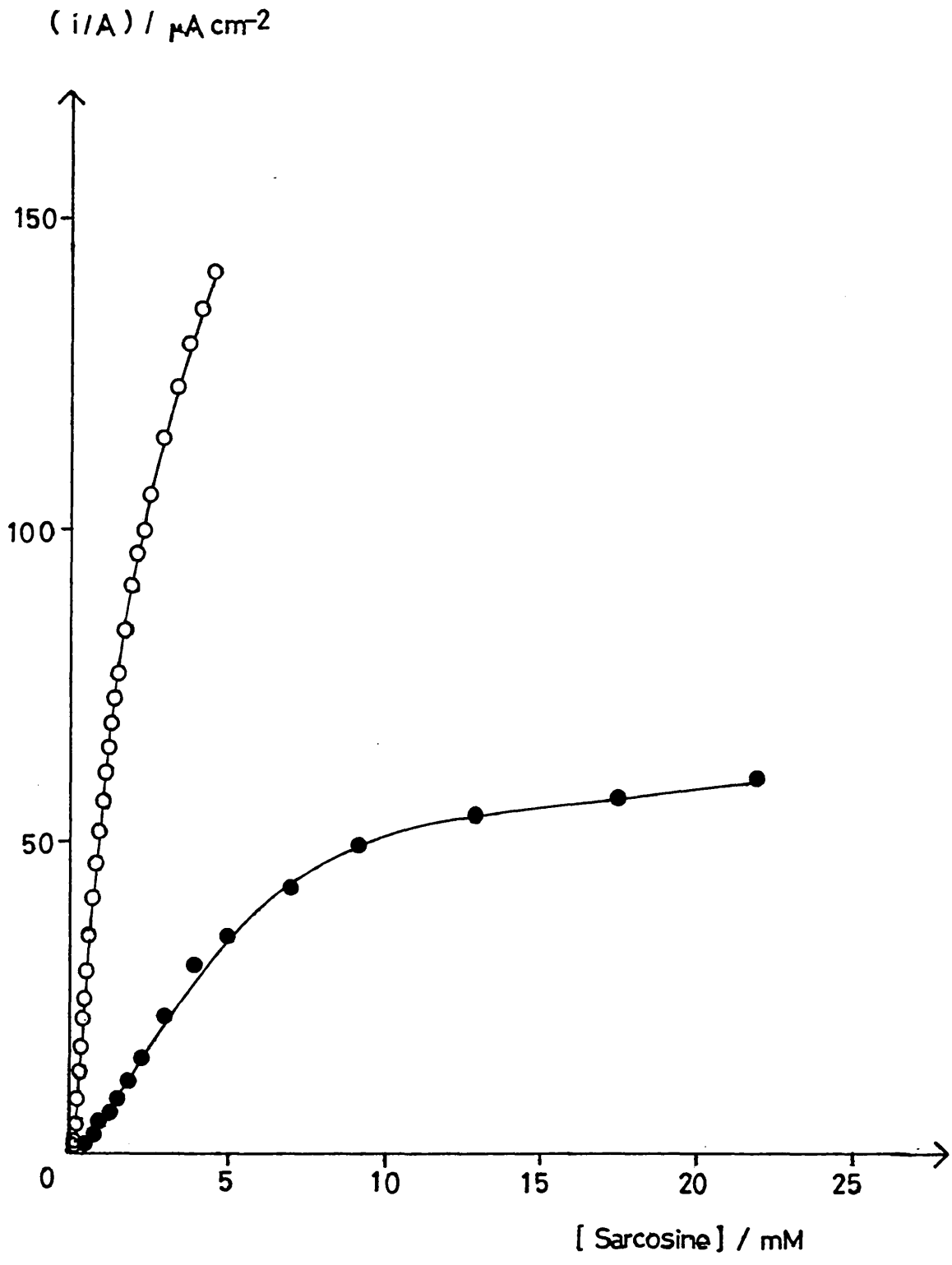
analyses of creatine and creatinine involve many-step chemical processes, the most famous of which is the Jaffé reaction and modifications thereof [109]. However it is not specific for creatine and creatinine, does not allow direct measurement of creatine and requires large quantites of serum.

High serum creatine levels are observed during fasting and in certain muscular diseases such as muscular dystrophy. Industrial applications for the measurement of creatine occur in the meat industry. The level of creatine in slaughtered animals appears to be directly proportional to the muscle protein content, thus giving an indication of meat quality [110]. Creatinine is a byproduct of the degradation of phosphocreatine; kidney malfunction results in increased levels in serum and decreased levels in urine.

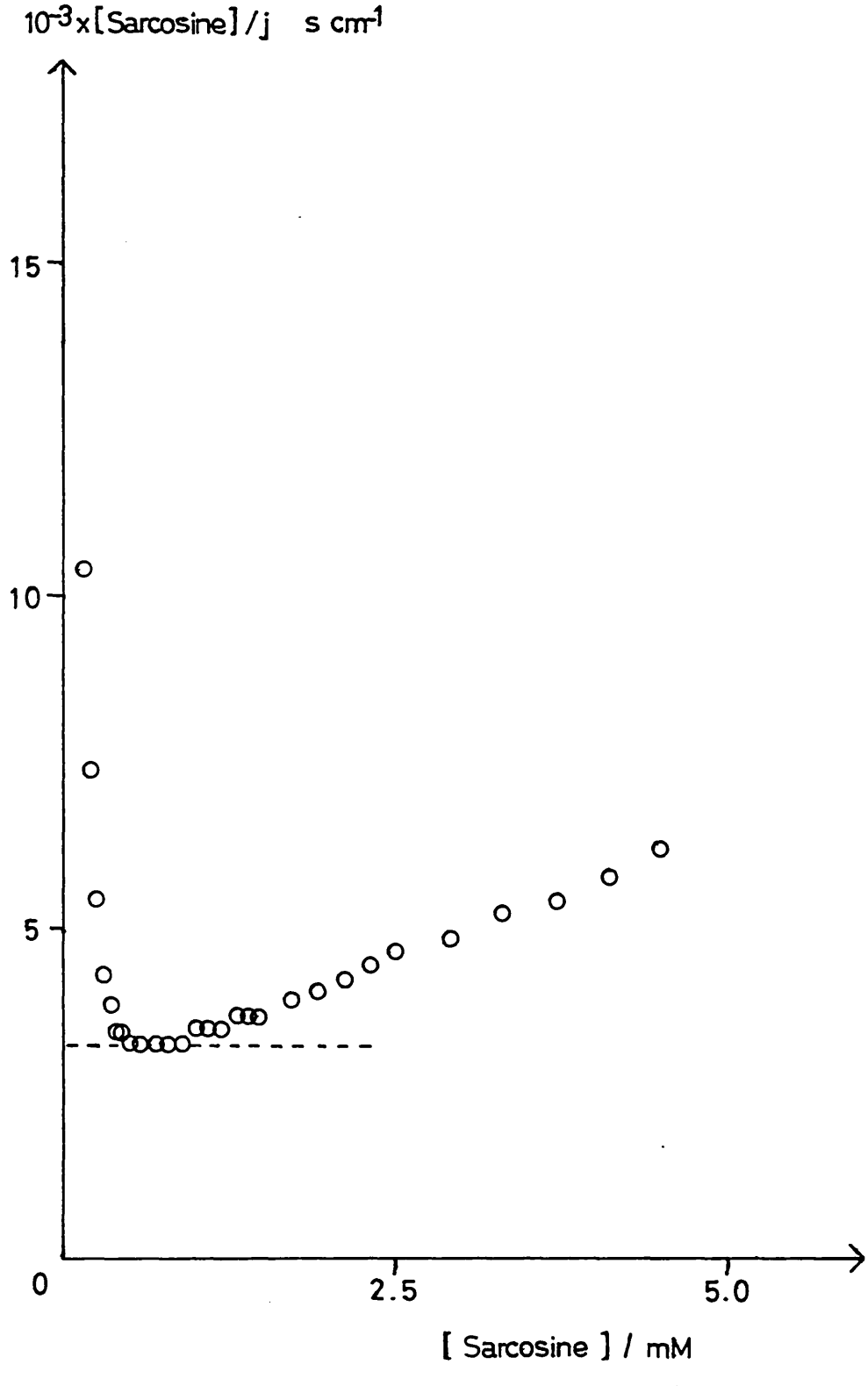
3.4.1.2 Sarcosine oxidase results

The responses of sarcosine oxidase membrane electrodes to successive injections of sarcosine are shown in fig(3.5.1). At low substrate concentrations there is an apparent loss of response, in particular for the NMP TCNQ electrode. This is thought due to a small amount of oxygen in the bulk solution preferentially oxidizing reduced enzyme until it is depleted. This effect is commonly seen with conducting organic salt electrodes and is discussed below in section 3.5.1.

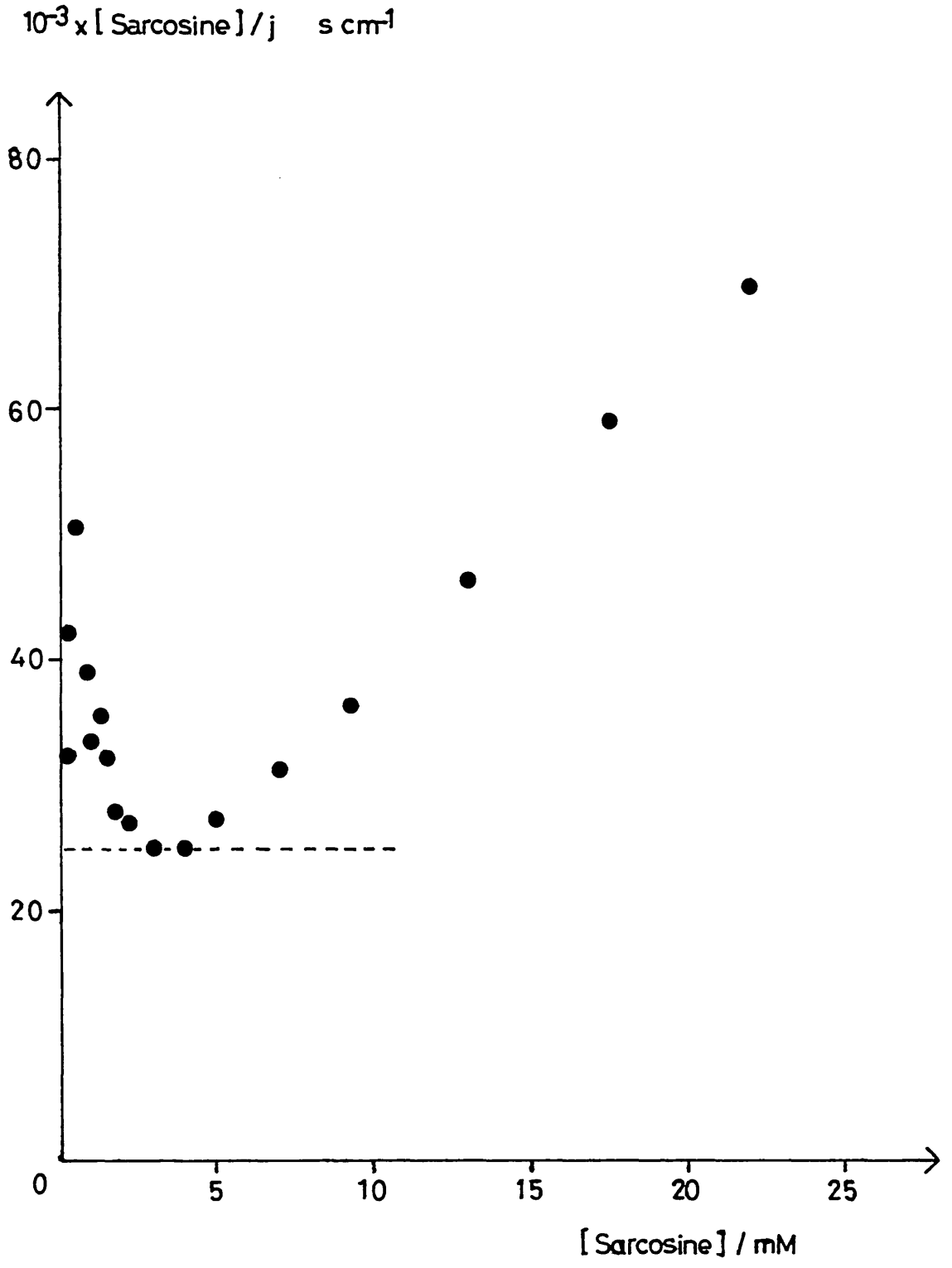
The data are analysed according to the Hanes plot (eqn. (3.12)) and presented in figs(3.5.2.a) and (3.5.2.b). Both electrodes exhibit a plateau at low concentrations of substrate, which is characteristic of membrane control. The intercept at low substrate concentration is



Fig(3.5.1) Sarcosine oxidase membrane electrode response profiles: • denotes TTF TCNQ and o denotes NMP TCNQ.



Fig(3.5.2.a) The Hanes plot for a sarcosine oxidase membrane electrode with NMP TCNQ as the electrode material. Note that the first point is not shown.



Fig(3.5.2.b) The Hanes plot for a sarcosine oxidase membrane electrode with TTF TCNQ as the electrode material.

used to calculate the electrochemical rate constant, k'_{ME} , for the unsaturated electrode.

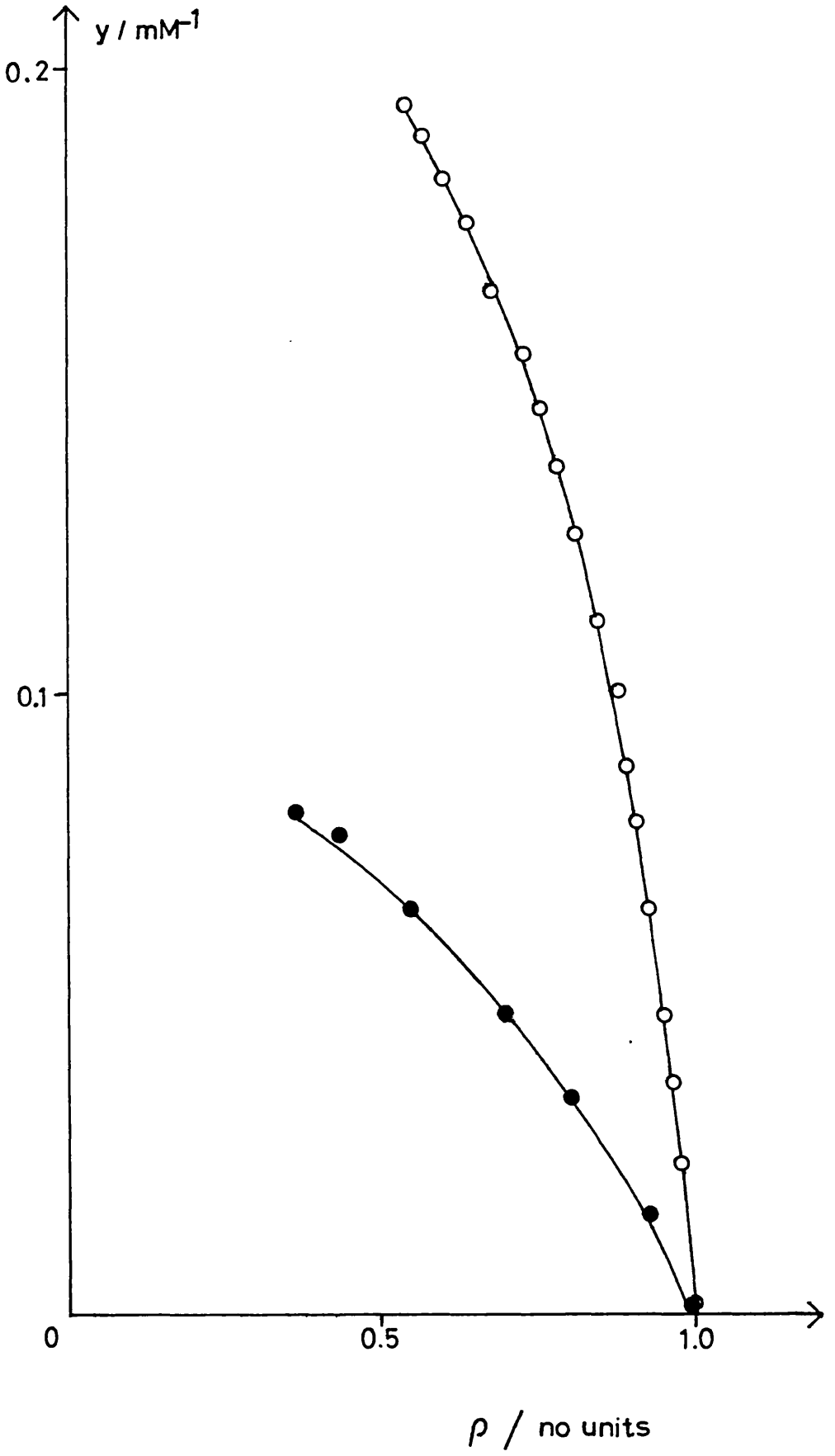
From eqn. (3.13), it is seen that the relative sizes of the unsaturated enzyme rate constant and the membrane rate constant will determine k'_{ME} . The experimentally determined values of k'_{ME} and the calculated values of $Lk_{cat}e_{\Sigma}/ K_M$ and k'_S are given in table 3.4. k'_S is calculated assuming a value of K_S equal to unity (since the molecular weight cutoff of the membrane is much greater than the molecular weight of the diffusing species) and L_M as twice the dry thickness of the membrane [111]. The actual value D_S has not been determined for the substrates used in this thesis, but it has been determined for glucose to be 10^{-6} $cm^2 s^{-1}$ [112], and will be assumed to be the same for these calculations. L, the thickness of the electrolyte layer, is assumed to be $\approx$ 10 μm. This has been confirmed experimentally [79].

On inspection of table 3.4 it is observed that $Lk_{cat}e_{\Sigma}/ K_M$ is greater than k'_S by approximately one order of magnitude. This suggests membrane control of the unsaturated electrode kinetics. The difference between k'_{ME} and k'_S may be explained by the inaccuracy in assuming the D_S for sarcosine to be the same as for glucose.

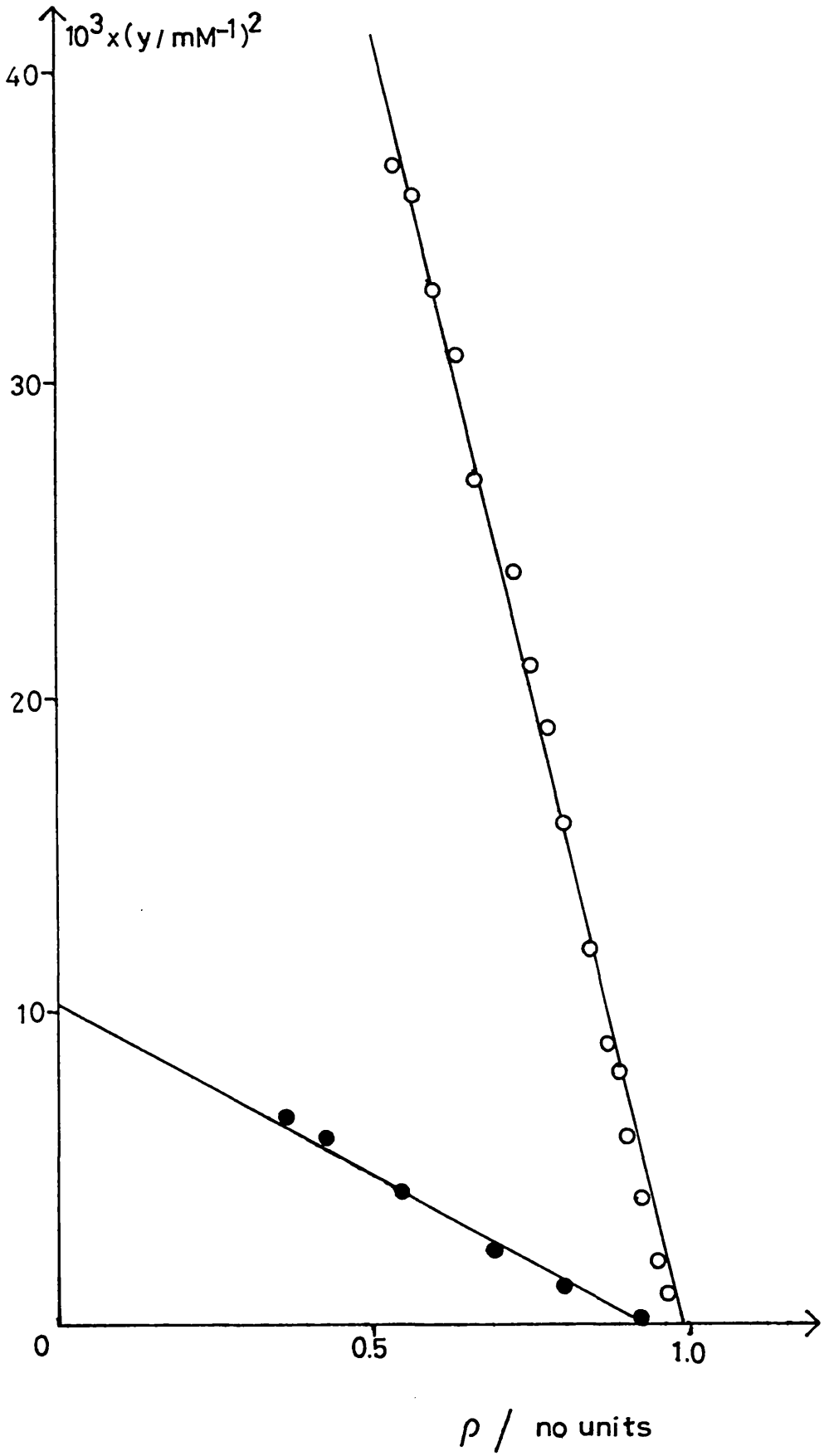
Using these values for k'_{ME} , ρ-plots are made in fig(3.5.3). These are clearly curved, passing through ρ=1 at y=0. This is characteristic of product inhibition caused by either ES or E'P being the most stable form of the enzyme. This case is given in the bottom right hand corner of the case diagram for product inhibition in fig(3.4). A plot of y^2 vs. ρ should be linear according to eqn. (3.25); these plots are shown in fig(3.5.4). It is satisfying to observe that the secondary plots are linear.

Electrode material	k_{ME}' /cm s^{-1}	$K_S D_S/L_M$ /cm s^{-1}	$e_\Sigma Lk_{cat}/K_M$ /cm s^{-1}	(j_{max}/e_Σ) /cm s^{-1}	Lk_{cat} /cm s^{-1}	K_{ME}' /mM
TTF TCNQ	4.0×10^{-5}	2.2×10^{-4}	1.3×10^{-3}	4.2×10^{-4}	5.8×10^{-3}	4.9
NMP TCNQ	3.0×10^{-4}	2.2×10^{-4}	2.7×10^{-3}	4.6×10^{-4}	5.8×10^{-3}	1.4

Table 3.4 Sarcosine oxidase kinetic data



Fig(3.5.3) The ρ-plot for sarcosine oxidase membrane electrodes: • denotes TTF TCNQ and o denotes NMP TCNQ.



Fig(3.5.4) Test for product inhibition: plots of y^2 vs. ρ for sarcosine oxidase membrane electrodes.
• denotes TTF TCNQ and o denotes NMP TCNQ.

It has been noted above in section 3.4.1.1 that formaldehyde, a product of the enzyme reaction, inhibits the enzyme. Thus it may be concluded that the reduced enzyme: formaldehyde complex is the most stable form of the enzyme. At low substrate concentrations, product inhibition is not observed since the rate controlling process is the diffusion of substrate through the membrane.

A value of $\rho_o = 1$ implies that $k'_{ME} = k'_S$ (seen from eqn. (3.20)) and so at low substrate concentrations, membrane control is observed, in agreement with the Hanes plot. K'_{ME} can be calculated by drawing a tangent to the curve at $\rho = 1$ and taking the point where it intercepts on the y-axis. The values for K'_{ME} are given in table 3.4, along with the values of j_{max}/ e_Σ and Lk_{cat}.

Comparison of the experimentally determined rate constant for the saturated electrode (j_{max}/ e_Σ) and the calculated rate constant for saturated enzyme kinetics (Lk_{cat}) allows the nature of the saturated electrode kinetics to be determined, as seen from eqn. (3.15). It is observed that Lk_{cat} is greater than j_{max}/ e_Σ and so it is concluded that the saturated electrode kinetics are determined by the electrode rate constant, k'. Also $K'_{ME} < K_M$ for the enzyme, which, on inspection of table 3.1, also implies the saturated electrode response is governed by the electrode rate constant.

3.4.2.1 Glycolate oxidase

Glycolate oxidase (EC 1.1.3.1) exists as two isozymic forms, which preferentially oxidize either short chain aliphatic hydroxy acids (form A) or long chain and aromatic hydroxy acids (form B). All experiments reported herein were carried out with form A of the

enzyme, which oxidizes glycolate to glyoxalate and L-lactate to pyruvate respectively:

$$\text{glycolate} + {}^{\cdot}O_2 \longrightarrow \text{glyoxalate} + H_2O_2 .$$

The enzyme is specific for glycolate and L-lactate, with L-lactate having half the turnover number of glycolate [97].

The prosthetic group of the enzyme is FMN. This enzyme is particularly interesting since its structure has been determined by x-ray crystallography [98,113]. This is the only known crystallographic structure of a flavoprotein. The enzyme consists of octamers of molecular weight 35,000 - 40,000, of diameter about 100 Å. The octamers are approximately spherical and pack together to give an enzyme molecule with a large central hole, of between 15 - 20 Å diameter. Each octamer has a barrel structure and the active site of the enzyme is at the end of the barrel.

It would be desirable to correlate kinetic data i.e. the ease of electron transfer between the enzyme and a conducting organic salt electrode, with the physical availability of the active site for a series of flavoenzymes. This could give information about the nature of the mechanism of electron transfer. Unfortunately this is not possible due to the lack of crystallographic data.

Glycolate is metabolised by plants during photorespiration [98] and so measurement of glycolate would be a useful monitor of their activity. For example, in the on-line fermentation of algae and cyanobacteria, millimolar concentrations of glycolate are excreted.

3.4.2.2 Glycolate oxidase results

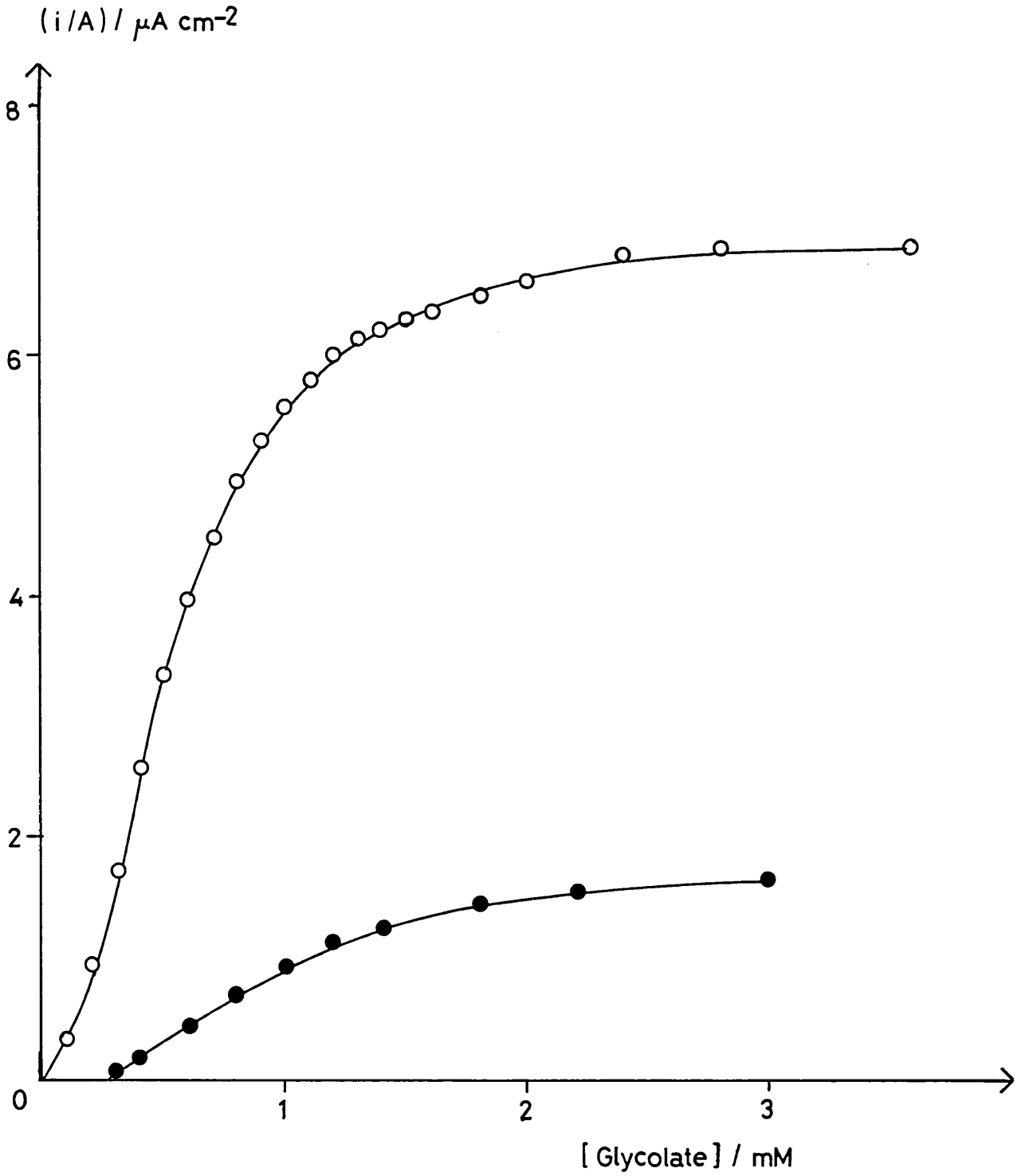
The responses of glycolate oxidase membrane electrodes to successive injections of glycollic acid are shown in fig(3.6.1). With TTF TCNQ, there is initially observed a drop in current, i.e. a reduction current, on injection of glycolate. This is most probably due to some oxygen present in the bulk solution being converted in the enzyme reaction to hydrogen peroxide, which may then be reduced at the electrode surface [114]. This suggests reduced enzyme is preferentially oxidized by oxygen rather than TTF TCNQ. The effect of oxygen is discussed more fully in section 3.5.1.

The data are analysed according to the Hanes plot and presented in fig(3.6.2). Both electrodes exhibit a plateau region at low concentrations, indicative of membrane control; the effect of oxygen is observed, distorting the initial points as for sarcosine oxidase.

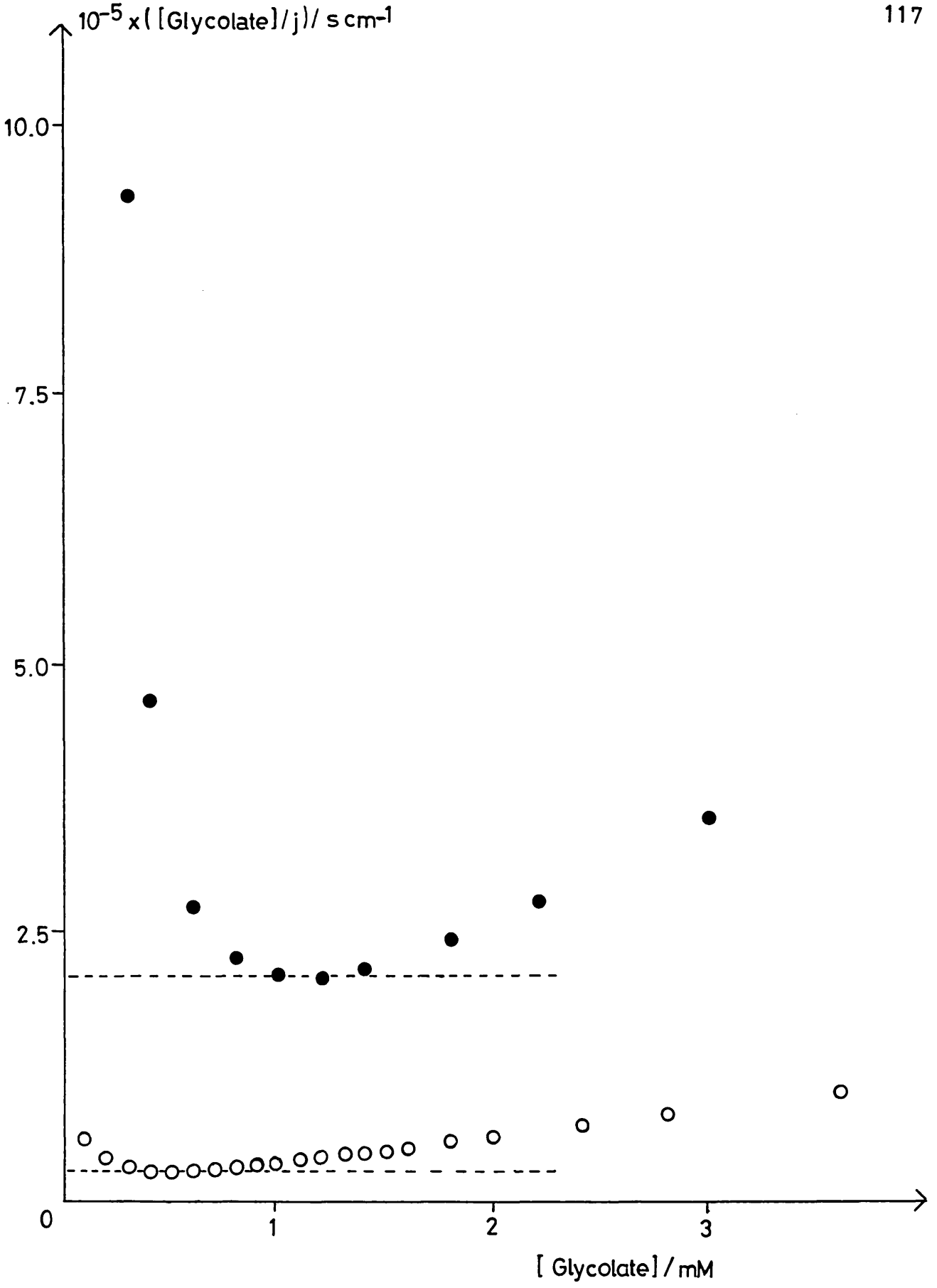
The k'_{ME} values are calculated, also $Lk_{cat}e_{\Sigma} / K_M$ and k'_S , and these are presented in table 3.5. The unsaturated enzyme rate constant as faster than the membrane rate constant, and so diffusion of substrate through the membrane is rate limiting at low substrate concentrations.

The ρ-plots are presented in fig(3.6.3). Both ρ-plots give $\rho_o = 1$, which is indicative of membrane control of the unsaturated electrode response. Comparison of j_{max}/e_{Σ} and Lk_{cat} , in table 3.5 , shows that j_{max}/e_{Σ} is approximately 100 times smaller than Lk_{cat} . Hence it is concluded that the saturated electrode response is determined by the electrode rate constant, k'.

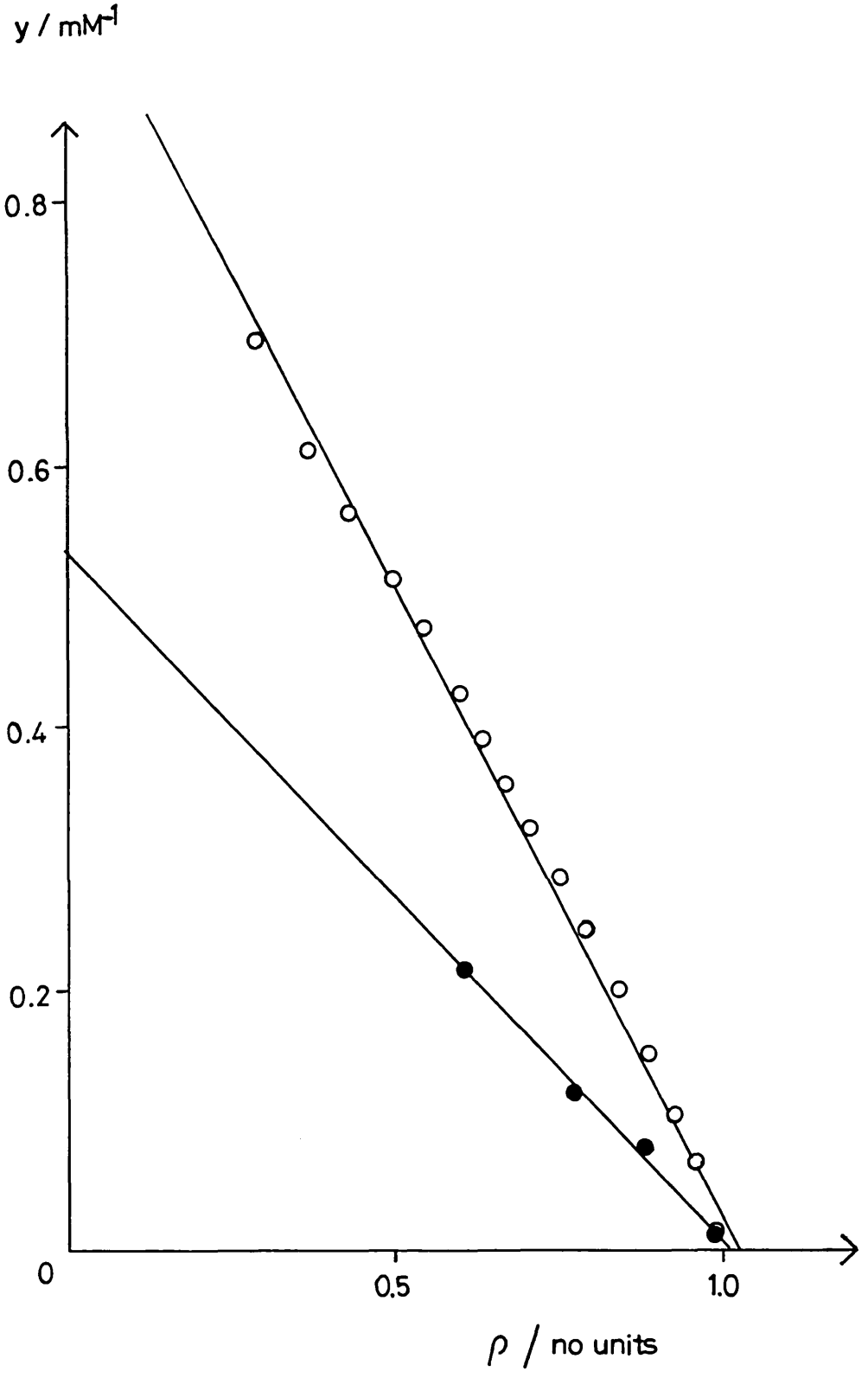
Values of K'_{ME} are given in table 3.5. It is satisfactory that these are larger than K_M for the enzyme of 0.38 mM, indicating that



Fig(3.6.1) Glycolate oxidase membrane electrodes response profiles: • denotes TTF TCNQ and o denotes NMP TCNQ.



Fig(3.6.2) The Hanes plots for glycolate oxidase membrane electrodes: • denotes TTF TCNQ and o denotes NMP TCNQ.



Fig(3.6.3) The ρ-plots for glycolate oxidase membrane electrodes: • denotes TTF TCNQ and o denotes NMP TCNQ.

Electrode material	k_{ME}' /cm s^{-1}	$K_S D_S/L_M$ /cm s^{-1}	$e_\Sigma Lk_{cat}/K_M$ /cm s^{-1}	(j_{max}/e_Σ) /cm s^{-1}	Lk_{cat} /cm s^{-1}	K_{ME}' /mM
TTF TCNQ	4.7 $x10^{-6}$	2.0 $x10^{-4}$	7.6 $x10^{-3}$	1.0 $x10^{-4}$	3.5 $x10^{-2}$	1.8
NMP TCNQ	3.5 $x10^{-5}$	2.0 $x10^{-4}$	8.0 $x10^{-3}$	4.1 $x10^{-4}$	3.5 $x10^{-2}$	1.1

Table 3.5 Glycolate oxidase kinetic data

membrane control is truly occuring in the unsaturated response region.

3.4.3.1 L-lactate-2-monooxygenase

L-lactate-2-monooxygenase (EC 1.13.12.4), also known as lactate oxidase, catalyses the oxidative decarboxylation of L-lactate:

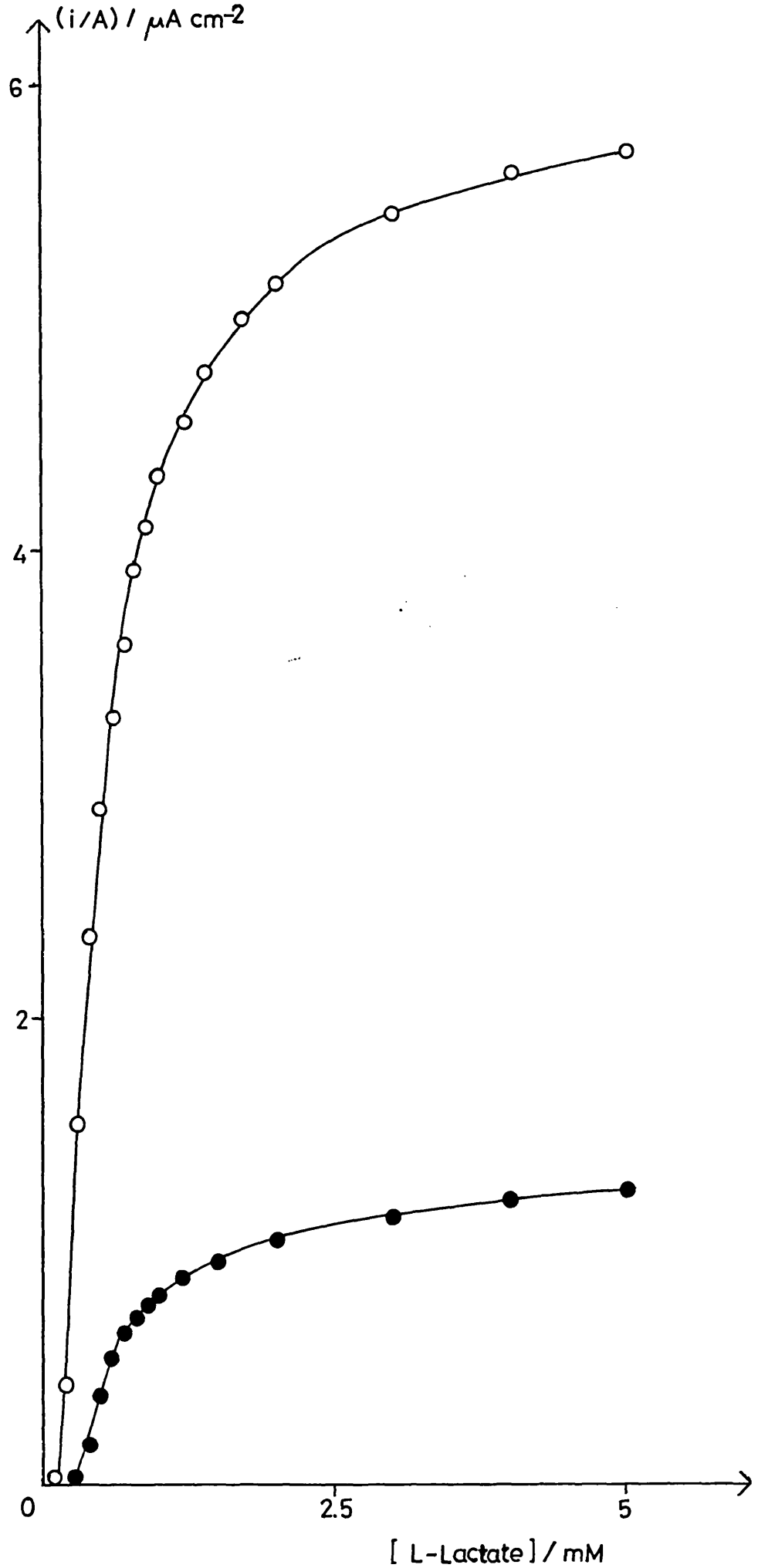
$$\text{L-lactate} + O_2 \longrightarrow \text{acetate} + CO_2 + H_2O_2$$

The purified enzyme is specific for L-lactate [101]. The cofactor for the enzyme is FMN. The enzyme is made up of two identical subunits [99], with one FMN per sub unit. Spectrographic analysis reveals the presence of copper [101], but this is not thought to take part in the enzymatic reaction.

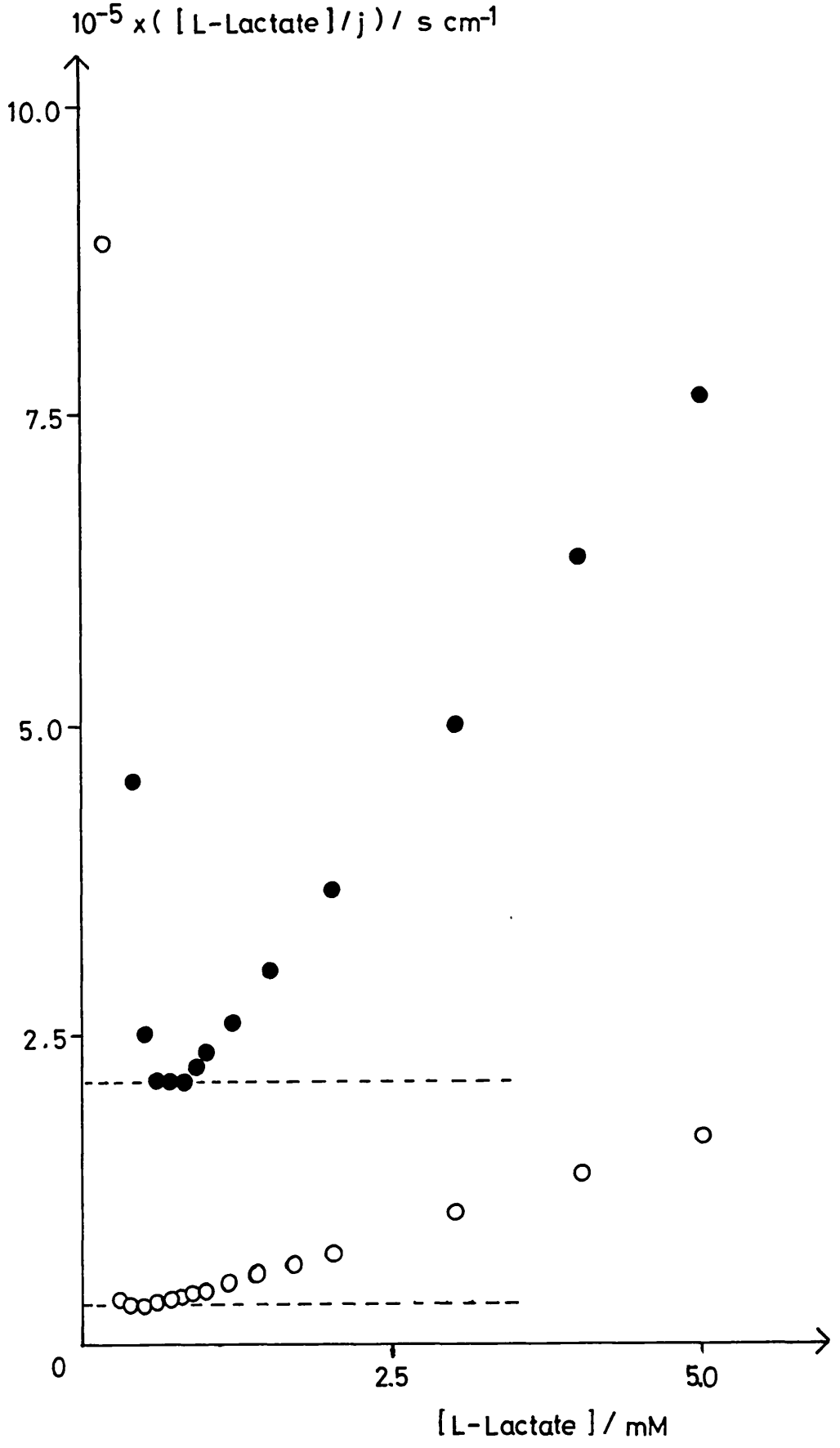
Lactate is routinely measured at present. The measurement of lactate is desirable clinically, since increased levels are associated with tissue hypoxia associated with liver disease, circulatory failure and hematological disorders.

3.4.3.2 L-lactate-2-monooxygenase results

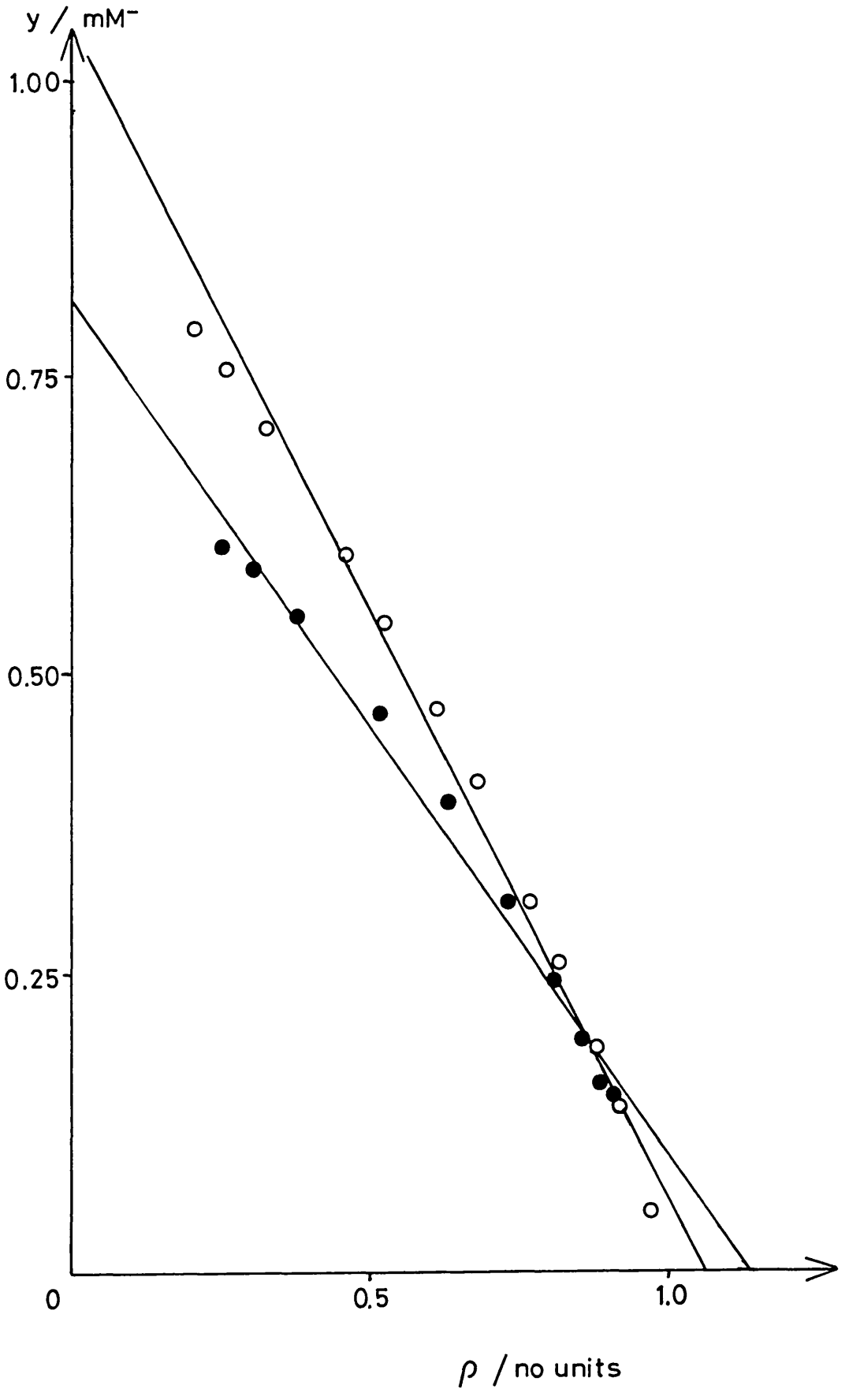
The responses of l-lactate-2-monooxygenase membrane electrodes to successive injections of L-lactic acid are shown in fig(3.7.1). This data has been analysed and presented as a Hanes plot in fig(3.7.2). Again, at low substrate concentrations, there is a plateau region indicative of membrane control.



Fig(3.7.1) The response profiles for L-lactate-2-monooxygenase membrane electrodes:
• denotes TTF TCNQ and o denotes NMP TCNQ.



Fig(3.7.2) The Hanes plots for L-lactate-2-monooxygenase membrane electrodes: • denotes TTF TCNQ and o denotes NMP TCNQ. Note that the first point is not shown for both plots.



Fig(3.7.3) The ρ-plots for L-lactate-2-monooxygenase membrane electrodes: • denotes TTF TCNQ and o denotes NMP TCNQ.

Electrode material	k_{ME}' /cm s^{-1}	$K_S D_S/L_M$ /cm s^{-1}	$e_\Sigma Lk_{cat}/K_M$ /cm s^{-1}	(j_{max}/e_Σ) /cm s^{-1}	Lk_{cat} /cm s^{-1}	K_{ME}' /mM
TTF TCNQ	5.3 $x10^{-6}$	2.0 $x10^{-4}$	6.5 $x10^{-5}$	1.8 $x10^{-4}$	2.7 $x10^{-2}$	1.3
NMP TCNQ	2.9 $x10^{-5}$	2.0 $x10^{-4}$	7.0 $x10^{-5}$	6.9 $x10^{-4}$	2.7 $x10^{-2}$	1.0

Table 3.6 Lactate oxidase kinetic data

Values of k'_{ME} , k'_S and $Lk_{cat}e_\Sigma / K_M$ have been calculated and presented in table 3.6 . In this instance, it is seen that the unsaturated enzyme rate constant is smaller than the membrane transport rate constant, which suggests that the unsaturated electrode kinetics could be controlled by the enzyme kinetics. However two points disagree with this:

(1) : D_S for lactate may well be less than for glucose, and so k'_S would be reduced;

(2) : the shape of the Hanes plot is typical of membrane control.

A further test is whether the ρ-plots pass through unity on the ρ-axis. The ρ-plots are shown in fig(3.7.3). Clearly the $\rho_o = 1$ for both plots and so it is concluded that the unsaturated electrode response is determined by the rate of diffusion of L-lactate through the membrane, and there is an error in calculating k'_S due to a lower value of D_S for L-lactate compared to glucose.

Comparison of j_{max}/e_Σ and Lk_{cat} , in table 3.6 , also indicates that the saturated electrode response are determined by the electrode rate constant. The values of K'_{ME} are much less than K_M for the enzyme, indicating that the electrode kinetics are really quite slow i.e. the electrode saturates at low concentrations of substrate.

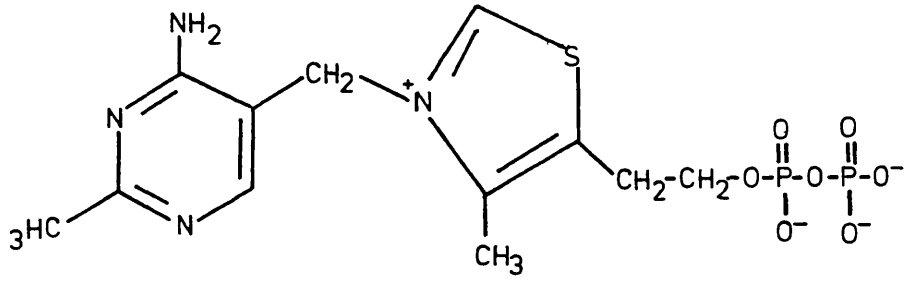
3.4.4.1 Pyruvate oxidase

Pyruvate oxidase (EC 1.2.3.3) catalyses the oxidative decarboxylation of pyruvate to acetate:

$$\text{pyruvate} + 1/2\ O_2 \xrightarrow{\text{TPP}} \text{acetate} + CO_2$$

where TPP is thiamin pyrophosphate.

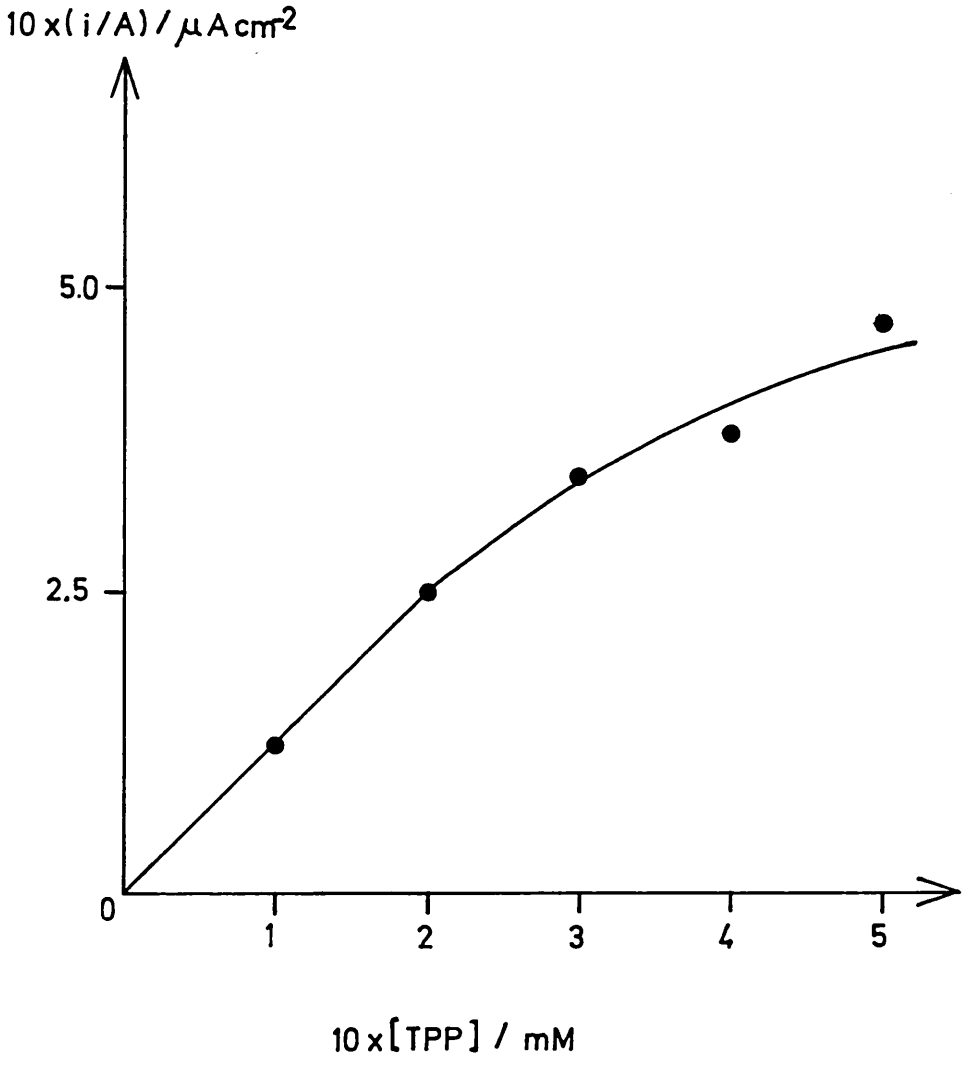
The enzyme is specific for pyruvate. It is a flavoenzyme and consists of four identical subunits, each of which contains one FAD residue [102]. It requires two cofactors: FAD and TPP [102]. TPP is also known as cocarboxylase tetrahydrate or vitamin B1:



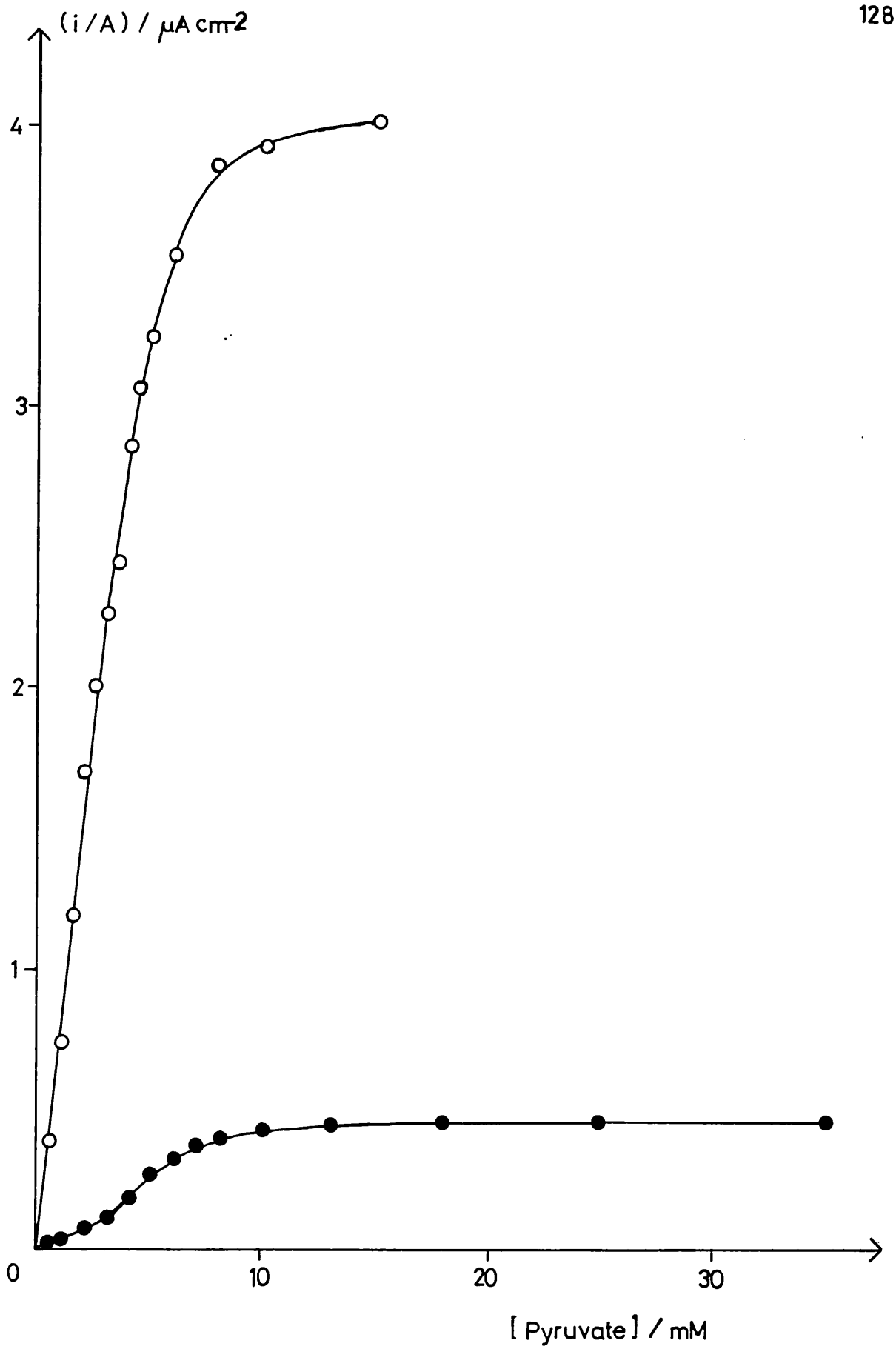
Pyruvate is routinely measured at present to detect increased levels associated with neuromuscular disorders, hepatic cirrhosis, diabetes mellitus, vitamin deficiencies, uremia and congestive heart failure.

3.4.4.2 Pyruvate oxidase results

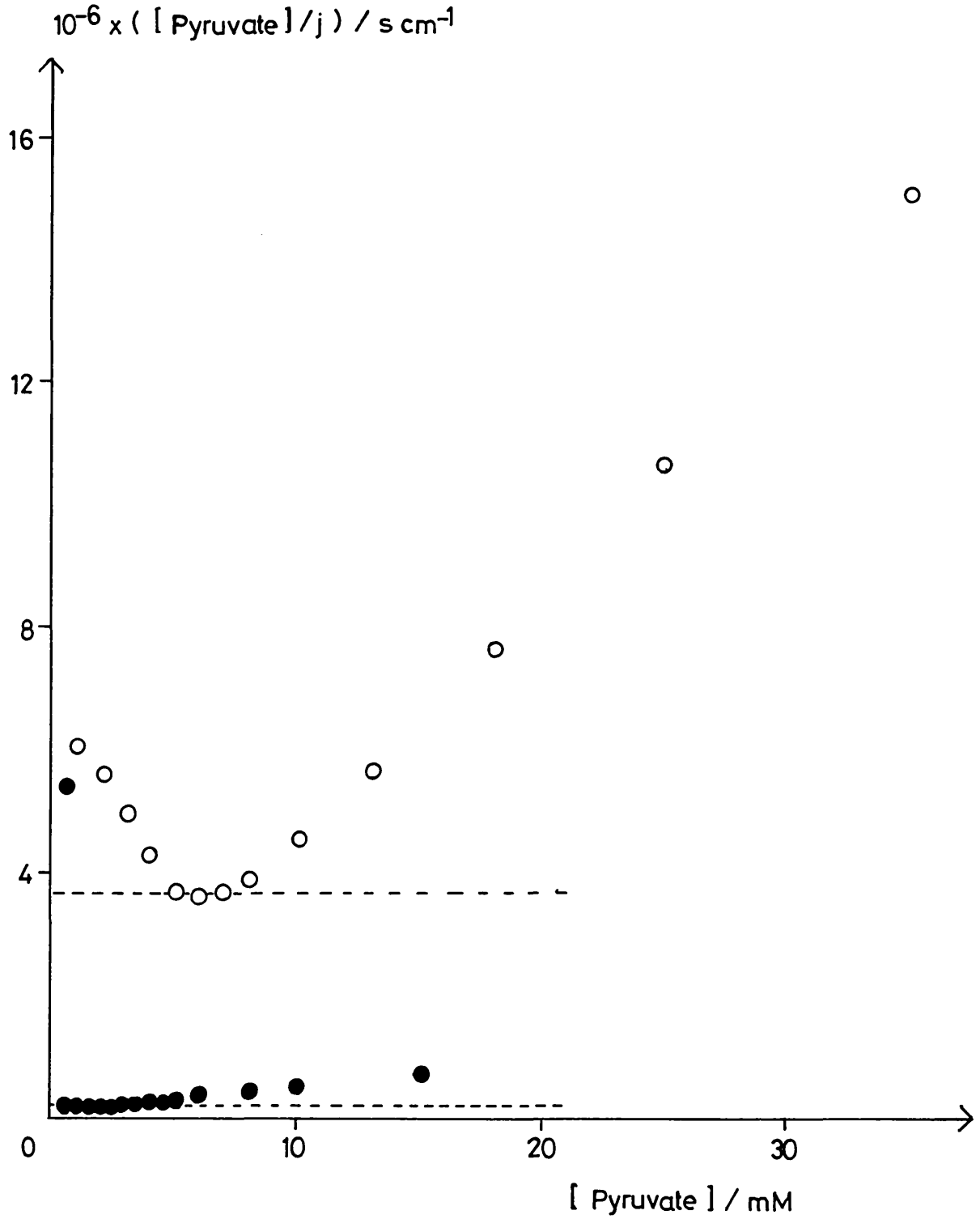
As noted above, pyruvate oxidase has a second cofactor: TPP. The K_M for TPP is 1.2 μM [115]. In order to simplify the response of the electrode, it was thought best to work with a saturating concentration of TPP. The response of a pyruvate oxidase membrane electrode to successive injections of TPP was measured in the



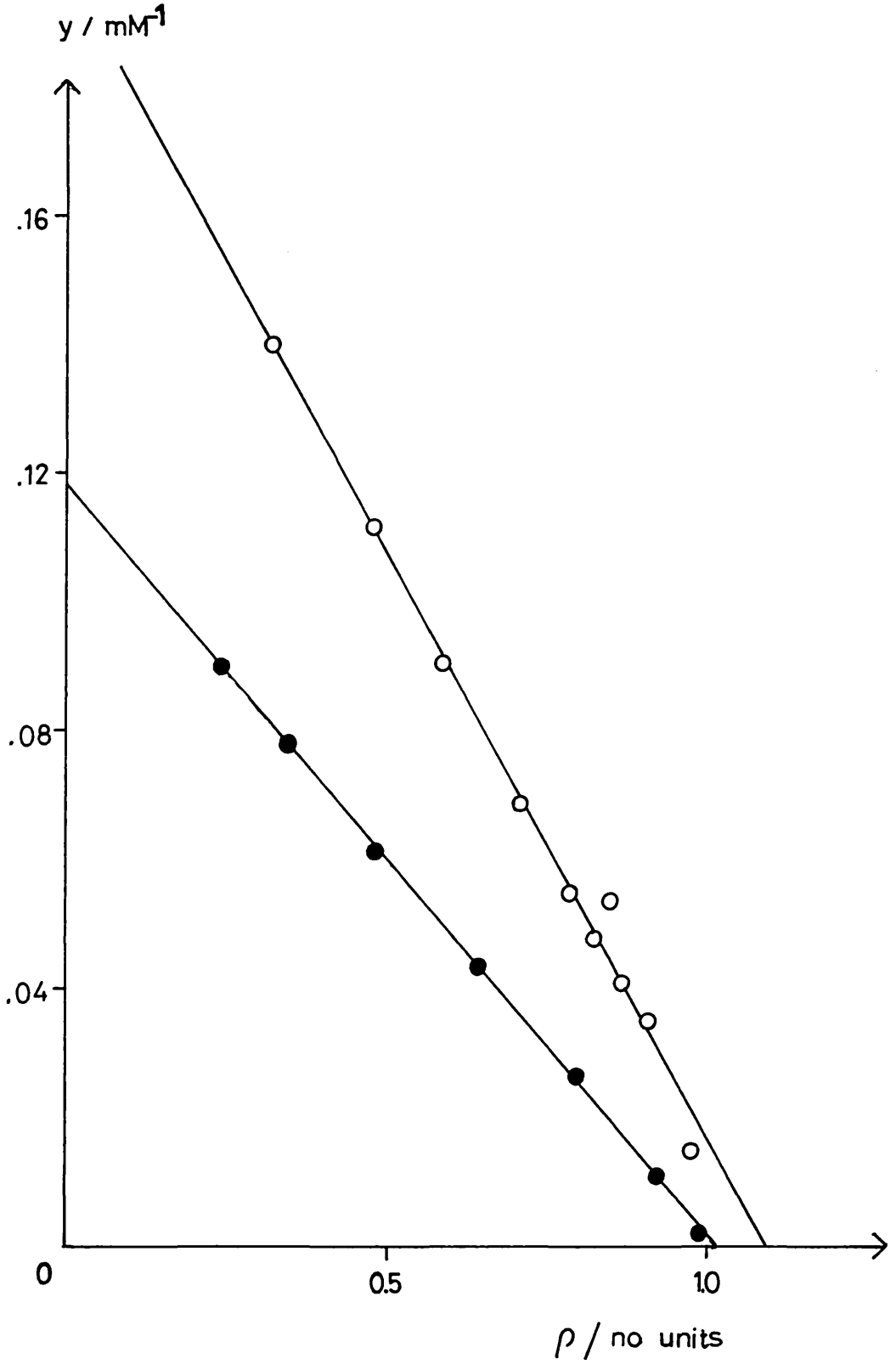
Fig(3.8.1) The response of a pyruvate oxidase membrane electrode to TPP in the presence of 2 mM sodium pyruvate. The electrode material was TTF TCNQ.



Fig(3.8.2) The response profiles of pyruvate oxidase membrane electrodes in the presence of 500 μM TPP: • denotes TTF TCNQ and o denotes NMP TCNQ.



Fig(3.8.3) The Hanes plots for pyruvate oxidase membrane electrodes: • denotes TTF TCNQ and o denotes NMP TCNQ. Note that the first point is not shown for the NMP TCNQ plot.



Fig(3.8.4) The ρ-plots for pyruvate oxidase membrane electrodes: • denotes TTF TCNQ and o denotes NMP TCNQ.

Electrode material	k_{ME}' /cm s^{-1}	$K_S D_S/L_M$ /cm s^{-1}	$e_\Sigma Lk_{cat}/K_M$ /cm s^{-1}	(j_{max}/e_Σ) /cm s^{-1}	Lk_{cat} /cm s^{-1}	K_{ME}' /mM
TTF TCNQ	2.8 $x10^{-7}$	2.0 $x10^{-4}$	7.8 $x10^{-2}$	2.7 $x10^{-5}$	9	8.5
NMP TCNQ	4.3 $x10^{-6}$	2.0 $x10^{-4}$	8.0 $x10^{-2}$	2.3 $x10^{-4}$	9	5.3

Table 3.7 Pyruvate oxidase kinetic data

presence of 2 mM sodium pyruvate in bulk. In the absence of TPP, no response was observed indicating that it was essential for electron transfer to the electrode to occur. The response is shown in fig(3.8.1). The electrode response drifted slowly and steadily positive, and took approximately 1 hour to steady; therefore the response was measured 15 mins after injection of TPP. The steady drift suggests that TPP binds to the enzyme quite slowly. The electrode did not saturate, although the magnitude of the response to successive injections did decrease. A concentration of 500 μM was adopted for all subsequent experiments since this is significantly larger than the K_M for TPP.

The response of pyruvate oxidase membrane electrodes to successive injections of sodium pyruvate, in the presence of 500 μM TPP, are shown in fig (3.8.2). The Hanes plots are presented in fig(3.8.3). The TTF TCNQ electrode indicates some interference from oxygen at low substrate concentrations. Both electrodes exhibit a small plateau region, indicative of membrane control. Values of k'_{ME}, k'_S and $Lk_{cat}e_\Sigma / K_M$ are given in table 3.7.

Comparison of the membrane rate constant and the unsaturated enzyme rate constant indicates that membrane transport determines the unsaturated electrode response. It should be noted that the value for k'_{ME} for the TTF TCNQ electrode is significantly lower than k'_S . Possibly the membrane used was particularly poor. It should also be remembered that the value of D_S used in calculating k'_S is possibly quite high, thus distorting the comparison of k'_{ME} and k'_S .

The ρ-plots for the electrodes are presented in fig(3.8.4). Both give $\rho_o = 1$, indicating the unsaturated electrode kinetics are indeed controlled by membrane transport kinetics. Comparison of the

values of j_{max}/e_{Σ} and Lk_{cat} indicate that the saturated electrode response is determined by the electrode rate constant, k'. The values of K'_{ME} have been calculated and are given in table 3.7. These are comparable to the K_M for pyruvate (10 mM), indicating in this case that either the electrode kinetics or the saturated enzyme kinetics are governing the saturated electrode response. However since $j_{max}/e_{\Sigma} << Lk_{cat}$, it is reasonable to assume that the saturated electrode response is governed by the electrode kinetics.

3.4.5.1 Oxalate oxidase

Oxalate oxidase (EC 1.2.3.4) catalyses the oxidation of oxalate:

$$\text{oxalate} + 2H^+ + O_2 \longrightarrow H_2O_2 + 2CO_2 .$$

The enzyme is highly specific for oxalate [104], and exhibits substrate inhibition [103].

The prosthetic group of the enzyme is unknown, and the enzyme does not require any added cofactor [103]. None the less the activity is found to increase in the presence of flavins, with riboflavin being the most efficient activator [103], followed by FMN then FAD. This activation suggests the possibility of flavin as a prosthetic group for the enzyme. However two facts disagree with this:

(1) : the purified enzyme is a white crystalline powder i.e. it exhibits neither the yellow colour nor the uv/visible spectrum characteristic of flavoproteins;

(2) : there is no evidence of flavin binding to the enzyme and the reduced enzyme does not quench the flavin fluorescence.

It is possible that riboflavin acts by having some protective effect against inhibition of the enzyme by fluoride ions [103]. The enzyme is also activated more than 500% by 0.4 mM 8-hydroxy quinoline [103].

High concentrations of 8-hydroxy quinoline or riboflavin eliminate the substrate inhibitor effect [103]; thus it is possible from the close similarity in behaviour that they act in a similar manner. It has been suggested that 8-hydroxy quinoline has some chelating effect with heavy metal ions, which deactivates the enzyme [116]. Divalent metal ions also deactivate the enzyme [103], as do the halide salts of sodium [104].

Oxalate is routinely measured at present in both clinical and manufacturing sectors. Increased urinary oxalate excretion is characteristic of renal calculii and urinary tract stones and hyperoxaluria, the genetic disorder of oxalate metabolism. Traditional methods of determination isolate the oxalate from the urine by precipitation, extraction or ion-exchange prior to assay. Clearly a more direct determination involving minimal sample pretreatment would be advantageous.

Oxalate sensing enzyme electrodes have been reported [117,118]. Of particular interest is the use of enzyme from the acetone extracted pulp from banana skins [118]. Such a cheap source of enzyme would be very desirable, particularly if any activators are separated with the enzyme.

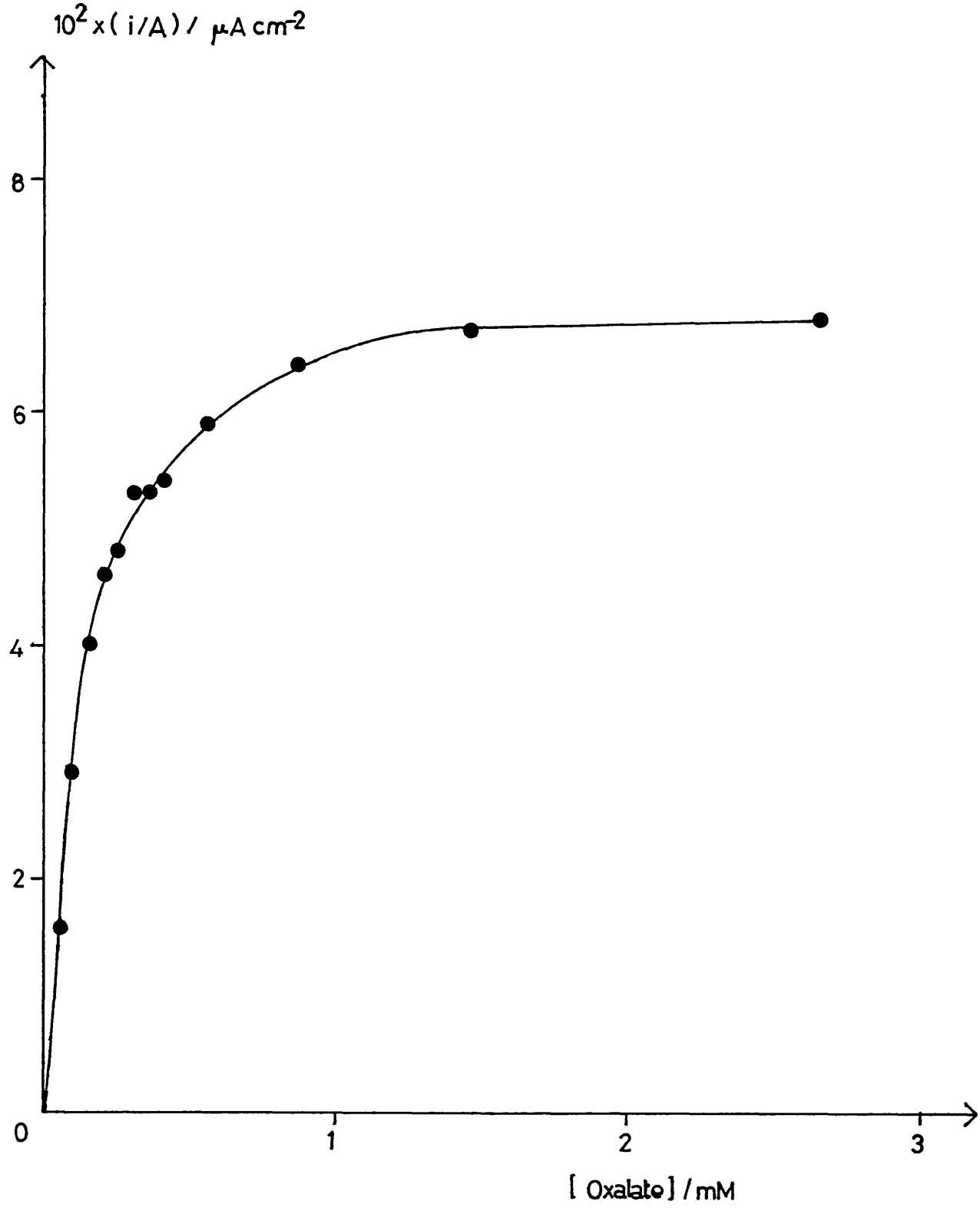
3.4.5.2 Oxalate oxidase results

Since FMN is a known activator for the enzyme, all experiments were carried out in the presence of 4 μM FMN [103]. This was particularly necessary because of the very low activity of the enzyme (2.5 u/ml).

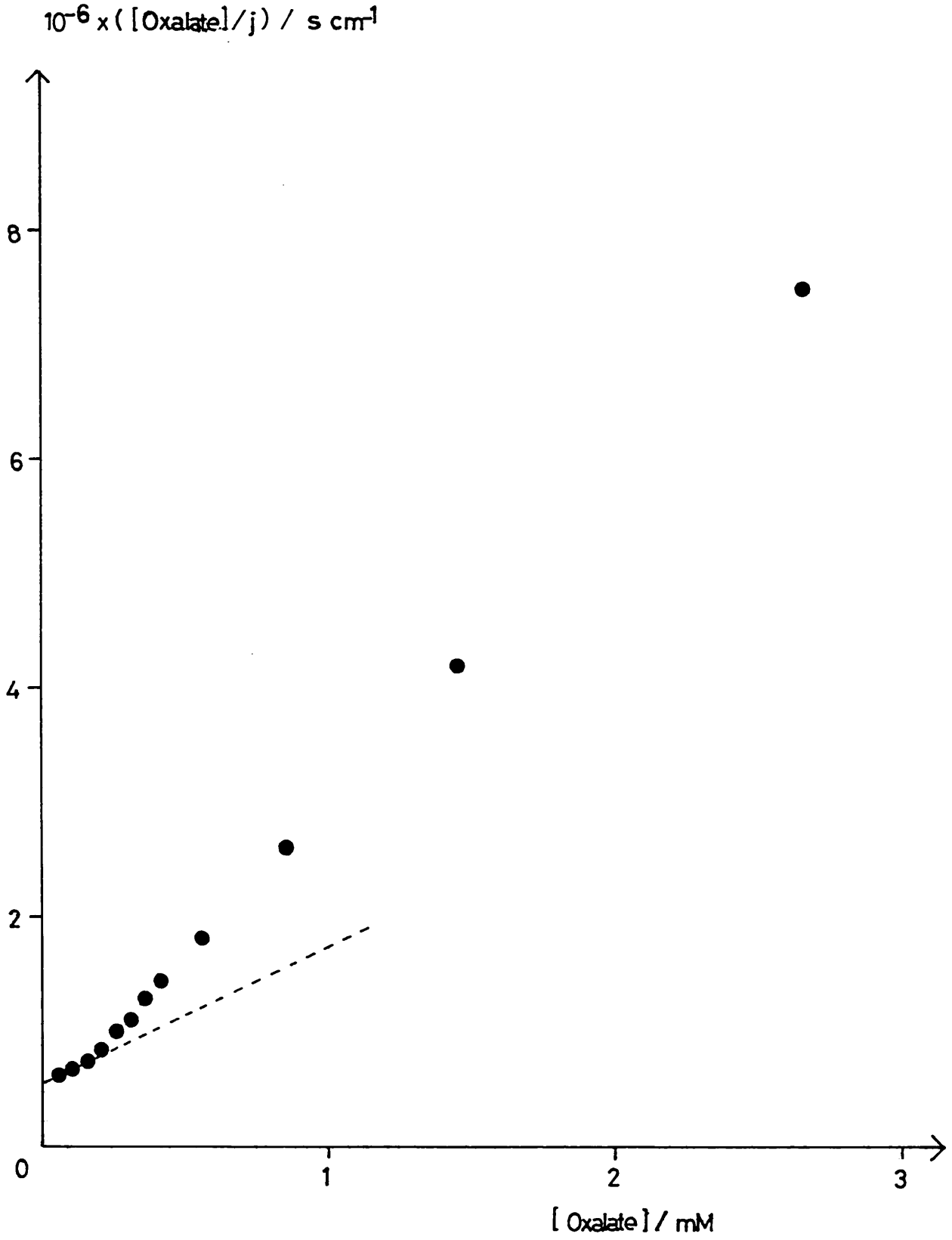
No response could be observed for the TTF TCNQ membrane electrode on successive injections of sodium oxalate. Consequently the potential of the working electrode was increased from +50 mV to +100 mV vs. SCE, since it was hoped that any small currents would be magnified, assuming the electrode response was potential dependent as observed for glucose oxidase [79]. This higher potential was used throughout all subsequent experiments. Still no response with TTF TCNQ was observed. The lack of response on TTF TCNQ could either be because oxalate oxidase is not electroactive on TTF TCNQ, or because the enzyme activity was too low to observe any current above the background current.

A very small response was observed for a NMP TCNQ membrane electrode, and is shown in fig(3.9.1). Again, the very low enzyme activity severely limits the response of the electrode. It should be noted that the bulk solution was initially yellow due to the oxidized FMN species; by the end of the experiment, the bulk solution was colourless. This could indicate that the FMN was reduced in the presence of oxalate oxidase and oxalate. Alternatively it could be that FMN was photolysed.

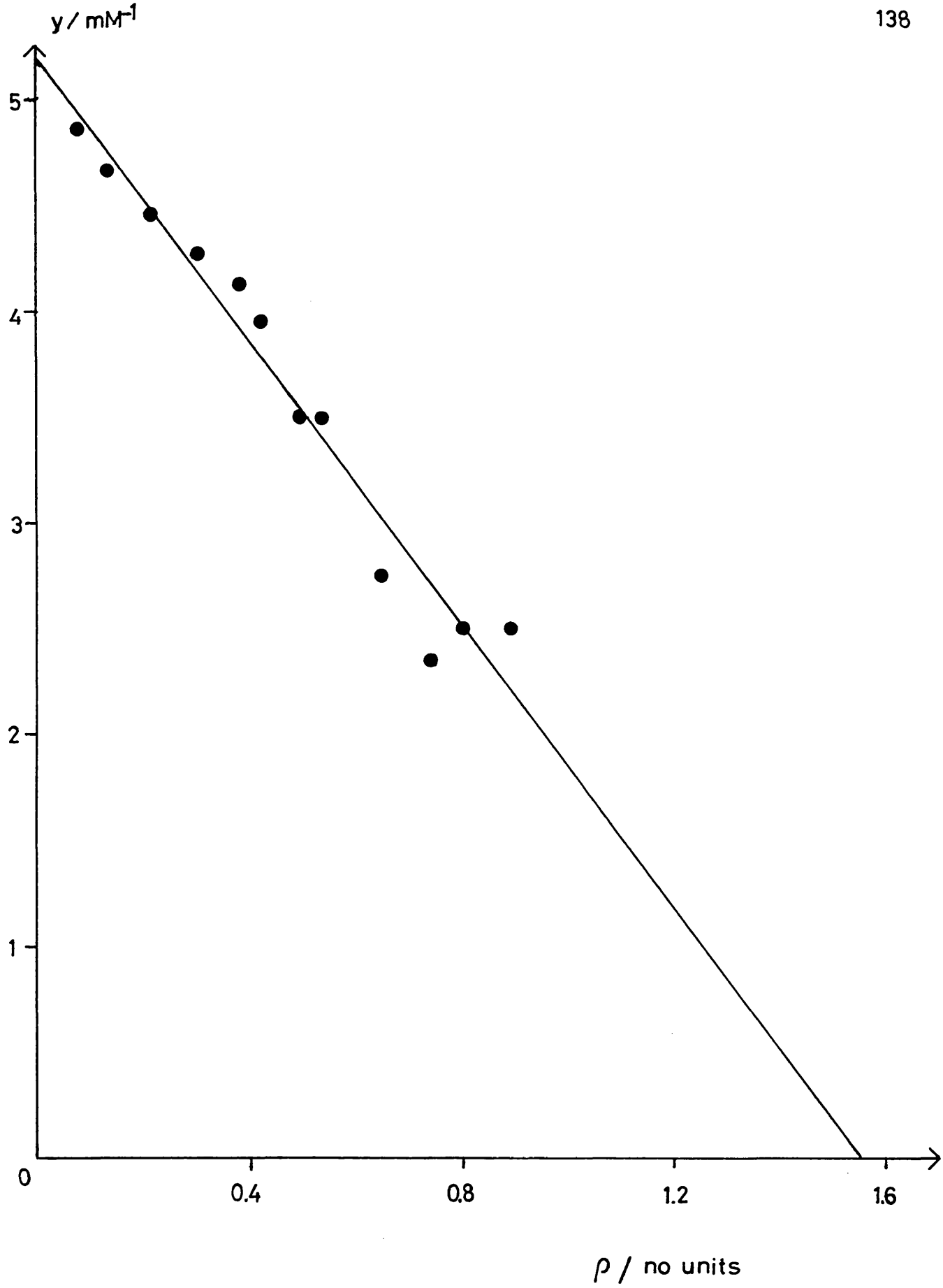
The Hanes plot is presented in fig(3.9.2). The electrode does not exhibit clean membrane control; there is no clear plateau region. It is possible that some degree of unsaturated enzyme kinetics control



Fig(3.9.1) The response of an oxalate oxidase membrane electrode in the presence of 4 μM FMN. The electrode material was NMP TCNQ.



Fig(3.9.2) The Hanes plot for the oxalate oxidase membrane electrode.



Fig(3.9.3) The ρ-plot for the oxalate oxidase membrane electrode.

Electrode material	k_{ME}' /cm s^{-1}	$K_S D_S/L_M$ /cm s^{-1}	$e_\Sigma Lk_{cat}/K_M$ /cm s^{-1}	(j_{max}/e_Σ) /cm s^{-1}	Lk_{cat} /cm s^{-1}	K_{ME}' /mM
NMP TCNQ	1.9 $x10^{-6}$	2.2 $x10^{-4}$	—	5.3 $x10^{-6}$	—	0.19

Table 3.8 Oxalate oxidase kinetic data

is occuring. The value for k'_{ME} is given in table 3.8. Comparison with k'_S indicates that it is much smaller. Unfortunately the k_{cat} for oxalate oxidase is unknown and so comparison of the unsaturated enzyme rate constant with k'_{ME} and k'_S cannot be made.

The ρ-plot is presented in fig(3.9.3). The value of $\rho_o = 1.55$. This clearly indicates both the membrane and unsaturated enzyme kinetics are controlling the unsaturated electrode kinetics, since $\rho = k'_S / k'_{ME}$ (eqn. (3.20)). The experimentally determined value of k'_{ME} is 2.88×10^{-6} cm s^{-1} , significantly lower than the calculated value of k'_S . This gives the calculated value of k'_S as 4.46×10^{-6} cm s^{-1}. Then using eqn. (3.13) , $Lk_{cat}e_\Sigma / K_M$ is calculated to be 5.25×10^{-6} cm s^{-1} . Unfortunately this value cannot be compared to the theoretical value since k_{cat} is unknown.

The value for j_{max} / e_Σ is given in table 3.8. It is not known whether the saturated electrode kinetics are governed by the electrode kinetics or the saturated enzyme kinetics, since comparison with Lk_{cat} cannot be made. The K_{ME} value is found to be 0.19 mM, which is less than the K_M for the enzyme (0.42 mM). If the saturated electrode response was limited by saturated enzyme kinetics, one would expect the K_{ME} value to be equal to or greater than the K_M for the enzyme. Thus it is concluded that the electrode rate constant determines the saturated electrode response.

3.4.6.1 Bilirubin oxidase

Bilirubin oxidase (EC 1.3.3.5) catalyses the oxidation of bilirubin to biliverdin:

$$\text{bilirubin} + O_2 \longrightarrow \text{biliverdin} + H_2O \ .$$

Biliverdin is further oxidised by the enzyme to other so far unidentified products, with 50% the activity of bilirubin [105]. Other substrates for bilirubin oxidase include catechol, pyrogallol, hydroquinone and p-phenylene diamine [106]. All substrates of the enzyme are tetrapyrrolic [106]. They can easily dissociate into dipyrrolic and monopyrrolic fragments and reassemble at random giving new, isomeric tetrapyrrolic structures. The process is favoured by visible light, acidic pH, oxygen and heat [119]. Bilirubin is also easily oxidised to biliverdin in the absence of the enzyme; the process is catalysed by oxygen and light, and slowed significantly in darkness, low temperature, in red light and in a deaerated atmosphere [119].

Bilirubin is not soluble in acidic media; thus all experiments should be carried out in alkali media in addition to being protected from light and oxygen (solutions should be used immediately after preparation).

Atomic absorption spectroscopy shows that bilirubin oxidase contains one copper atom per molecule of enzyme. There is no NAD, NADP, FMN or FAD [120]. Thus the active site of the enzyme would appear to be copper [106]. The enzyme is inactive in the absence of oxygen [120].

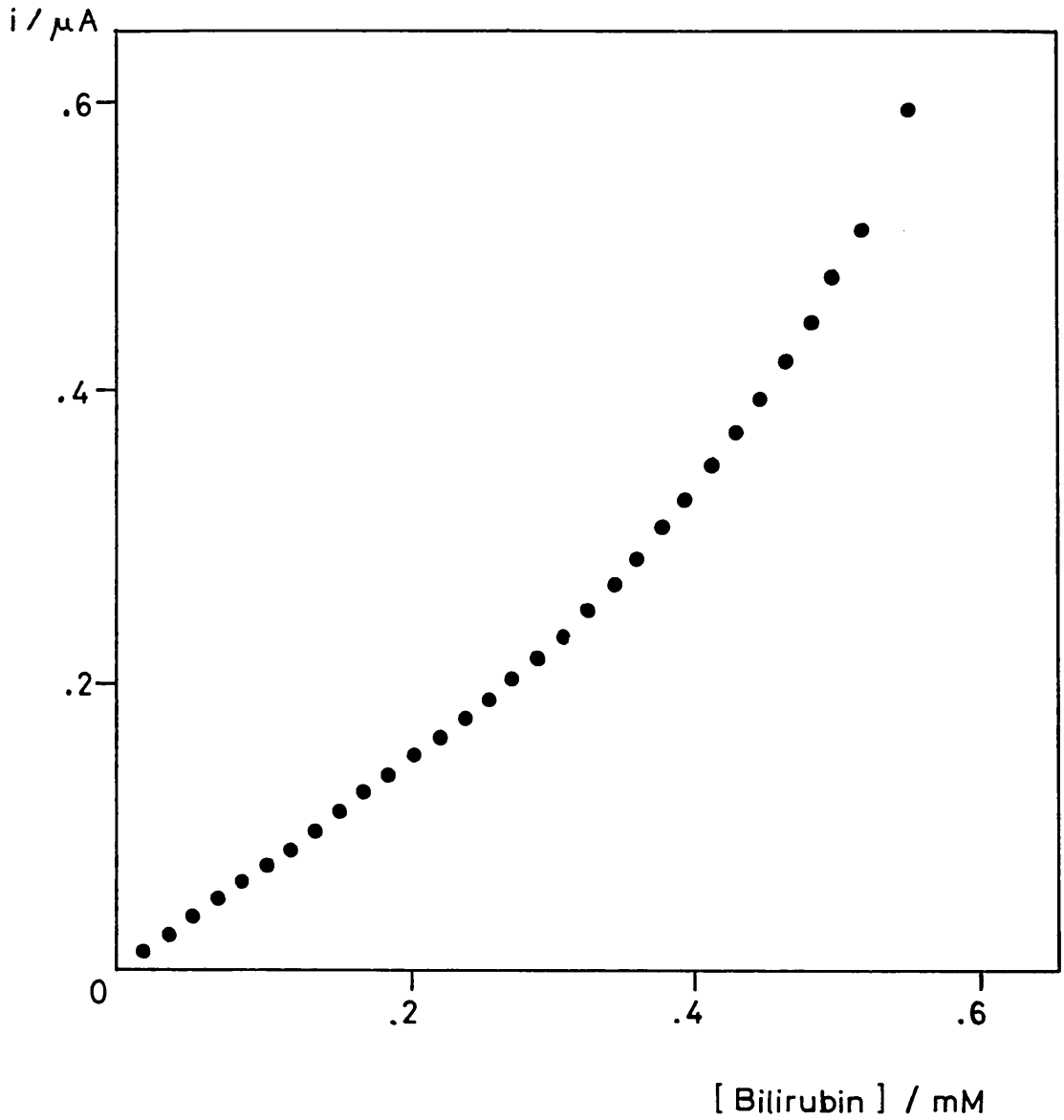
In vivo, bilirubin is derived from the breakdown of haemoglobin, myoglobin and haemoproteins. There are several isomers of bilirubin and its derivatives. The varying amounts of these isomers may be used to diagnose certain diseases [119]. Abnormally high levels of bilirubin are characterised by yellow skin, resulting in

jaundice. Bilirubin binds to cellular and mitochondrial membranes causing cell death in a variety of tissues. Clinically, bilirubin toxicity may lead to mental retardation, cerebral palsy, deafness, seizures and death [105]. Jaundice is particularly apparent in newborn infants; 20% accumulate a sufficient amount to contract jaundice. The two most common treatments for jaundice are blood transfusions (in extreme cases) and phototherapy. In phototherapy, the patient is exposed to blue light which converts bilirubin to a less toxic isomer [105]. Thus a measure of bilirubin could be useful to determine the extent of jaundice in patients.

3.4.6.2 Bilirubin oxidase results

Bilirubin itself was found to be electroactive, giving large currents on TTF TCNQ, shown in fig(3.10.1). Thus construction of a bilirubin oxidase membrane electrode was not possible. Biliverdin exhibited 10% the oxidation current of bilirubin. Thus it was thought possible that the bilirubin oxidation current could contain some proportion due to the oxidation of biliverdin, produced either by the oxygen or electrode activated oxidation of bilirubin. However UV/ visible spectroscopy indicated that the bulk solution of bilirubin contained no detectable amounts of biliverdin, and also the bilirubin oxidation current was independent of the ambient oxygen concentration. Thus it was concluded that biliverdin made no significant contribution to the bilirubin oxidation current.

The response of the electrode to bilirubin exhibits two distinct regions. Above $\approx$ 350 μM, the electrode appears to become activated towards oxidation. At this concentration, bilirubin was observed to



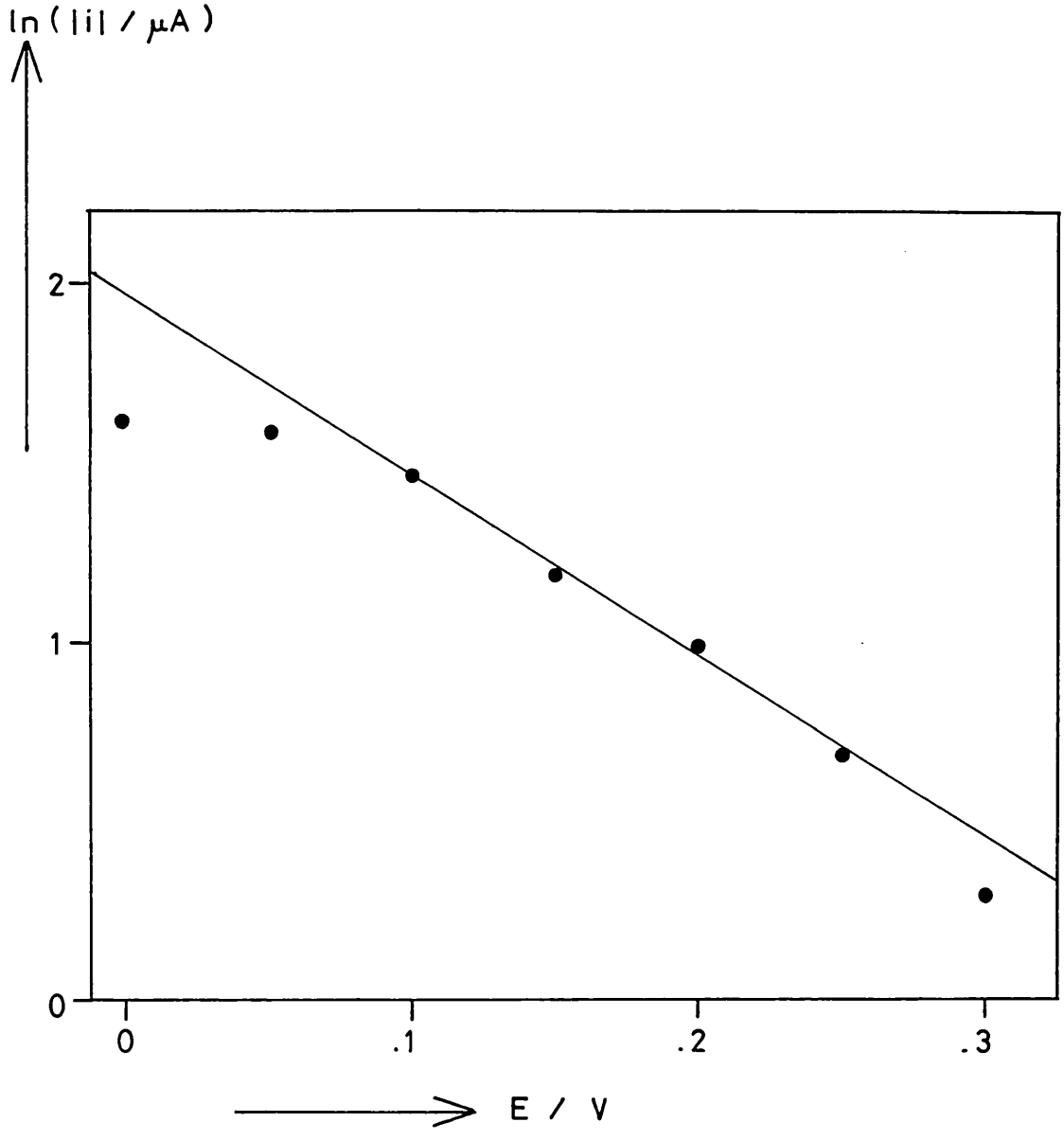
Fig(3.10.1) The current response profile of a TTF TCNQ electrode to successive injections of bilirubin.

be precipitating from solution on to any available solid surface. Thus it is likely that the activation effect is caused by the adsorption of bilirubin onto the electrode surface.

Bilirubin oxidase itself appeared to be electroactive in the absence of bilirubin. It should be noted that the enzyme is inactivated by NaCl [121]; consequently all experiments were carried out using KBr as electrolyte. A membrane electrode prepared with 3910 u/ml enzyme gave a reduction current on TTF TCNQ. It was thought possible that the observed current could be due to the presence of some electroactive impurity in the bilirubin oxidase preparation. Subsequently an experiment was carried out with a membrane entrapping buffer over a fresh electrode, with enzyme in the bulk solution only. No current was observed; however on removal of the membrane a reduction current was again observed. Thus it seems likely that bilirubin oxidase can be reduced at a TTF TCNQ electrode.

Deoxygenating the solution with nitrogen resulted in a steady decrease in the reduction current back to the background current. On ceasing to degas with nitrogen, the reduction current was restored. This suggests bilirubin oxidase is capable of being reduced by a TTF TCNQ electrode and subsequently oxidized by oxygen. Removal of the oxygen source did not allow the enzyme to be reoxidized, and so the bulk concentation of the oxidized enzyme was depleted and the reduction current fell.

The potential dependence of the bilirubin oxidase reduction was measured between 0 and +300 mV vs SCE, in steps of +50 mV. The Tafel plot is shown in fig(3.10.2). $n\alpha$ was calculated according to the Tafel equation [122]:



Fig(3.10.2) The Tafel plot for bilirubin oxidase on a TTF TCNQ electrode.

$$\ln i = \ln i_o + \alpha nFE/RT$$

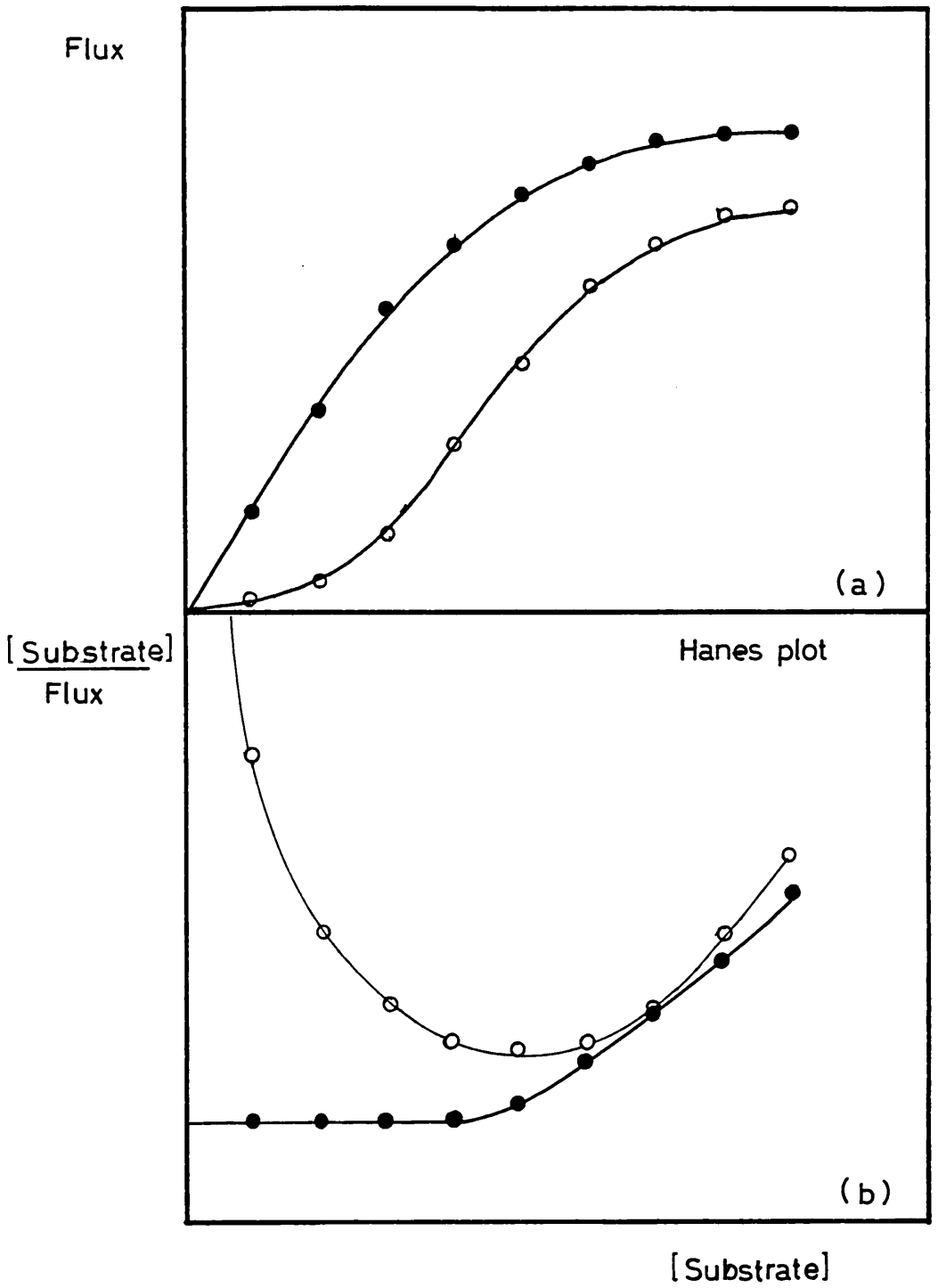
where E is the applied electrode potential. The gradient of the E vs. log i plot is given by $\alpha nF/RT$ and hence $n\alpha$ can be found. $n\alpha$ was found to be $\approx$ 0.15, which is quite low and suggests the electron transfer is not very facile.

3.5 Problems encountered

3.5.1 The oxygen effect

In all membrane electrode experiments, the bulk solution was degassed with nitrogen. However the surface of the bulk solution was exposed to the atmosphere throughout, and thus some oxygen could dissolve into the bulk solution. The amount of dissolved oxygen would be variable, being dependent on the rate of nitrogen flow through the bulk. Thus the effect on the electrode current cannot be quantified.

Qualitatively, a small amount of dissolved oxygen in the bulk solution would preferentially oxidize any reduced enzyme compared to the electrode i.e. for glucose oxidase, $k(O_2)$ = 1,150 s^{-1} [123], giving $Lk(O_2) \approx 1.15$ cm s^{-1} compared to the electrode rate constant for TTF TCNQ of 9 x 10^{-2} cm s^{-1} [62]. Thus the observed electrode response would be reduced from its maximum value in the absence of oxygen, until the bulk oxygen is depleted. The effect of oxygen is seen as a drop in the electrode response at low substrate concentrations. This is shown in fig(3.11.a). Consequently, in the Hanes plot the initial points are anomalously high, and distort the plateau region. This is



Fig(3.11) The effect of dissolved oxygen (a) on the membrane electrode response profile and (b) on the corresponding Hanes plot. • denotes deoxygenated solution and o denotes solution containing dissolved oxygen.

shown in fig(3.11.b). These points at low substrate concentrations are best ignored in the Hanes plot analysis.

In addition to the competition between oxygen and the electrode for the reduced enzyme, the reaction between reduced enzyme and oxygen can produce hydrogen peroxide. This can be reduced on conducting organic salt electrodes [114]. Thus a negative current may be observed at low substrate concentrations e.g. glycolate oxidase in section 3.4.2.2.

3.5.2 Reproducibility

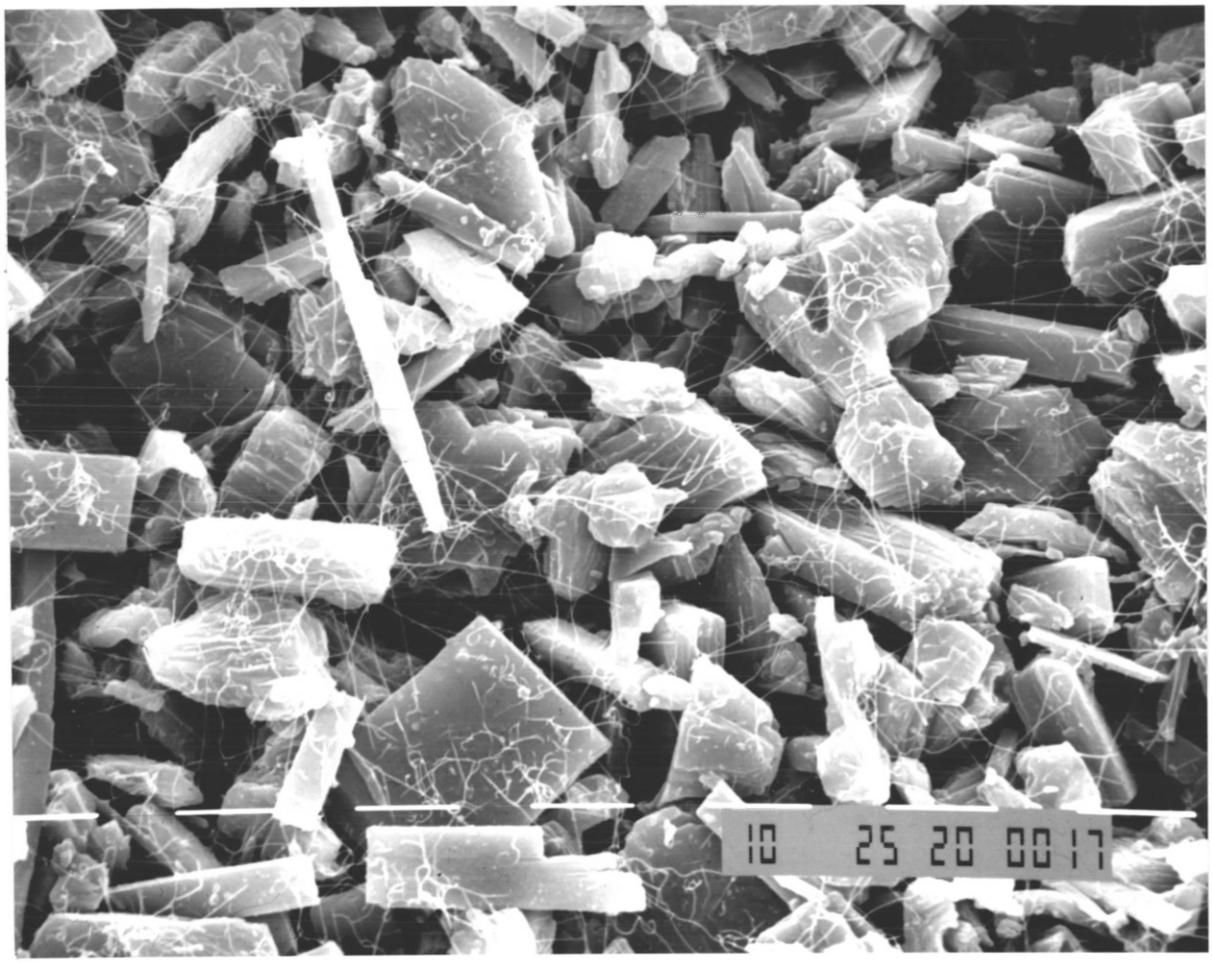
For electrodes prepared with polymer paste, a great variation in saturation current was observed. A good electrode would give ≈140 $\mu A cm^{-2}$ at saturation, with an enzyme loading of ≈100 u/ml (sarcosine oxidase). However, much less current was often observed, and sometimes the electrode was totally resistive and unsuitable for use. The latter case was generally caused by a loss of contact between the conducting organic salt and the platinum disc. It was thought that the variation in saturation current could be due to the random method of packing the electrode with the PVC polymer : salt paste. The paste was pressed into the cavity with a wooden applicator: clearly irreproducible and uneven pressures could result in a unique electrode surface for each electrode. Generally it was observed that electrodes with a high saturation current ("good" electrodes) had a rough, more crystalline surface, while electrodes with low saturation currents ("poor" electrodes) had a smoother, more shiny surface.

3.5.3 Scanning electron microscopy

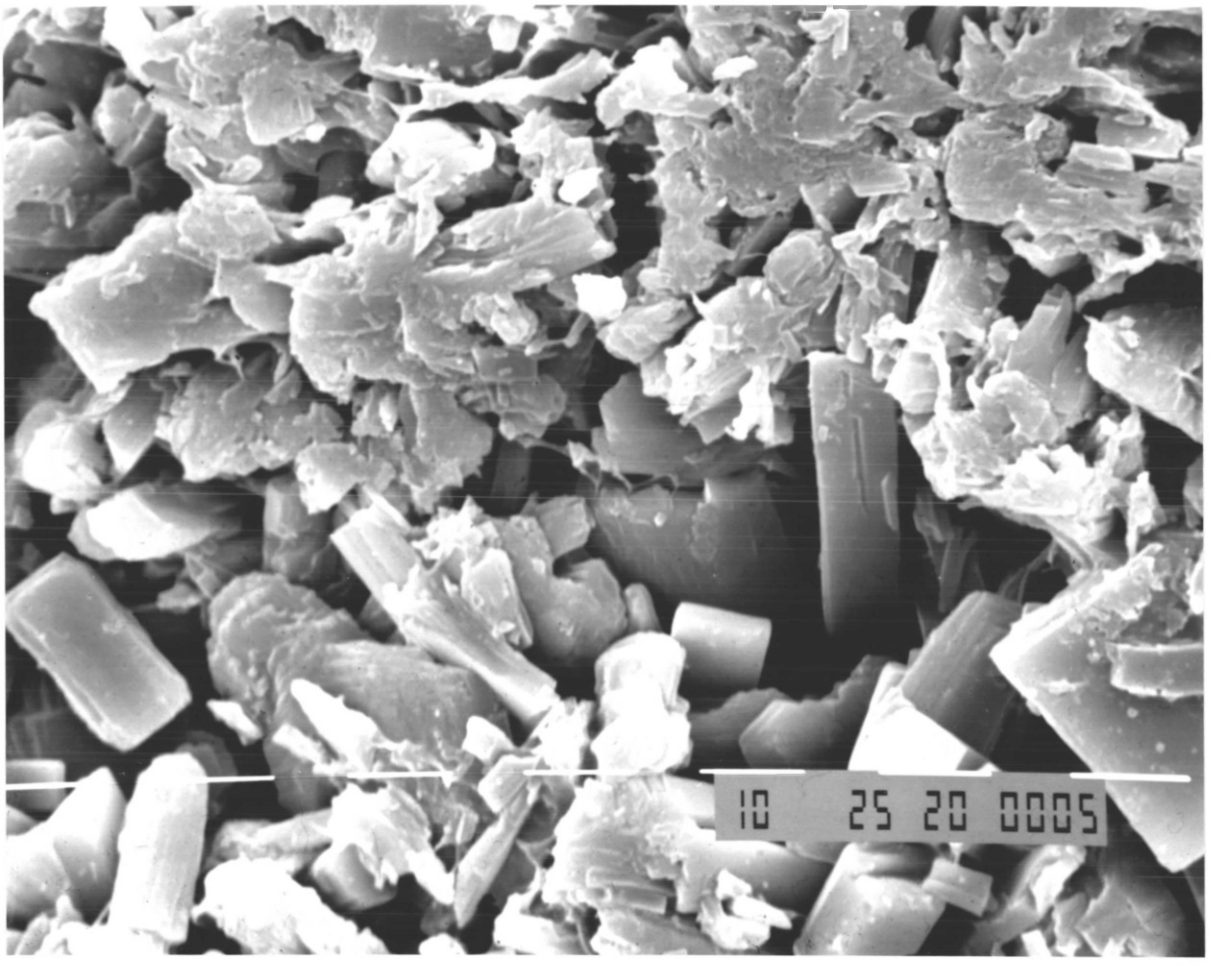
It was thought that inspection of the surface of the electrodes by electron microscopy might yield further information. A number of electrodes were prepared using a screw top cavity electrode. Some electrodes were prepared simply by one or two applications of the PVC : salt slurry and minimum use of the wooden applicator. Others were prepared by pressing the salt hard into the cavity in between applications of the slurry; in this case it was necessary to apply more slurry, so it can be concluded that these electrodes were more densely packed.

The electrodes were made into membrane electrodes using glucose oxidase (250 u/ml). They were held at +50 mV wrt SCE, and the responses of the electrodes to successive injections of 1 M glucose were measured, and the saturation currents noted. This allowed each electrode to be labelled as either "good" or "poor". A correlation was noted between "good" and "poor" electrodes and the method of packing. Those electrodes prepared with the minimum of applications and little use of the applicator were "good", while those that were very densely packed were "poor". The electrode material was then removed from the cavity and prepared for electron microscopy.

The scanning electron micrographs of a "good" and a "poor" TTF TCNQ electrode for glucose oxidase are shown in figs(3.12.1) and (3.12.2). The "good" electrode has a very rough surface with a great number of crystals projecting out of the surface and available to solution. Strands of PVC can be seen lying over the crystal surface, holding the crystallites together. The "poor" electrode has far fewer



Fig(3.12.1) Scanning electron micrograph of a "good" TTF TCNQ packed cavity electrode prepared with PVC binder. Each line across the bottom of the micrograph represents a certain number of μm; this number is given by the left most number in the box on the right hand side of the photograph i.e. in this case, the line represents 10 μm.



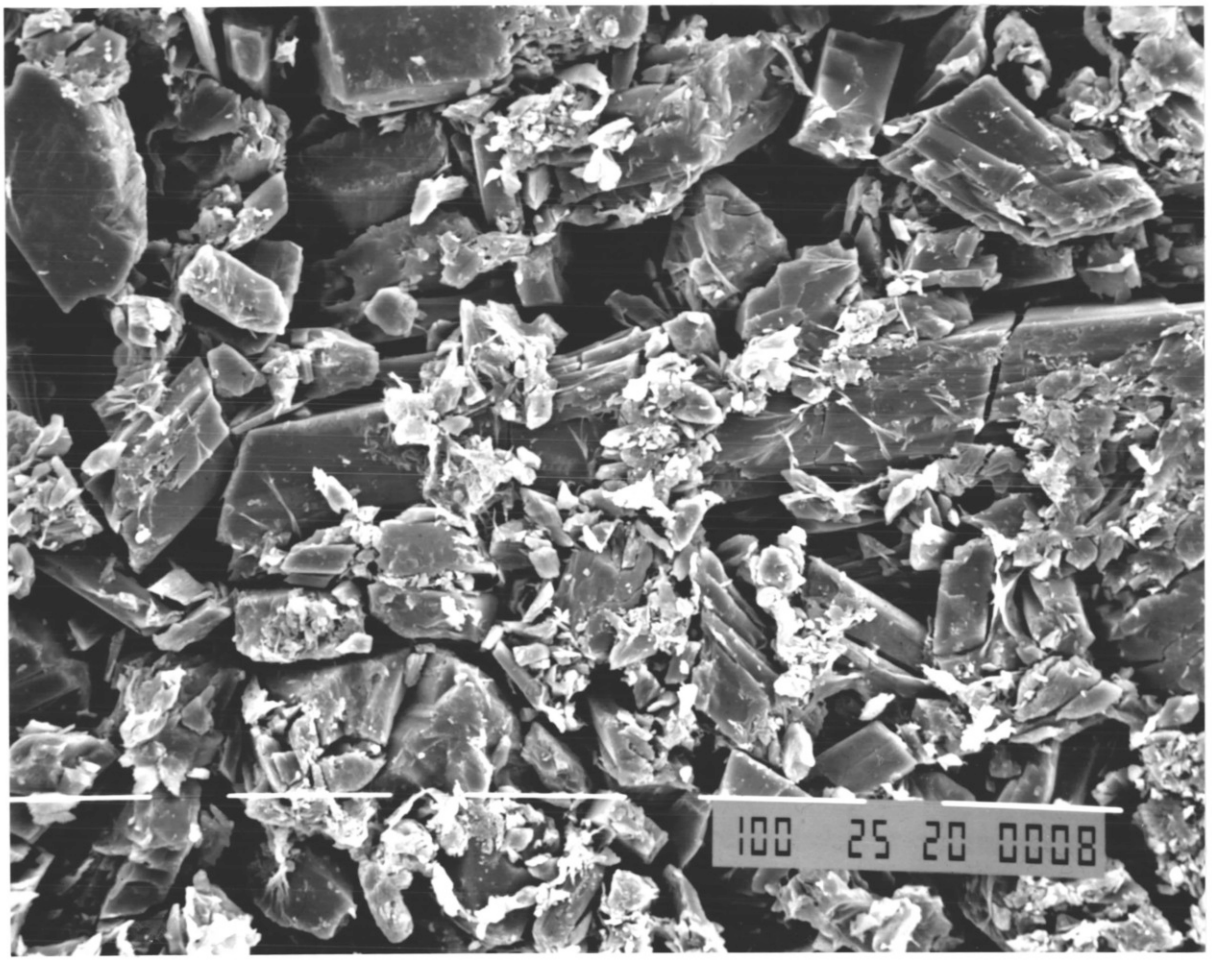
Fig(3.12.2) Scanning electron micrograph of a "poor" TTF TCNQ packed cavity electrode prepared with PVC binder.

individual crystals showing, and the majority of the surface is covered by a mass of PVC and crystals bound together in a compact lump. The crystals generally appear smaller, suggesting they could have been broken by the use of the wooden applicator during the preparation of the electrode.

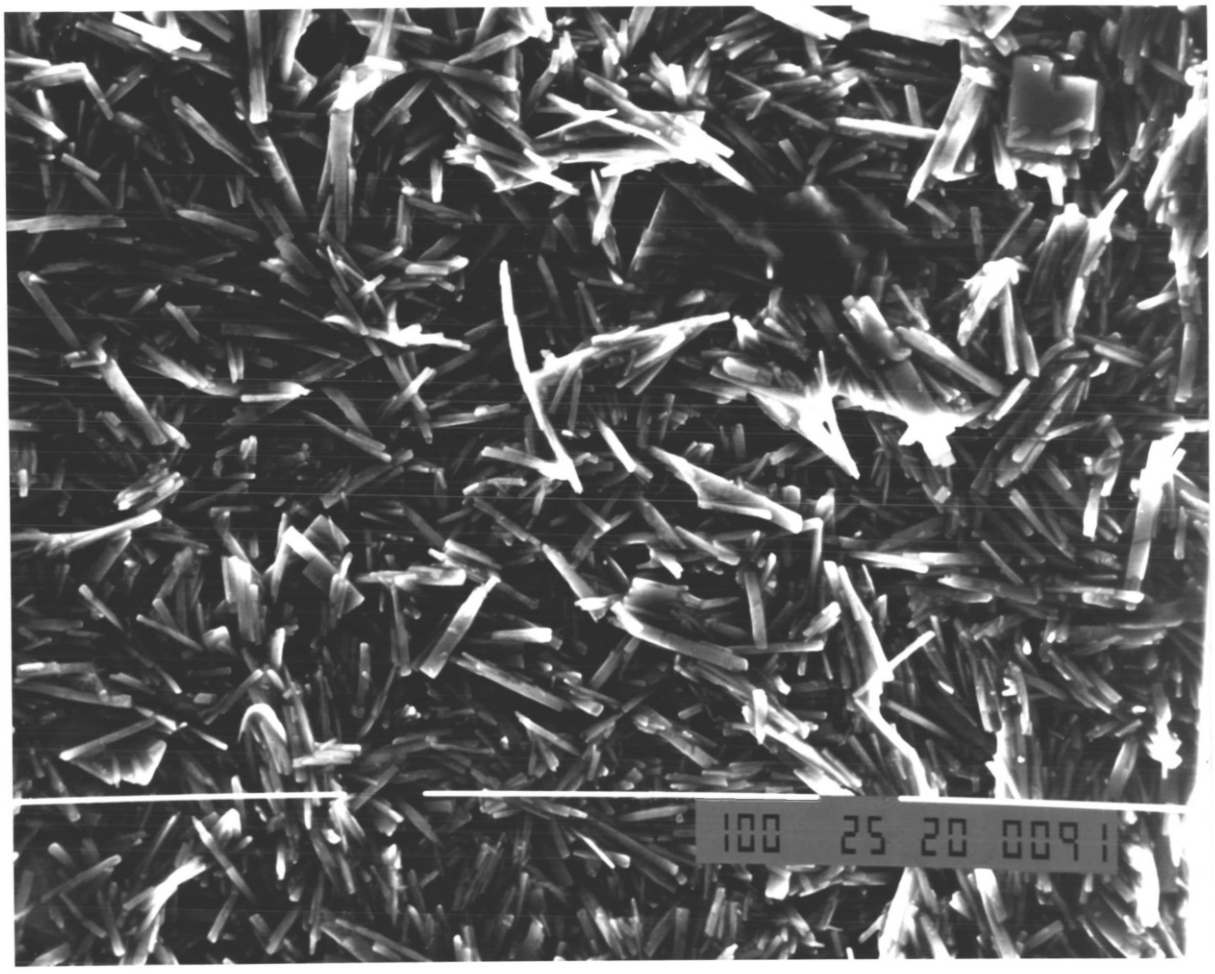
For comparison a "good" NMP TCNQ electrode (111 μA cm^{-2} saturation current) is shown in fig(3.12.3). The individual crystals are much larger than for TTF TCNQ (100 μm compared to 10 - 20 μm), and the surface is quite rough. In this case no individual strands of PVC can be seen; there are some areas of much smaller crystallites on top of the larger ones - the NMP TCNQ crystals have a much greater variety of size than TTF TCNQ.

A Si oil : TTF TCNQ electrode is shown in fig(3.12.4). It has been noted above (section 2.4.1) that all electrodes prepared with Si oil were found to be universally "good", although in general, lower saturation currents were observed. The electrode surface is very rough, and the individual crystals are quite uniformally sized crystals of ≈ 30 μm length (note that this was a different TTF TCNQ sample from those used in figs(3.12.1) and (3.12.2)). It should be noted that these electrodes are prepared with minimal use of force.

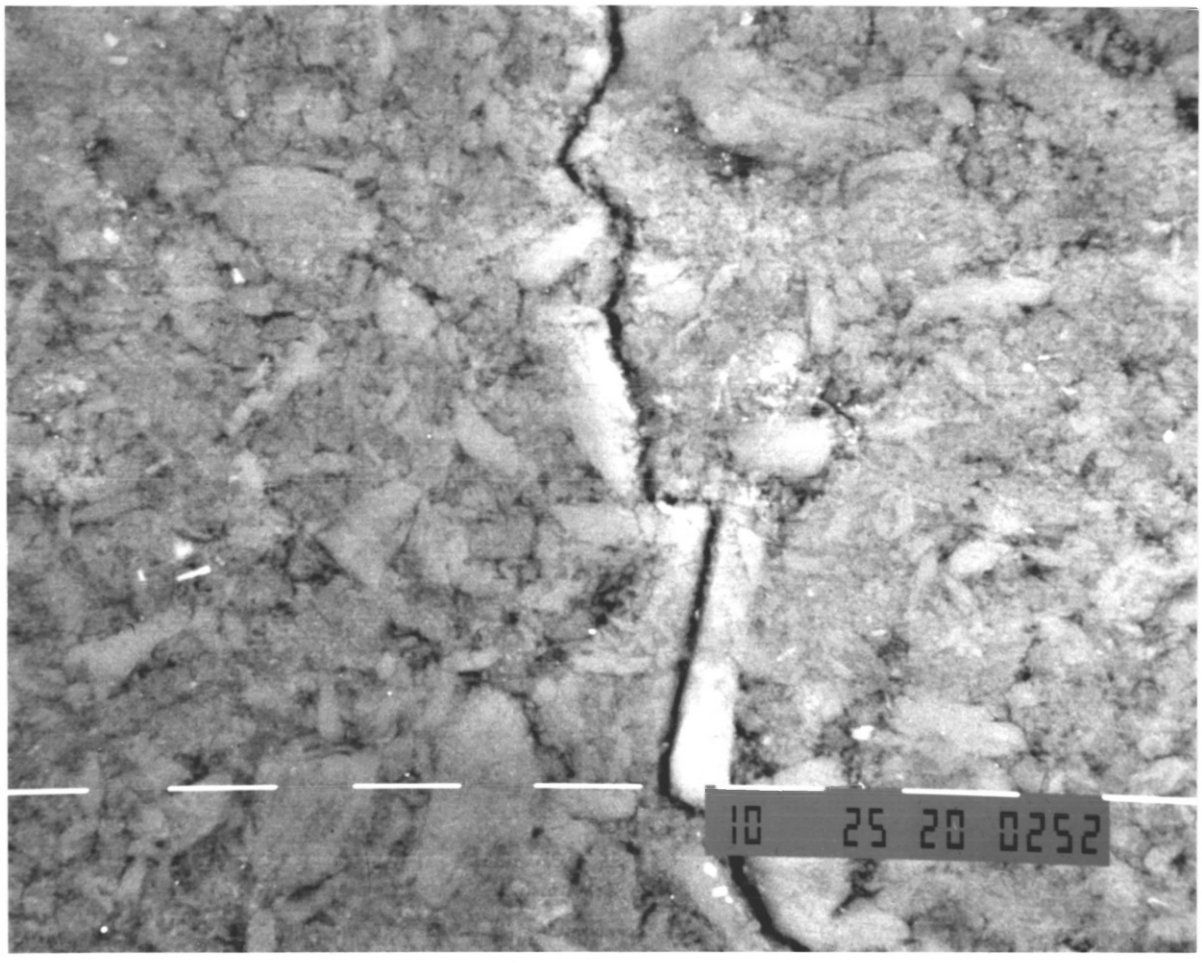
Fig(3.12.5) shows an NMP TCNQ pressed pellet electrode; this was prepared using no binder following the method given in section 2.2.2. Pressed pellet electrodes give very low saturation currents (10 μA cm^{-2}) and it is not surprising that the surface of the electrode is very smooth. The outlines of individual crystals can be observed where they have been compressed into the electrode surface. Across the picture from left to right runs a crack in the electrode surface; this kind of fault is quite common to pressed pellet electrodes.



Fig(3.12.3) Scanning electron micrograph of a "good" NMP TCNQ packed cavity electrode prepared with polystyrene binder.



Fig(3.12.4) Scanning electron micrograph of a Si oil : TTF TCNQ paste electrode.



Fig(3.12.5) Scanning electron micrograph of an NMP TCNQ pressed pellet electrode.

Then in conclusion, the magnitude of the saturation current of an electrode is directly proportional to the roughness, or available surface area, of that electrode. This in turn depends on the method of preparation of the electrode: methods which apply large pressures on the crystals result in more uniform packing and smaller surface area, and possibly also affect the conductivity of individual crystals by introducing faults into them. Methods involving lying down the crystals with the minimum of force result in rougher, generally less uniform surfaces; in this case, conductivity between individual crystals relies on the haphazard connections through the electrode surface.

3.5.4 The mediated reaction layer thickness

It was noted at the end of the introduction that there is some controversy over whether the mechanism of electron transfer between an enzyme and a conducting organic salt electrode occurs directly, by heterogeneous redox catalysis or by a mediated mechanism. Consideration of the electron micrographs gives some evidence to support the mediated theory.

The electron micrograph of a "good" TTF TCNQ electrode (fig(3.12.1)) reveals the intercrystallar spacing between the surface TTF TCNQ crystals to be of the order of 10 μm, in some cases less. This intercrystallar spacing can be compared with the reaction layer thickness for the mediated electron transfer proposed by J.J. Kulys [70]. The reaction layer thickness, χ_M , is given by:

$$\chi_M = (D_M / k_M [E])^{1/2}$$

where D_M is the diffusion coefficient of any mediated species, typically 5 $x10^{-6}$ cm^{-2} s^{-1}; k_M is the second order rate constant for the enzyme - mediator reaction: this was found to be 3 x 10^6 $M^{-1}s^{-1}$ for $TCNQ^o$ and was the highest rate constant obtained for the possible mediator species from an NMP TCNQ electrode [70]; and [E] is the enzyme concentration, typically 5 x 10^{-6} M (250 u/ml) for glucose oxidase. Then χ_M is found to be:

$$\chi_M > 5\ \mu m\ .$$

Then the reaction layer thickness can be less than the intercrystallar distance, and consequently the roughness of the electrode surface will determine the total area over which the mediated electron transfer reaction can take place and also the saturation current of the electrode.

This argument is supported by the comparison of the saturation currents at a single crystal electrode and a packed cavity electrode [72]. Comparison of the fluxes gives a roughness factor of 10^2 - 10^3 . Clearly the porous electrode has the advantage over the single crystal, which is explicable if the spacing between crystallites in the packed cavity electrode is greater than the reaction layer thickness.

It should be noted that the calculated value of χ_M is very approximate, and at present the actual mediator species and hence k_M are unknown. However in the case of NMP TCNQ, the intercrystallar spacing is greater and more variable (fig(3.12.3)) being $\approx$10 - 30 μm , which is much greater than the proposed reaction layer thickness.

Thus this argument, based on the inspection of the electron micrographs, does not exclude the possibility of the mediated electron transfer reaction taking place.

3.6 Conclusions

It has been shown that a large number of enzymes are capable of being oxidized at the surface of a conducting organic salt electrode. The membrane electrode theory developed by W.J. Albery and P.N. Bartlett has been shown to be applicable to a number of enzyme electrodes. The theory shows that the unsaturated electrode response is governed by the rate of transport of substrate through the membrane, while the saturated electrode response is governed by the rate of oxidation of reduced enzyme at the electrode surface. Exceptions to this are oxalate oxidase, for which the unsaturated electrode response had contributions from both the transport of substrate through the membrane and the unsaturated enzyme kinetics, and bilirubin oxidase, which was reduced at the electrode surface in the absence of substrate. It is of interest to note that sarcosine oxidase exhibited product inhibition: this is the first example found for a flavoenzyme electrode. It is further evidence of the validity of the theory for the p-plot.

The effect of the electrode flux having half order dependence on the reduced enzyme concentration has also been considered for the membrane electrode theory. It was found that the membrane electrode analysis still held true and allowed the rate limiting steps for both the unsaturated and the saturated electrode response to be

determined in the same manner as before. The analysis for product inhibition was also unaffected.

The values of k'_S , the membrane transport rate constant, are given in table 3.9 for the enzyme electrodes reported both in this chapter and elsewhere. One would expect all the values to be approximately the same, since they are determined by the same type of membrane (Spectra/Por). With the exception of sarcosine oxidase, some values reported for electrodes in this chapter are $\approx$ 1 order of magnitude smaller than those previously reported. This may be because the membranes were from a different batch, or because they were not prepared and stored in exactly the same manner, and so different transport properties may have resulted. The values for pyruvate oxidase are particularly slow, possibly because of the diffusion of the relatively bulky TPP through the membrane could be blocking it.

It is noticeable for the results reported in this thesis that k'_S values for electrodes prepared with NMP TCNQ are greater than for those prepared with TTF TCNQ. Ideally the k'_S values should be independent of the electrode material. Thus it appears that the choice of electrode material can influence the electrode response in the region where membrane transport is rate limiting. This implies that some process involving the electrode material is important in this region. It is possible that a different mechanism could be occuring that gives rise to the same response profile i.e. a linear region in the response profile and a plateau region in the Hanes plot. Quite what this mechanism could be is open to speculation. However the k'_S values do cast doubts on the validity of the basic assumption of direct electron transfer in the membrane electrode theory.

Enzyme	k_S'/ cm s^{-1} TTF TCNQ	k_S'/ cm s^{-1} NMP TCNQ
Glucose oxidase [62]	4.7×10^{-5}	3.0×10^{-5}
Sarcosine oxidase	4.0×10^{-5}	3.0×10^{-4}
Glycolate oxidase	4.7×10^{-6}	3.5×10^{-5}
Lactate oxidase	5.3×10^{-6}	2.9×10^{-5}
Pyruvate oxidase	2.8×10^{-7}	4.3×10^{-6}
Oxalate oxidase	—	4.5×10^{-6}
Xanthine oxidase [63]	1.1×10^{-4}	—
D-amino acid oxidase [63]	2.6×10^{-5}	—
L-amino acid oxidase [63]	2.8×10^{-5}	—
Choline oxidase [63]	1.2×10^{-4}	—

Table 3.9 k_S' values for enzymes electroactive on conducting organic salt electrodes

The values of k', the electrochemical rate constant, determined for the enzyme electrodes described herein and others previously investigated in these laboratories, are given in table 3.10. Nearly all the k' values are greater than 10^{-4} cm s^{-1}, indicating the satisfactory nature of the electron transfer at these conducting organic salt electrodes. Of those exhibiting k' values less than 10^{-4} cm s^{-1} (that is pyruvate oxidase on TTF TCNQ and oxalate oxidase on NMP TCNQ), both require an added cofactor (TPP and FMN respectively). It is expected that a thorough determination of the dependence of these electrodes on the cofactors will allow optimization of the electrode responses.

It is seen in table 3.10 that for the results reported in this thesis, k' for NMP TCNQ is greater than k' for TTF TCNQ. This is explicable if NMP TCNQ has faster kinetics i.e. is the better choice of electrode material. This disagrees with the k' values for glucose oxidase where TTF TCNQ was the material of choice, although this could either be because of the different enzymes employed or because of the different preparations of electrode material.

It should be realised that the determination of the rate controlling process for both the unsaturated and saturated electrode response is not simply an academic exercise but is necessary in order to optimize the response of the electrode. For example, if the electrode response is limited by the enzyme rate constant, then increasing the thickness of the membrane will decrease the membrane transport rate constant, and when the membrane is sufficiently thick, the transport of substrate through the membrane will become rate limiting. Thus the linear range of the electrode can be increased and the electrode

Enzyme	k'/ cm s^{-1} TTF TCNQ	k'/ cm s^{-1} NMP TCNQ
Glucose oxidase [62]	9 $x10^{-2}$	8 $x10^{-2}$
Sarcosine oxidase	4.2 $x10^{-4}$	4.6 $x10^{-4}$
Glycolate oxidase	1.0 $x10^{-4}$	4.1 $x10^{-4}$
Lactate oxidase	1.8 $x10^{-4}$	6.9 $x10^{-4}$
Pyruvate oxidase	2.7 $x10^{-5}$	2.3 $x10^{-4}$
Oxalate oxidase	—	5.3 $x10^{-6}$
Xanthine oxidase [63]	3.7 $x10^{-4}$	—
D-amino acid oxidase [63]	2.4 $x10^{-4}$	—
L-amino acid oxidase [63]	4.6 $x10^{-4}$	—
Choline oxidase [63]	3.0 $x10^{-3}$	—

Table 3.10 k' values for enzymes electroactive on conducting organic salt electrodes

response can become independent of the enzyme activity behind the membrane.

A summary of all the enzymes tested in these laboratories is given in table 3.11. It is seen that the flavoenzymes, that is, enzymes with either FMN or FAD as cofactor, are all redox active at these electrodes with the exception of cholesterol oxidase. Difficulties were encountered in solubilizing the cholesterol, and it was felt that this, rather than the enzyme, resulted in no observable current [125].

Of the enzymes containing copper as their active site, galactose oxidase gave no response and bilirubin oxidase appeared to be reduced at the electrode in the absence of substrate. It would be desirable to know the potential for the reduction of bilirubin oxidase, to confirm this conclusion. Unsurprisingly bilirubin was electroreduced. It has a highly delocalized nature which is capable of stabilizing an oxidized form.

Scanning electron micrography has revealed that electrodes with a high saturation current have rougher, more irregular surfaces, while electrodes with low saturation currents have much smoother and more compact surfaces. The roughness of an electrode surface is dependent on the method of manufacture of the electrode: electrodes prepared with minimum compaction of the crystals are rougher.

Inspection of the electron micrograph of TTF TCNQ has revealed that the intercrystallar distance is $\approx$ 10 - 20 μm. This is greater than the reaction layer thickness for the mediated electrode theory of $>$ 5 μm, suggesting that the roughness of the electrode determines the total surface area over which the mediated electron transfer can take place. It should be noted that the calculation of the reaction layer

Enzyme	EC number	Cofactor
Glucose oxidase [62]	1.1.3.4	FAD
L-amino acid oxidase [63]	1.4.3.2	FAD
D-amino acid oxidase [63]	1.4.3.3	FAD
Xanthine oxidase [63]	1.1.3.22	FAD/MoFe centre
Choline oxidase [63]	1.1.3.17	FAD
Sarcosine oxidase	1.5.3.1	FAD
Pyruvate oxidase	1.2.3.3	FAD/TPP
Oxalate oxidase	1.2.3.4	(FMN)
Lactate oxidase	1.13.12.4	FMN
Glycolate oxidase	1.1.3.15	FMN
Bilirubin oxidase	1.3.3.5	Copper
Galactose oxidase [124]	1.1.3.9	Copper
Cholesterol oxidase [125]	1.1.3.6	FAD

Table 3.11 Active sites of enzymes tested on conducting organic salt electrodes

thickness is very approximate since the second order rate constant for the mediated electron transfer is unknown. However the argument does not preclude the possibility of the electron transfer occuring by a mediated mechanism.

Chapter 4

The mechanism of electron transfer between an enzyme and a conducting organic salt electrode

4.1 Introduction

This chapter is concerned with the mechanism of electron transfer between a conducting organic salt electrode and an enzyme. To date, there has been no irrefutable proof to support either of the proposed mechanisms, namely homogeneous mediation or heterogeneous redox catalysis. The experimental observations that have led to the proposal of these theories are outlined below, and a theoretical description of each mechanism is given. A number of cases are found for each theory. Each case will predict some or no dependence of the electrode current on the four experimental variables: the concentrations of enzyme and substrate, the rotation speed of the electrode and the potential at which the electrode is held.

Experimental data obtained from a rotating TTF TCNQ disc electrode with glucose oxidase are presented and analysed according to the two theories. These data may traverse a number of cases and determination of the variation of the electrode current with the experimental variables will allow the case or cases which best fit the experimental data to be identified. Comparison of the analyses allows the validity of each theory to be determined.

4.2 Current understanding of the mechanism

The first work on conducting organic salt enzyme electrodes was carried out by J.J. Kulys in 1980 [61]. Kulys measured the second order rate constants for the oxidation of reduced glucose oxidase by the various electron acceptors that could exist on either an NMP TCNQ or NMA TCNQ (N-methyl acridinium tetracyanoquinodimethane) electrode [70]. The maximum second order rate constant observed was 3 $x10^6$ $M^{-1}s^{-1}$ for $TCNQ^o$. Kulys proposed that species from the electrode dissolved into the solution and acted as mediators for the electron transfer between the reduced enzyme and the electrode. He gave a mathematical treatment for the saturated electrode response and using this the concentration of mediator required for the observed saturation current was calculated. This concentration was 13.5 μM for $TCNQ^o$.

Subsequent work by the enzyme electrode group at Imperial College, London discredited the mediated theory. Ring-disc experiments with NMP TCNQ gave no current, placing an upper limit on the mediator concentration of less than 10^{-6} M [62]. This concentration of mediator was too low to explain the observed currents by the mediated theory. Consequently it was assumed that the electron transfer reaction between the enzyme and the electrode was direct [62,93].

However later work on single crystals of TTF TCNQ carried out by P.N. Bartlett gave a half order dependence on enzyme concentration [72]. This was inexplicable by the direct electron transfer theory, which proposed a first order dependence on enzyme concentration. However it could be explained by the mediated theory, although the original objections to this theory remained. Also electron microscopy

of the electrode surface did not discount the possibility of the mediated electron transfer theory of Kulys occurring [section 3.5.4]. Thus neither theory was supported conclusively.

Consequently a new theory was proposed by W.J. Albery to explain the half order dependence on enzyme concentration observed by P.N. Bartlett. This mechanism was called heterogeneous redox catalysis. It proposed that the electrode material could dissociate into neutral species on the electrode surface. The donor species (A) would be oxidized at the electrode while the acceptor species (D) would be reduced by the reduced enzyme. The resultant A^+ and D^- species would then recombine. The limited solubility of these species would result in all reactions taking place on, or in a very small reaction layer next to, the electrode surface.

B.J. Driscoll of Imperial College, London has used a rotating TTF TCNQ electrode with glucose oxidase under saturated electrode conditions to investigate the homogeneous mediation and the heterogeneous redox catalysis mechanisms [79]. The dependences of the electrode current on the concentration of the enzyme, the rotation speed of the electrode and the potential of operation were measured and comparisons made between the observed and the theoretical dependences. He concluded that neither model was favoured conclusively. Both models could adequately explain the dependence of current on each of these variables taken in isolation but not as a whole. Diagnostic plots favoured homogeneous mediation, although potential dependence was best explained by heterogeneous redox catalysis. Thus it was concluded that a more rigorous investigation of these theories was necessary.

It was proposed that the dependence of the electrode on substrate concentration, in addition to the other parameters used by B.J.

Driscoll above, would yield more conclusive evidence. The pattern of change of dependencies over a wide range of concentrations of enzyme and substrate, in addition to the change in dependence on rotation speed, would allow a much better assignment of the theoretical cases to experimental data. In this chapter, work of this type is presented and analysed according to the two theories.

4.3 Introduction to the theories

In this section, the two theories are outlined to show how they may be applied to experimental data. The two complete theories are given in the Appendices A and B. Each theory gives a mathematical solution for the flux of electrons at the electrode in terms of three dimensionless parameters. The relative sizes of these parameters allow particular cases to be derived. There are seven cases for the homogeneous mediation theory and six for the heterogeneous redox catalysis theory. Certain cases may be eliminated for the particular experimental conditions employed in this thesis. Analysis of the experimental data will show that this is justifiable.

4.3.1 Introducing the homogeneous mediation mechanism

For the work in this thesis, the source of mediator is the electrode itself, and the bulk concentrations of the reduced and oxidized forms of the mediator are zero. It should be noted that the analysis can also be made applicable to the case where the mediator is supplied from the bulk of solution, where it is present in the reduced form.

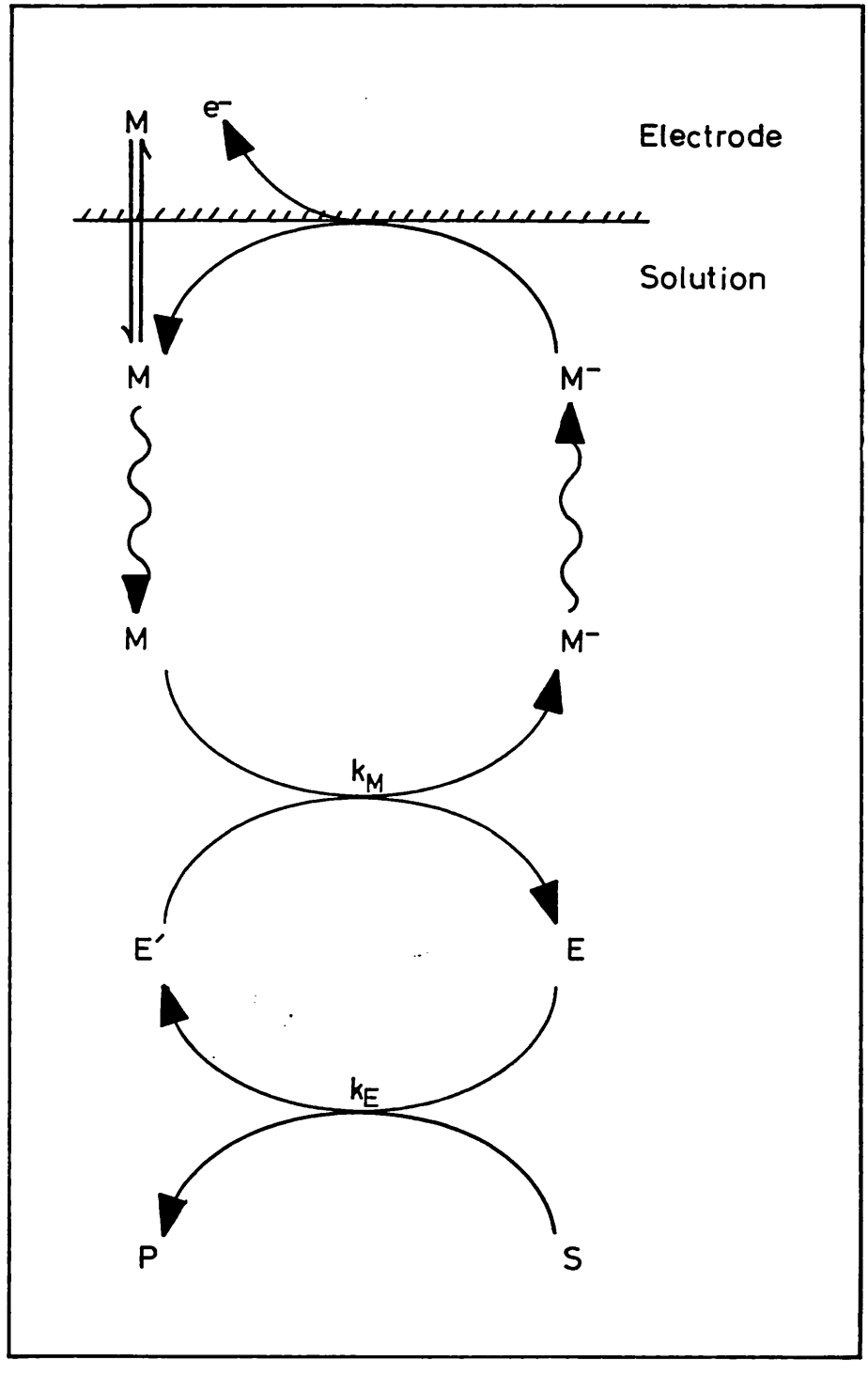
The scheme for the homogeneous mediation model is shown in fig(4.1). Mediation is assumed to take place in the solution. Enzyme reacts with substrate with the Michaelis-Menten rate constant, k_E:

$$k_E = k_{cat} [S] / (K_M + [S]) \ .$$

If the enzyme is unsaturated, $k_E = (k_{cat}/ K_M) [S]$ (it will be shown below that this is a reasonable approximation). If the enzyme is saturated, $k_E = k_{cat}$. It is assumed that [S] is large enough for no concentration polarization of substrate to occur in the diffusion layer of the electrode. Confirmation of this assumption is given in section 4.5.8.1.

It is assumed that the concentration of substrate is large enough for all the enzyme in the bulk solution to be present in the reduced form. Reduced enzyme reacts with mediator, M , in solution, with the second order rate constant k_M. The reduced mediator, M' , is then reoxidized at the electrode surface. It is assumed that this reaction is fast and not rate limiting, and that all M' reaching the electrode is oxidized.

The mathematical treatment of this mechanism is given in Appendix A. The differential equations describing the diffusion and reaction kinetics of all M and E species are expressed in dimensionless variables (eqn.s (A.15) and (A.16)); application of the boundary conditions gives an expression for the concentration gradient of reduced mediator at the electrode surface, $(\delta u'/\delta \chi)_0$ (eqn. (A.24)). This expression may be solved for various cases and boundaries between cases, depending on the relative sizes of the dimensionless variables κ_E, κ_M and γ. Placing the solution into eqn.



Fig(4.1) The scheme for the homogeneous mediation mechanism.

(A.20) then gives the flux of electrons at the electrode for each case or case boundary.

The seven cases obtained from considering the relative sizes of these variables are shown in fig(A.9); $\gamma > 1$ throughout. This form of the case diagram is not very amen able to use, since all three axes, $\log \kappa_E$, $\log \kappa_M$ and $\log \gamma$ depend on an experimental variable, ([S], [E] and [S] respectively). Thus in order to follow a change in both [E] and [S] would involve a translation in a 3- dimensional diagram, which would be difficult to visualize. Therefore the case diagram is redrawn in the new co-ordinates $\log (1/ \gamma)$, $\log \beta$ and $\log \phi$, where:

$$1/ \gamma = k_E / k_M m_o$$

$$\beta = D_E e_\Sigma / D_M m_o$$

and

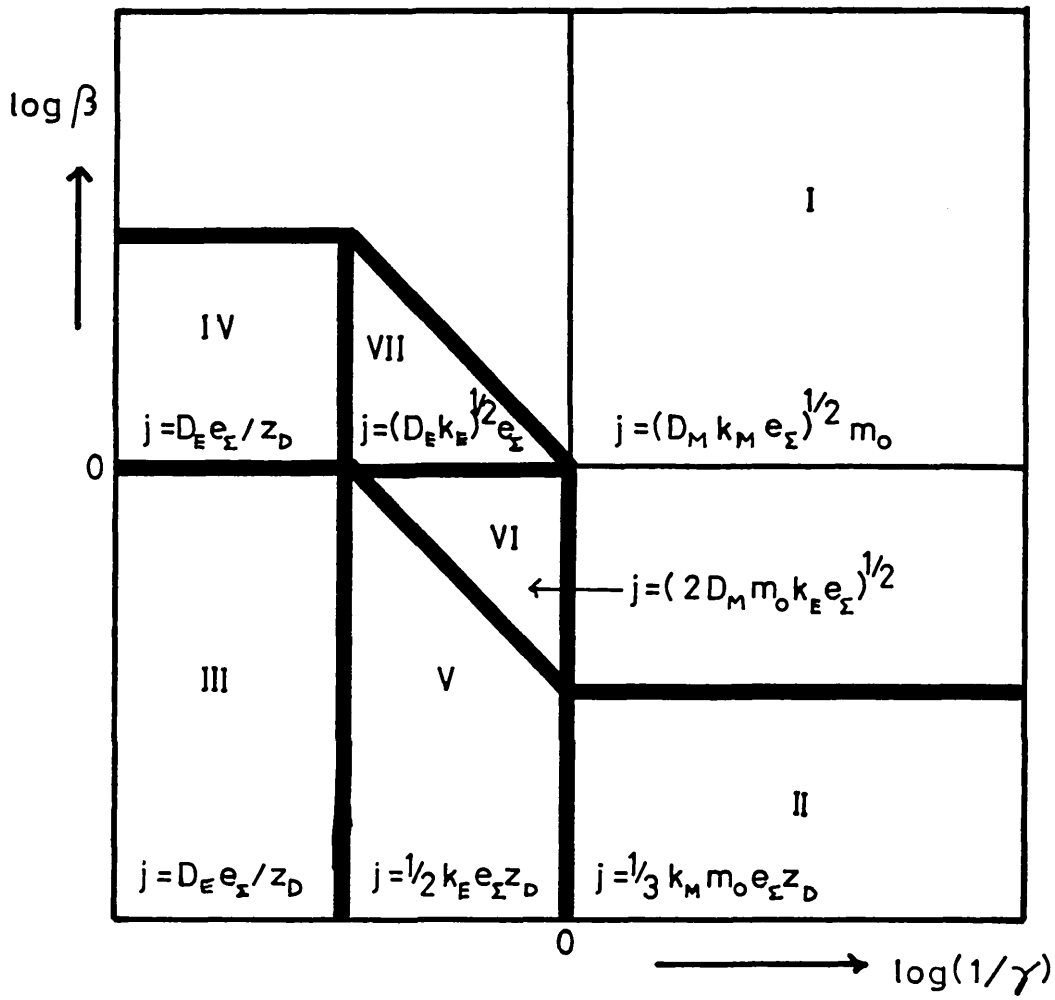
$$\phi = k_M m_o z_D^2 / D_E .$$

$1/ \gamma$ depends on [S] , β depends on [E] and ϕ is independent of both [E] and [S]. The new case diagram is shown in fig(4.2); $\phi > 1$ throughout.

The values of $1/ \gamma$, β and ϕ can be calculated for the particular experimental conditions used in this thesis. This allows the most likely position of the experimental data in the case diagram to be identified. z_D is given by [126] :

$$z_D = 0.643 \, \nu^{1/6} D^{1/3} \omega^{-1/2} \quad . \qquad (4.1)$$

ν, the kinematic viscosity, is typically 0.01 $cm^2 s^{-1}$ [127]. Values for D for various species are given in table 4.1 where known. The values



Fig(4.2) The case diagram for the homogeneous mediation mechanism : the $\phi >> 1$ plane.

Species	10^7 D/ $cm^2 s^{-1}$
Glucose oxidase	4.1 [128]
TTF^+	60 [129]
glucose	67 [112]

Table 4.1 Values of D for various species

Species	10^4 k_M / $mol^{-1}dm^3 s^{-1}$
TTF^+	"efficient" [130]
$TCNQ^o$	300 [70]
$TCNQ^-$	6.6 [70]

Table 4.2 Values of k_M for various mediator species where known

of D for TTF^{o}, $TCNQ^{o}$ and $TCNQ^{-}$ do not appear to have been measured, although it may be assumed that the values would be approximately the same as for TTF^{+} since the species are similar in size and not highly charged. Then using D for glucose oxidase, z_D (at ω = 1 Hz) is 2.2 x 10^{-3} cm.

The value of m_o is assumed to be less than 10^{-6} M (see section 4.2). The values of k_M for various mediator species are given in table 4.2 . We shall assume a maximum value of 3 x 10^{6} $M^{-1}s^{-1}$ for k_M in all these calculations. For glucose oxidase, k_{cat} is 3400 s^{-1} [131] and K_M is 33 mM [128] (for pH 5.6 and 25°C in the presence of air). Then ϕ is typically $\approx$ 3 - 21 (no units). The assumption that the $\phi > 1$ plane should be used is corroborated. Note that the uncertainty in m_o and k_M does not allow very accurate calculation of the theoretical parameters.

The range of e_Σ values used is 2.5 x10^{-12} - 5 x10^{-9} mol cm^{-3} , assuming the molecular weight of glucose oxidase is 186,000 [128]. Then β is between 2.0 x10^{-4} - 0.41 i.e. $\beta < 1$, and we may confine our consideration of the case diagram to those cases below this value of β. Again the inaccuracy in the calculation due to m_o should be noted.

The range of [S] used is 0.01 - 200 mM, giving the range of $1/\gamma$ between $\approx$ 0.3 - 1000. Then $\gamma < \phi$ always and we can confine our consideration of the ($1/\gamma$) axis to cases where ($1/\gamma$) > ($1/\phi$). It should be noted that the line ($1/\gamma$) = 1 can be crossed on increasing [S] if a very low initial [S] , i.e. 0.01 mM, is used.

If $1/\gamma$ = 1, then $k_M m_o = k_E$ and using the values given above, this occurs when [S] $\approx$ 0.03 mM. This is much less than K_M , and so the approximation made above for the unsaturated enzyme rate constant is reasonable. This approximation applies to cases V, VI and VII, all of which are to the left of the line ($1/\gamma$) = 1 and include the term k_E

in the expression for the electrode flux. For cases to the right of this line (i.e. higher [S]), k_E is not important and this implies that for the particular conditions used in this thesis, only the unsaturated enzyme kinetics can be rate determining. Note that for another enzyme with a different K_M / k_{cat} value, the saturated enzyme kinetics may be possible before the line $(1/ \gamma) = 1$ is crossed.

Then in conclusion, $\phi > 1$, so we are restricted to the $\phi > 1$ plane. Also, $\beta << 1$ and $(1/ \gamma) > (1/ \phi)$. Thus it is seen from fig(4.2) that the most likely cases to occur are cases I, II, V and VI. It should be noted that since both ϕ and γ depend on $k_M m_o$, the ratio of ϕ to γ is independent of $k_M m_o$. Thus the experiments should always be described by cases to the right of the line $1/ \phi = 1/ \gamma$.

The dependence of current on [E], [S] and ω are shown in table 4.3 for each of the cases. Plots of the current against the experimental variables raised to the relevant orders will be made to determine which cases are most likely to describe the experimental data.

In the second part of the analysis, each set of data is fitted to a theoretical curve describing the boundary between two cases. For experiments involving increasing [S] , the boundaries of interest will be the case V - II boundary, the case V - VI boundary and the case VI - I boundary. For experiments involving increasing [E], the boundaries of interest are the case V - VI boundary and the case II - I boundary.

4.3.1.1 The case V - VI boundary

The case V - VI boundary is unique in this theory; there is a sharp transition between cases V and VI, and no expression exists for

Case	order wrt [E]	order wrt [S]	order wrt ω
I	+1/2	0	0
II	1	0	-1/2
III & IV	1	0	+1/2
V	1	1	-1/2
VI	+1/2	+1/2	0
VII	1	+1/2	0

Table 4.3 Dependence of current on [E], [S] and ω according to the homogeneous mediation theory
(wrt = with respect to)

the boundary between the two cases. For all other boundaries between cases, the transition is more gradual. In case V, j is described by eqn. (A.42):

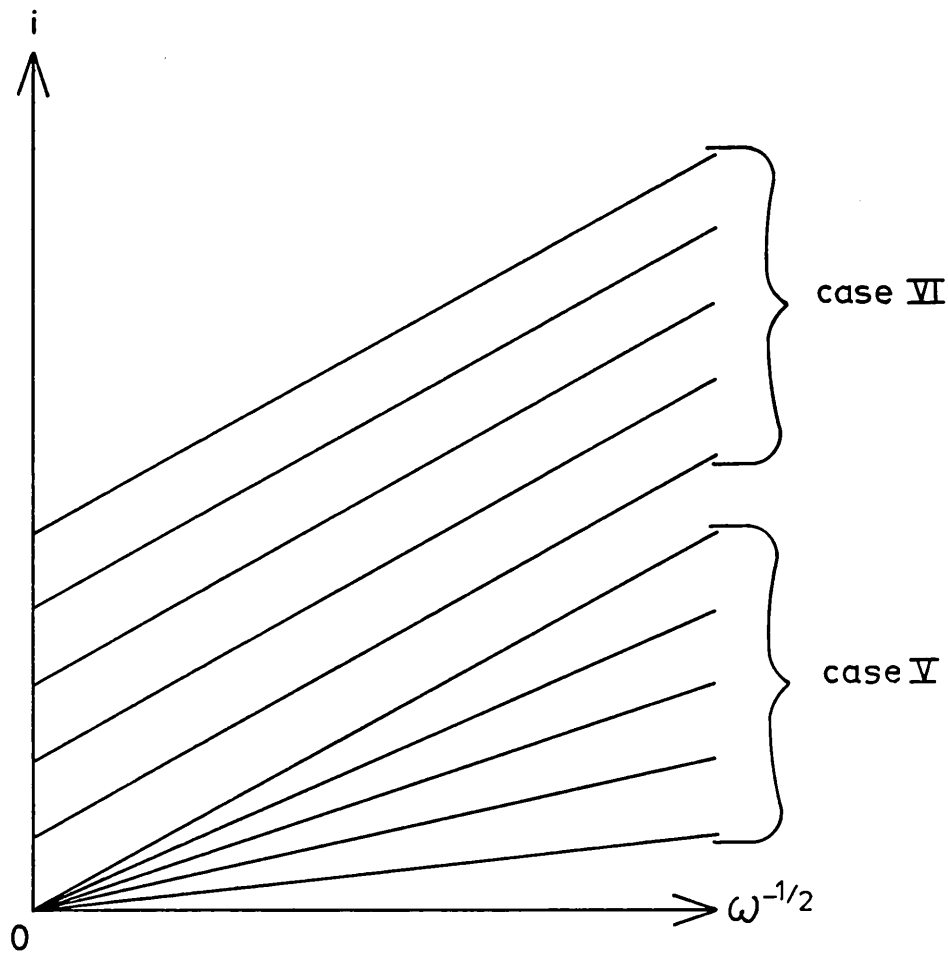
$$j = 1/2\ n\ k_E\ e_\Sigma\ z_D \quad . \qquad (\ 4.2\ )$$

In case VI, j is described by eqn. (A.51):

$$j = n\ (\ 2\ D_M\ m_o\ k_E\ e_\Sigma\ )^{1/2} - (\ n\ D_M\ m_o\ )\ /\ z_D \qquad (\ 4.3\ )$$

where j is related to i by j = i/FA (A is the area of the electrode) and z_D is related to ω by eqn. (4.1).

Then in case V, plotting i vs. $\omega^{-1/2}$ for successive concentrations of S or E should result in a series of straight lines passing through the origin, with gradients increasing linearly with concentration of species being varied. In case VI, the dependence on rotation speed is given by the second term in eqn. (4.3). The inverse dependence on z_D results in this term increasing with ω; however since it is subtracted from the first term in eqn. (4.3), the observed rotation speed dependence will be inversely dependent on ω. Plotting i vs. $\omega^{-1/2}$ will result in a straight line with a positive intercept on the i axis, the magnitude of which is given by the first term and will depend on either $[\ E\ ]^{1/2}$ or $[\ S\ ]^{1/2}$, depending on which is being varied. The gradient of the line is given by the second term and should be constant with respect to [E] and [S]. Thus the transition between cases V and VI may be observed by plotting i vs. $\omega^{-1/2}$. The predicted plot for the case V - VI boundary is shown in fig(4.3).



Fig(4.3) The predicted plot for the case V - VI boundary.

4.3.1.2 The case VI - I boundary

The case VI - I boundary is described by eqn. (A.82):

$$(\delta u'/\delta \chi)_o = \{ (2\kappa_M/\gamma) [1- 1/\gamma \ \ln (1 + \gamma)] \}^{1/2} - 1 \qquad (4.4)$$

leading to:

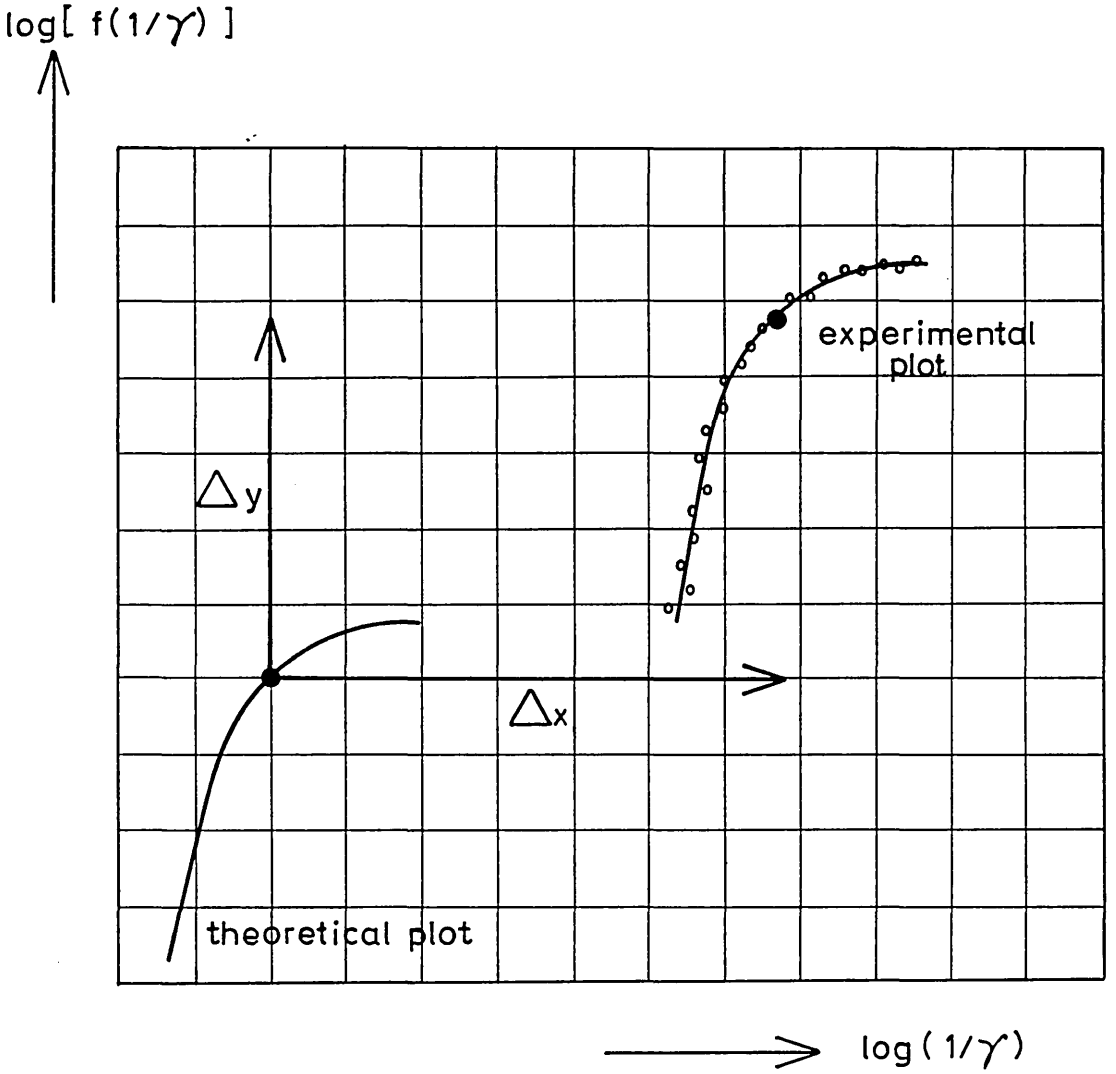
$$j = 2n(D_M m_o^2 k_M e_\Sigma)^{1/2} [1/\gamma - 1/\gamma^2 \ln (1 + \gamma)]^{1/2} - nD_M m_o/z_D \ . \qquad (4.5)$$

Only the second term in eqn. (4.5) is dependent on ω. Plotting i vs. $\omega^{-1/2}$ for increasing values of [S] should give a series of straight lines with constant gradients and increasing intercepts on the i-axis, denoted i_o:

$$i_o = 2nAF (D_M m_o^2 k_M e_\Sigma)^{1/2} [1/\gamma - 1/\gamma^2 \ln (1 + \gamma)]^{1/2} \ . \qquad (4.6)$$

The dependence of i_o on [S] is given by the terms in γ . This term cannot be accurately evaluated since it is a complex function, involving the unknown variables $k_M m_o$ in the γ term. A theoretical plot must be made of $\log[1/\gamma - 1/\gamma^2 \ln (1 + \gamma)]^{1/2}$ vs. $\log (1/\gamma)$. The experimental data are plotted as $\log (i_o / e_\Sigma^{1/2})$ vs. $\log [S]$. The experimental plot is fitted to the theoretical plot by translational movements in the direction of the x- and y- axes. This is shown schematically in fig(4.4).

The values of Δx and Δy allow calculation of the unknown variables $k_M m_o$ and $D_M m_o^2 k_M$ respectively. This can be seen by taking the log of eqn. (4.6) above:



Fig(4.4) Fitting theoretical data to experimental data for the case VI - I boundary.

$$\log (i_o / e_\Sigma^{1/2}) = \log [2nAF (D_M m_o^2 k_M)^{1/2}] + \log [1/\gamma - 1/\gamma^2 \ln (1 + \gamma)]^{1/2} . \quad (4.7)$$

Then Δy is given by:

$$\Delta y = \log [2nAF (D_M m_o^2 k_M)^{1/2}] , \quad (4.8)$$

and $D_M m_o^2 k_M$ may be calculated. Similarly, taking the log of $1/\gamma$ gives:

$$\log (1/\gamma) = \log [S] + \log (k_{cat}/ K_M k_M m_o) , \quad (4.9)$$

and Δx is given by:

$$\Delta x = \log (k_{cat}/ K_M k_M m_o) . \quad (4.10)$$

Thus $k_M m_o$ can be calculated. The ratio of this value to that for $D_M m_o^2 k_M$ will give $D_M m_o$.

4.3.1.3 The case V - II boundary

The case V - II boundary is described by eqn. (A.78):

$$(\delta u'/\delta \chi)_o = (\kappa_M/ \gamma) [1/2 - 1/\gamma - 1/\gamma^2 \ln (1 + \gamma)]. \quad (4.11)$$

This gives the expression for i as:

$$i = nAF (k_M m_o e_\Sigma z_D)[1/(2 \gamma)- 1/\gamma^2 - 1/\gamma^3 \ln (1 + \gamma)] . \quad (4.12)$$

As for the case VI - I boundary, the dependence of i on [S] is given by the γ terms and cannot be calculated. Then substituting for z_D using eqn. (4.1) and taking logs of both sides gives:

$$\log (i/ \omega^{-1/2} e_\Sigma) = \log nAF (0.643 \nu^{1/6} D^{1/3} k_M m_o) + \log [1/2 \gamma - 1/\gamma^2 - 1/\gamma^3 \ln (1 + \gamma)]. \quad (4.13)$$

A theoretical plot of $\log [1/(2 \gamma) - 1/\gamma^2 - 1/\gamma^3 \ln (1 + \gamma)]$ vs. $\log (1/ \gamma)$ is made and a fit made to the experimentally determined plot of $\log (i/ \omega^{-1/2} e_\Sigma)$ vs. log [S].

Δx is obtained as for the case VI - I boundary. Δy is given by :

$$\Delta y = \log nAF (0.643 \nu^{1/6} D^{1/3} k_M m_o) . \quad (4.14)$$

$k_M m_o$ can be calculated from Δx and from Δy as before.

4.3.1.4 The case II - I boundary

The case II - I boundary is given by eqn. (A.26):

$$(\delta u'/\delta \chi)_o = \kappa_M^{1/2} \coth (\kappa_M^{1/2}) - 1 . \quad (4.15)$$

i is given by:

$$i = nAF D_M m_o/ z_D [\kappa_M^{1/2} \coth (\kappa_M^{1/2}) - 1] . \quad (4.16)$$

Dividing both sides by $\kappa_M^{1/2}$ and rearranging eqn. (4.16) gives:

$$(i / nAF)(D_M m_o^2 k_M e_\Sigma)^{-1/2} = \coth (\kappa_M^{1/2}) - \kappa_M^{-1/2}. \qquad (4.17)$$

The function coth ($\kappa_M^{1/2}$) cannot be evaluated, since it involves the unknown variables k_M and D_M . Then a theoretical plot of log [coth ($\kappa_M^{1/2}$) - $\kappa_M^{-1/2}$] vs. log (κ_M) is made and compared with an experimentally determined plot of log (i/ $e_\Sigma^{1/2}$) vs. log (e_Σ/ ω) .

Δx and Δy are given by:

$$\Delta x = - \log [0.643 \, k_M \nu^{1/6} D^{1/3} / D_M] , \qquad (4.18)$$

and

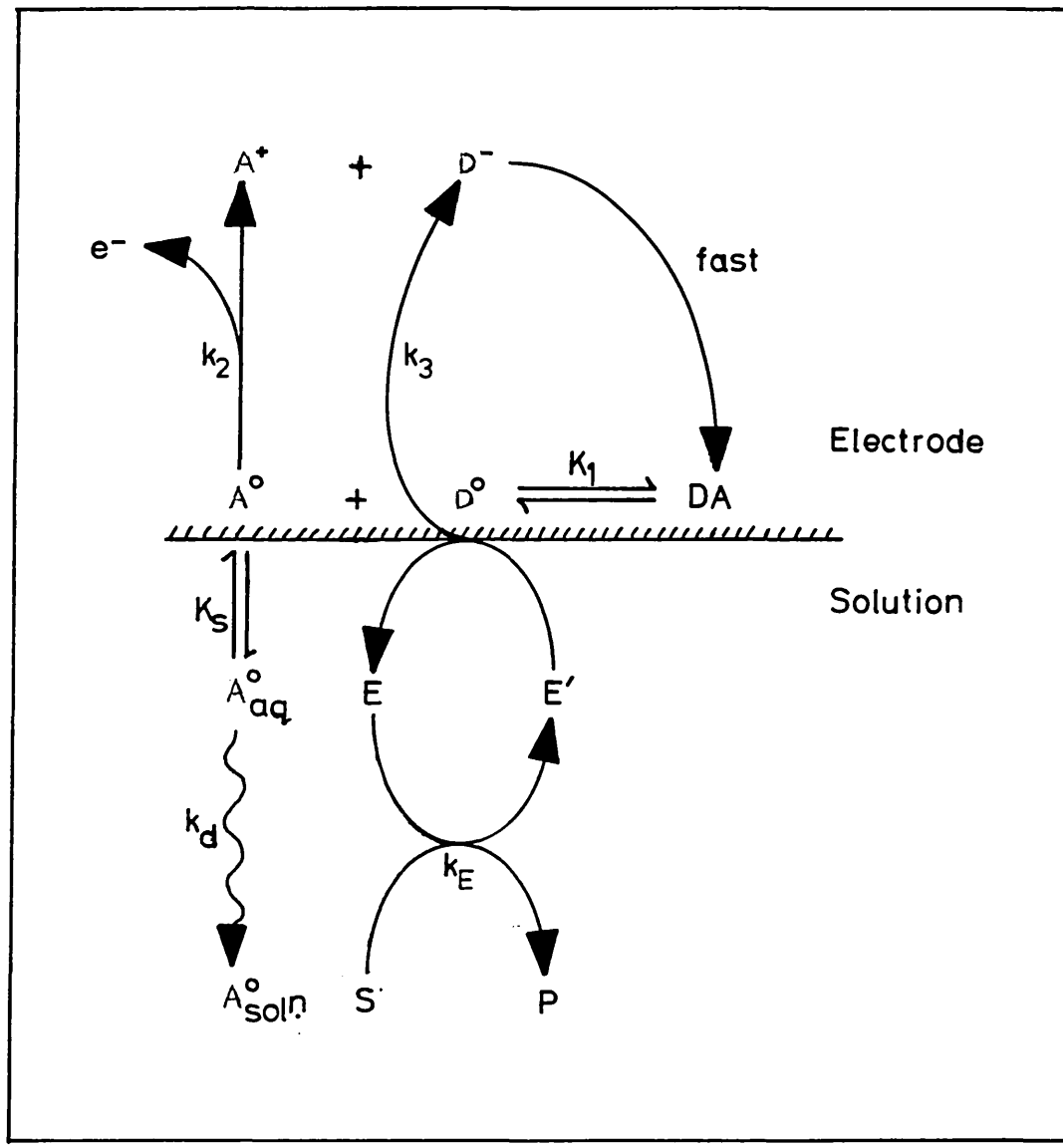
$$\Delta y = \log [nAF (D_M k_M m_o^2)^{-1/2}] . \qquad (4.19)$$

From Δx , k_M/ D_M and from Δy, ($D_M k_M m_o^2$) can be obtained.

4.3.2 Introducing the heterogeneous redox catalysis mechanism

The reaction scheme for heterogeneous redox catalysis is shown in fig(4.5). The theory is outlined below, and given in greater detail in Appendix B.

It is assumed that on the surface of a conducting organic salt, $A^+ D^-$, there is a labile equilibrium involving the two energetic species A^o and D^o, described by the equilibrium constant K_1. A^o can be oxidized to A^+ at the electrode with the first order rate constant k_2. The reduced enzyme E' is oxidized by D^o with the second order rate constant k_3. E' may require more than one molecule of D^o for its oxidation. This is allowed for by introducing n, the number of D^o equivalents required, in the expression describing the flux of electrons. It is assumed that the removal of only the first electron



Fig(4.5) The scheme for the heterogeneous redox catalysis mechanism.

from the enzyme is rate limiting. The A^+ and D^- formed on the surface by the k_2 and k_3 reactions will combine readily to form the original salt. This recombination reaction is not assumed to be rate limiting.

So far all reactions have been assumed to take place on the electrode surface; this does not allow any rotation speed dependence of the observed current. Then to introduce the possibility of rotation speed dependence, it is assumed that A^o can be lost from the electrode surface by dissolving into the solution and diffusing away from the electrode. K_S (cm^{-1}) describes the solubility of A^o and k_D ($cm\ s^{-1}$) is the mass transfer rate constant for A^o :

$$k_D = D_A / z_D \tag{4.20}$$

where D_A is the diffusion coefficient of A and z_D is the thickness of the diffusion layer. In the steady state, the flux of A^o dissolving in the solution must be matched by an equal flux of D^- leaving the electrode surface.

In the solution, enzyme E reacts with its substrate S, regenerating E' and product P. The rate of the enzyme reaction is described by k_E , which is the normal Michaelis Menten expression:

$$k_E = k_{cat} [S] / (K_M + [S]) \ . \tag{4.21}$$

It is assumed that the concentration of S is sufficiently large for there to be no concentration polarization of the substrate. The justification for this assumption is given in section 4.5.8.1.

The full mathematical treatment of this mechanism is given in Appendix B. The steady state fluxes at the electrode are considered,

and combined with an expression describing the diffusion and reaction kinetics of E'. The equations are expressed in terms of three dimensionless variables (consistent with the homogeneous mediation mechanism), κ_E , ρ and θ :

$$\kappa_E = k_E z_D^2 / D_E$$

$$\rho = (ne_\Sigma / K_1 k_2 k_3) (D_E / z_D)^2$$

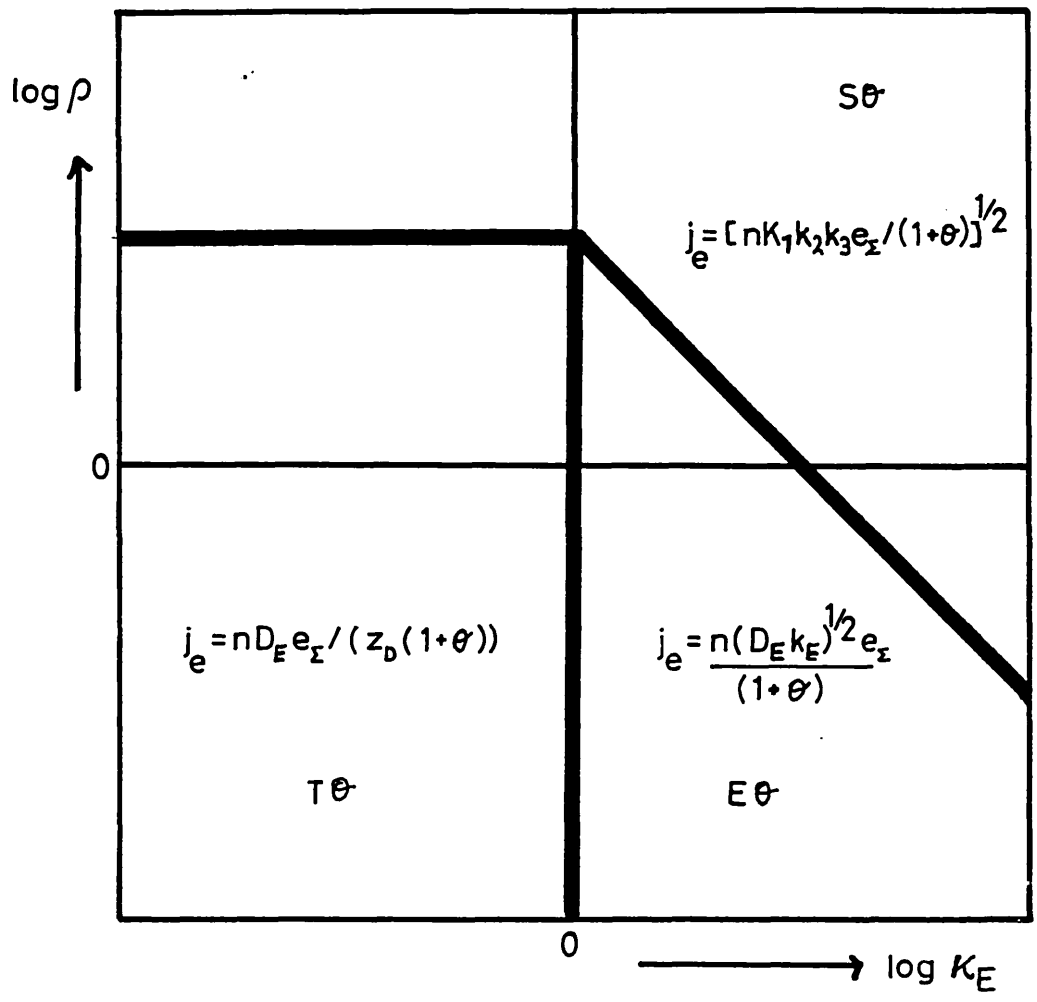
and

$$\theta = K_S k_d / k_2 .$$

Note that this expression for κ_E is identical to that in the homogeneous mediation theory.

An expression is obtained for $(\delta v / \delta \chi)_0$, the concentration gradient of E' at the electrode surface. This is then used to find an expression for f, a dimensionless parameter in the expression for j_e , the flux of electrons at the electrode surface. The parameter f is dependent on the three dimensionless variables mentioned above, and the relative sizes of these variables will determine individual cases in the case diagram. The three theoretical variables can be used to construct a three-dimensional case diagram with the x , y and z axes represented by κ_E , ρ and θ respectively. Depending on the size of the variables, six cases are obtained. Three of the cases are shown in fig(4.6), for the $\theta >> 1$ plane. They are denoted Tθ, Eθ and Sθ.

We can attempt to find our position on the case diagram by calculating the dimensionless parameters, as for the homogeneous mediation case diagram (section 4.3.2). The value of θ cannot be calculated from experimentally determined values, since K_S and k_2



Fig(4.6) The case diagram for the heterogeneous redox catalysis mechanism : the $\theta >> 1$ plane.

are unknown. However it will be seen that in all experiments, some degree of dependence of the current on the rotation speed is observed, and so it can be assumed that $\theta >> 1$ throughout. For the sake of completeness, the dependence of the case boundaries on θ is given in Appendix B. Similarly, ρ cannot be calculated since it depends on $K_1 k_2 k_3$, all of which are unknown.

However κ_E can be calculated, using the values for z_D , D_E , k_{cat} and K_M given in section 4.3.2. The range of values of [S] used is 0.01 - 200 mM, giving κ_E between 12.2 - 3.5 x 10^4 respectively (no units). Then $\kappa_E > 1$ always, and it is expected that the experimental data should be explicable by either the enzyme regeneration case (Eθ) or the surface kinetics case (Sθ).

The dependences of current on [E], [S] and ω are shown in table 4.4 for each of the three cases. Note that in case Eθ , the dependence of current on [S] is described by $k_E^{1/2}$, and hence could describe either unsaturated or saturated enzyme kinetics i.e. [S]$^{1/2}$ through to [S]^0. The dependence of the current on ω can be described by a range of values for each case since it is dependent on the magnitude of θ .

The preliminary analysis of plotting current vs. relevant order for each experimental variable allows the most likely theoretical case describing the data to be identified. The second part of the analysis is confined to cases Eθ and Sθ only, since $\kappa_E > 1$ always. Plots are made for the case boundary between Eθ and Sθ . There are two plots applicable, depending on whether the experimental variable is [E] or [S]. The plots are derived by considering eqn. (B.23) for $\kappa_E > 1$. Under this condition, $\tanh(\kappa_E^{1/2}) \approx 1$. Eqn. (B.23) then becomes:

$$f = (1/2\rho) \{ [1/\kappa_E + 4\rho/(1 + \theta)]^{1/2} - 1/\kappa_E^{1/2} \} . \quad (4.22)$$

Case	order wrt [E]	order wrt [S]	order wrt ω
Tθ	1	0	0 - +1/2
Eθ	1	+1/2 - 0	-1/2 - 0
Sθ	1/2	0	-1/4 - 0

Table 4.4 Dependence of current on [E], [S] and ω according to the heterogeneous redox catalysis theory

This equation can be rearranged and substitutions made for ρ , f and κ_E so that plots for data at constant [E] and constant [S] can be derived.

4.3.2.1 Heterogeneous plot for data at constant [E]

Eqn. (4.22) can be rearranged to give:

$$\rho f^2 + f/\kappa_E^{1/2} = 1/(1 + \theta) \quad . \tag{4.23}$$

Using eqn.s (B.21) and(B.18) for ρ and f, and substituting for κ_E this becomes:

$$j_e^2/ ne_\Sigma K_1 k_2 k_3 + j_e/ ne_\Sigma (D_E k_E)^{1/2} = 1/(1 + \theta) \quad . \tag{4.24}$$

This is rearranged and using eqn. (4.21) for k_E we obtain:

$$1/ j_e^2 = (1 + \theta)/ ne_\Sigma K_1 k_2 k_3 + (1 + \theta) [(K_M/k_{cat})^{1/2}/ j_e n D_E^{1/2} e_\Sigma] (1/[S] + 1/K_M)^{1/2}. \tag{4.25}$$

j_e is related to i by $j_e = i/AF$. Thus plotting $1/i^2$ vs. $1/i$ $(1/[S] + 1/K_M)^{1/2}$ should give a straight line for constant e_Σ . Now $\theta = (K_S D_A/k_2 z_D)$ so that $\theta_{9Hz} = 3\theta_{1Hz}$, since from eqn. (4.1) we see that z_D depends on $\omega^{-1/2}$. Thus the ratio of the gradients and of the intercepts are given by:

$$grad_{1Hz}/grad_{9Hz} = int_{1Hz}/int_{9Hz} = (1 + \theta_{1Hz})/(1 + \theta_{9Hz}) = (1 + \theta_{1Hz})/(1 + 3\theta_{1Hz}) \tag{4.26}$$

where grad and int denote gradient and intercept respectively. Thus θ_{1Hz} can be found and hence $K_1k_2k_3$ can be calculated from the intercepts.

4.3.2.2 Heterogeneous plot for data at constant [S]

For data at constant [S], we rearrange eqn. (4.24) to give:

$$j_e = nK_1k_2k_3/(1 + \theta)\,(e_\Sigma/j_e) - K_1k_2k_3/(D_Ek_E)^{1/2} \quad . \qquad (4.27)$$

Then plotting i vs. e_Σ/i should give a straight line. The ratio of the gradients at different rotation speeds enables θ_{1Hz} to be calculated as before (section 4.3.3.1). $K_1k_2k_3$ can be calculated from the gradient. k_E can be calculated from the intercept using the value of $K_1k_2k_3$ found from the gradient. The intercept is independent of e_Σ and ω and so should be constant for data at different ω. This a test of the validity of the plot.

4.4 Choice of experimental conditions

It should be realised that in order to correlate experimental results to theoretical cases, as many orders of magnitude of concentration as possible should be used, since the theoretical plots are sometimes made in logarithmic units. Thus in experiments varying [S] , concentrations from 0.01 to 200 mM were used, giving 4 orders of magnitude. Similarly in experiments varying [E], concentrations from 0.1 to 200 u/ml were used, giving three orders of magnitude. It should be noted that for constant [E] experiments,

the lowest concentration of enzyme that could give measurable responses at low [S] , i.e. 0.01 mM, was 1 u/ml. The highest [E] was fixed by the cost of the experiment. For constant [S] experiments, the lowest [S] that could be used was 0.5 mM ; any lower concentration would be consumed by the enzyme too quickly for the whole experiment to be completed.

Rotation speed dependence was observed measuring the steady state current at 1 Hz and 9 Hz, using 9 Hz as the baseline rotation speed, since it would enable better mixing of injections of substrate. Although using more rotation speeds would have increased the accuracy of the measured dependence on ω , it would also have significantly increased the time scale of the experiment, which was particularly crucial at low concentrations.

A complete set of experiments were carried out at two potentials It had been thought possible that changing the electrode potential could cause a switch over from one mechanism to the other. Thus the need for carrying out the experiment at different potentials was observed. The experiments were carried out at +200 mV and +300 mV wrt SCE ; these potentials were chosen since at high [S] , they gave a significant difference in current between otherwise identical experimental conditions. Working below +200 mV gives little difference in saturation current, while experiments above +300 mV are not possible due to decomposition of the electrode material outside its stable range. Experiments at +300 mV are most accurate since larger currents are obtained, and so the error in measuring responses is smaller.

Thus in total six experiments are reported for each potential: three at constant [E] and three at constant [S]. The experiments at constant [E] were carried out at 1, 5 and 50 u/ml GOD. The

Potential in mV	[S] : constant or variable ?	[E] : constant or variable ?	ω / Hz
+200	0.5 mM	variable	1 & 9
+200	5 mM	variable	1 & 9
+200	50 mM	variable	1 & 9
+200	variable	1 u/ml	1 & 9
+200	variable	5 u/ml	1 & 9
+200	variable	50 u/ml	1 & 9
+300	0.5 mM	variable	1 & 9
+300	5 mM	variable	1 & 9
+300	50 mM	variable	1 & 9
+300	variable	1 u/ml	1 & 9
+300	variable	5 u/ml	1 & 9
+300	variable	50 u/ml	1 & 9

Table 4.5 Experimental conditions for series of mechanistic experiments

experiments at constant [S] were carried out at 0.5, 5 and 50 mM glucose. For each experiment, the electrode current was measured at both 1 and 9 Hz. The complete set of experiments is shown in table 4.5.

4.4.1 Glucose oxidase

All the mechanistic experiments reported in Chapters 4 and 5 have been performed with the flavoenzyme glucose oxidase (GOD). Glucose oxidase (EC 1.1.3.4) catalyses the oxidation of glucose to gluconolactone:

$$\text{D-glucose} + O_2 \longrightarrow \text{gluconolactone} + H_2O_2 .$$

The enzyme is highly specific for the β anomer of D-glucose. It also oxidizes 2-deoxy-D-glucose, D-mannose, D-galactose and D-xylose, although the turnover numbers for these sugars are much lower [123]. The physiological electron acceptor is oxygen, although a number of mediators can also act as acceptors [38]. The reduced form of the enzyme is inactivated by H_2O_2 [132].

The cofactor for the enzyme is FAD: there are two molecules of firmly bound FAD per molecule of enzyme [128]. The molecular weight of the enzyme is 186,000 [128]. The enzyme is very stable and has a high specific activity, and its kinetics have been studied in great detail [123], [128] and [131]. It is also very cheap to buy, hence it is a good choice of flavoenzyme for use in these mechanistic experiments.

4.5 Preliminary analysis of results

In this section, the dependences of current on the experimental variables [E], [S] and ω are determined. For [E] and [S], plots are made of current against experimental variable to the appropriate order.' The best straight line is fitted to the data. The correlation coefficient for the line is calculated. For ω, this analysis is not appropriate and the data is presented as ω vs. log [S].

4.5.1 Dependence of current on [E]^1

At low concentrations of enzyme first order dependence is observed, shown in figs (4.7.a) - (4.7.f). Points at higher [E] have been omitted in order to display the data to its best advantage. The analyses of the data are given in table 4.6. Correlation coefficients are good.

Fig 4.7.a Plot of i vs. [E]
Data at +200 mV and 0.5 mM glucose

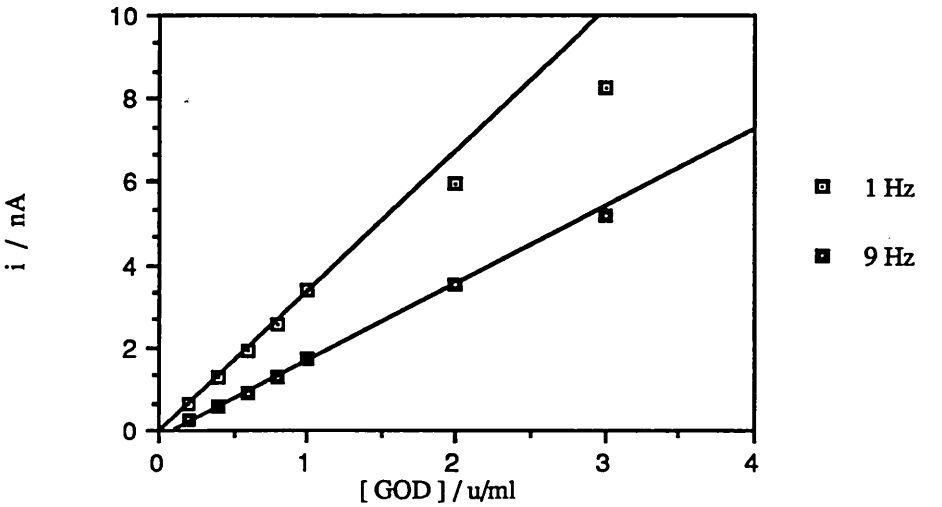


Fig 4.7.b Plot of i vs [E]
+200 mV and 5 mM glucose

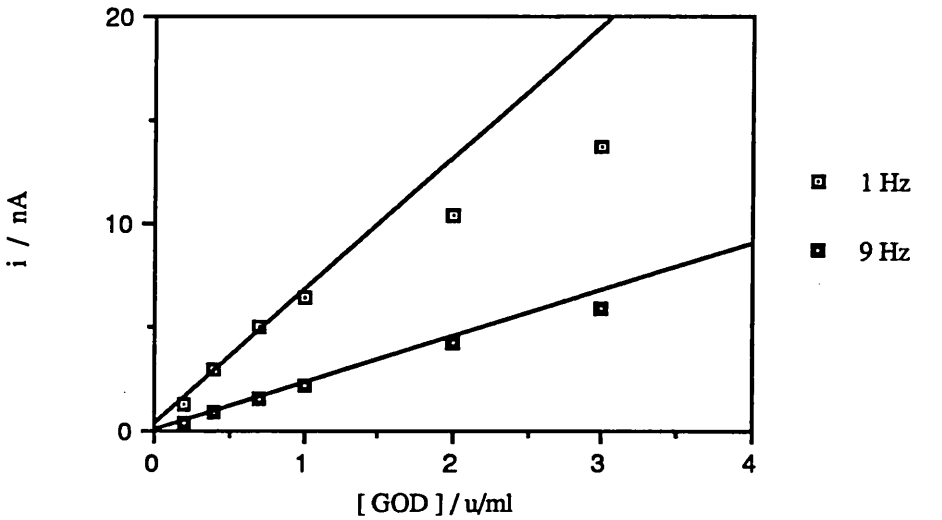


Fig 4.7.c Plot of i vs. [E]
Data at +200 mV and 50 mM glucose

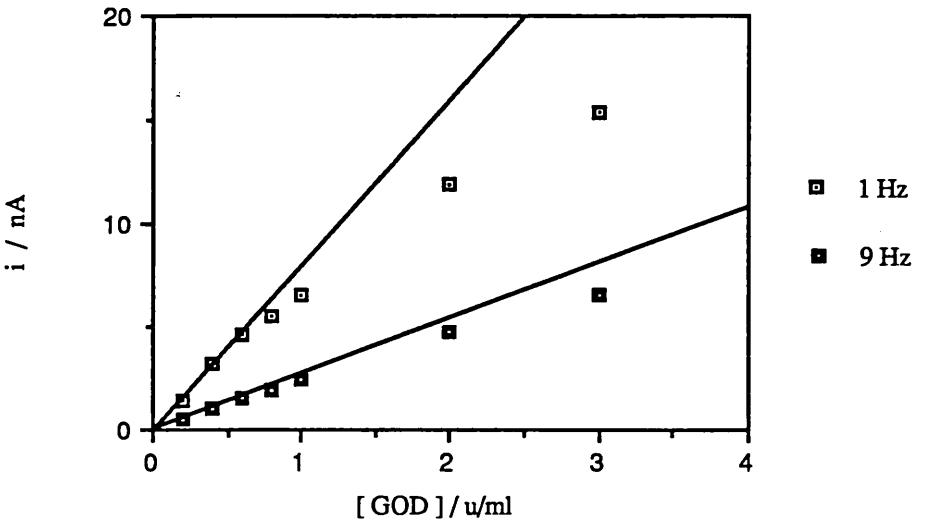


Fig 4.7.d Plot of i vs. [E]
Data at +300 mV and 0.5 mM glucose

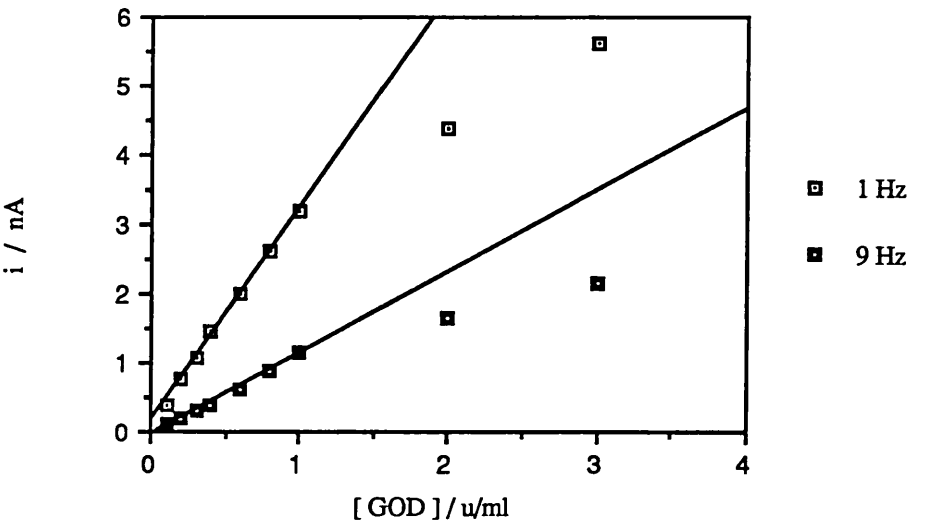


Fig 4.7.e Plot of i vs. [E]
Data at +300 mV and 5 mM glucose

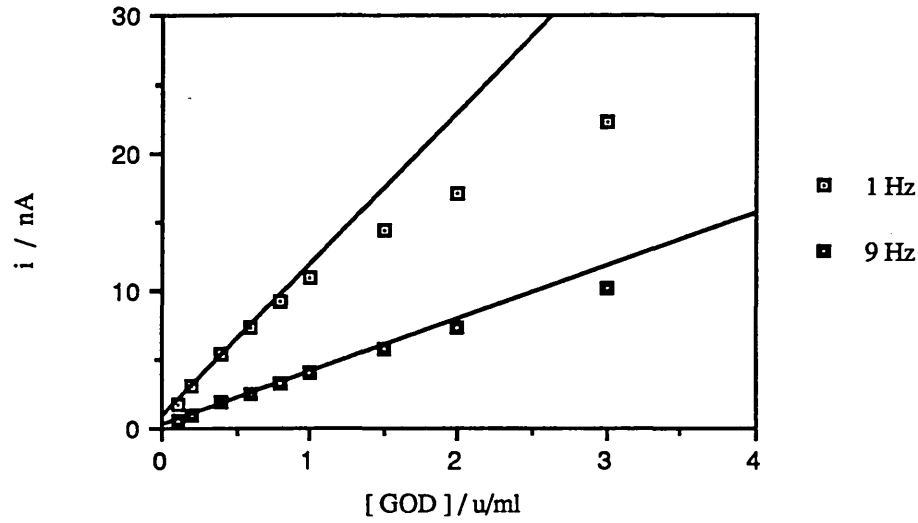
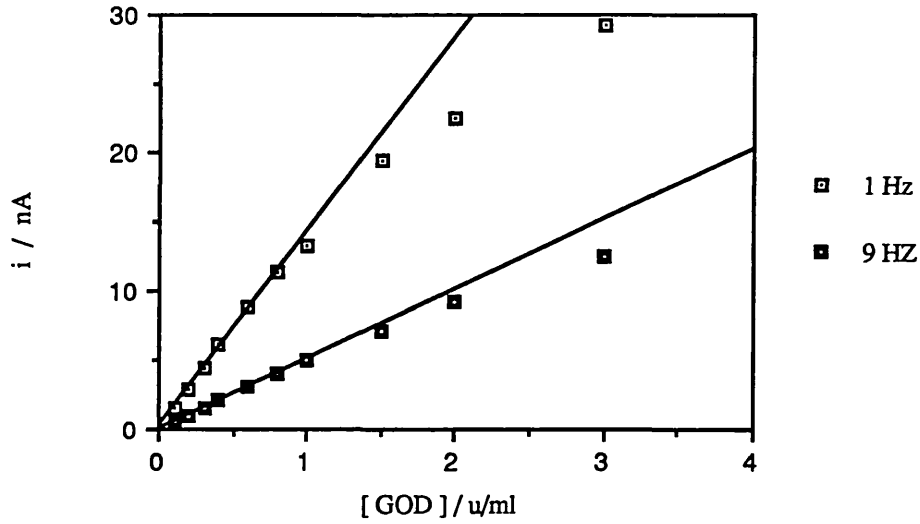


Fig 4.7.f Plot of i vs. [E]
Data at +300 mV and 50 mM glucose



E / mV	[S] / mM	ω / Hz	linear between? / u/ml	number of points	correlation coefficient
+200	0.5	1	0.2 - 1.0	5	0.99843
+200	0.5	9	0.2 - 1.0	5	0.99750
+200	5	1	0.2 - 1.0	4	0.99405
+200	5	9	0.2 - 1.0	4	0.99920
+200	50	1	0.2 - 0.6	3	0.99899
+200	50	9	0.2 - 0.6	3	0.99909
+300	0.5	1	0.1 - 1.0	7	0.99884
+300	0.5	9	0.1 - 1.0	7	0.99635
+300	5	1	0.1 - 0.6	4	0.99907
+300	5	9	0.1 - 0.6	4	0.99863
+300	50	1	0.1 - 0.8	6	0.99904
+300	50	9	0.1 - 0.8	6	0.99987

Table 4.6 Analysis of the plots of i vs. [E][1]

4.5.2 Dependence of current on [E]$^{1/2}$

Half order plots for the same experimental data are shown in figs (4.8.a) - (4.8.f), with values at higher [E] included. The plots are seen to give the best straight lines at higher concentrations. The analyses of the data are given in table 4.7. Again, correlation coefficients are good.

It should be noted that the experiments at +300 mV and 0.5 and 5 mM glucose show some drop in half order dependence above 20 and 50 u/ml respectively. This is most probably due to substrate depletion.

Thus it can be concluded that at low [E], first order dependence is observed while at higher [E], the dependence becomes half order, with intermediate orders of dependence between these two regions. The exact concentration at which the dependence changes between first order and half order cannot be determined accurately.

Fig 4.8.a Plot of i vs. [E]^0.5
Data at +200 mV and 0.5 mM

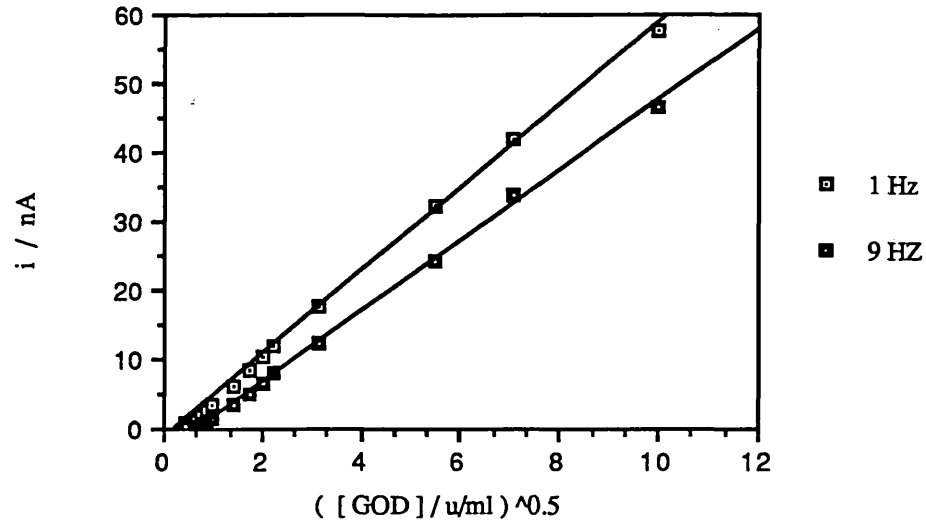


Fig 4.8.b Plot of i vs. [E]^0.5
Data at +200 mV and 5 mM glucose

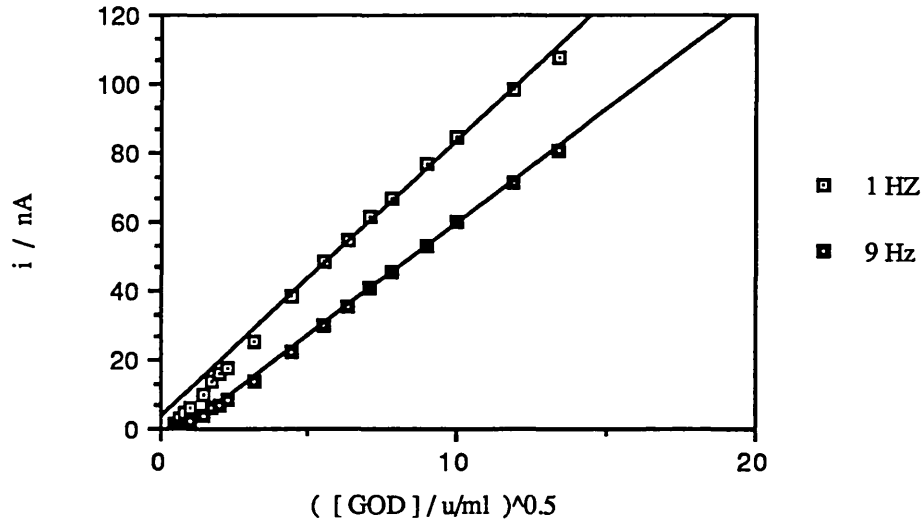


Fig 4.8.c Plot of i vs. [E]^0.5
Data at +200 mV and 50 mM glucose

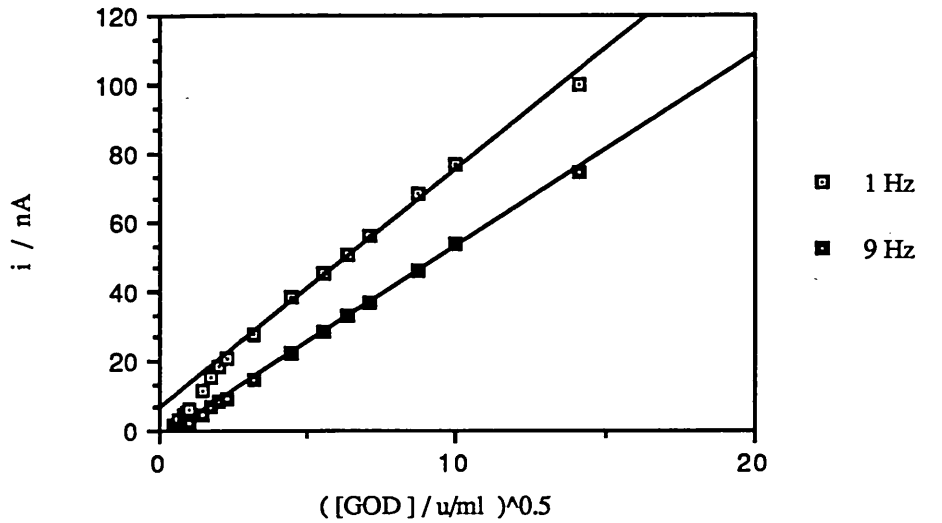


Fig 4.8.d Plot of i vs. [E]^0.5
Data at +300 mV and 0.5 mM glucose

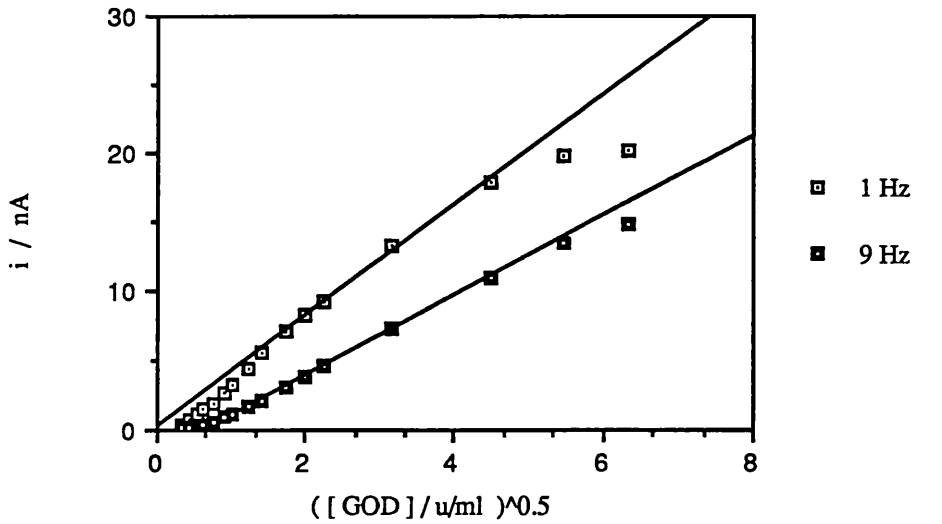


Fig 4.8.e Plot of i vs. [E]^0.5
Data at +300 mV and 5 mM glucose

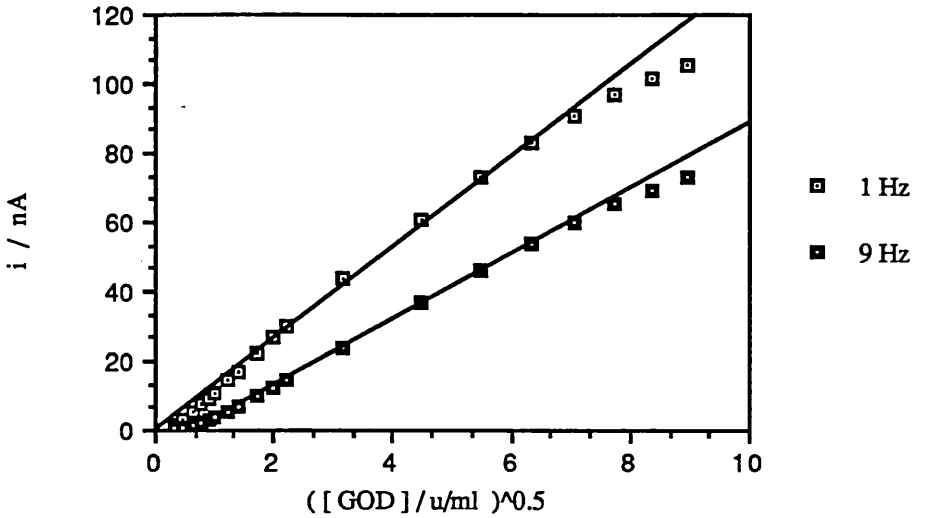
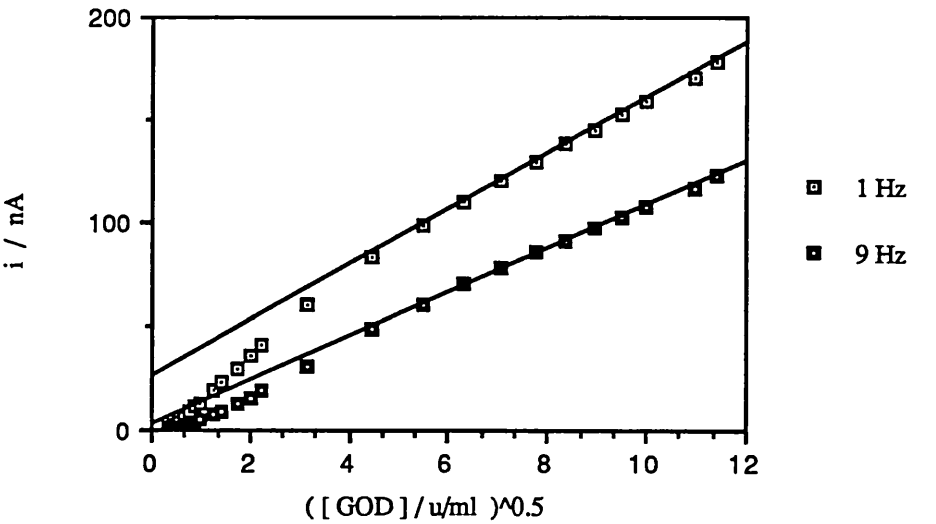


Fig 4.8.f Plot of i vs. [E]^0.5
Data at +300 mV and 50 mM glucose



E / mV	[S] / mM	ω / Hz	linear between? / u/ml	number of points	correlation coefficient
+200	0.5	1	4 - 100	6	0.99944
+200	0.5	9	4 - 100	6	0.99913
+200	5	1	10 - 180	10	0.99777
+200	5	9	10 - 180	10	0.99953
+200	50	1	3 - 200	11	0.99725
+200	50	9	3 - 200	11	0.99953
+300	0.5	1	2 - 20	6	0.99824
+300	0.5	9	2 - 20	6	0.99993
+300	5	1	1.5 - 50	10	0.99860
+300	5	9	1.5 - 50	10	0.99985
+300	50	1	20 - 130	11	0.99935
+300	50	9	20 - 130	11	0.99914

Table 4.7 Analysis of the plots of i vs. $[E]^{1/2}$

4.5.3 Dependence of current on [S]^1

We now turn to experiments carried out at constant [E]. First order plots at low [S] are shown in figs (4.9.a) - (4.9.f). At 1 and 5 u/ml, first order dependence is observed. For experiments at 50 u/ml, there is no first order dependence, although if more injections could have been made below 0.2 mM, first order dependence might have been observed. In practise this was not possible due to the substrate depletion effect observed at high [E].

The analyses of the data are given in table 4.8. Correlation coefficients are good.

Fig 4.9.a Plot of i vs. [S]
Data at +200 mV and 1 u/ml GOD

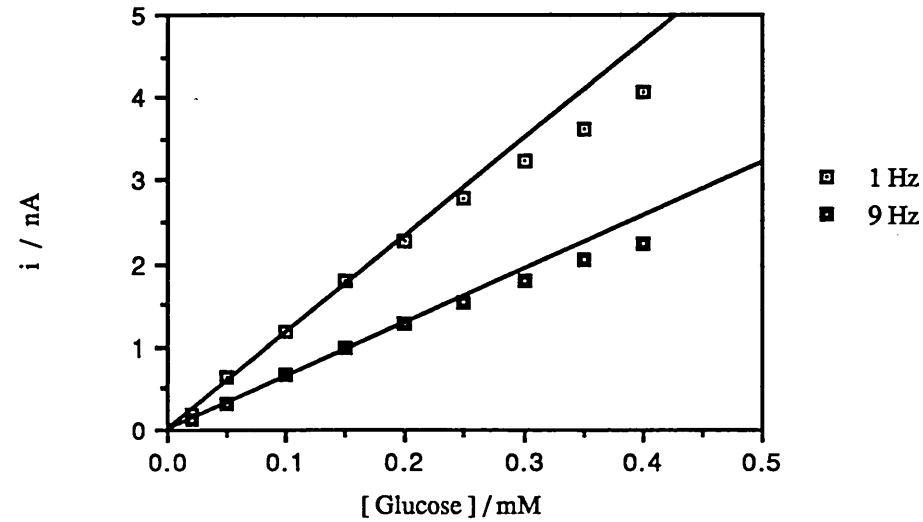


Fig 4.9.b Plot of i vs. [S]
Data at +200 mV and 5 u/ml

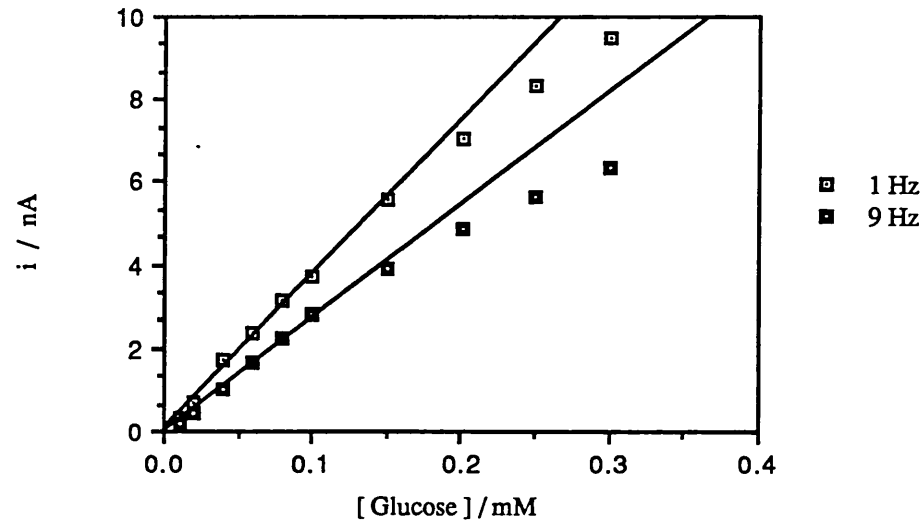


Fig 4.9.c Plot of i vs. [S]
Data at +200 mV and 50 u/ml GOD

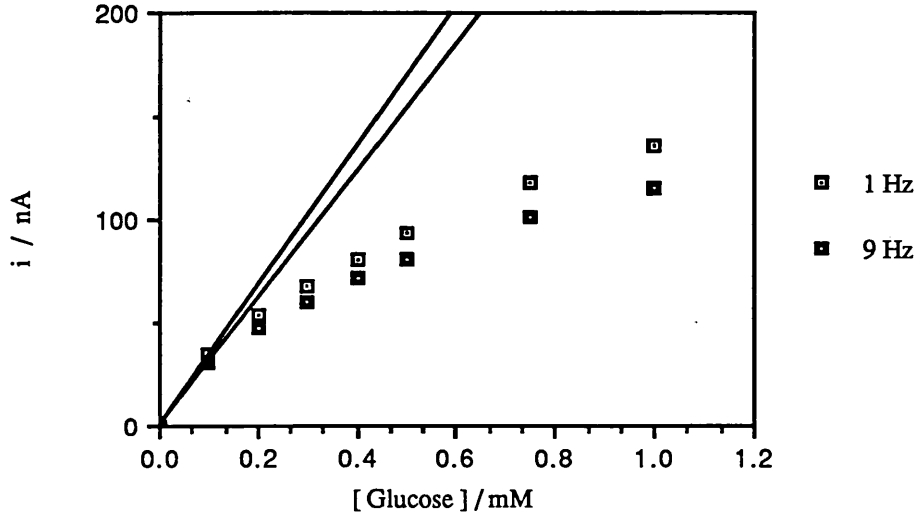


Fig 4.9.d Plot of i vs. [S]
Data at +300 mV and 1 u/ml GOD

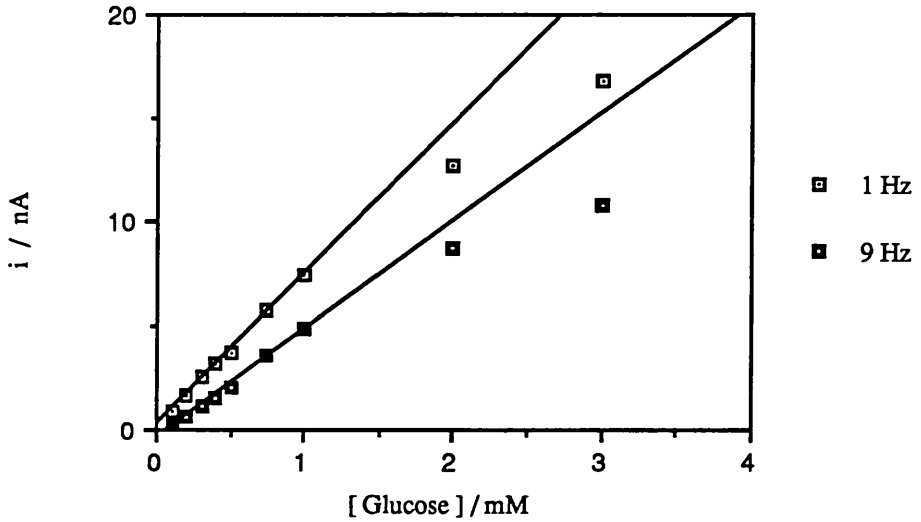


Fig 4.9.e Plot of i vs. [S]
Data at +300 mV and 5 u/ml GOD

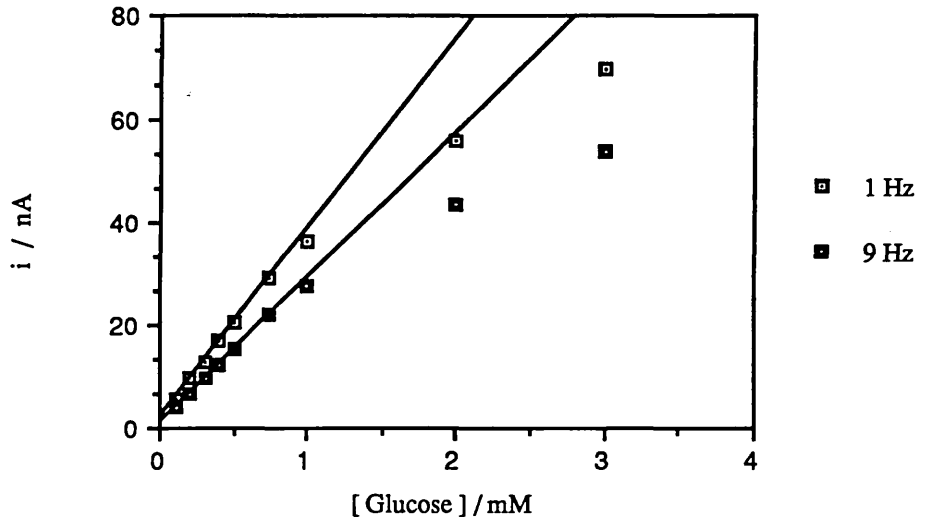
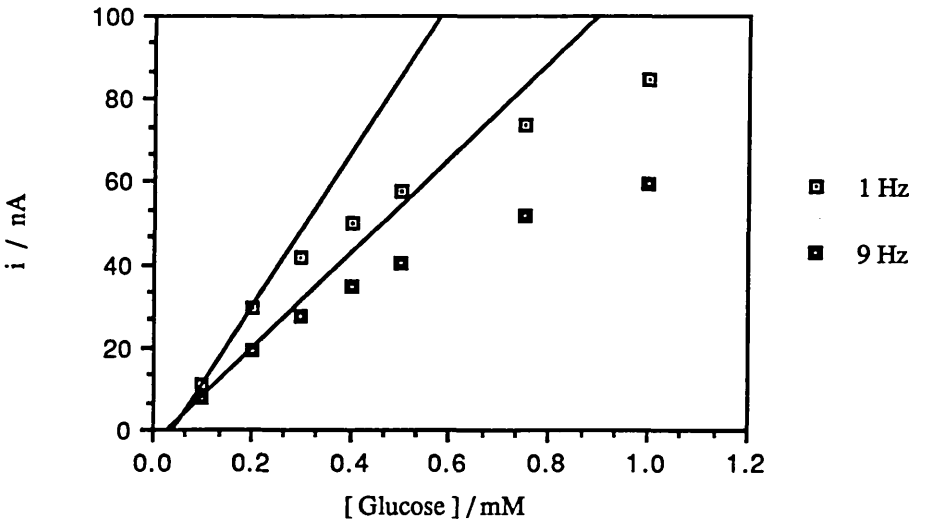


Fig 4.9.f Plot of i vs. [S]
Data at +300 mV and 50 u/ml GOD



E / mV	[E] / u/ml	ω / Hz	linear between? / mM	number of points	correlation coefficient
+200	1	1	0.02 - 0.2	5	0.99866
+200	1	9	0.02 - 0.2	5	0.99914
+200	5	1	0.01 - 0.15	7	0.99817
+200	5	9	0.01 - 0.15	7	0.99707
+200	50	1	—	—	—
+200	50	9	—	—	—
+300	1	1	0.1 - 1.0	7	0.99910
+300	1	9	0.1 - 1.0	7	0.99739
+300	5	1	0.1 - 0.75	6	0.99973
+300	5	9	0.1 - 0.75	6	0.99983
+300	50	1	0.1 - 0.2	2	—
+300	50	9	0.1 - 0.2	2	—

Table 4.8 Analysis of the plots of i vs. [S][1]

4.5.4 Dependence of current on [S]$^{1/2}$

Half order plots for the same experiments are shown in figs (4.10.a) - (4.10.f), with values at higher [S] included. For intermediate values of [S], half order dependence is observed. It is noticeable that the half order dependence occurs at a lower [S] for data at +200 mV compared to data at +300 mV. For this reason the plots for +200 mV have more points in this analysis, since the equivalent points in the +300 mV data are first order in [S]. This is seen from the analyses of the data in table 4.9, and on comparison of this table with table 4.8.

Fig 4.10.a Plot of i vs. [S]^0.5
Data at +200 mV and 1 u/ml GOD

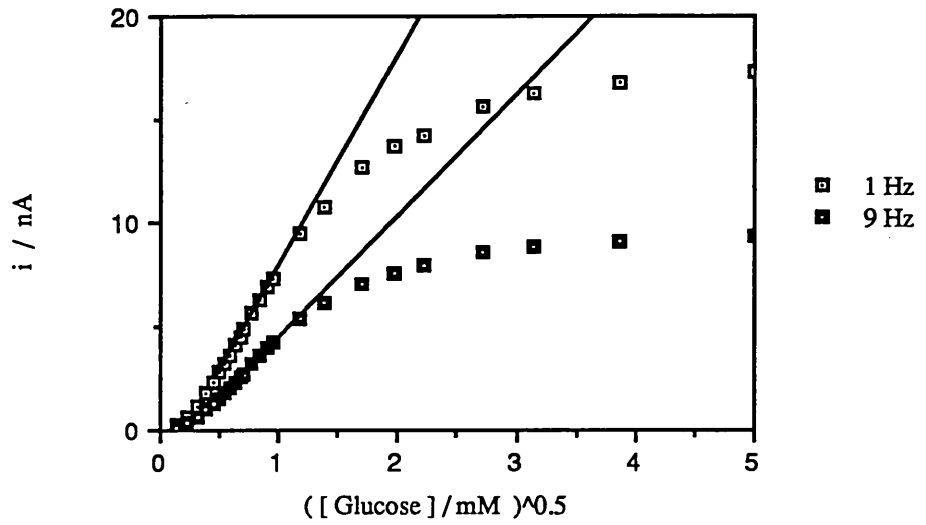


Fig 4.10.b Plot of i vs. [S]^0.5
Data at +200 mV and 5 u/ml GOD

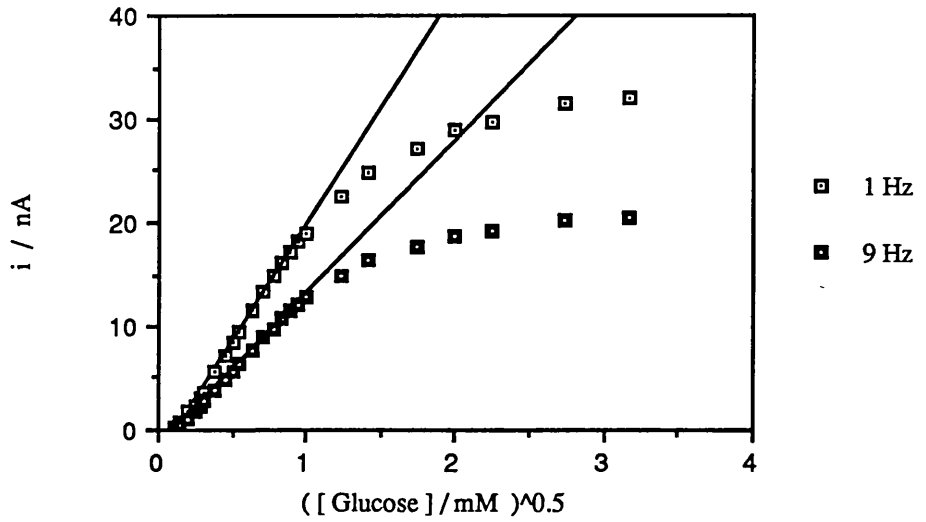


Fig 4.10.c Plot of i vs. [S]^0.5
Data at +200 mV and 50 u/ml GOD

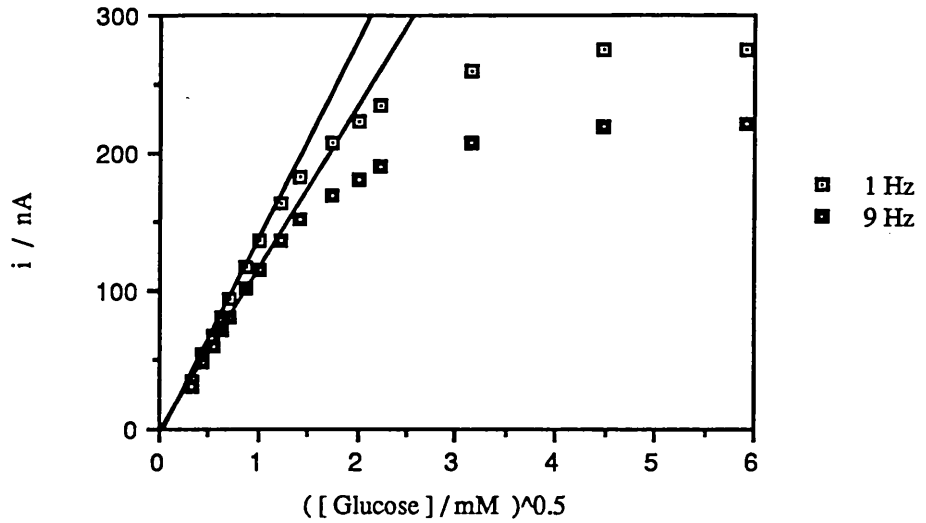


Fig 4.10.d Plot of i vs. [S]^0.5
Data at +300 mV and 1 u/ml GOD

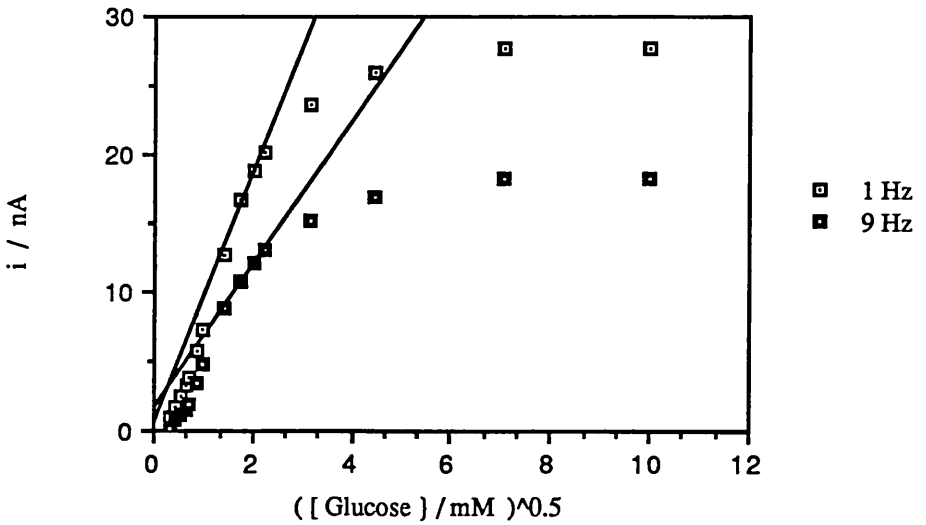


Fig 4.10.e Plot of i vs. [S]^0.5
Data at +300 mV and 5 u/ml GOD

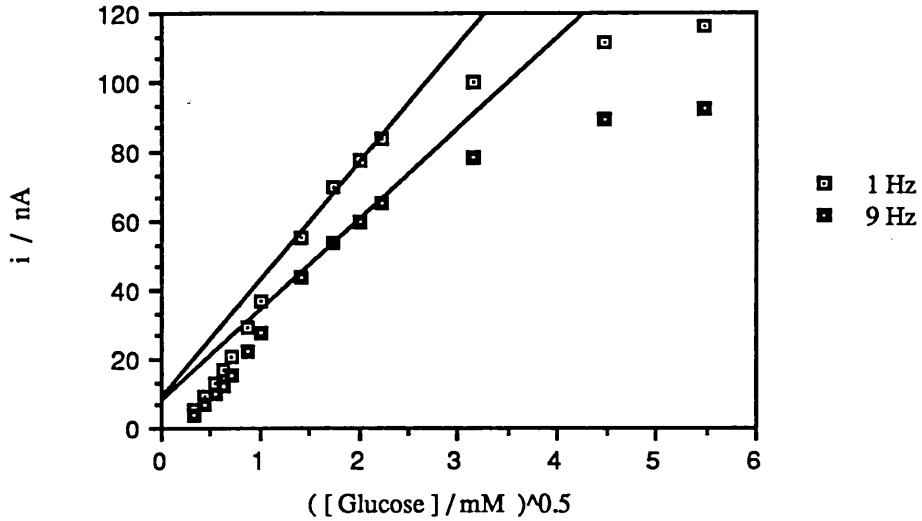
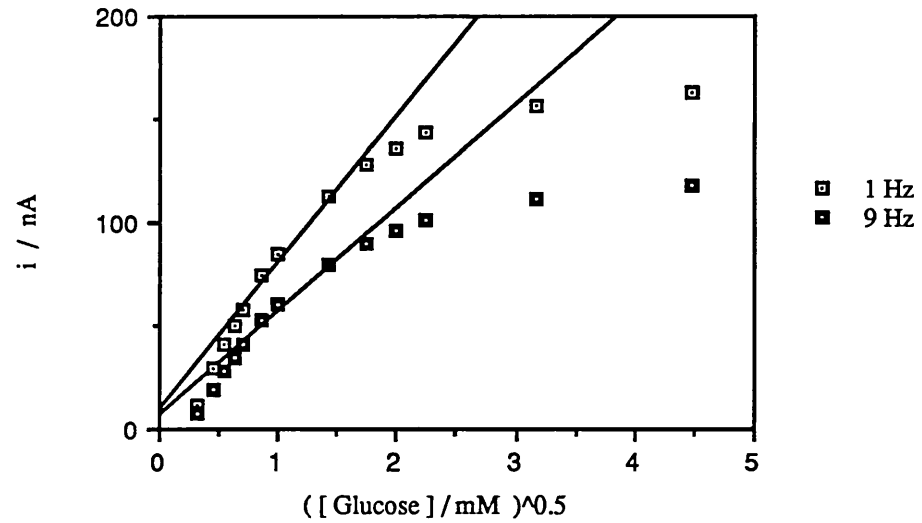


Fig 4.10.f Plot of i vs. [S]^0.5
Data at +300 mV and 50 u/ml GOD



E / mV	[E] / u/ml	ω / Hz	linear between? / mM	number of points	correlation coefficient
+200	1	1	0.25 - 1.4	11	0.99929
+200	1	9	0.25 - 1.4	11	0.99863
+200	5	1	0.20 - 0.90	9	0.99909
+200	5	9	0.20 - 0.90	9	0.99927
+200	50	1	0.1 - 1.5	8	0.99870
+200	50	9	0.1 - 1.5	8	0.99770
+300	1	1	3.0 - 5.0	3	0.99577
+300	1	9	3.0 - 5.0	3	0.99859
+300	5	1	2.0 - 5.0	4	0.99229
+300	5	9	2.0 - 5.0	4	0.99649
+300	50	1	0.4 - 3.0	6	0.99233
+300	50	9	0.4 - 3.0	6	0.99658

Table 4.9 Analysis of the plots of i vs. $[S]^{1/2}$

4.5.5 Dependence of current on [S]^0

The order of dependence on [S] is observed to decrease from first order, through intermediate orders to zero order i.e. the electrode becomes saturated and i depends on [S]^0 . This can be seen from figs (4.10.a) - (4.10.f) . The concentrations at which zeroth order dependence on [S] occurs are given in table 4.10.

E / mV	[E] / u/ml	ω / Hz	linear between? / mM	number of points
+200	1	1 & 9	24.9 - 99.9	3
+200	5	1 & 9	20 - 100	3
+200	50	1 & 9	20 - 100	4
+300	1	1 & 9	20 - 100	3
+300	5	1 & 9	30 - 100	3
+300	50	1 & 9	20 - 100	3

Table 4.10 Data for i dependent on [S]^0

4.5.6 Dependence of current on ω

The order of dependence of current on ω is given by n, a dimensionless constant. n is determined from :

$$n = - \log (i_{1Hz} / i_{9Hz}) / \log 9 \ . \qquad (4.28)$$

For all experiments, inverse dependence of current on ω was observed.

The variation of n with [E] is shown on figs(4.11.a) and (4.11.b). The concentration of enzyme is given in logarithmic units to show the spread of values. It is seen that at the lowest [E] , $n \approx -0.5$. This is the region where first order dependence on [E] is observed. At higher concentrations of E , the value of n is seen to steadily decrease and to approach zero. There is little dependence of n on the bulk concentration of S.

The variation of n with [S] is shown in figs (4.11.c) and (4.11.d); again, logarithmic units are used. The variation of n with [S] is very small, with the exception of the experiment at +300 mV and 1 u/ml GOD, which exhibits a change in n from ≈ -0.53 to a final value of -0.19. There appears to be no correlation between the order of substrate dependence and the value of n. For the experiments at +200 mV, the value of n appears to decrease i.e. approach zero, as the bulk concentration of E is increased. This effect is less clearly observed at +300 mV, with the value of n for 50 u/ml GOD being intermediate between the values for 1 and 5 u/ml GOD.

Fig 4.11.a Plot of n vs. log [E]
Data at +200 mV

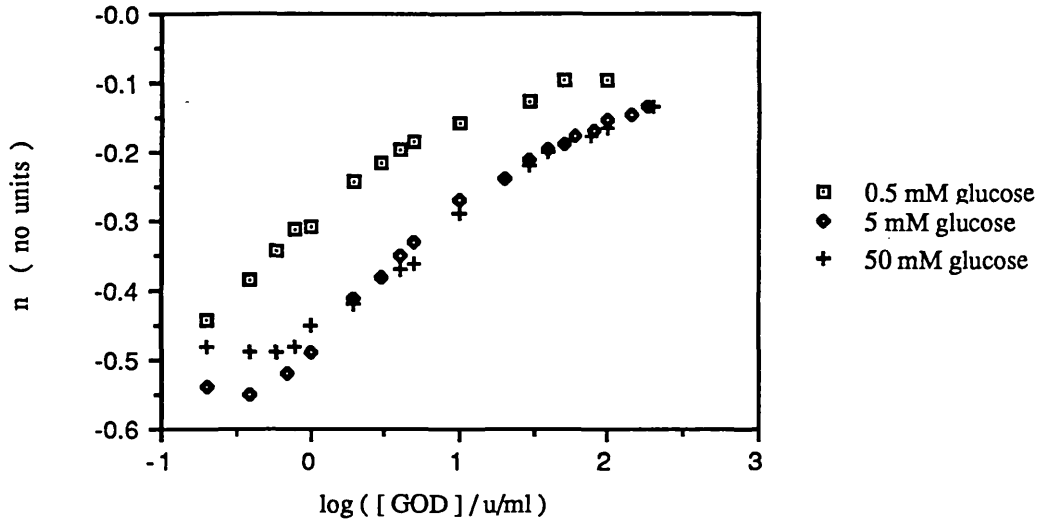


Fig 4.11.b Plot of n vs. log [E]
Data at +300 mV

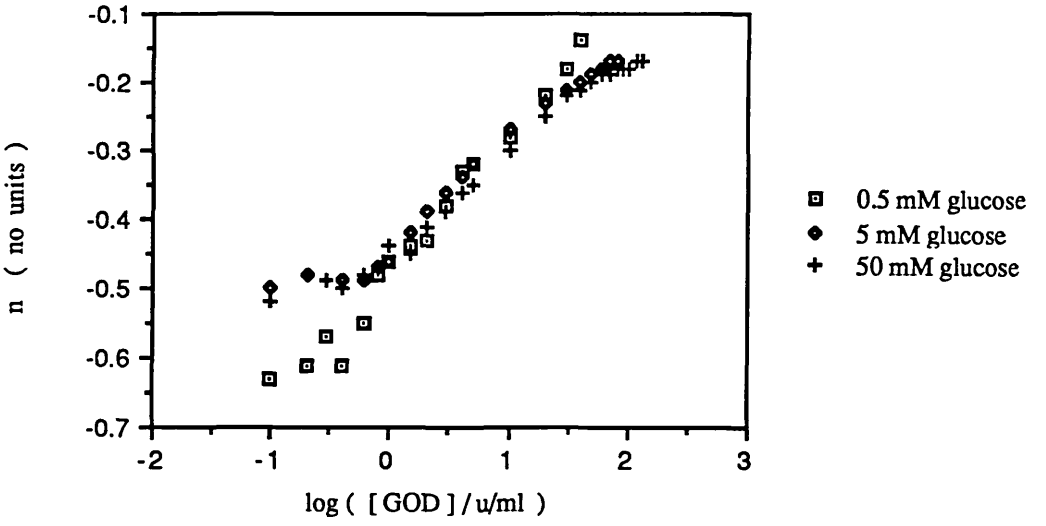


Fig 4.11.c Plot of n vs. log [S]
Data at + 200 mV

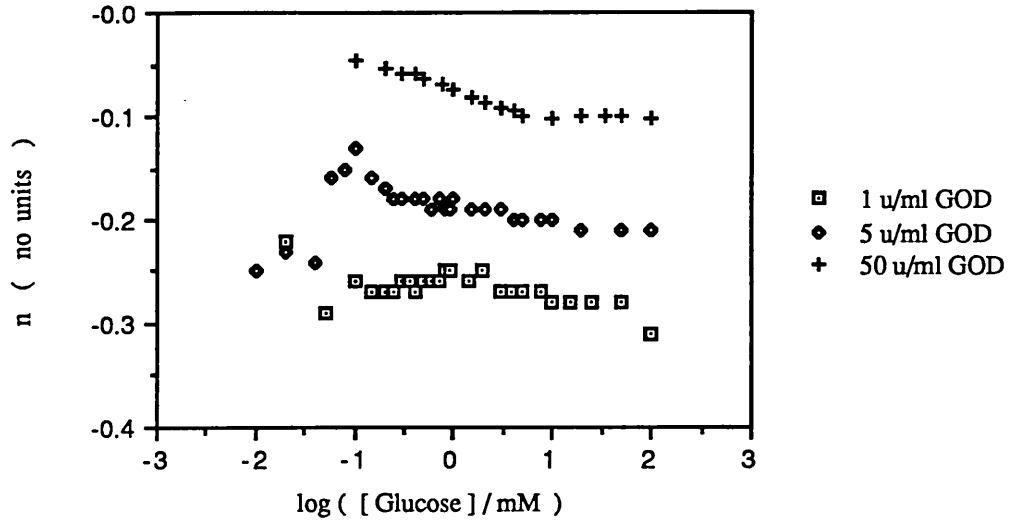
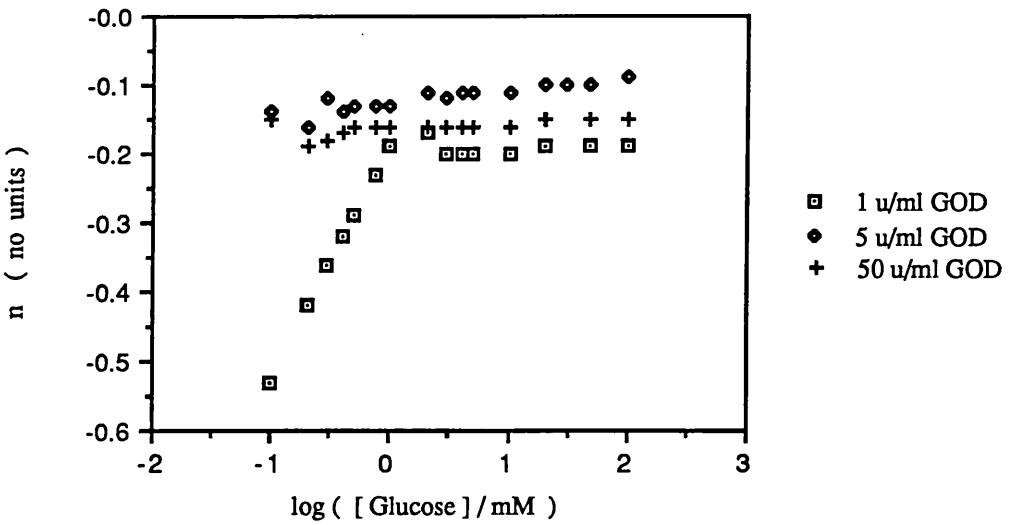


Fig 4.11.d Plot of n vs. log [S]
Data at +300 mV



4.5.7 Dependence of current on potential

This is the most difficult relationship to determine from this data since each experiment was carried out at a single potential with a new electrode, and so some variations will occur due to factors such as the rate of degassing with nitrogen and electrode roughness. However the general observations can be made that at very low concentrations of either S or E , where first order dependence is observed, there is virtually no potential dependence, while at saturating concentrations of S or high concentrations of E, currents at +300 mV are generally larger than at +200 mV. The potential dependence of current will be examined much more thoroughly in Chapter 5.

4.5.8 Summary of the preliminary analysis

For experiments at constant [S] , the current is found to depend on $[E]^1$ at low concentrations and $[E]^{1/2}$ at high concentrations, with ω dependence varying from n $\approx$ -0.5 to $\approx$ -0.1 respectively. This dependence on [E] is explicable by both theories. In the homogeneous mediation theory, a vertical translation from case V to case VI or from case II to case I both describe $\{ [E]^1, \omega^{-1/2} \}$ to $\{ [E]^{1/2}, \omega^0 \}$ dependence. Although $\omega^{-0.1}$ rather than ω^o dependence is observed, close to the case II - I boundary values of ω between -0.5 and 0 are allowed, whereas on the case V - VI boundary the transition is very sharp and so intermediate values of ω are not possible. Thus for the homogeneous mediation theory, the case II - I boundary best explains data on varying [E].

In the heterogeneous redox catalysis theory, a vertical translation from Eθ to Sθ describes the $[E]^1$ to $[E]^{1/2}$ behaviour. However the rotation speed dependence is less well explained: if in Eθ , $n \approx -0.5$, then in Sθ , because of the square root dependence on (1 + θ) and since θ should be constant throughout each experiment, n should become ≈ -0.25 . However much lower values of n are observed, which are not explicable.

For experiments at constant [E] , the current is found to depend on $[S]^1$ at low concentrations, $[S]^{1/2}$ at intermediate concentrations and $[S]^0$ at high concentrations. First order dependence on [S] is observed up to a higher concentration at +300 mV compared to +200 mV. With the exception of the experiment at +300 mV and 1 u/ml GOD, the ω dependence does not vary greatly with [S] and is between ≈ -0.3 and -0.1 . At +300 mV and 1 u/ml GOD, the ω dependence varies from ≈ -0.5 in the $[S]^1$ region to ≈ -0.3 at saturation.

According to the homogeneous theory, this dependence on [S] can be described by a horizontal translation either from case V to case II, or from case V, through case VI to case I. However both situations require n = -0.5 when the dependence on [S] is first order, and this is only observed for the experiment at +300 mV and 1 u/ml GOD. However if the data are very close to the line $1/\gamma = 1$ and to the case II - I boundary, then intermediate orders of n are possible since in case II, n = -0.5 and in case I, n = 0, so on the case II -I boundary $0 > n > -0.5$.

The homogeneous mediation theory can also explain why the first order dependence on [S] is seen to higher concentrations at +300 mV compared to +200 mV. The region where first order dependence is observed is to the left of the line $1/\gamma = 1$. If potential is increased

i.e. from +200 to +300 mV, then m_o will increase and hence for $1/\gamma = 1$ to hold true, k_E must increase. This is only possible if [S] on the boundary increases. Then the concentration of substrate below which first order dependence is observed is higher at +300 mV compared to +200 mV.

Also the $\omega^{-0.5}$ dependence observed at +300 mV and 1 u/ml GOD can be explained by the homogeneous mediation theory. At this potential, we have seen that at very low [S], we are more to the left of the line $1/\gamma = 1$ than at lower potentials i.e. we are further into case V. Also at +300 mV, β will be smaller compared to the value at +200 mV since m_o has increased, and with 1 u/ml GOD (the lowest value of GOD used), β is at an absolute minimum for the whole series of experiments described above. Hence the experiment at +300 mV and 1 u/ml GOD starts furthest into case V and $\omega^{-0.5}$ can be observed.

In the heterogeneous redox catalysis theory, first order dependence on [S] is inexplicable, although $[S]^{1/2}$ to $[S]^0$ dependence is possible by a horizontal translation from Eθ to Sθ , or by saturation of the enzyme within Eθ itself. The ω dependence is inexplicable by an Eθ to Sθ transition, since n should halve on crossing from Eθ to Sθ , but is observed to remain approximately constant. However the ω dependence is explicable if the $[S]^{1/2}$ to $[S]^0$ data are explained by case Eθ , since it should be constant throughout this case. Thus suggests that all experiments at constant [E] should be in case Eθ ; however at 50 u/ml GOD, we know from experiments varying [E] that half order dependence on [E] is obtained and thus experiments at 50 u/ml should be in case Sθ. Thus the best, although very poor, explanation of the data at constant [E] is a transition from case Eθ to Sθ.

Thus it is seen that the homogeneous mediation theory is supported most strongly. The first order dependence on [S] is the most destructive criticism of the heterogeneous redox catalysis model. One possible explanation of this $[S]^1$ dependence is that at such low concentrations of substrate, the current becomes controlled by the rate of mass transport of substrate from the bulk solution to the electrode. This is discussed in more detail in the following section.

4.5.8.1 Concentration polarization of substrate

It has been assumed in both theories that the concentration of S is sufficiently large to be constant throughout the diffusion layer. However at very low concentrations this may no longer be true. If the supply of S cannot match the rate at which it is consumed by the enzyme, then concentration polarization of S in the diffusion layer may result, and the mass transport of S could become rate limiting. In such a situation, the variation of electrode current with [S] is described by the Levich equation for a rotating disc electrode [133]:

$$i_L = 1.554\ nFAD^{2/3}\nu^{-1/6}\omega^{1/2}\ [S]_\infty \qquad (4.29)$$

where ν is the kinematic viscosity in $cm^2\ s^{-1}$ and ω is the rotation speed of the electrode in Hz. For an electrode of radius 0.5 mm and taking $\nu = 0.01\ cm^2\ s^{-1}$, D (glucose) = $6.7 \times 10^{-6}\ cm^2\ s^{-1}$ [112], n = 1 and ω =1 Hz , eqn. (4.29) becomes:

$$i_L = 0.902\ [S]_\infty \qquad (4.30)$$

Potential/mV	[E] / u/ml	linear up to?	gradient / $mM^{-1}nA$
+200	1	0.2 mM	11.5
+200	5	0.15 mM	37.1
+300	1	1.00 mM	7.4
+300	5	0.75 mM	39.3

Table 4.11 Linear region of i vs. $[S]^{1}$ plots

where $[S]_\infty$ is in mol cm^{-3} and i_L is in Amps.

Only the β-anomer of D-glucose is active for GOD, and this is present as 63.6% of an equilibriated glucose solution [134], so that eqn. (4.30) becomes:

$$i_L = 0.574 [S]_\infty \ . \qquad (4.31)$$

Then for $[S]_\infty$ = 0.1 mM, a current of 57.4 nA would be observed and for $[S]_\infty$ = 1 mM, a current of 574 nA would be observed. These currents are much greater than the experimentally determined values in the region where linear dependence on [S] is observed. Table 4.11 gives the current observed in the linear portion of figs (4.8.a) - (4.8.f) in section 4.5.3.

Thus it can be concluded that concentration polarization of S is not an adequate explanation of the first order dependence of current on [S]. It should also be noted that the Levich current demands +1/2 dependence of current on ω, which is never experimentally observed.

4.6 Fitting experimental data to theoretical plots: the homogeneous mediation theory

In this section, experimental data are plotted in the correct fashion for each particular theoretical plot on crossing the case boundary between two cases. These plots have been outlined in sections 4.3.2 for the homogeneous theory. There are a number of possible cases that could be applied to the data. In this analysis, experiments at constant [S] i.e. varying [E], are considered first. The cases under consideration are cases V and VI, and cases II and I. Various constants can be calculated from the plots. It should be noted that

both k_M and m_o are unknown and so comparison with the experimentally determined values is not very informative.

4.6.1 Cases V and VI : varying [E]

Plots of i vs. $\omega^{-1/2}$ were made according to section 4.3.1.1 and are shown in figs (4.12.a) - (4.12.f). The theory predicts that in case V (low [E]), the lines should intercept the i-axis on the origin and the gradient of the line should be proportional to [E] ; on crossing the sharp boundary into case VI, the intercept on the i-axis should increase as $[E]^{1/2}$ is increased, while the gradient remains constant. The plots show that initially the conditions for case V are obeyed; however once the intercept is greater than zero, the gradients of the lines are not constant. Then it is concluded that in the region where i depends on $[E]^1$, a good dependence of i on $\omega^{-1/2}$ is observed which is explicable by case V, but higher concentrations of E are not explicable by case VI.

It should be noted that case II also depends on $[E]^1$ and $\omega^{-1/2}$, so that at low concentrations these graphs could also agree with case II. In both cases V and II, the gradients of the lines from the i vs. $\omega^{-1/2}$ plots should be proportional to $[E]^1$. Plots of gradient vs. [E] are shown inset on each graph and the correlation coefficients are quoted. It is satisfactory that each plot gives a good linear relationship. The gradient of the derived plot can be used to calculate k_E , according to eqn. (A.42) for case V and to calculate $k_M m_o$, according to eqn. (A.28) for case II. Calculated values are given in table 4.12, along with real values of k_E , using the values for K_M and k_{cat} given in section 4.3.1.

Fig 4.12.a Plot for case V - VI boundary
Data at +200 mV and 0.5 mM glucose

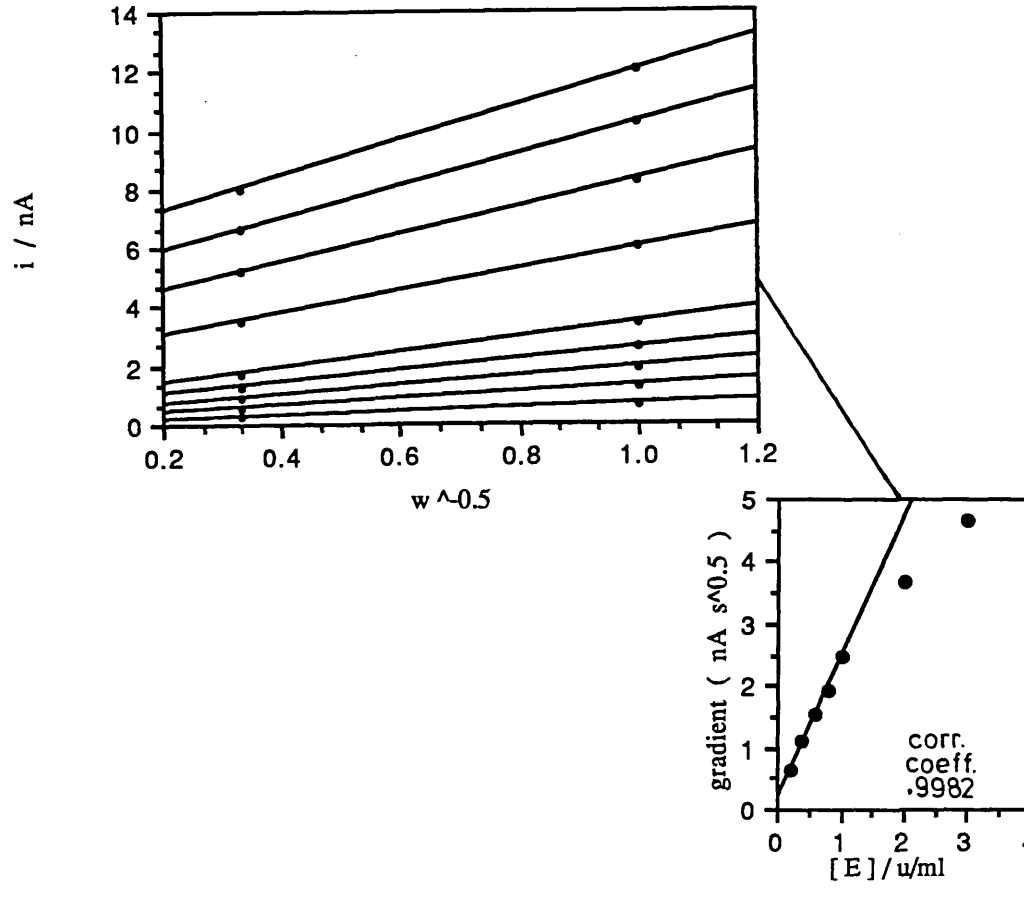


Fig 4.12.b Plot for case V - VI boundary
Data at +200 mV and 5 mM glucose

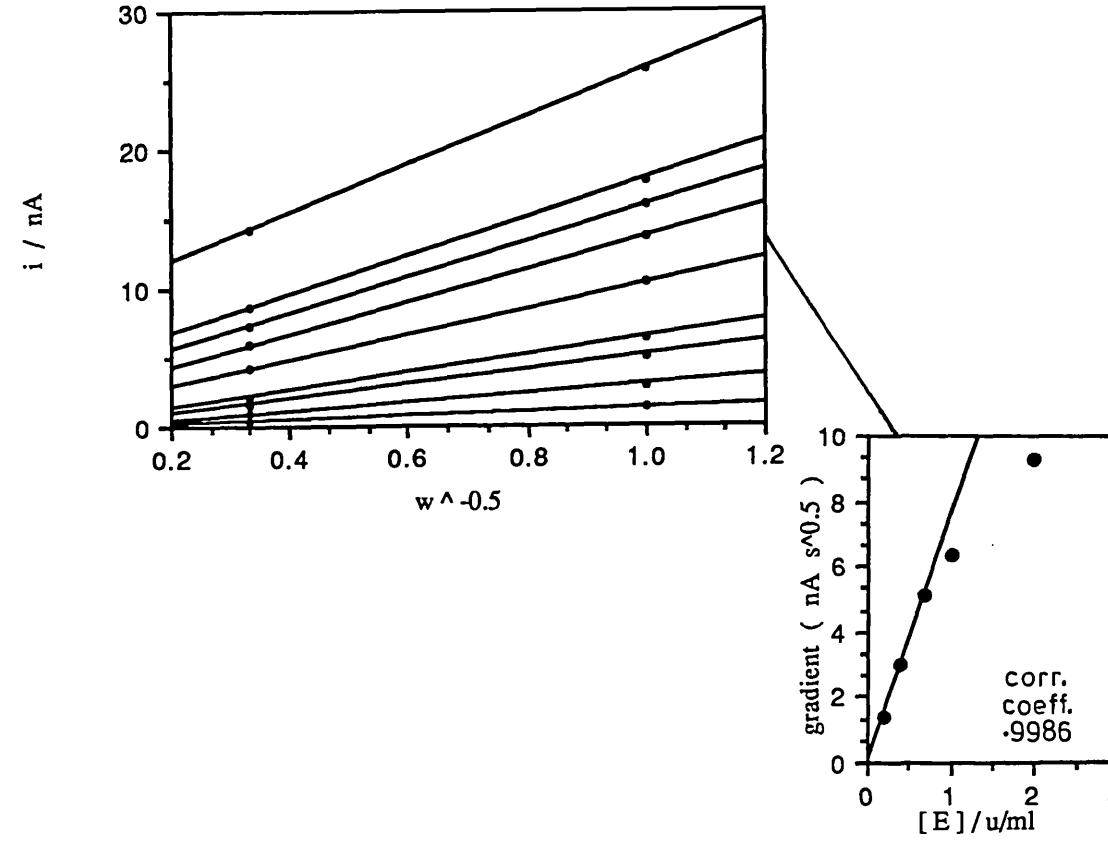


Fig 4.12.c Plot for case V - VI boundary
Data at +200 mV and 50 mM glucose

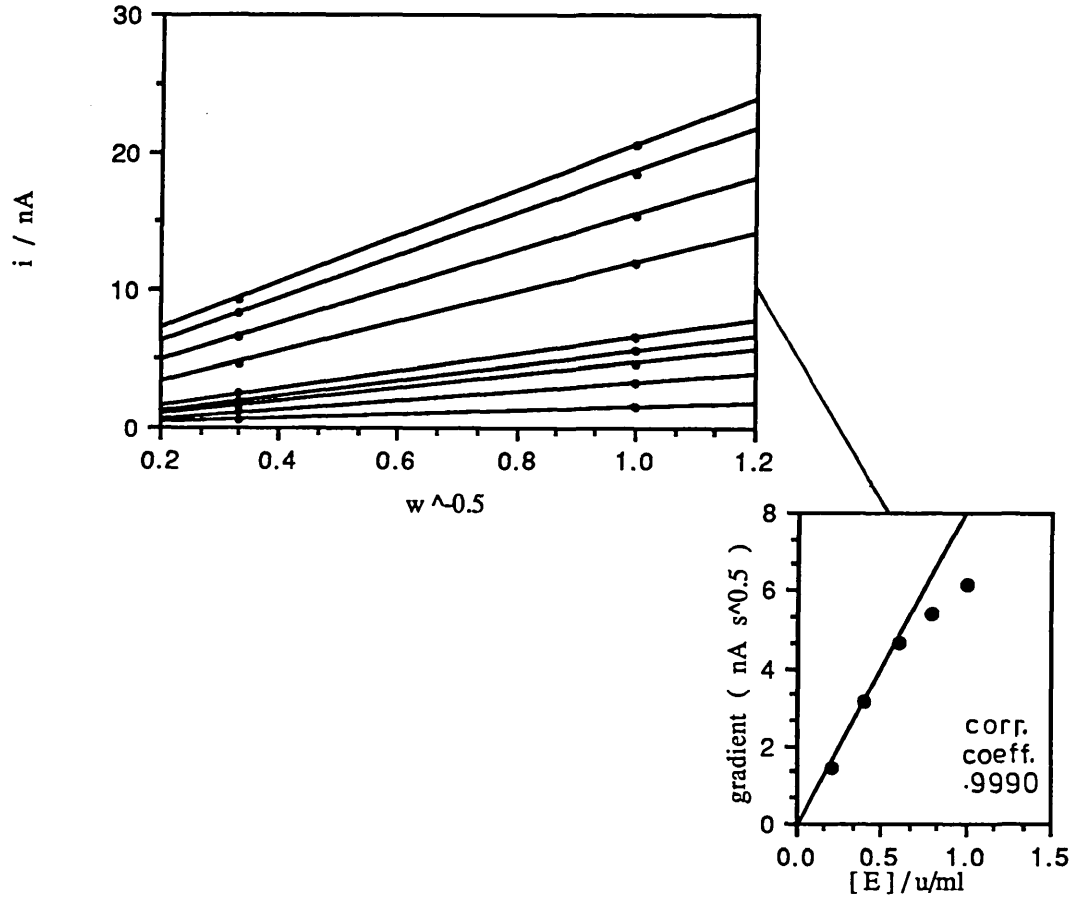


Fig 4.12.d Plot for case V - VI boundary
Data at +300 mV and 0.5 mM glucose

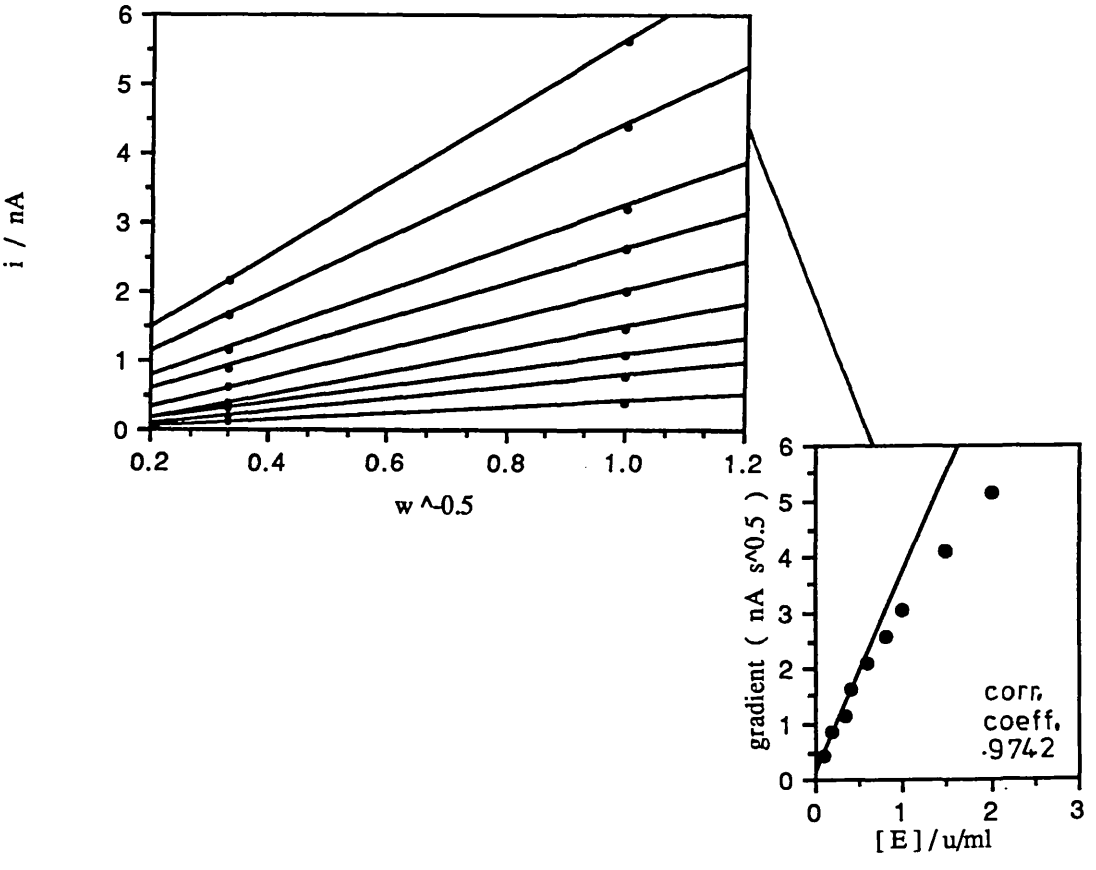


Fig 4.12.e Plot for case V - VI boundary
Data at +300 mV and 5 mM glucose

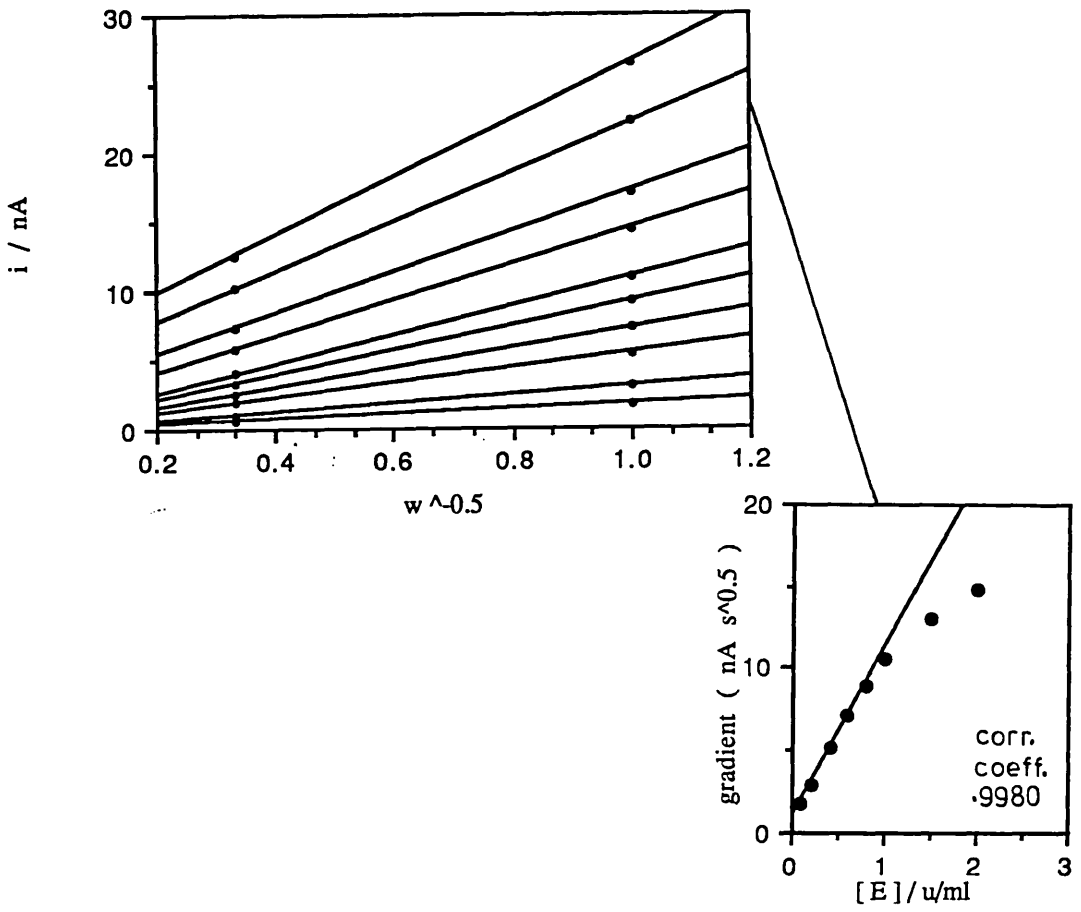
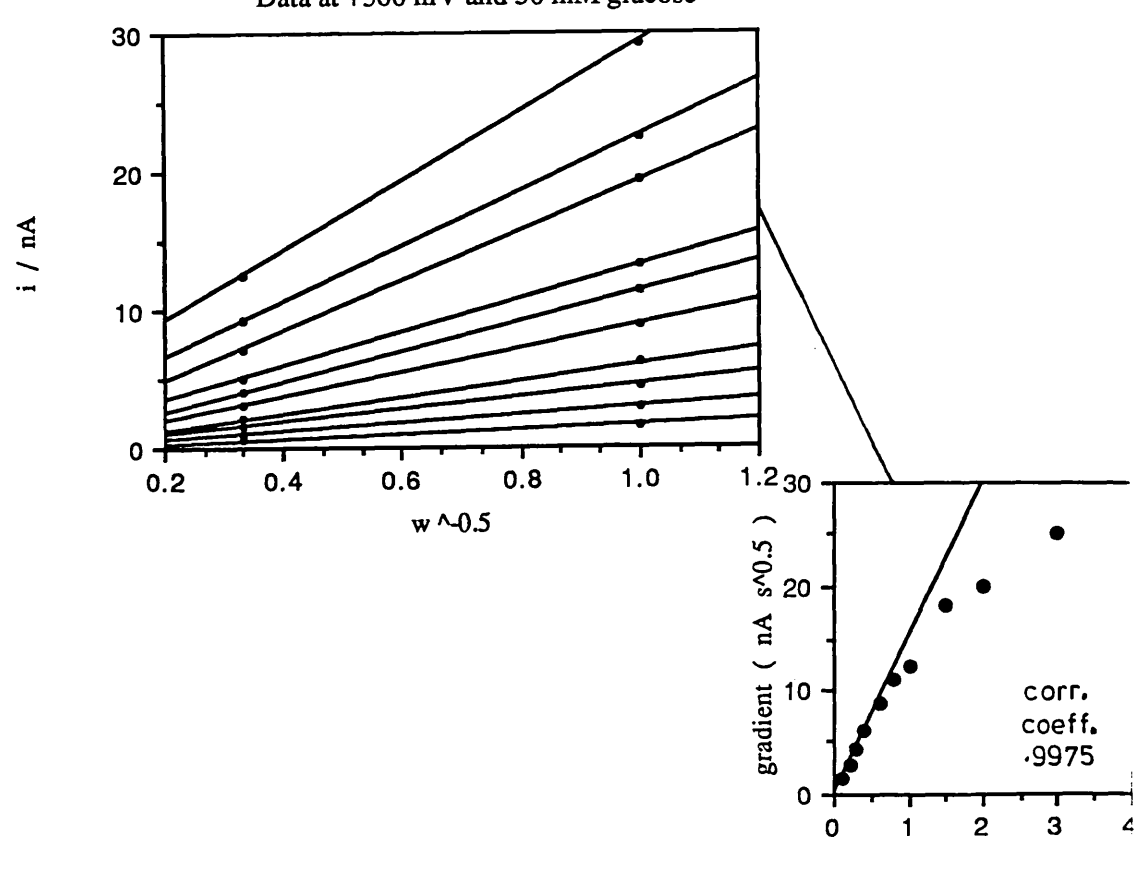


Fig 4.12.f Plot for case V - VI boundary
Data at +300 mV and 50 mM glucose



The calculated value of k_E only shows reasonable agreement with the real value at 0.5 mM glucose. The values of $k_M m_o$ appear to be somewhat high if values of k_M of 3 x10^6 $mol^{-1} dm^3 s^{-1}$ and $m_o < 10^{-6}$ mol dm^{-3} are used, giving a value for $k_M m_o$ of 3.0 s^{-1} (see section 4.3.1).

E / mV	[S] / mM	correlation coefficient	number of points	k_E / s^{-1} (calc.)	k_E / s^{-1} (real)	$k_M m_o$ / s^{-1}
+200	0.5	0.9982	5	35.5	51.5	53.2
+200	5	0.9986	3	117.2	447.4	179
+200	50	0.9990	3	124.2	2048	186
+300	0.5	0.9931	5	52.3	51.5	78
+300	5	0.9992	4	169.0	447.4	253
+300	50	0.9987	5	222.3	2048	333

Table 4.12 Data from case V - VI boundary analysis for experiments varying [E]

4.6.2 Cases II and I

Plots of log ($i/E^{1/2}$) vs. log ([E] / ω) were made according to section 4.3.1.4 and are shown in figs (4.13.a) - (4.13.f), with the theoretical plots superimposed over the experimental plots. The fits are quite good, although at high values of log ([E] / ω) , the experimental data are sometimes seen to drop below the theoretical plot. This is most probably due to the dilution of the bulk concentrations of both enzyme and substrate, since at say, 200 u/ml GOD and 5 mM glucose, a total of 4 ml enzyme solution will have been added, resulting in a true concentration of enzyme of 166.66 u/ml, and 4.17 mM glucose. Fig(4.13.g) shows data being replotted using the true [E], calculated according to the formula:

$$[E]_{TRUE} = 20 [E] / \{ 20 + 0.02 [E] \} \quad . \qquad (4.32)$$

Using $[E]_{TRUE}$ improves the plot to a small extent, although it is still not perfect. This is probably because no correction can be made for the true bulk concentration of S. This is particularly important for data at low [S], since it is closer to the line $1/\gamma = 1$ and so [S], through the term k_E , influences the current to some extent. Also for data at 0.5 mM glucose, substrate depletion occurs at high enzyme concentrations.

Values of k_M and m_o have been calculated according to section (4.3.1.4) and values are presented in table 4.13. D_M was taken to be 5×10^{-6} $cm^2 s^{-1}$, and the value of k_M calculated from Δx was used to calculate m_o. Values of k_M are one order of magnitude larger than the biggest k_M value reported by Kulys [70]. However this may be possible if some mediator species not measured by Kulys is

Fig 4.13.a Plot for the case II - I boundary
Data at +200 mV and 0.5 mM glucose

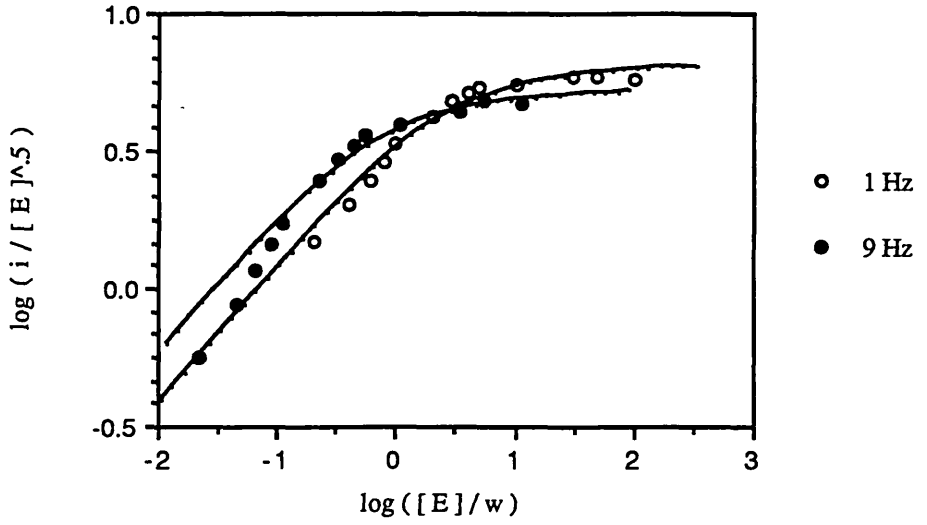


Fig 4.13.b Plot for case II - I boundary
Data at +200 mV and 5 mM glucose

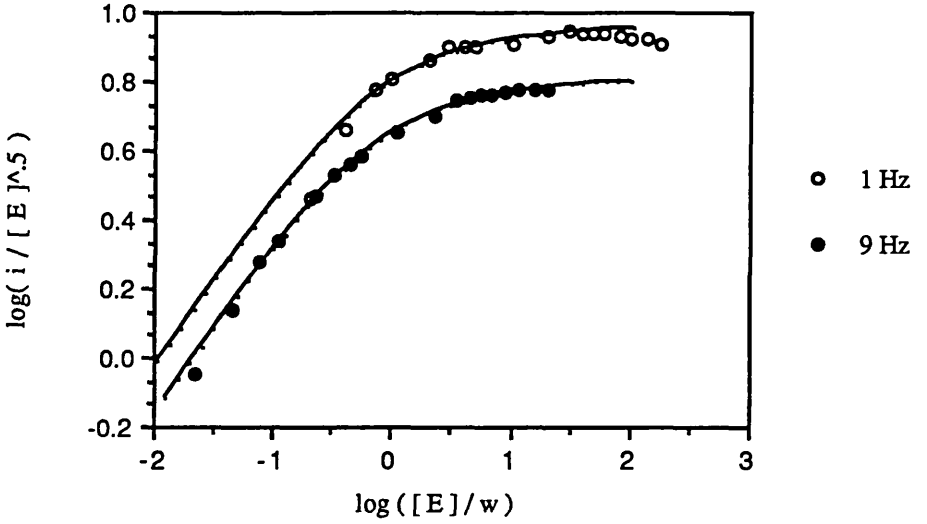


Fig 4.13.c Plot for case II - I boundary
Data at +200 mV and 50 mM glucose

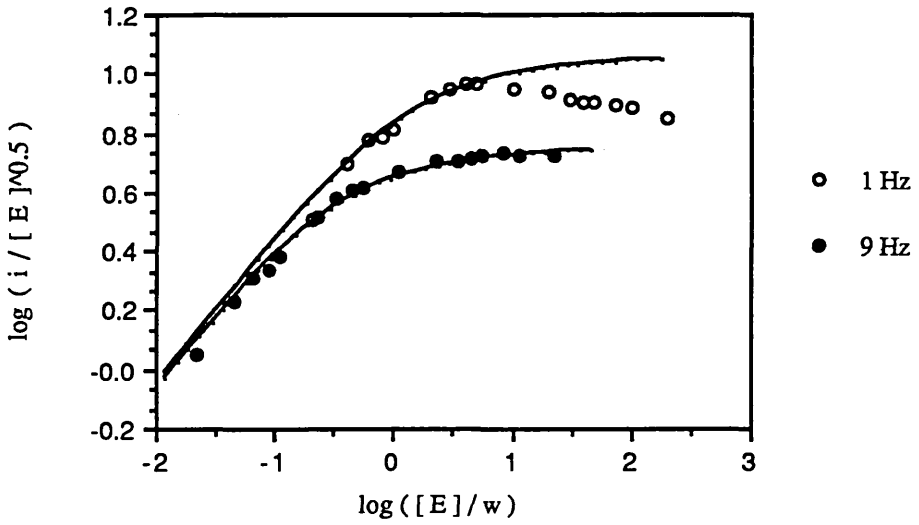


Fig 4.13.d Plot for case II - I boundary
Data at +300 mV and 0.5 mM glucose

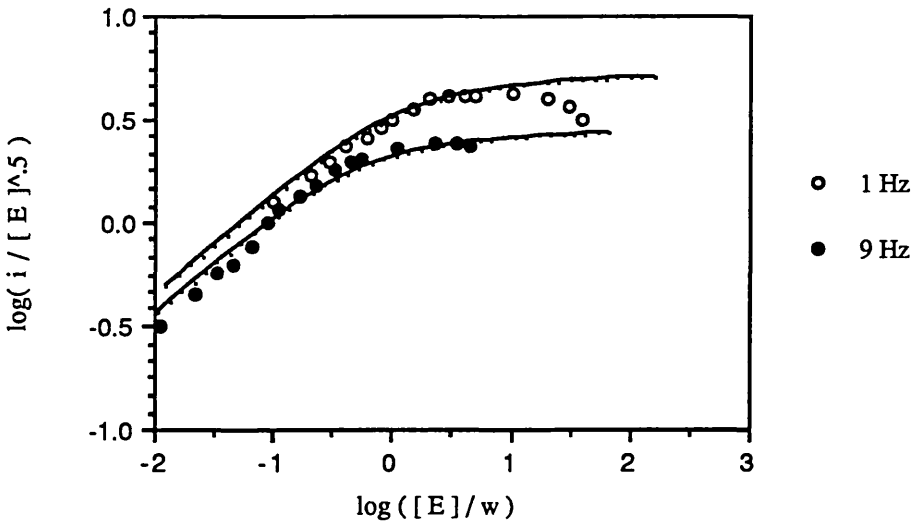


Fig 4.13.e Plot for case II - I boundary
Data at +300 mV and 5 mM glucose

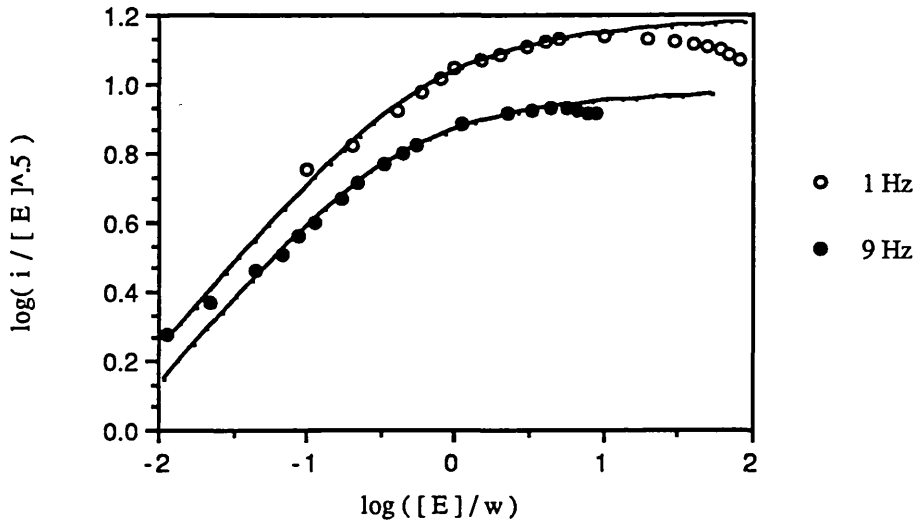


Fig 4.13.f Plot for case II - I boundary
Data at +300 mV and 50 mM glucose

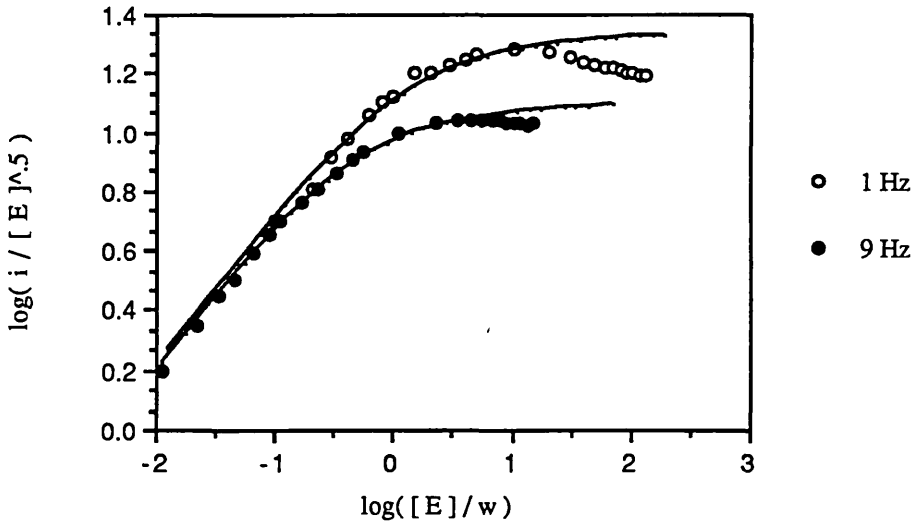
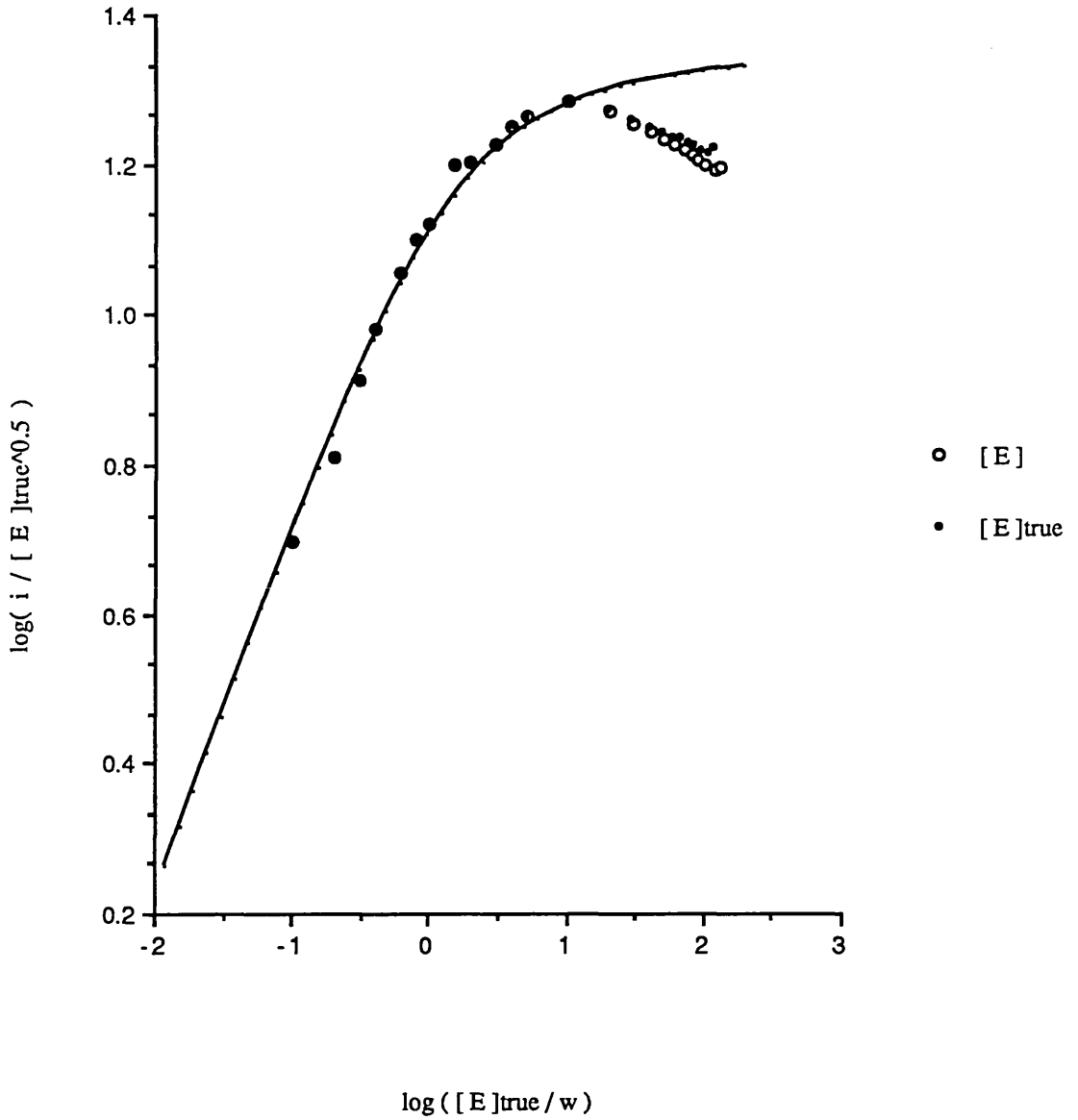


Fig 4.13.g Replotting fig 4.13.f for data at 1 Hz
with [E]true from eqn. (4.32)



E mV	[S] mM	ω Hz	10^{-7} x k_M $mol^{-1}dm^3 s^{-1}$	10^{-5} x $1/m_o(1/k_M D_M)^{1/2}$ $mol^{-1/2}$ $cm^{-1/2}$ $s^{1/2}$	m_o μM
+200	0.5	1	1.50	6.08	6.1
+200	0.5	9	1.81	2.56	13.0
+200	5	1	4.64	4.34	4.8
+200	5	9	1.65	2.05	17.0
+200	50	1	2.73	3.49	7.8
+200	50	9	3.54	2.36	10.1
+300	0.5	1	3.14	7.72	3.3
+300	0.5	9	2.45	4.82	5.9
+300	5	1	5.55	2.62	7.3
+300	5	9	3.08	1.41	18.1
+300	50	1	2.61	1.83	15.1
+300	50	9	2.39	1.05	27.6

Table 4.13 Data from case II - I boundary analysis

responsible for the mediated process. Similarly, the values of m_o are 1-2 orders of magnitude larger than expected from the ring-disc experiments of D.H. Craston [62], although in those experiments a different salt (NMP TCNQ) was under study, and no substrate or enzyme was present, and so different behaviour may be expected. There is little obvious variation of m_o with potential, which would be expected; however the subjective nature of the fit between real and theoretical plots could give a range of m_o values, and so not too much emphasis should be placed on the precision of these values.

In conclusion, the case II - I boundary is a better fit for experiments varying [E] , than the case V - VI boundary. Both boundaries explain the first order dependence on [E], but the case II - I boundary is generally a better fit for higher [E] compared to case VI, where no fit at all was obtained.

4.6.3 Cases V and VI : varying [S]

Plots of i vs. $\omega^{-1/2}$ are shown in figs (4.14.a) - (4.14.f) . The predicted behaviour of these plots has been outlined in section 4.3.1.1. Clearly the plots are a bad fit for the case V - VI boundary. In the region where first order dependence on [S] occurs (see section 4.3.1.1), the intercepts from the plots do not pass through the origin for any data. Similarly the lines are not parallel to each other at any point. Thus it is concluded that the case V - VI boundary is a bad fit for the experimental data. No further analysis is made for this boundary.

Fig 4.14.a Plot for case V - VI boundary
Data at +200 mV and 1 u/ml GOD

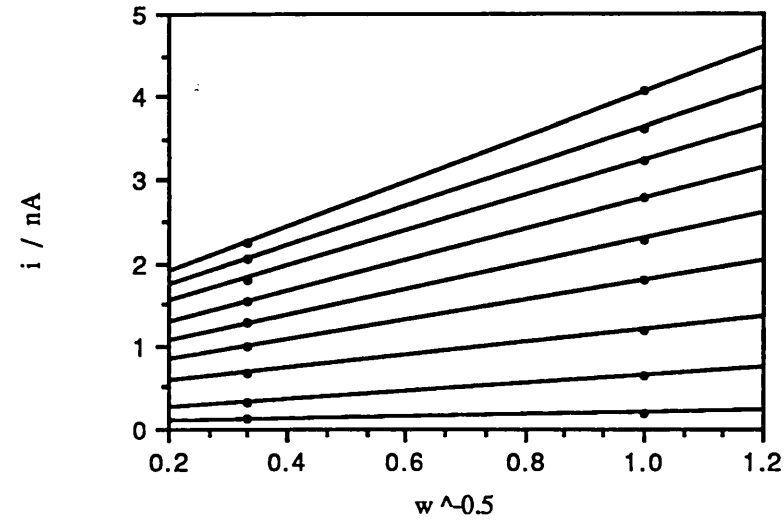


Fig 4.14.b Plot for case V - VI boundary
Data at +200 mV and 5 u/ml GOD

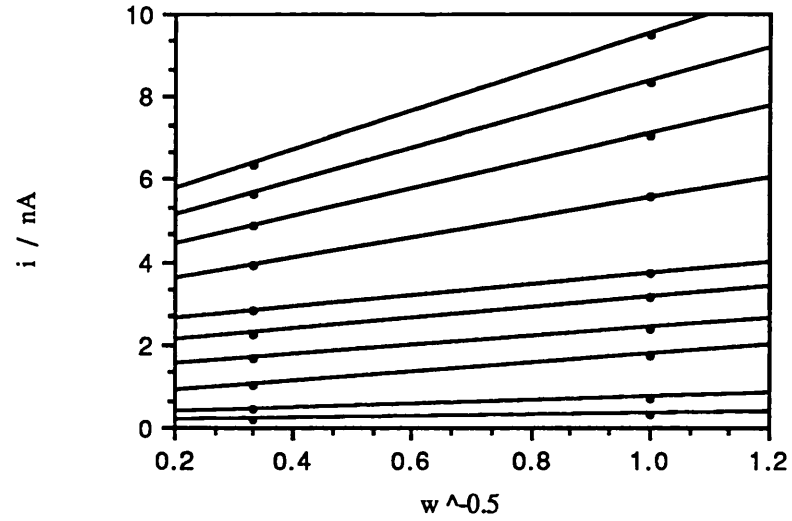


Fig 4.14.c Plot for case V - VI boundary
Data at +200 mV and 50 u/ml GOD

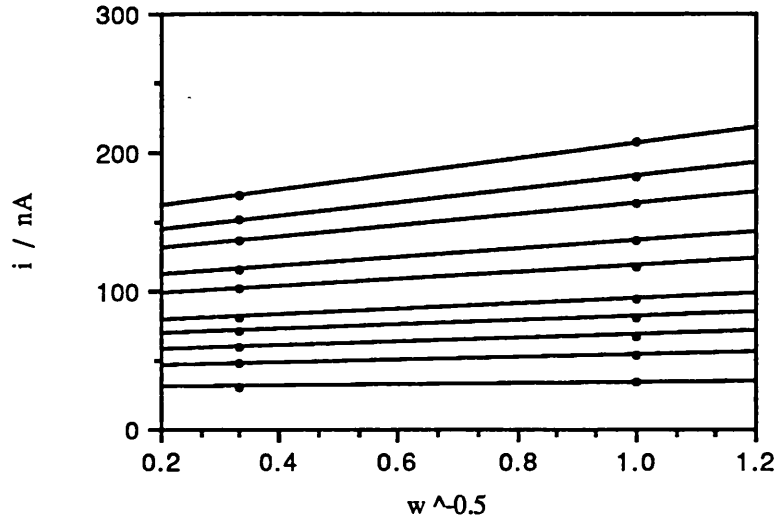


Fig 4.14.d Plot for case V - VI boundary
Data at +300 mV and 1 u/ml GOD

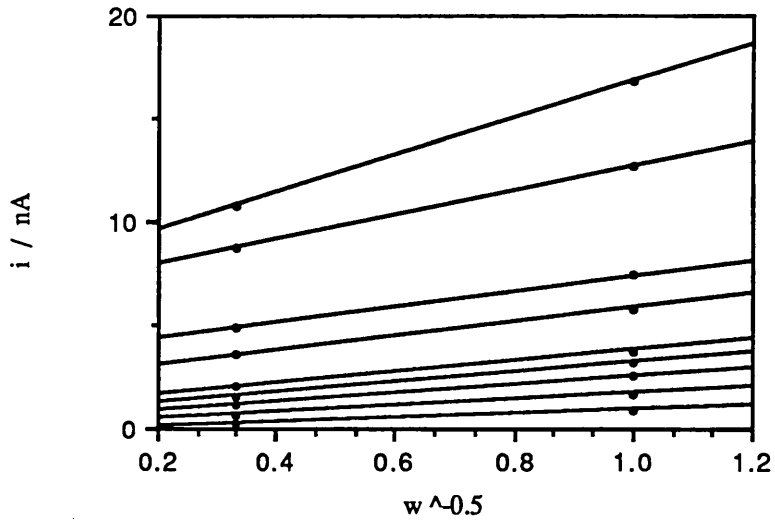


Fig 4.14.e Plot for case V - VI boundary
Data at +300 mV and 5 u/ml GOD

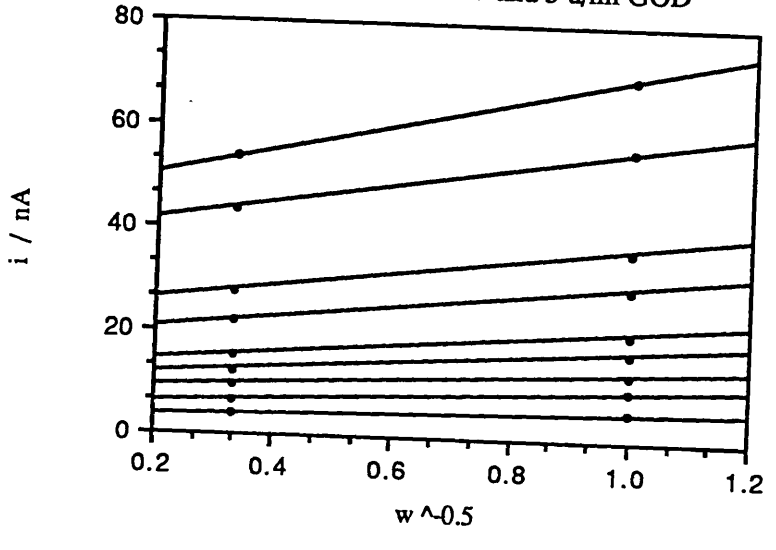
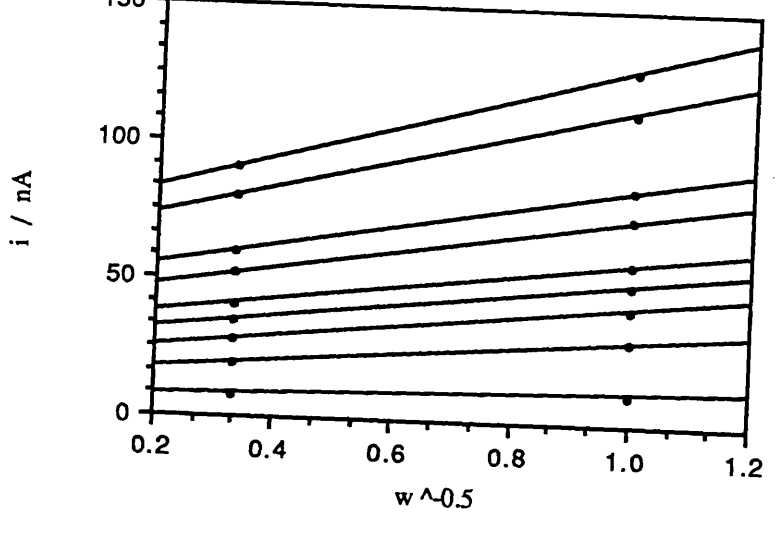


Fig 4.14.f Plot for case V - VI boundary
Data at +300 mV and 50 u/ml GOD



4.6.4 Cases VI and I

In order to complete the analysis, the case VI - I boundary must be considered, although the very poor behaviour of the case V - VI fit makes this unlikely to be good. Plots of log ($i_o / e_\Sigma^{1/2}$) vs. log [S] have been made according to section 4.3.1.2 and fits of the theoretical plot of $\log[1/\gamma - 1/\gamma^2 \ln (1 + \gamma)]^{1/2}$ vs. log ($1/\gamma$) were made. These plots are shown in figs (4.15.a) - (4.15.f). The plots are poor at 1 u/ml GOD, but are seen to improve as [E] is increased, so that at 50 u/ml GOD , reasonable fits are observed. This suggests that only data at 50 u/ml fit the case VI - I boundary. This is consistent with the preliminary analysis in section 4.5.3, where it was observed that at 50 u/ml , no first order dependence on [S] is obtained. Values of $k_M m_o$ and $k_M m_o^2$ have been calculated from Δx and Δy respectively and are presented in table 4.14. m_o is calculated from $k_M m_o$ and $k_M m_o^2$. Thus it is concluded that the case VI - I boundary is a good fit only for data at 50 u/ml.

Fig 4.15.a Plot for case VI - I boundary
Data at +200 mV and 1 u/ml GOD

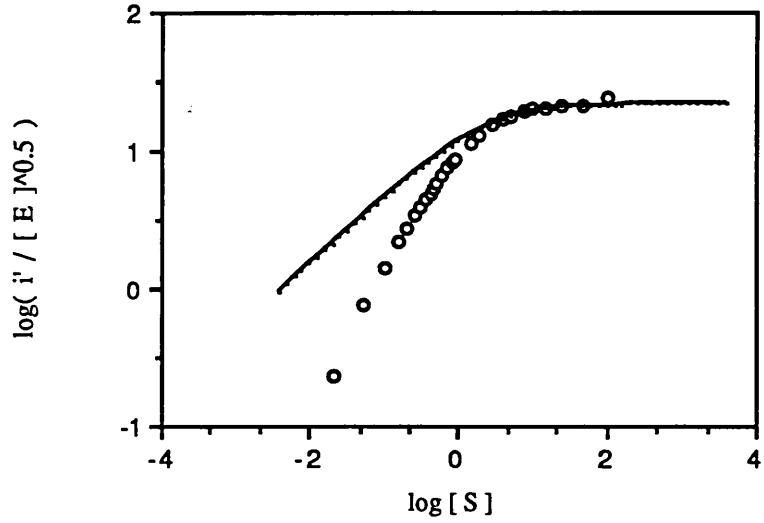


Fig 4.15.b Plot for case VI - I boundary
Data at +200 mV and 5 u/ml GOD

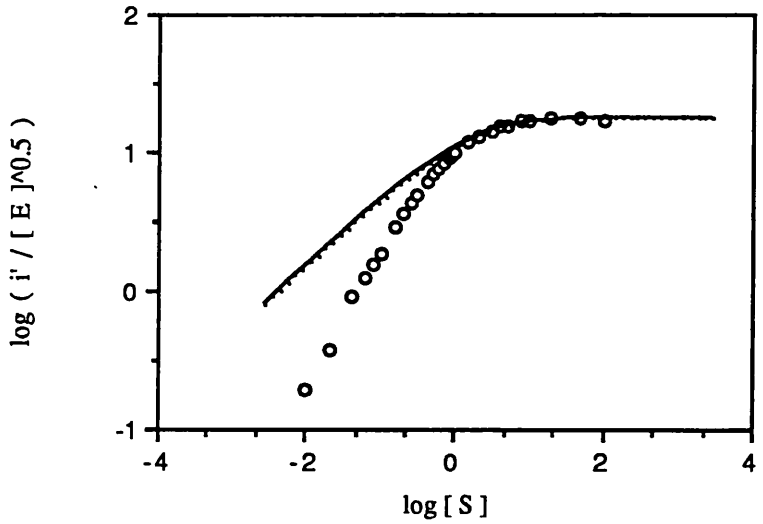


Fig 4.15.c Plot for case VI - I boundary
Data at +200 mV and 50 u/ml GOD

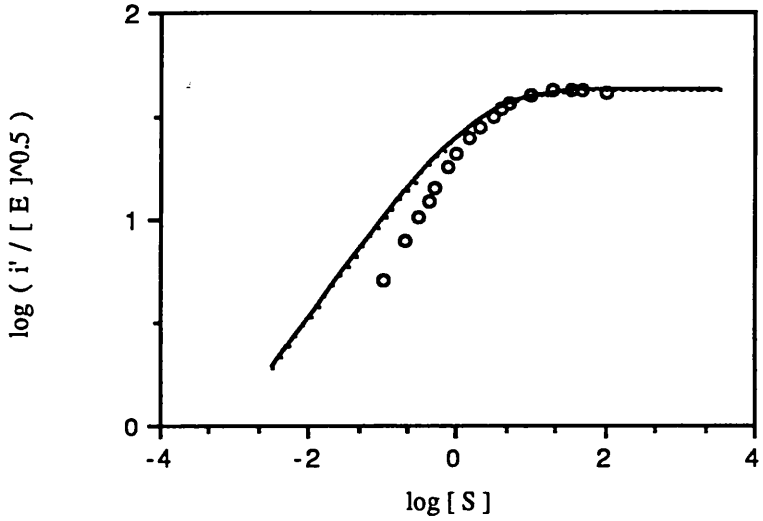


Fig 4.15.d Plot for case VI - I boundary
Data at +300 mV and 1 u/ml GOD

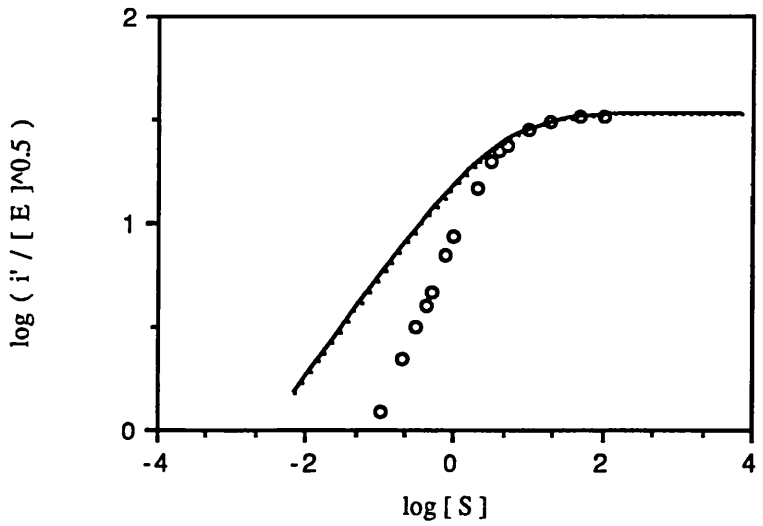


Fig 4.15.e Plot for case VI - I boundary
Data at +300 mV and 5 u/ml GOD

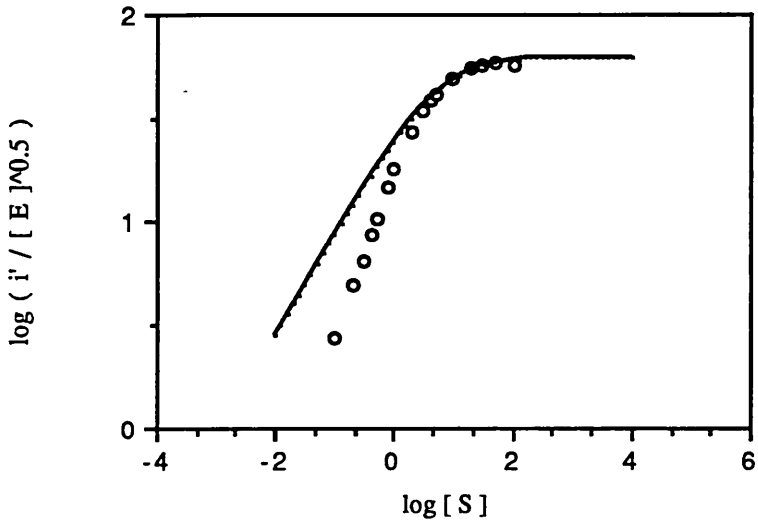
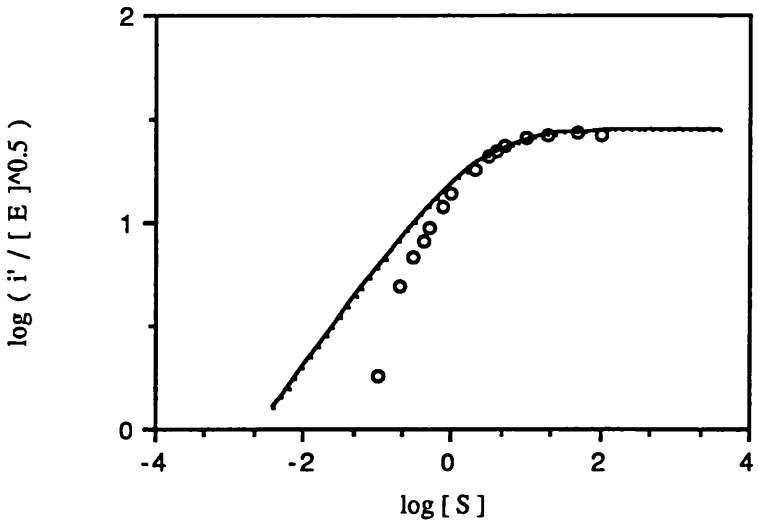


Fig 4.15.f Plot for case VI - I boundary
Data at +300 mV and 50 u/ml GOD



E / mV	[E] / u/ml	$10^{-2} \times k_M m_o$ / s^{-1}	$10^{6} \times k_M m_o^2$ / mol cm^{-3} s^{-1}	m_o / μM
+200	1	4.10	5.76	14.1
+200	5	2.97	3.99	13.4
+200	50	3.45	22.3	65.0
+300	1	7.46	13.8	18.5
+300	5	10.30	47.9	46.5
+300	50	4.10	9.57	23.3

Table 4.14 Data from case VI - I boundary analysis

4.6.5 Cases V and II

Plots of log (i $\omega^{1/2}$ / e_Σ) vs. log [S] were made, and the best fits to a plot of log [$1/\gamma$ $-1/\gamma^2 + 1/\gamma^3$ ln ($1 + \gamma$)] vs. log ($1/\gamma$) were made, according to section 4.3.1.3. These plots are presented in figs (4.16.a) - (4.16.f). The fits are very good, with the exception of the effect of rotation speed: experiments carried out at the same potential and [E] should be coincident on the plots for both 1 Hz and 9 Hz response profiles, although this is clearly not the case.

Values of $k_M m_o$ calculated from both Δx and Δy are collected in table 4.15. The $k_M m_o$ values are larger than expected and show a large variation in size.

Fig 4.16.a Plot for case V - II boundary
Data at +200 mV and 1 u/ml GOD

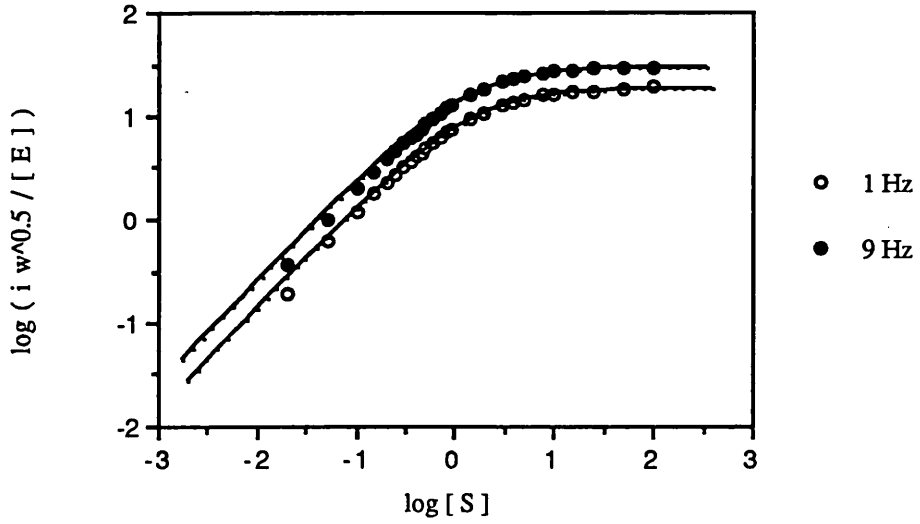


Fig 4.16.b Plot for case V - II boundary
Data at +200 mV and 5 u/ml GOD

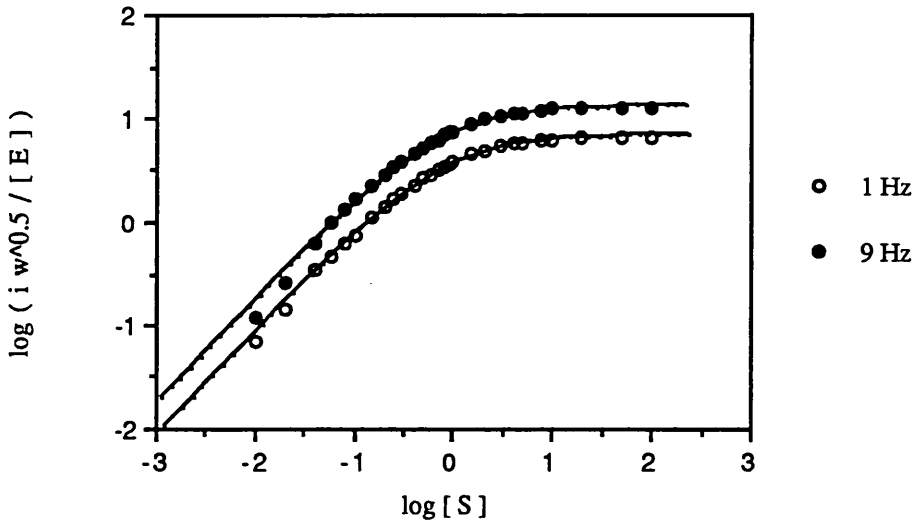


Fig 4.16.c Plot for case V - II boundary
Data at +200 mv and 50 u/ml GOD

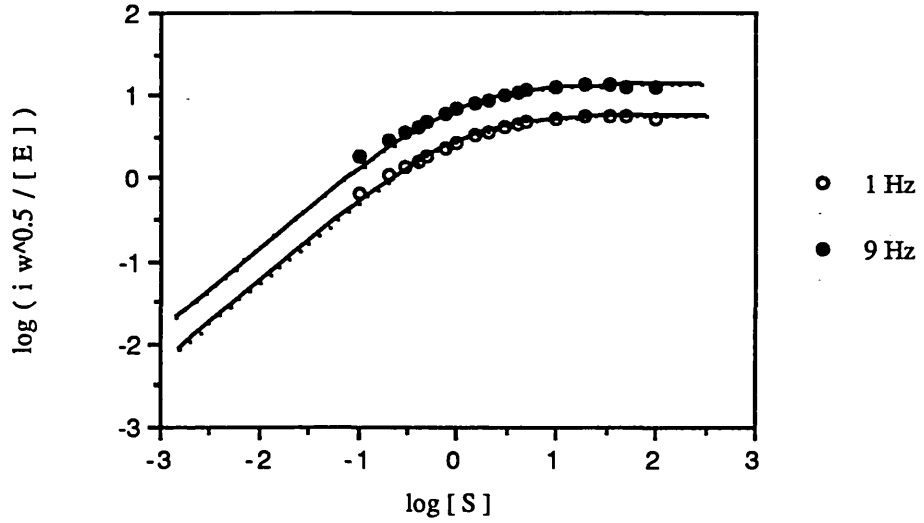


Fig 4.16.d Plot for case V - II boundary
Data at +300 mV and 1 u/ml GOD

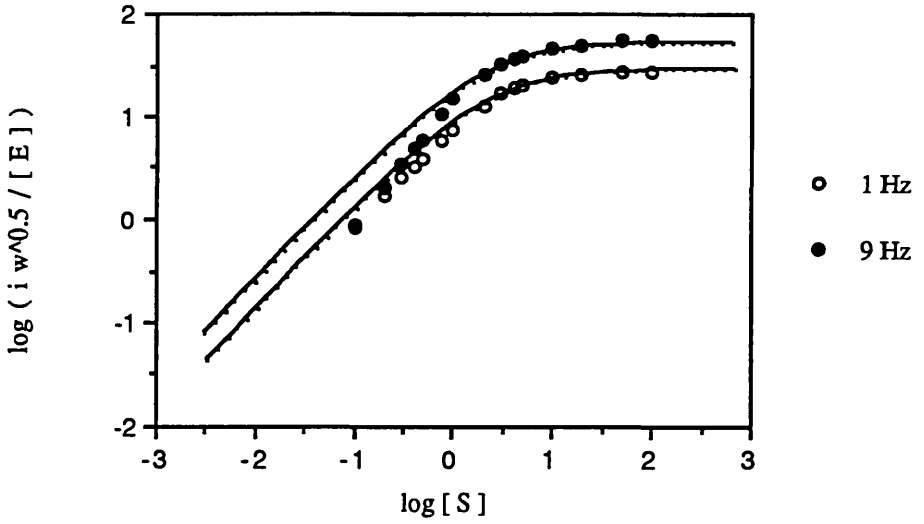


Fig 4.16.e Plot for case V - II boundary
Data at +300 mV and 5 u/ml GOD

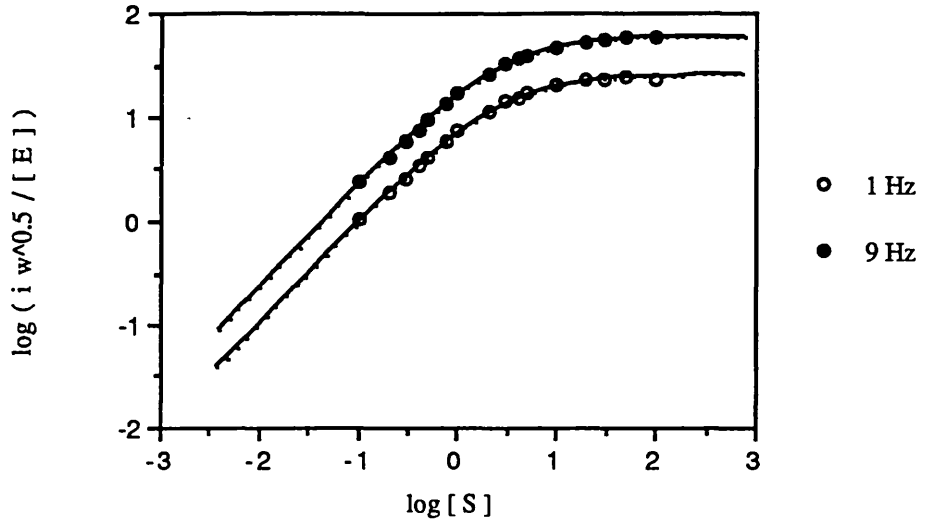
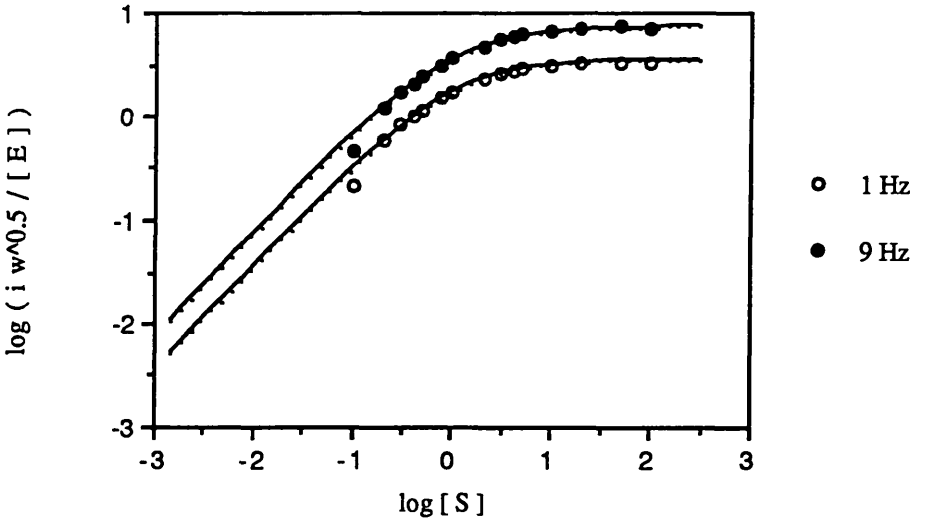


Fig 4.16.f Plot for case V - II boundary
Data at +300 mV and 50 u/ml GOD



E / mV	[E] / u/ml	ω / Hz	10^{-2} x $k_M m_o$/ s^{-1} from x-axis	10^{-2} x $k_M m_o$/ s^{-1} from y-axis
+200	1	1	1.99	4.30
+200	1	9	1.88	6.97
+200	5	1	1.19	1.63
+200	5	9	1.12	3.11
+200	50	1	1.58	1.36
+200	50	9	1.41	3.18
+300	1	1	3.35	6.81
+300	1	9	3.16	12.97
+300	5	1	3.76	5.92
+300	5	9	3.98	3.60
+300	50	1	1.50	0.81
+300	50	9	1.50	1.71

Table 4.15 Data from case V - II boundary analysis

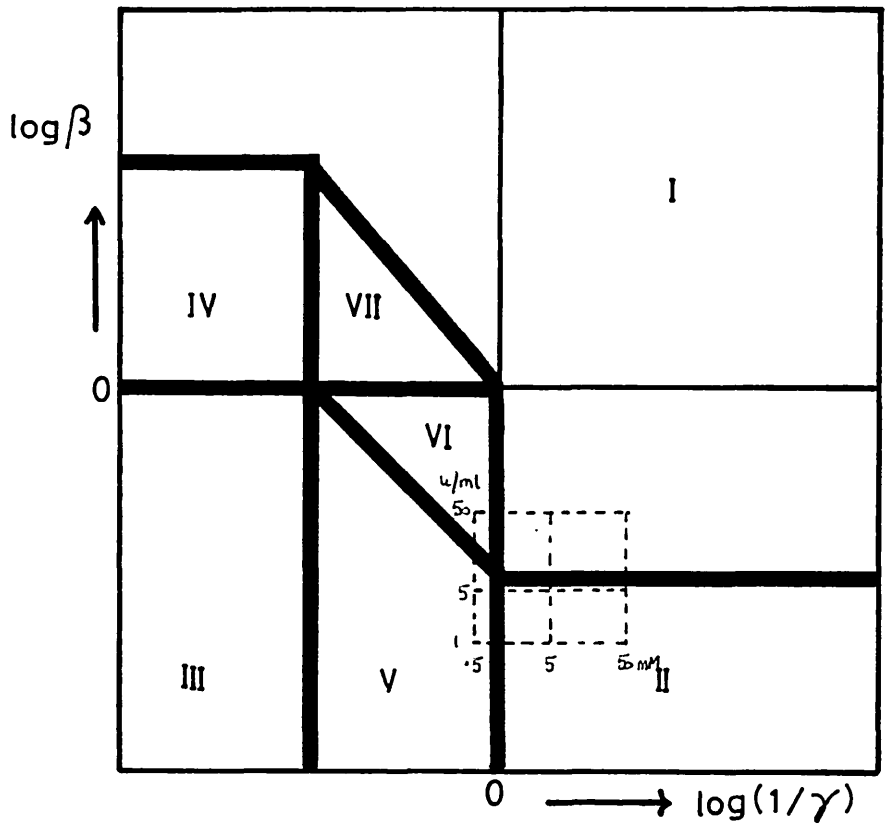
4.6.6 Summary of the homogeneous mediation fit

For data at constant [S] , the case II - I boundary best describes the data, and the behaviour of the dependence of current on both [E] and ω is adequately accounted for. It should be noted that in the region where current depends on $[E]^1$, the data can fit either case V or case II.

For data at constant [E] ,the case V - II boundary is the best description of the data. However it fails to adequately explain the rotation speed dependence of the results, since n = -0.5 is predicted throughout, and this is never observed (see figs(4.11.c) and (4.11.d)). The cases VI - I boundary is also a good fit for data at 50 u/ml.

In fig(4.17), an attempt is made to fit the experimental data on the theoretical case diagram. The explanation of the fit follows. For all experiments at constant [S] , first order dependence on [E] is seen up to or below 1 u/ml GOD. Then 1 u/ml GOD must lie on or just below the case II - I boundary. For all experiments at constant [E], first order dependence on [S] is seen up to or below 1 mM glucose for experiments at 1 and 5 u/ml GOD, hence 0.5 mM is approximately on the case V -II boundary, and at concentrations below 0.5 mM , first order dependence of current on [S] occurs. However at 50 u/ml, we must be above the case II - I boundary (since no first order dependence of i on [S] is observed). Hence at 50 u/ml GOD and at concentrations of glucose less than 0.5 mM, we must be in case VI , where half order dependence on [S] is observed.

The rotation speed dependences of experiments varying [E] are adequately described, since we are moving quite cleanly across the



Fig(4.17) Fitting the experimental data on the homogeneous mediation case diagram (the $\phi > 1$ plane).

case II - I boundary from $\omega^{-1/2}$ to ω^{0} dependence. The rotation speed dependence of experiments varying [S] can also be described when it is remembered that when data are close to the II - I boundary, i.e. at 1 and 5 u/ml GOD, ω dependence varies from -1/2 to 0. The boundaries are not sharp and so intermediate values of ω are observed. At 50 u/ml , we would expect to start in case VI, which has some degree of ω dependence as seen in section 4.3.2.1. Again, the data at 50 u/ml might be sufficiently close to the case II - I boundary for intermediate values of ω dependence to occur.

4.7 Fitting experimental data to theoretical plots: the heterogeneous redox catalysis theory

This analysis is much simpler. Only cases Eθ and Sθ can be applied to the data. Initially experiments varying [E] are considered.

4.7.1 Varying [E]

Plots of i vs. [E]/i were made according to section 4.3.2.2 and are presented in figs (4.18.a) - (4.18.f). The theory predicts that for each particular [S], the plot should be a straight line for each ω and the intercept should be independent of ω. Clearly the plots are not very linear. Thus straight lines were drawn through the data and forced to the same intercept.

Values calculated from the plots are given in table 4.16. θ_{1Hz} varies from ≈ 0.5 - 2. One would expect θ_{1Hz} to be constant at each potential, since the only variable in θ_{1Hz} is k_2. However this is not observed. Generally the values are inconclusive. k_2 should increase with potential, which implies $K_1k_2k_3$ should increase and K_S/k_2 should decrease on going from +200 mV to +300 mV. K_S/k_2 does decrease but there is too much scatter in the $K_1k_2k_3$ values to deduce anything. The values of $(D_E/k_E)^{1/2}$ are 10^2 - 10^3 orders of magnitude too large.

Fig 4.18.a Plot for heterogeneous analysis
Data at +200 mV and 0.5 mM glucose

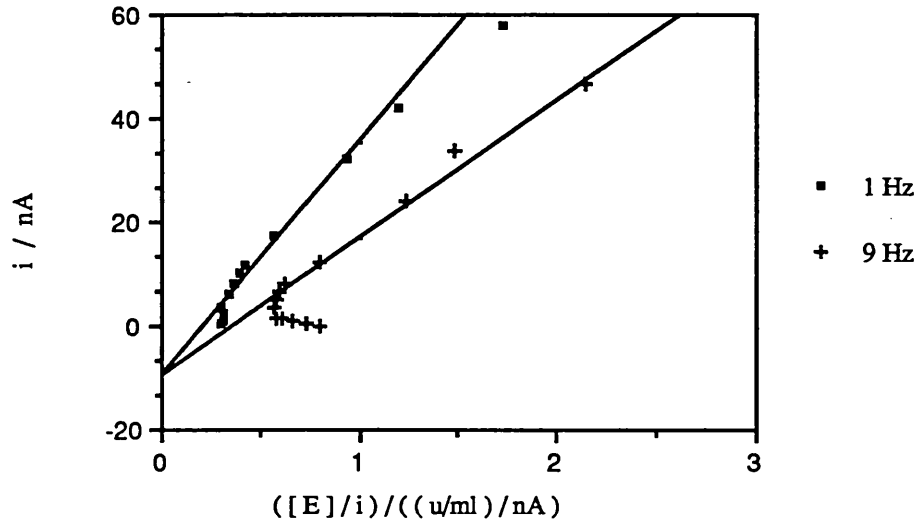


Fig 4.18.b Plot for heterogeneous analysis
Data at +200 mV and 5 mM glucose

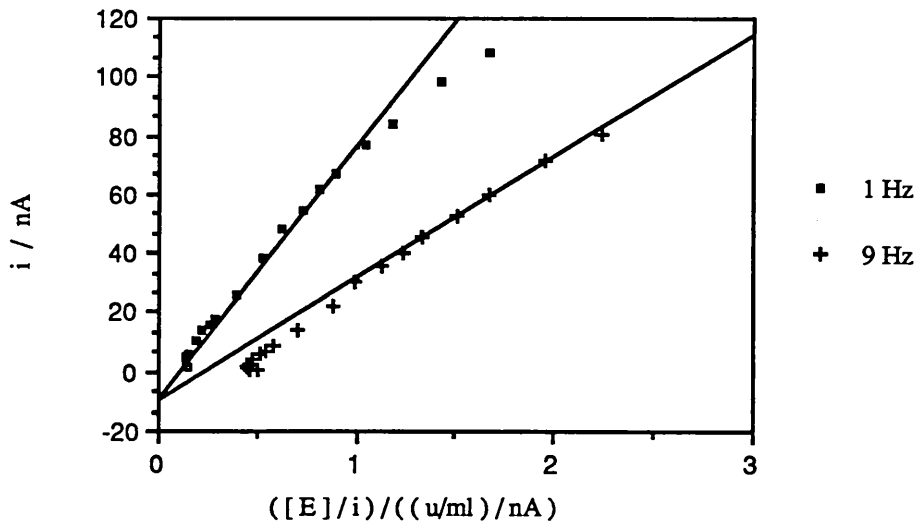


Fig 4.18.c Plot for heterogeneous analysis
Data at +200 mV and 50 mM glucose

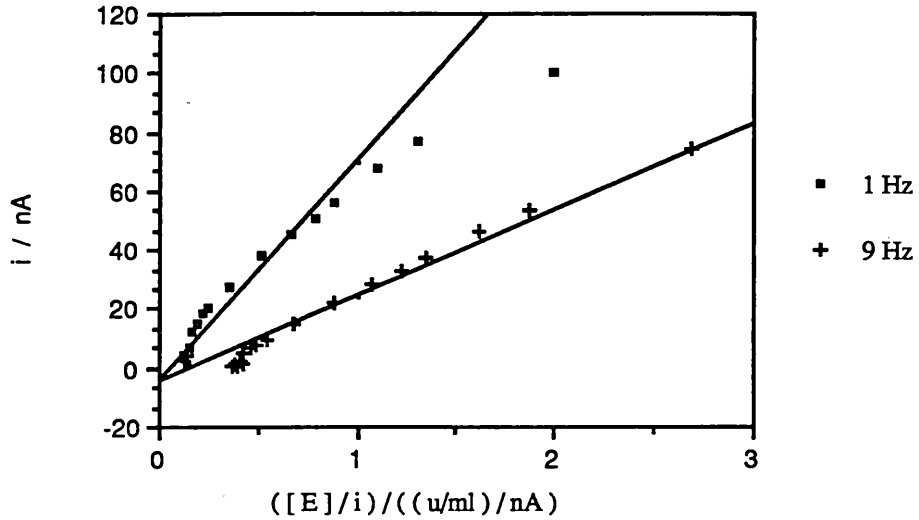


Fig 4.18.d Plot for heterogeneous analysis
Data at +300 mV and 0.5 mM glucose

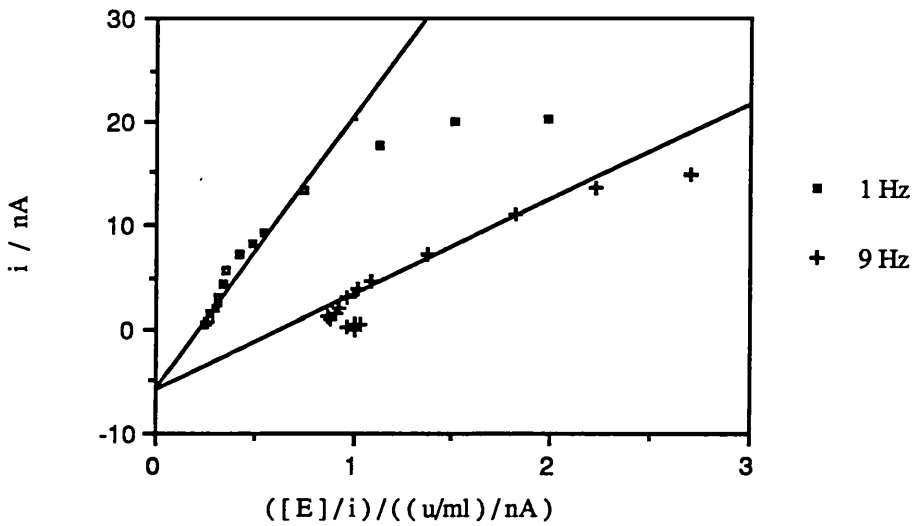


Fig 4.18.e Plot for heterogeneous analysis
Data at +300 mV and 5 mM glucose

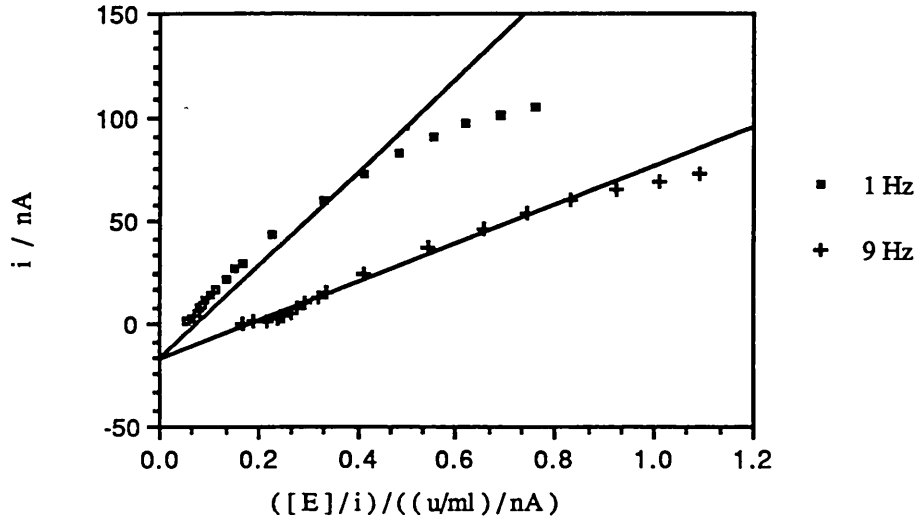
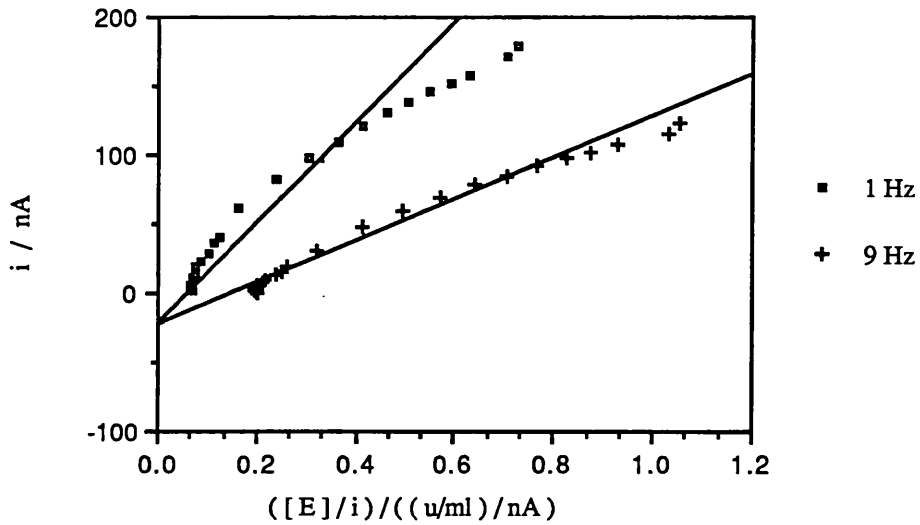


Fig 4.18.f Plot for heterogeneous analysis
Data at +300 mV and 50 mM glucose



E mV	[S] mM	θ_{1Hz} (no units)	K_S/k_2 cm^{-1} s	10^{-12} x $K_1k_2k_3$ mol cm^{-1} s^{-2}	$(D_E/k_E)^{1/2}$ cm s^{-1}
+200	0.5	1.87	4.78	7.9	0.60
+200	5	0.84	2.15	16.1	0.82
+200	50	0.27	6.97	5.8	1.14
+300	0.5	0.07	1.89	1.7	4.61
+300	5	0.45	1.15	19.9	1.19
+300	50	0.44	1.13	31.9	0.99

Table 4.16 Data from heterogeneous analysis at constant [S]

4.7.2 Varying [S]

Plots of $1/i^2$ vs. $1/i\ (\ 1/[\ S\ ] + 1/\ K_M\ )^{1/2}$ were made according to section 4.3.2.1 and are presented in figs (4.19.a) - (4.19.f). The theory predicts the plots should be a straight line and for each particular [E] and ω, the ratio of the gradients for data at 1 and 9 Hz should equal the ratio of the intercepts. In practice the plots were very poor: at low [S] the plots were very curved and only at high [S] was linear behaviour observed. In figs (4.19.a) - (4.19.f), only points at high [S] are shown. The best straight lines were taken through the points and the values of $\theta_{1\ Hz}$ were calculated from the ratio of the gradients and of the intercepts respectively. These values are given in table 4.17, along with the correletion coefficients for the plots and the number of points used in the analysis. The values of $\theta_{1\ Hz}$ calculated from the ratio of the gradients show most uniformity. A value of $\theta_{1\ Hz}$ between 0.55 and 0.09 indicates that the value of n for the rotation speed dependence of the electrode should be between -0.5 and 0, as is indeed observed (see figs (4.11.c) and (4.11.d)). However the values of $\theta_{1\ Hz}$ calculated from the ratio of the intercepts are very erratic and some negative values are obtained. These negative values are due to the ratio of the intercepts being less than 1/3. We can see this on rearranging eqn. (4.26) for calculating $\theta_{1\ Hz}$:

$$\theta_{1\ Hz} = (\ 1 - I\ )/(\ 3I - 1\ )$$

where $I = int_{1\ Hz}/int_{9\ Hz}$. If $\theta_{1\ Hz} < 0$, then either $I > 1$ or $I < 1/3$. Thus the analysis is very sensitive to the position of the straight line through the data. Redrawing the line can give a different intercept

Fig 4.19.a Plot for heterogeneous analysis
Data at +200 mV and 1 u/ml GOD

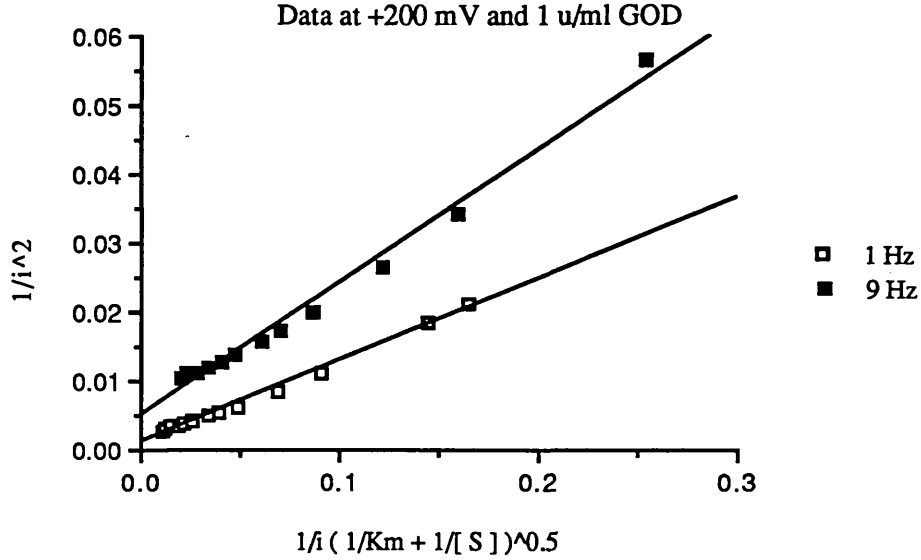


Fig 4.19.b Plot for heterogeneous analysis
Data at +200 mV and 5 u/ml GOD

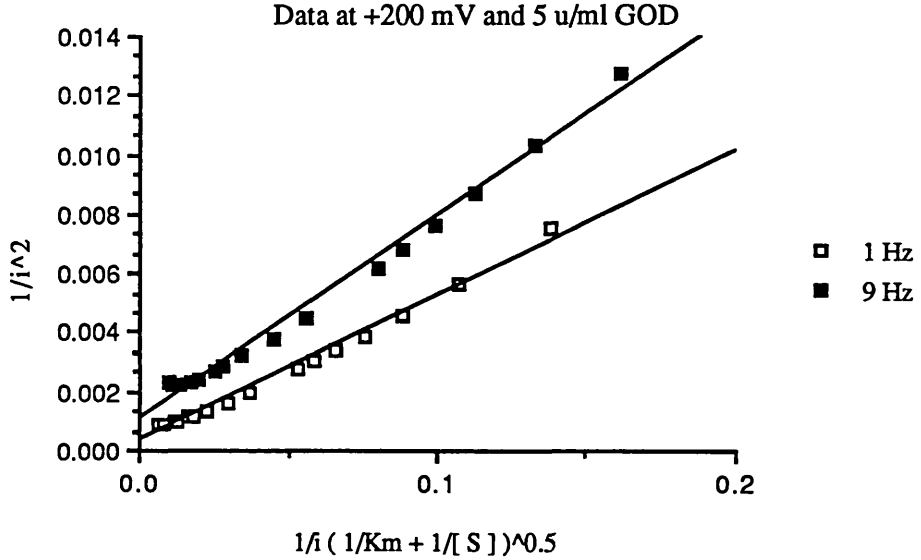


Fig 4.19.c Plot for heterogeneous analysis
Data at +200 mV and 50 u/ml GOD

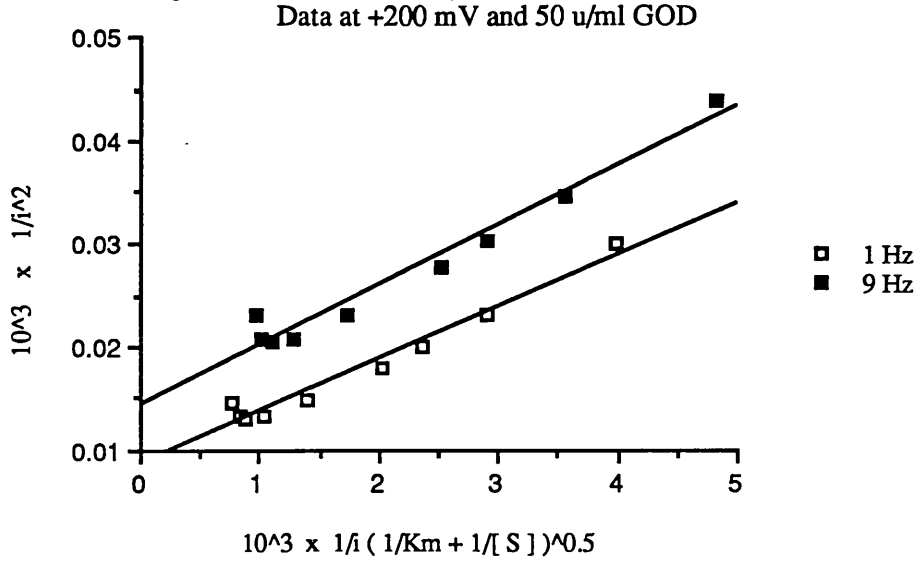


Fig 4.19.d Plot for heterogeneous analysis
Data at +300 mV and 1 u/ml GOD

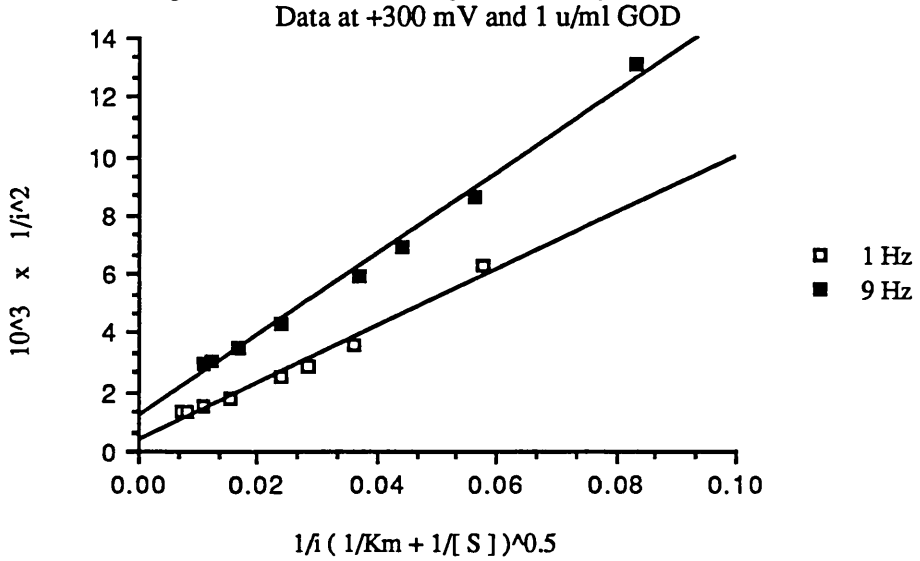


Fig 4.19.e Plot for heterogeneous analysis
Data at +300 mV and 5 u/ml GOD

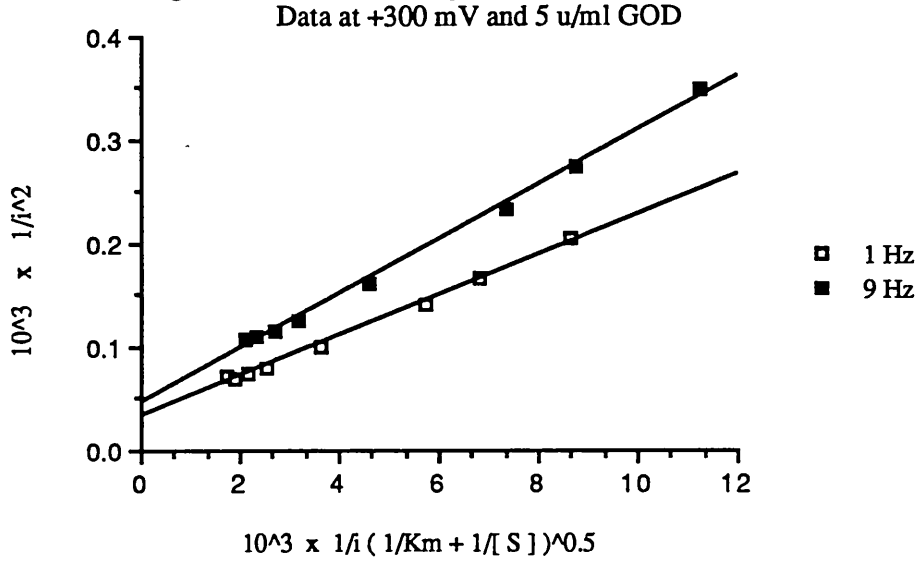
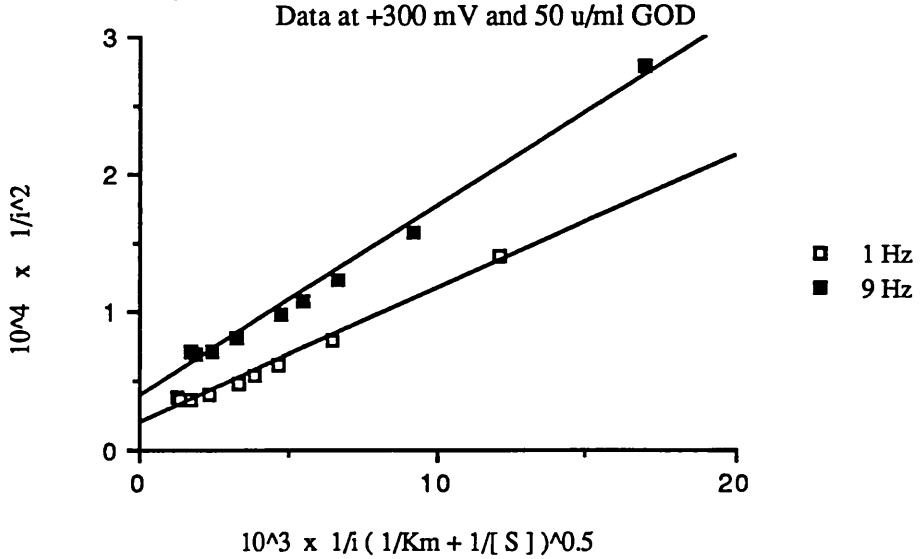


Fig 4.19.f Plot for heterogeneous analysis
Data at +300 mV and 50 u/ml GOD



E mV	[E] u/ml	ω Hz	number of points used (omitted)	correlation coefficient	$\theta_{1\ Hz}$ (no units) from		10^{11} x $K_1k_2k_3$ $molcm^{-1}s^{-2}$
					gradients	intercepts	
+200	1	1 9	13 (13)	0.99677 0.99549	0.55	-2.96	9.82 4.18
+200	5	1 9	17 (10)	0.99553 0.99448	0.34	5.19	5.54 3.13
+200	50	1 9	9 (8)	0.98079 0.98304	0.09	0.48	17.2 12.2
+300	1	1 9	8 (7)	0.99045 0.99648	0.28	≈ -45	23.5 2.21
+300	5	1 9	8 (8)	0.99778 0.99850	0.21	0.25	50.5 215
+300	50	1 9	9 (6)	0.99304 0.99553	0.27	0.87	8.90 6.55

Table 4.17 Data from the heterogeneous analysis at constant [E]

and thus a better value of $\theta_{1\ Hz}$; however the fit of the line to the points will be much poorer. Thus it can be concluded that the heterogeneous analysis is a very poor fit of the experimental data at constant [E]. Only data at high [S] can give a straight line, although very poor values of $\theta_{1\ Hz}$ are obtained.

The values of $K_1k_2k_3$ calculated from the intercept and using $\theta_{1\ Hz}$ calculated from the gradient are given in table 4.17. The values are fairly erratic. The values at +300 mV should be greater than those at +200 mV since k_2 increases with potential. Although some larger values of $K_1k_2k_3$ are observed at +300 mV, this is not a general trend.

4.7.3 Conclusion of the heterogeneous redox catalysis fit

The plots for data varying [E] and [S] are all poor, in particular for the latter case at low [S] i.e. in the region where first order dependence on [S] is known to occur. For plots varying [E], a fit is only obtained at high [E] i.e. in the region where $[\ E\ ]^{1/2}$ dependence is observed. Similarly for data varying [S], a fit is only obtained at high [S] i.e. in the region where $[\ S\ ]^{1/2}$ - $[\ S\ ]^{0}$ dependence is observed. Values of $\theta_{1\ Hz}$ obtained from the plots are erratic, although of approximately the correct order of magnitude. Thus it is concluded that the heterogeneous redox catalysis theory gives a very poor explanation of the data.

4.8 Conclusions

The dependences of the current of a rotating TTF TCNQ disc electrode on [E] , [S] and ω have been presented and analysed according to the homogeneous mediation theory and the heterogeneous redox catalysis theory. The preliminary analysis showed that for experiments at constant [S] , the current depends on $[E]^1$ at low concentrations and $[E]^{1/2}$ at high concentrations of enzyme, with the rotation speed dependence varying from $\approx \omega^{-0.5}$ to $\approx \omega^{-0.1}$ respectively. For experiments at constant [E] , the current depended on $[S]^1$ at very low concentrations, $[S]^{1/2}$ at intermediate concentrations and $[S]^0$ at high concentrations, with the rotation speed dependence approximately constant for each experiment and intermediate between $\approx \omega^{-0.3}$ to $\approx \omega^{-0.1}$. No significant effect of potential on the current was observed, except that $[S]^1$ dependence was observed up to a higher concentration at the higher potential. The effect of potential was difficult to understand from these experiments, since a new electrode was used for each. The potential dependence of the current is considered in more detail in Chapter 5.

The homogeneous mediation theory gave the best fit of the theoretical analysis; all aspects of the data could be satisfactorily explained. The data were fitted on to the theoretical case diagram in fig(4.17). The translation of the data in the case diagram on increasing [E] or [S] can be related to the actual physical situation occurring. At low [S] and [E], the data is in case V. We have seen that increasing [S] results in a translation into case II. In both cases V and II, the E' + M reaction is slow, but in case V, the regeneration of E' throughout the diffusion layer is rate determining. Increasing

[S] increases the rate of regeneration of E' (since κ_E increases), so that on entering case II, the E' + M reaction can become rate limiting.

If [E] is increased in case V, then the E' + M reaction becomes faster (since κ_M increases). Thus the mediator reaction layer decreases in size, so that in case VI, the mediator reaction layer is only very small at the electrode surface and no longer throughout the whole diffusion layer. However the regeneration of E' from E is still slow and so the rate limiting step in case VI is the regeneration of E' from E in a small enzyme reaction layer next to the mediator reaction layer at the electrode surface.

At low [ε] and high [ς], the data start in case II. Increasing [E] increases κ_M , so that the mediator reaction layer decreases. Thus on increasing [E] we move from case II, where the E' + M reaction is rate limiting throughout the whole diffusion layer, to case I, where the E' + M reaction is still rate limiting, but in a small reaction layer next to the electrode surface.

At low [S] and high [E], the data are in case VI. In this case, the rate determining step is the regeneration of E' from E in a small enzyme reaction layer next to the mediator reaction layer at the electrode surface. Increasing [S] increases the rate of regeneration of E' from E. Thus on moving from case VI to case I, the regeneration of E' from E increases and is no longer rate limiting, so that the reaction between E' + M in the small mediator reaction layer becomes the rate determining step.

The heterogeneous redox catalysis theory could only explain the dependence on enzyme concentration taken in isolation, but could not explain the associated rotation speed dependence. This theory totally failed to explain the dependence on [S], in particular the first order

dependence; the concentration polarization of the substrate within the diffusion layer was shown to be an inadequate explanation.

The experimental data were plotted in the form predicted by the two theories for each of the case boundaries most likely to to be crossed by the data. For the homogeneous theory, the data varying [E] gave a reasonable fit to the case II - I boundary, although at very high concentrations some departure from the theoretical plot was observed. This was thought due to the dilution of both the enzyme and the substrate at such high concentrations. It is satisfactory that this analysis agrees with that carried out by Bryan Driscoll [79] for the saturated electrode, who concluded that his data best fit the case II - I boundary. The data varying [S] gave an excellent fit to the case V - II boundary; in addition, the data at high constant [E] also fitted the case VI - I boundary. The position of the data in the case diagram agreed with the preliminary analysis and with the position predicted from calculating the theoretical variables in section 4.3.2. Values of k_M and m_o calculated from the plots are $\approx$ 10 - 100 times greater than the values previously assumed (section 4.3.2). For the heterogeneous theory, the fits of the experimental data to the theoretical plots were very poor indeed. Only data at very high [E] or [S] gave the predicted straight line.

Then, in conclusion, the homogeneous mediation theory can explain all the data obtained, while the heterogeneous redox catalysis theory can only explain the dependence of sections of the data taken in isolation. The biggest failing of the heterogeneous theory is the inability to explain the first order dependence of current on [S]. If the homogeneous mediation mechanism is indeed occurring, one would expect some mediator species to be present in the solution. Thus in Chapter 5, ring-disc electrode results are reported for a TTF

TCNQ disc electrode in the presence of glucose oxidase and its substrate, glucose.

Chapter 5

Further investigations of the mechanism of electron transfer

The dependence of the current of a TTF TCNQ disc electrode on [S], [E] and ω has been analysed at length in Chapter4, and it was concluded that the homogeneous mediation theory was the best fit of the experimental data. In this chapter, the dependence of the current on the remaining variable, the potential of the electrode, is considered. In order to relate the effect of a change of potential on the experimental data, the position of the data in the two theoretical case diagrams must be known. The analysis of the data in Chapter 4 makes this possible.

Also reported in this chapter are the results from a rotating ring-disc electrode study, using TTF TCNQ as the disc material, with both glucose oxidase and its substrate, glucose, in the bulk solution. The aim of the ring-disc electrode study was to detect a mediator species from the disc electrode. This was thought necessary in view of the very good fit of the homogeneous mediation theory to the experimental data in Chapter 4. The absence of any mediator species detected on the ring electrode would severely discredit the homogeneous mediation mechanism. In the only ring-disc experiment performed to date, using a NMP TCNQ electrode in the absence of enzyme and substrate, no ring currents were observed above the background current, placing a lower limit on the mediator concentration of $<10^{-6}$ M [62]. However, the introduction of enzyme and its substrate into the bulk solution might influence the flux of any possible mediator species from the disc electrode.

The potential dependence of the ring current was measured in order to discover the optimum potential at which to hold it, and also to discover something about the nature of the species detected on the ring. The ring and disc currents were measured for increasing concentrations of substrate in the presence of glucose oxidase. The disc current was analysed in terms of the homogeneous mediation theory and the heterogeneous redox catalysis theory, in order to find the position of the data in the two theoretical case diagrams. This allowed the collection efficiency of the ring electrode to be predicted according to the two theories. The collection efficiency for case V, case VI, case I and the case V - VI boundary are given. Analysis of the variation of the collection efficiency with [S] allowed the best fit of the collection efficiency to the two theories to be made.

5.1 Potential dependence of the electrode

In Chapter 4, the dependence of the current on [S], [E] and ω was studied at great length. The remaining experimental variable to be investigated is the potential of the electrode. Initially we must understand the effect of a change of potential on the case diagram for each theory.

5.1.1 The homogeneous case

m_o is the only potential dependent variable in this theory. It is assumed that m_o will increase with potential. ϕ is directly dependent on m_o , while $1/\gamma$ and β are inversely dependent on m_o . A decrease in potential of ΔE will result in a decrease in log ϕ by $-\Delta \log m_o$ and an increase in both $\log(1/\gamma)$ and $\log \beta$ by $+\Delta \log m_o$.

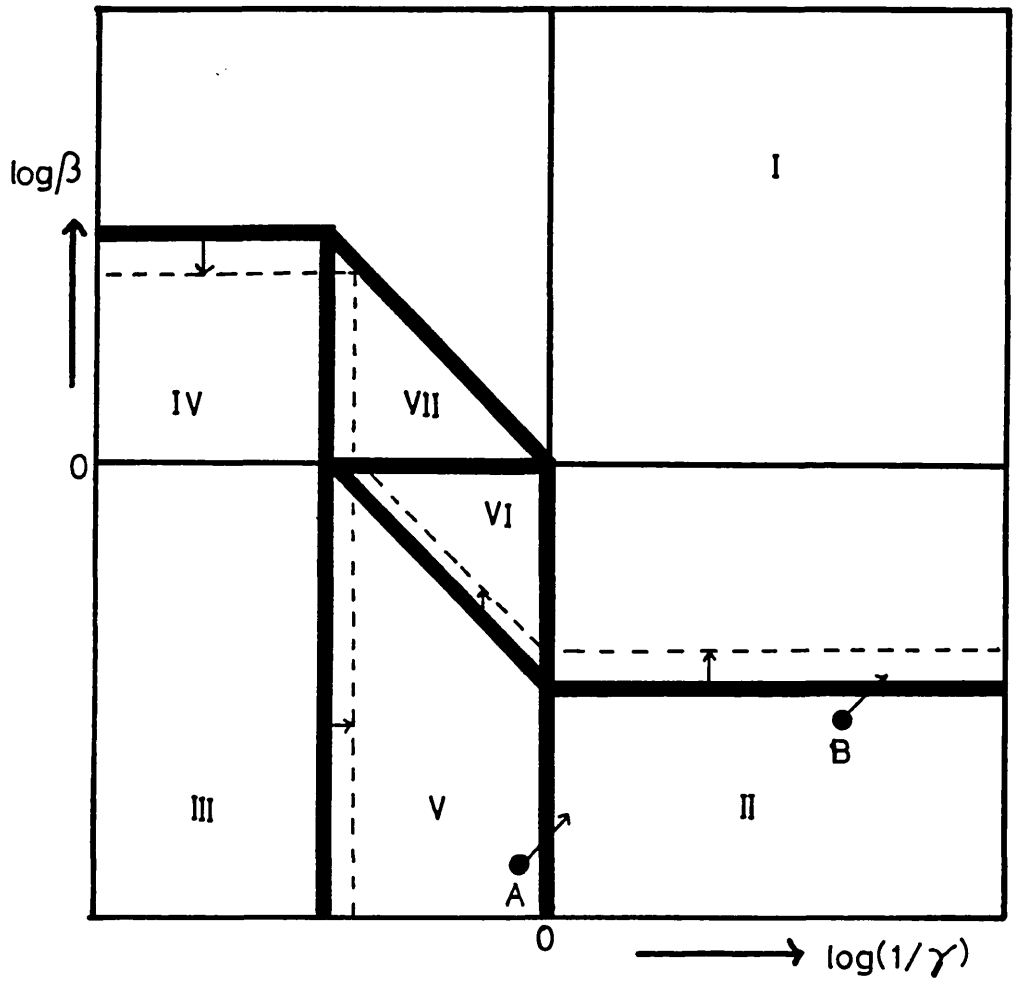
We must also consider the effect of a potential decrease on the case boundaries. The boundaries $\gamma = 1$ and $\beta = 1$ are independent of potential. The boundaries $1/\gamma = 1/\phi$ and $\beta = 1/\phi$ are inversely dependent on m_o and so will increase by $+\Delta\log\ m_o$. The boundary $\beta = \phi$ is directly dependent on m_o and so will decrease by $-\Delta\log\ m_o$. The boundary $\beta = \gamma$ must still intercept at the points $\beta = \gamma = 1$ and $\beta = \gamma = \phi$. The gradient of the boundary is given by $\log \beta\ /\ \log\ (\ 1/\gamma\ ) = -1$ i.e. it is constant and independent of potential.

The boundary $\beta\ \phi = \gamma$ is the most complex to consider. Taking the log of the boundary gives:

$$\log \beta = -\log\ (\ 1/\ \gamma\ ) - \log \phi$$

i.e. the gradient of the boundary is -1 and independent of potential. The intercept on the line $\beta = 1$ is given by $1/\ \gamma = 1/\phi$ and the intercept on the line $\gamma = 1$ is given by $\beta = 1/\phi$ and so the ends of the boundary are fixed as before. Then in effect the boundary has shifted both horizontally and vertically by $+\Delta\log\ m_o$, towards the top right hand side of the diagram.

The effect of a decrease in potential on the case diagram is shown in fig(5.1). For a particular point in the case diagram, say $(\ 1/\gamma\ ,\ \beta\ )$, a decrease in potential will result in a NW shift of the point to $(1/\gamma + \Delta\log\ m_o\ ,\ \beta + \Delta\log\ m_o)$. Then the point may shift to a new case depending on its position in the case diagram. For example, if a point is on or close to a case boundary which is independent of potential, it may be shifted to a new case e.g. point A in fig(5.1). However for a point on or near a case boundary that also shifts NW by $\Delta\log\ m_o$, then no new case can be entered since the point and the boundary do not move relative to one another e.g. point B in fig(5.1). Then in



Fig(5.1) The effect of a decrease in applied electrode potential on the case diagram for the homogeneous mediation theory (the $\phi > 1$ plane). ---- shows the new position of the case boundary. Point A shifts into a new case, while point B does not.

order to predict the effect of potential for a particular set of fixed experimental conditions i.e. [S], [E] and ω, the initial position in the case diagram must be known. For the experimental conditions used in these experiments, the position can be deduced from the previous discussions (section 4.5).

5.1.2 The heterogeneous case

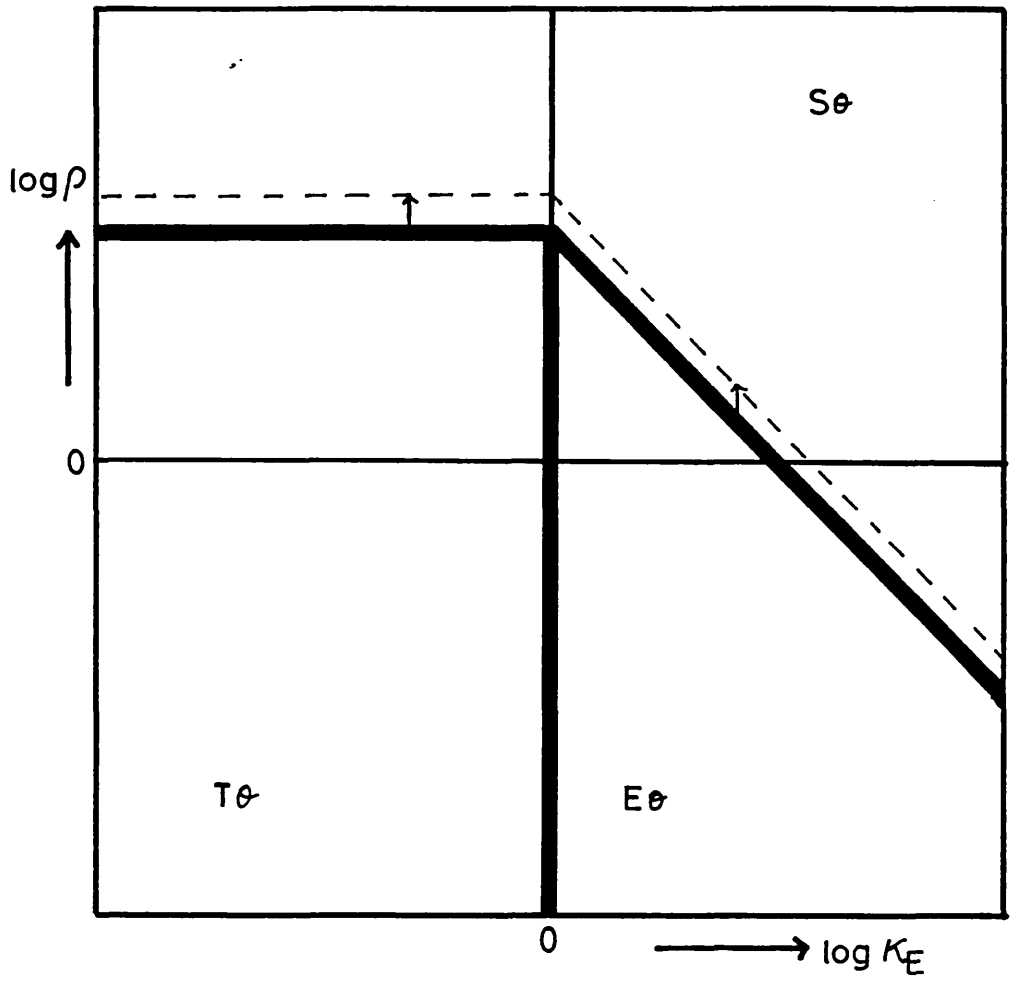
The only potential dependent variable in this theory is k_2. Of the three experimental variables, κ_E is independent of k_2 , while both ρ and θ are dependent on $1/k_2$. Thus a decrease in potential would result in a decrease in log k_2 to log k_2' and a corresponding increase in both log ρ and log θ by log (k_2/ k_2').

The case boundaries must also be considered. The boundary $\kappa_E = 1$ is independent of k_2 and therefore unaffected by a change in potential. The boundary $\rho = (1 + \theta)$ will shift up the log ρ axis by log (k_2/ k_2'). The boundary $\rho\ \kappa_E = (1 + \theta)$ is easier to understand if written in log form:

$$\log \rho = - \log \kappa_E + \log (1 + \theta).$$

Then the gradient of this boundary is -1 and independent of potential. The intercept on the line $\kappa_E = 1$ is given by log (1 + θ) and is thus increased by log (k_2/ k_2') if potential is decreased.

The effect of potential on the case diagram is shown in fig(5.2). For a point on the case diagram, say (log κ_E , log ρ), a decrease in potential will result in a shift upwards, parallel to the log ρ axis, of log (k_2/ k_2'). Thus a point next to a case boundary cannot be shifted



Fig(5.2) The effect of a decrease in applied electrode potential on the case diagram for the heterogeneous redox catalysis theory. ---- shows the new position of the case boundary.

into a new case on a change in potential, since the case boundary will shift by an equal amount.

5.1.3 The potential dependence results

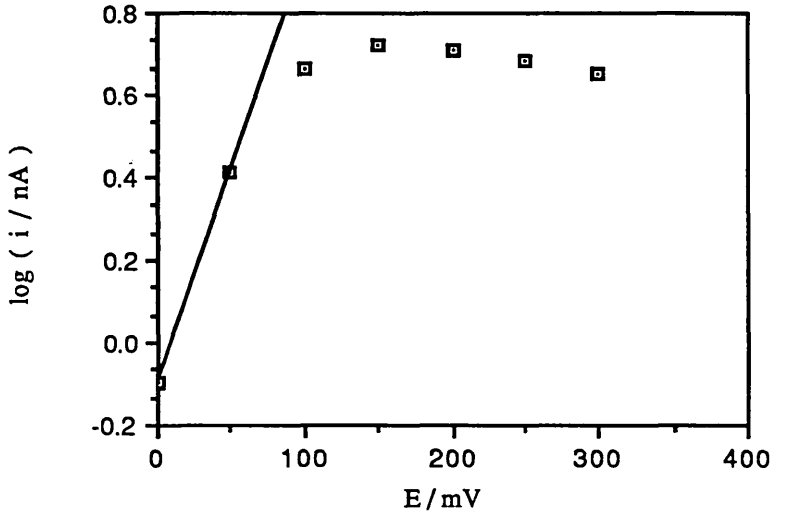
It was noted in section 5.1.1 that the position of the data in the case diagram must be known to interpret the data in terms of the two theories. Thus the experimental conditions were chosen after inspection of the data in section 4.5. An enzyme concentration of 5 u/ml was chosen, and the potential dependence of the electrode current was measured at 0.1, 1.0 and 50.0 mM glucose. These concentrations corresponded to the regions where data depended on substrate concentration to the first order, half order and zeroth order respectively, for the electrode held at both +200 and +300 mV. For the homogeneous theory, this corresponds to a horizontal shift from case V to case II, and for the heterogeneous theory, to a horizontal shift from case $E\theta$ to case $S\theta$ (although it should be noted that first order dependence on [S] is not explicable by the heterogeneous theory and the position of the data in the case diagram is extremely tenuous).

The potential dependence of the electrode current is shown in figs(5.3.a) - (5.3.c) for the three substrate concentrations. The data are plotted in the form E vs. log i according to the Tafel equation [122]:

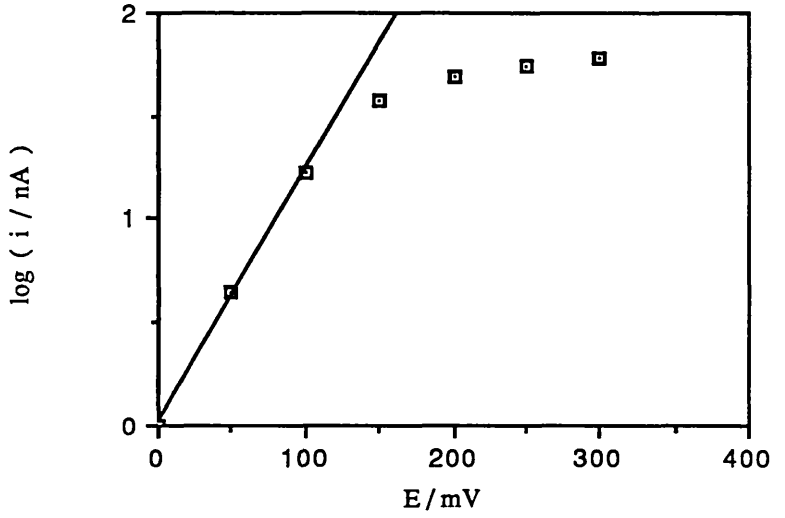
$$\log i = \log i_0 + \alpha n F E'/RT \quad (5.1)$$

where E' is the applied electrode potential. The gradient of the plot is given by $\alpha nF/RT$ and hence $n\alpha$ can be found.

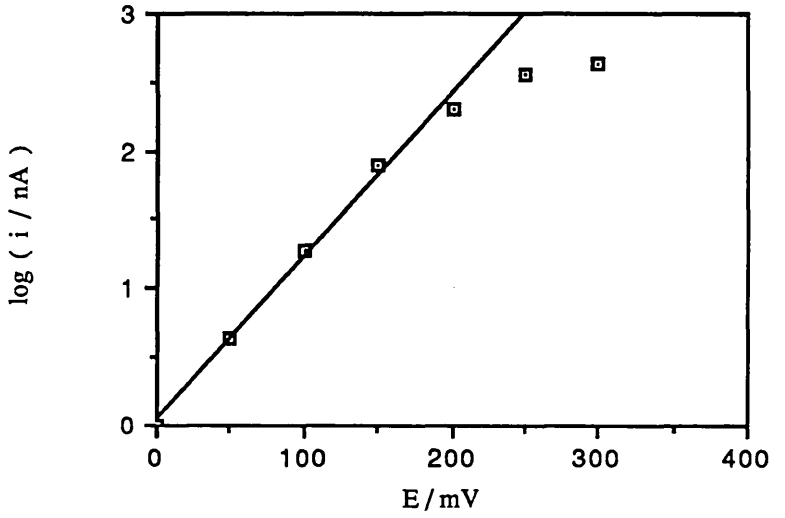
Fig(5.3.a) The potential dependence of the current at 0.1 mM glucose



Fig(5.3.b) The potential dependence of the current at 1 mM glucose



Fig(5.3.c) Potential dependence of the current at 50 mM glucose



From inspection of the plots, it is apparent that the potential dependence of the electrode current is much (greater) at lower potentials than at higher potentials, and that the potential below which high potential dependence is observed increases with substrate concentration. The values of $n\alpha$ have been calculated for each substrate concentration for the regions of both high and low potential dependence and are given in table 5.1. It should be noted that at 0.1 mM glucose in the high potential region, $n\alpha$ is calculated from two points and so is inherently inaccurate.

Initially the points are analysed in terms of the homogeneous theory. For an enzyme concentration of 5 u/ml and with 0.1 mM glucose, we are in the region where i depends on $[S]^1$ for both +200 and +300 mV, described by case V. In this case there is no m_0 term in the expression for j and hence no potential dependence is expected. Decreasing the potential will result in a shift in the case diagram in the NW direction. If we are close to the case V - II boundary (which is potential independent), then it is possible we will shift into case II at low potentials. In case II, the expression for j is dependent on m_0 and hence some potential dependence is expected at lower potentials i.e. 0 - +50 mV.

Increasing [S] to 1.0 mM implies we are close to the case V - II boundary, because $[S]^{1/2}$ dependence is observed at this concentration and this is intermediate between case V ($[S]^1$ dependence) and case II ($[S]^0$ dependence). Thus it is expected that the potential at which we shift into case II will be higher than at 0.1 mM glucose. This is indeed observed in fig(5.3.b), where (strong) potential dependence occurs between 0 to +150 mV.

At 50 mM glucose, we know $[S]^0$ dependence is observed at both +200 and +300 mV. Thus we expect to be in case II at all potentials,

[S] / mM	nα (no units)	
	(high) potential strong dependence	low potential dependence
0.1	0.62 (0 - 50 mV)	≈ 0 (100 - 300 mV)
1.0	0.72 (0 - 100 mV)	0.05 (200 - 300 mV)
50.0	0.74 (0 - 150 mV)	0.10 (250 - 300 mV)

Table 5.1 nα values for the data in figs(5.3.a) - (5.3.c)

and to observe potential dependence throughout. Although potential dependence is observed to a higher potential than at 1 mM glucose, at +250 and +300 mV it is minimal. This is explicable if at these higher potentials, we are still close to the case V - II boundary, where intermediate behaviour is expected. It is interesting to note that if we are indeed crossing the case V - II boundary, the regions of (high) potential dependence should have the same $n\alpha$ value, independent of [S], given by case II. This is approximately observed with $n\alpha$ between $\approx$ 0.6 and 0.75.

Now we turn to the heterogeneous redox catalysis theory. It is difficult to interpret the data in terms of this theory, since the initial position of the data at 0.1 mM glucose (i.e. where $[S]^1$ dependence is observed) is unknown. At 1.0 mM glucose, $[S]^{1/2}$ dependence is observed for data at +200 and +300 mV; this is explicable by case Eθ. Any change in [S] results in a horizontal shift in the $\theta >> 1$ plane. Thus it shall be assumed that at 0.1 mM glucose, we are in case Eθ, to the left of the position occupied by 1.0 mM glucose. On decreasing potential from +300 mV, we will shift vertically up the case diagram; however the case Eθ-Sθ boundary will also shift upwards by an identical amount and so we can never enter case Sθ. This argument also applies to data at 1.0 mM glucose. Thus the potential dependence is described by k_2 in the $1/(1 + \theta)$ term in eqn. (B.32). Thus some degree of potential dependence is expected. Clearly the data do not agree with the theory, since potential dependence is only observed at lower potentials, and not throughout the whole range of potentials examined..

For data at 50 mM glucose, we know that at +200 and +300 mV, $[S]^0$ dependence is observed. It was seen in section 4.5.8 that case Sθ was the best explanation of this behaviour. Decreasing the

potential from +300 mV results in a vertical shift further into case Sθ, and so at 50 mM glucose the potential dependence of the current should be explicable by this case for all potentials. In case Sθ, the potential dependence is given by the $[k_2/(1 + \theta)]^{1/2}$ term in eqn. (B.27) i.e. some degree of potential dependence is expected. It can be seen , from fig(5.3.c), that potential dependence is observed up to +200 mV only, and once more the behaviour of the data does not agree with the heterogeneous theory.

5.1.4 Conclusion of the potential step experiment

The homogeneous theory explains the potential dependence of the current very well, by placing the data close to the case V - II boundary. In particular, this theory can explain why potential dependence is observed up to a higher potential at higher glucose concentrations. The case V - II boundary predicts the nα values should be independent of [S], which is indeed approximately observed.

The heterogeneous theory fails to explain the potential dependence at all substrate concentrations. The theory predicts that potential dependence should be observed at all potentials; however at each [S], regions of high and low potential dependence were observed.

One possible way the heterogeneous theory could allow regions of high and low potential dependence is if k_2 were to reach its limiting value at some potential in the experimental range. However, this would predict that the regions of high and low potential dependence should always occur at the same potentials, since k_2 would always

reach its limiting value at the same potential. This is not observed, and so clearly this explanation is not adequate.

It should be noted that the nature of the potential dependence of m_o is ambiguous. m_o could be potential dependent for one of two reasons:

(1): the solubility of m_o increases with potential. In this case one would not expect the solubility to reach a maximum as potential is increased.

(2): the rate constant for the $M' \rightarrow M + e^-$ reaction is potential dependent. In this case, one would expect m_o to reach a maximum at some potential i.e. in the mass transport limited region. At lower potentials, not all M' reaching the electrode would be oxidized. Thus the concentration gradients of M' and M at the electrode would decrease. This violates one of the initial assumptions of the theory.

If m_o is potential dependent, then the values of $k_M m_o$ calculated for the case V - II boundary should increase with potential, assuming k_M to be potential independent. Values of $k_M m_o$ are given in table 4.15. Comparing data at both 1 and 5 u/ml GOD shows that $k_M m_o$ is indeed higher at +300 mV. One would also expect the value of $k_M m_o$ to be approximately constant at each potential. This is seen for the value calculated from Δx, but much wider variation is seen for Δy, possibly due to the greater error in measuring current as opposed to concentration. The data at 50 u/ml are in cases VI - I and so the $k_M m_o$ values are meaningless.

5.2 Ring-disc electrode studies

In this section, a ring-disc electrode study is reported, the aim of which was to detect any redox species being lost from the TTF TCNQ disc. Both the homogeneous mediation theory and the heterogeneous redox catalysis theory predict the loss of a redox species from the electrode to the bulk. For the former theory, this is M and/or M', and for the latter theory, it is A^{o}.

Results are reported for the potential dependence of the ring current. This enables the ring to be held at the potential for the limiting current for the redox species in subsequent experiments. It also gives some information on the chemical identity of the redox species.

The ring and disc currents were measured in the presence of glucose oxidase and increasing concentrations of glucose. The disc current is analysed in terms of the two theories, to discover the position of the data in the case diagrams. This enables the behaviour of the M and M' species, and the A^{o} species, to be interpret ed for the appropriate cases and hence the dependence of the collection efficiency on [S] to be predicted. Comparison of the observed collection efficiency with the theoretical collection efficiencies allows the theory most appropriate for the data to be identified.

In the ring-disc electrode experiments reported below, the same conditions were employed as for the series of mechanistic experiments described in Chapter 4 and section 5.1, i.e. the disc electrode is held at +300 mV, there is 5 u/ml GOD in the bulk solution and successive injections of glucose are made. It was necessary to work in an Argon atmosphere, since any small amount of contaminating oxygen could react with the reduced enzyme to give

H_2O_2 , which in turn could be oxidized at the platinum ring giving rise to spurious results. This in turn allowed measurements to be taken at three rotation speeds since substrate depletion at low concentrations would no longer be a problem, and so the time scale of the experiment was not so important.

The theory for the rotating ring-disc electrode will not be given in this thesis. Readers are referred to standard texts [122], [133] and [135].

5.2.1 Collection efficiency

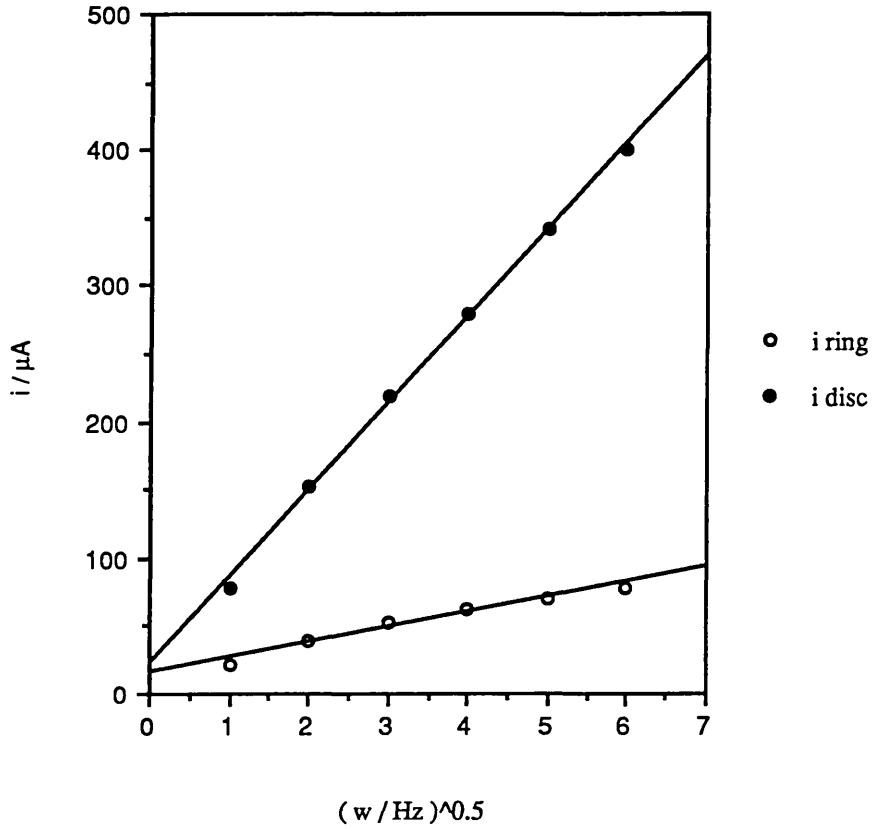
The collection efficiency, N, of the ring-disc electrode was measured using 10 mM $K_3Fe(CN)_6$ made up with pH 7.4 phosphate buffer. N is given by [133]:

$$N = - i_{ring}/i_{disc} \qquad (5.2)$$

for the case where A → B on the disc, and B → A on the ring. For this experiment, we identify $Fe(CN)_6^{3-}$ with A. The ring and disc electrode currents are shown in fig(5.4). The data are plotted in the form of the Levich equation (eqn. (4.29)).

The i vs. $\omega^{1/2}$ profiles are seen to be non-linear at high ω values. This was also observed by D.H. Craston [138], who proposed the roughness of the electrode was responsible for this behaviour. At high rotation speeds i.e. 36 Hz, the diffusion layer thickness is $\approx 9 \times 10^{-4}$ cm, which is approximately equal to the intercrystallar distance ($\approx 10^{-3}$ cm), so it is quite possible for roughness to be causing this effect. It is also observed that at $\omega = 0$ there is some current on both ring and disc electrodes. The calculated

Fig 5.4 The Levich plot for the ring and disc currents with 10 mM ferricyanide



values for N are given in table 5.2. Also given is N', the collection efficiency calculated by subtracting the currents at ω=0 from both ring and disc electrode currents. These values should be compared with the theoretical value of N, determined to be 0.23 from the purely geometric consideration of the electrode, using eqn. (3.12) from reference [133] and the values for the ring-disc electrode dimensions given in section 2.4.4. Then clearly N' gives better agreement with the theoretical value than N.

The current at ω=0 is presumably due to the slow rate of electron transfer between $Fe(CN)_6^{3-}$ and the TTF TCNQ electrode. The Koutecky-Levich plot for the disc is shown in fig(5.5). The Koutecky-Levich equation is given by [139]:

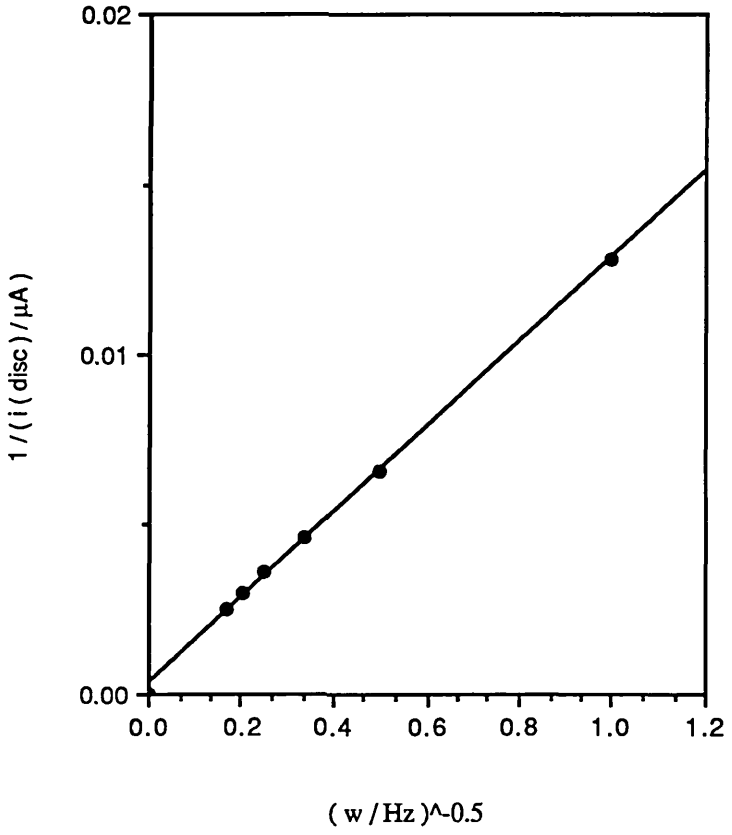
$$1/ i = 1/ nAFk'[S]_\infty + 1.554\, \upsilon^{1/6}/ nAFD^{2/3}\, \omega^{1/2} [S]_\infty . \quad (5.3)$$

This plot enables determination of the rate constant, k', for the rate limiting step at infinitely high ω i.e. when mass transport of the electroactive species is no longer rate limiting. We assume that for our electrode, this rate constant is the electrode rate constant. The intercept at $\omega^{-1/2} = 0$ ($\omega \rightarrow \infty$) gives a value for the electrode rate constant of 1.39 $x10^{-2}$ cm s^{-1} , which is indeed quite slow.

5.2.2 Potential dependence of the ring current

In the next stage, the potential dependence of the ring current was measured over the range -0.6 V to +0.8 V vs. SCE in steps of +100 mV, with the disc electrode held at +300 mV throughout. This was necessary to determine at what potentials, if any, the redox species could be detected. The potential range was scanned a

Fig 5.5 The Koutecky-Levich plot for the disc current in fig 5.4



$\omega^{1/2}$ / $(Hz)^{1/2}$	N no units	N' no units
1	0.282	0.230
2	0.257	0.230
3	0.237	0.220
4	0.221	0.210
5	0.208	0.196
6	0.200	0.187

Table 5.2 N and N' values for the platinum ring electrode measured using 10 mM $K_3Fe(CN)_6$

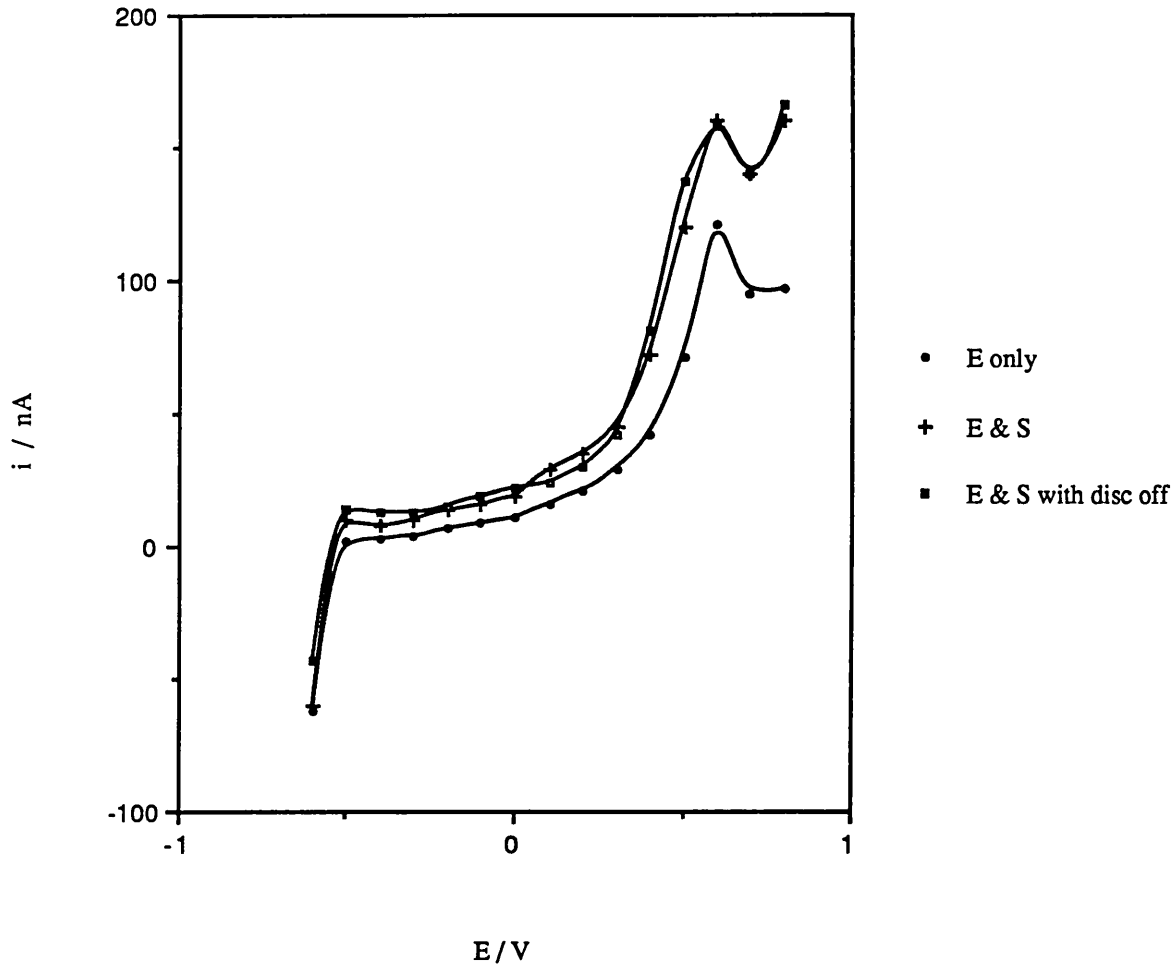
number of times, in the absence of both enzyme and substrate, in the presence of the enzyme, and finally in the presence of both the enzyme and a saturating concentration of the substrate (50 mM). The results are shown in fig(5.6). A large increase in ring current is observed on injecting substrate. This increase is roughly maintained on switching the disc electrode to open circuit potential. This is shown in fig(5.7), where the ring current for the situation where only enzyme is in the pot is subtracted from the ring current for the situations where both enzyme and substrate are in the bulk solution and where the disc ele ctrode is switched to open circuit potential. It can be concluded that the disc electrode need not be doing any bioelectrochemistry for the ring current to be observed.

We can see in fig(5.6) that the ring current, in the presence of saturated enzyme, increases with potential until at +300 mV it is approximately constant. Above this potential, a 3-4 fold increase in the ring current is observed, reaching a maximum at ≈ +600 mV. The oxidation current at +300 mV is assigned to the mass transport limited region for the first oxidation reaction of the redox species. The peak at +600 mV is assigned to the second oxidation reaction. It should be noted that the second oxidation peak is anomalously large in comparison to the first limiting oxidation current. One would expect only double the oxidation current for the second oxidation reaction. Also of note is the absence of any reduction current.

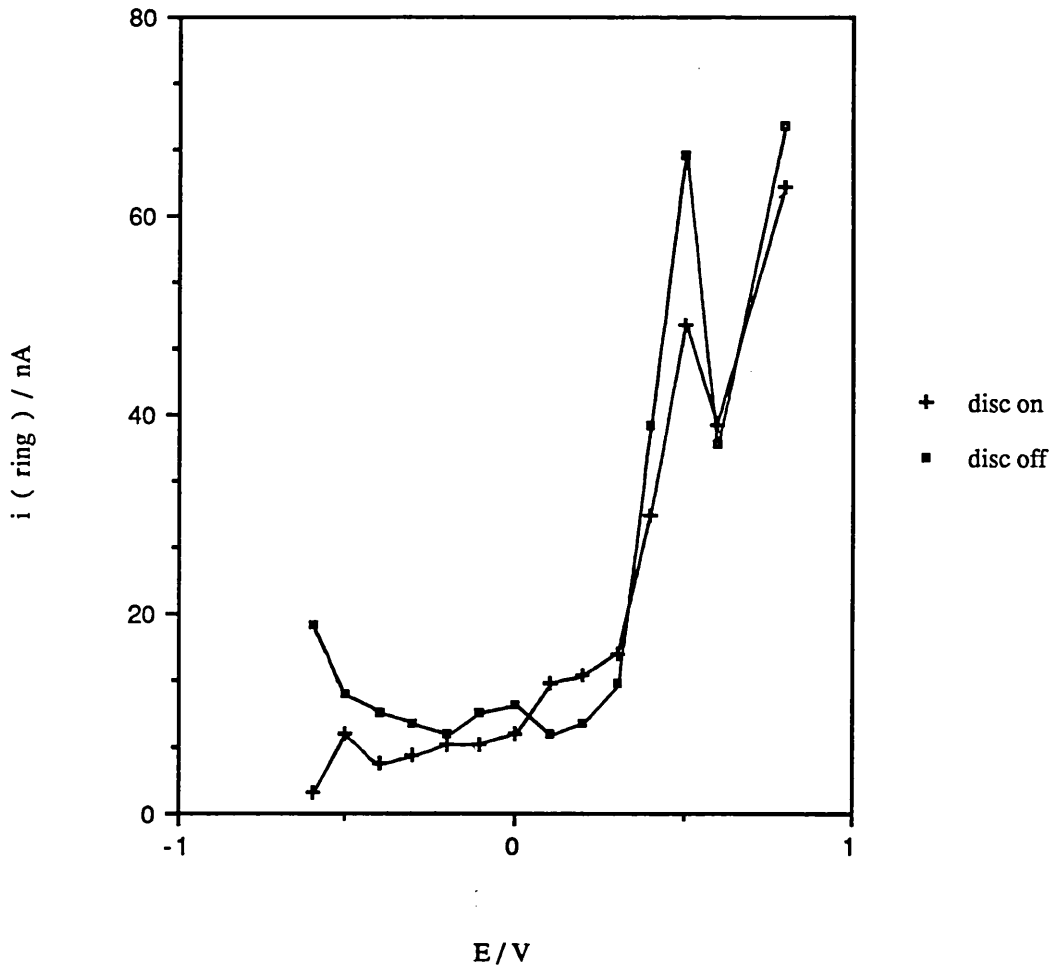
5.2.3 Identification of the redox species

To interpret the potential dependence of the ring current, we must initially consider what each of the theories predicts about the nature of the redox species. In the homogeneous mediation theory, it

Fig(5.6) The potential dependence of the ring current



Fig(5.7) The potential dependence of the ring current



can be seen from section 4.5 that at 5 u/ml GOD and 50 mM glucose we are in case I. The concentration profiles for the M and M' species in this case are shown in fig(A.2). In this case, M is totally consumed in a very small reaction layer next to the electrode surface. M' has a linear concentration profile from very close to the electrode surface to the outside edge of the diffusion layer. Thus only M' is expected to be lost to the bulk and hence to reach the ring electrode. This predicts that we will see the oxidation of M' from M on the ring. Thus M will be regenerated at the ring itself. This poses the question of whether we will also be able to see the reduction of M on the ring electrode. However when the ring electrode is held at a reducing potential, no M is being regenerated from the oxidation of M' at the ring, and hence in case I we do not expect to see any reduction current. It should be noted that the M' species may be capable of undergoing two one-electron oxidation reactions, thus giving rise to the two oxidation peaks observed in fig(5.6).

The heterogeneous redox catalysis theory predicts that A^o will diffuse from the electrode surface into the bulk. For the diffusion of A^o to be significant, the condition $\theta > 1$ must be obeyed (this is seen from section B.3). This condition requires the electrode current to have rotation speed dependence, and since this is always experimentally observed, it can be concluded that the diffusion of A^o away from the electrode surface is occurring at a significant rate. Thus the theory predicts that the oxidation of A^o to A^+ could be observed on the ring electrode, and that a second oxidation reaction may be possible to A^{2+}. For TTF TCNQ, A^o is identified with TTF^o. Thus no reduction current is predicted for the ring electrode.

It is concluded that the two theories both allow first and second one-electron oxidation reactions to occur, and expect no reduction

reaction. Thus no distinction can be made between the two theories on this basis.

Now we must attempt to assign the observed oxidation peaks to the redox species. The species we shall consider are TTF^{o}, TTF^{+} and $TCNQ^{-}$. All these species can undergo a one-electron oxidation reaction, although only TTF^{o} can undergo a second one-electron oxidation. Thus if one of the other species were the redox species being measured, another explanation must be found for the second oxidation peak. The oxidation and reduction potentials of these species are given in table 5.3. From inspection of this table, it is seen that either TTF^{o} or $TCNQ^{-}$ could be responsible for the oxidation current below +300 mV. However for the second oxidation current above +300 mV, the only possible reaction is $TTF^{+} \rightarrow TTF^{2+} + e^{-}$. If we then identify the redox species with TTF^{o} i.e. $TTF^{o} = M'$ or A^{o} depending on which theory is under consideration, the solubilities of TTF^{o} and its first and second oxidation products are crucial.

If the redox species is assigned as TTF^{o}, then the anomalously large second oxidation peak can be explained in terms of the solubility of TTF in its various oxidation states. Eddowes and Gratzel [129] do not consider the second oxidation step of TTF^{o} to be a simple process: they propose TTF^{o} is oxidised to TTF^{2+} at the electrode. Then in solution TTF^{2+} recombines with TTF^{o} to give 2 TTF^{+} , which in turn are oxidized at the electrode. TTF^{o} is relatively insoluble and will have a slower diffusion coefficient than either TTF^{+} or TTF^{2+}. Thus in the second oxidation peak, TTF^{+} will have enhanced mass transport compared to TTF^{o} and a larger oxidation peak will result.

The assignment of the redox species to TTF^{o} has been confirmed by using TTF^{o} as a mediator in the bulk solution [141]. TTF^{o} was able to mediate the electron transfer between reduced glucose oxidase

Redox reaction	$E^{o'}$ / V vs. SCE
$Cl^-(aq) + TTF^o(s) \rightarrow TTF^+Cl^-(s) + e^-$	+ 0.13 [85] + 0.17 [129]
$TTF^+Cl^-(s) \rightarrow TTF^{2+}(aq) + Cl^-(aq) + e^-$	+ 0.39 [85] + 0.50 [129]
$Na^+TCNQ^-(s) \rightarrow TCNQ^o(s) + Na^+(aq) + e^-$	+ 0.26 [140]

Table 5.3 The potentials for the oxidation of various redox species existing on a TTF TCNQ electrode within its stable range

and a platinum electrode. Two oxidation peaks coincident with those observed in fig(5.6) were found, with the second oxidation peak anomalously larger than the first.

Thus it can be concluded that that redox species detected on the ring electrode is most likely to be TTF^{o}. From fig(5.6) it is observed that the limiting current of the first oxidation reaction is observed at +300 mV. Thus the ring electrode should be held at this potential for all subsequent ring-disc electrode experiments.

5.2.4 The dependence of the ring and disc currents on the concentration of substrate

The dependence of the ring current on substrate concentration can yield further information about the validity of the two theories. In the homogeneous theory, the diffusion of M and/or M' into the bulk is dependent on the particular case describing the data. Thus the dependence of the disc current on substrate concentration must be analysed in order to discover the case or cases applicable and to predict the behaviour of the ring current. In the heterogeneous theory, the diffusion of A^{o} into the bulk is independent of both [E] and [S], and thus if this theory is correct, the ring current should always remain constant on increasing the substrate concentration. Also, the rate of diffusion of A^{o} is given by k_D (eqn. (B.1)) which is inversely dependent on z_D and hence dependent on $\omega^{1/2}$ (seen from eqn. (A.83)). Thus the ring current should show positive rotation speed dependence. For the homogeneous mediation theory, the rotation speed dependence of the ring current can be seen from considering eqn. (5.2) for N. For this experiment, $i_R = N\, i_D$, since both ring and disc electrodes are oxidizing M'. Thus if the disc

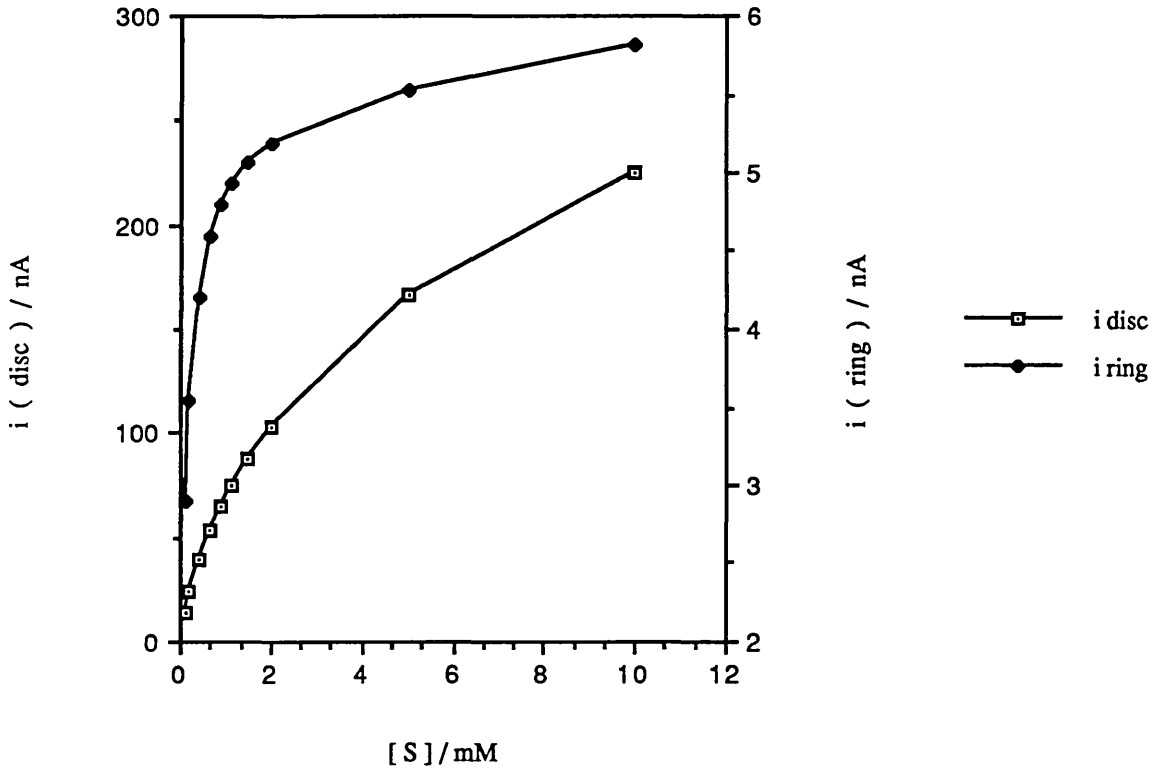
current has negative rotation speed dependence, this should also be observed for the ring current.

The responses of the ring and disc electrodes to successive injections of glucose were measured with 5 u/ml GOD in the bulk solution, and holding both the ring and disc electrodes at +300 mV. These responses are shown in fig(5.8). The ring current increases for each injection of substrate. The ring current always exhibits negative rotation speed dependence: this is shown in fig(5.9) for increasing [S]. Thus immediately we can discard the heterogeneous redox catalysis theory as a possible explanation of the ring current, since it always requires the ring current to exhibit no dependence on [S] and to have positive dependence on rotation speed. The remainder of the discussion of the ring-disc electrode study will be confined to the homogeneous mediation theory. It should be noted that the negative rotation speed dependence of the ring current supports the homogeneous mediation theory.

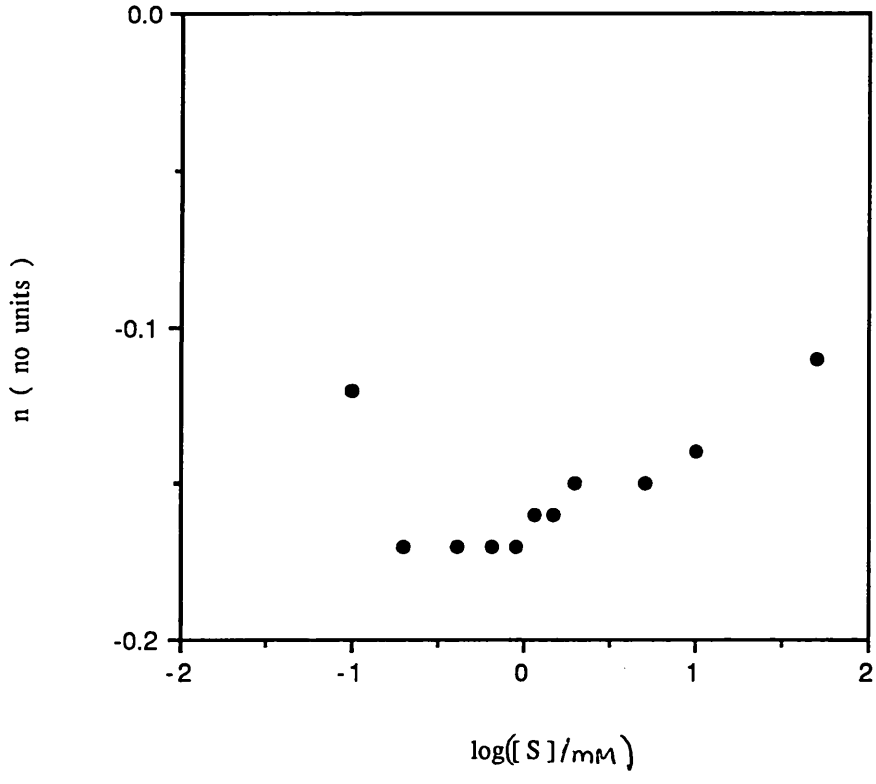
As we have noted above, the disc current must be analysed in order to discover which case(s) is most applicable to the data. From previous discussions in section 4.5, it was concluded that at 5 u/ml GOD , the experiment would start in case V at low [S] and move into case II as [S] was increased, although the data would be very close to the case II - I boundary.

Plots of i vs. $[S]^{1}$ and $[S]^{1/2}$ are shown in figs(5.10.a) and (5.10.b) for the disc current. Some points at high concentrations have been ignored in fig(5.10.a) to present the data to its best advantage. At very low [S], the data are almost first order. At higher [S], the data is half order, apart from the point at highest concentration. This analysis is in agreement with the previous analyses of experimental data at +300 mV and 5 u/ml GOD, with the

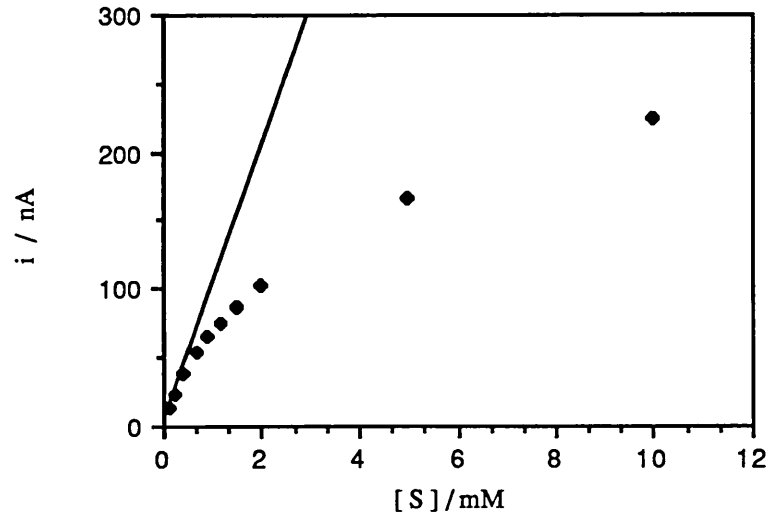
Fig(5.8) Plot of ring and disc currents vs.
[S] for data at 9 Hz



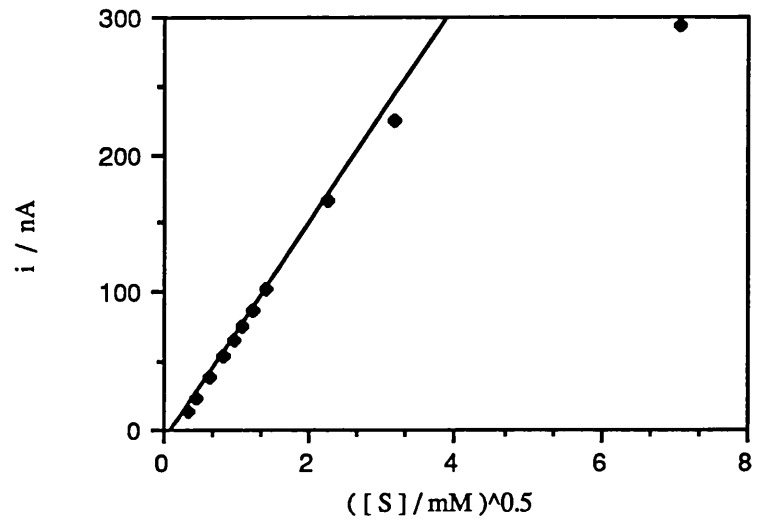
Fig(5.9) The rotation speed dependence
of the ring current



Fig(5.10.a) Plot of current vs. [S] for the disc at 9 Hz



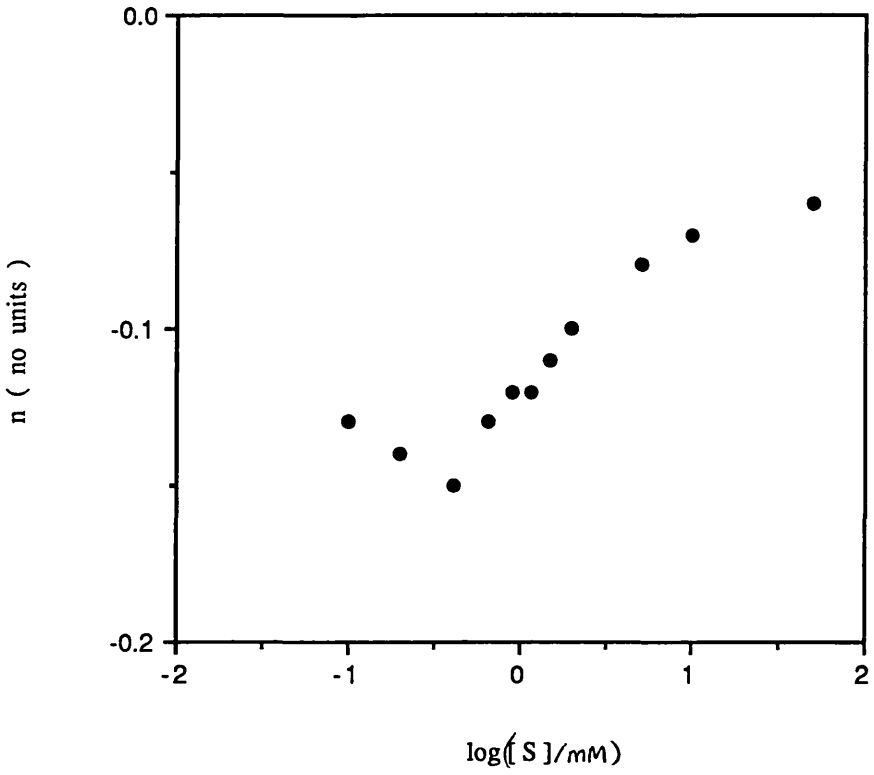
Fig(5.10.b) Plot of current vs. [S]^0.5 for the disc at 9 Hz



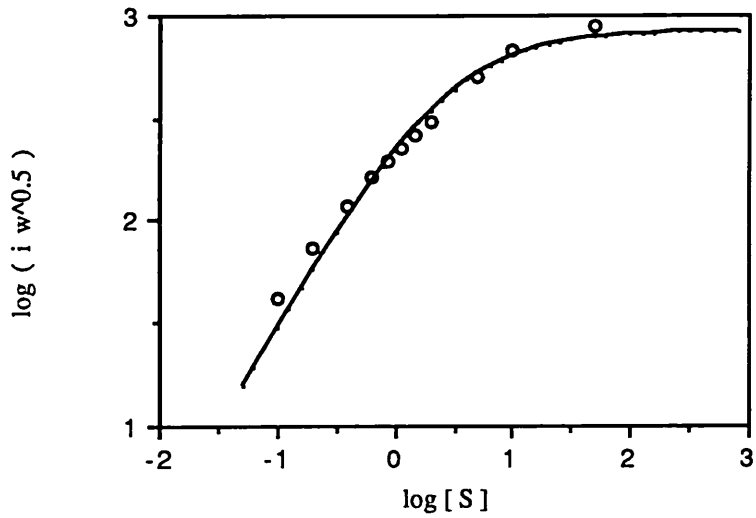
exception that first order dependence was more positively observed in the previous experiments. It should be noted that for the ring-disc experiment, we have not started at such low [S] compared to the experiments in Chapter4, since it was feared that any change in ring current would be too low to be observed. Thus it is not surprising that such a small region of $[S]^1$ dependence is observed. The ω dependence of the disc electrode is shown in fig(5.11). n is always negative and $\approx$ -0.15 to -0.06 i.e. it is intermediate between $\omega^{-0.5}$ and ω^0.

The pattern of dependence of the disc current on [S] and ω is in agreement with the data starting just inside case V, then either shifting through case VI to case I, or into case II, as observed in section 4.5. The intermediate order of ω dependence indicates the data are close to the case II - I boundary. Thus the data has been plotted in the appropriate form for both the case V - II boundary (see section 4.2.1.3) and the case VI - I boundary (see section 4.3.1.2). These plots are shown in figs(5.12.a) and (5.12.b). The case V - VI boundary analysis has not been carried out since only the first two to three points are likely to be in case V. Inspection of the fit of the theoretical plots to the experimental data gives no clear indication of which boundary is being crossed; both plots are reasonable. This is suggestive of the data being on the case II - I boundary i.e. intermediate between both cases. It is fortunate that the precise position need not be known for the following discussion of the collection efficiency, but it is satisfactory to know that the data gives the same pattern of behaviour observed in Chapter 4 and that the homogeneous theory is applicable.

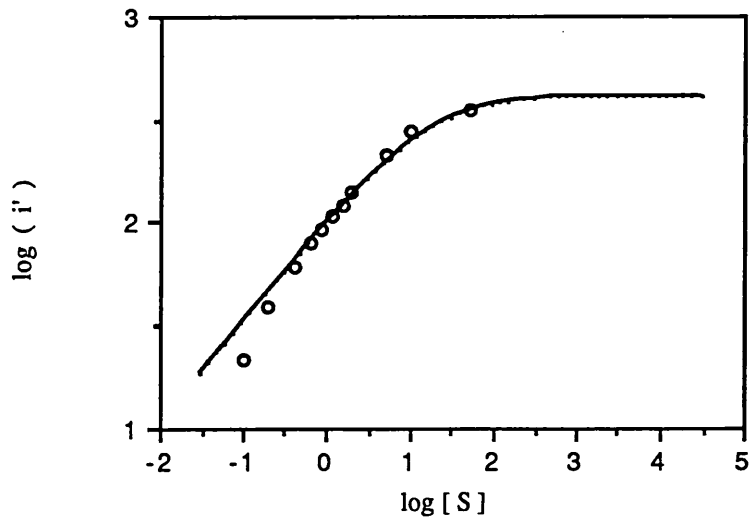
Fig(5.11) Rotation speed dependence of the disc current



Fig(5.12.a) Plot for the case V - II boundary for data at 9 Hz



Fig(5.12.b) Plot for the case VI - I boundary



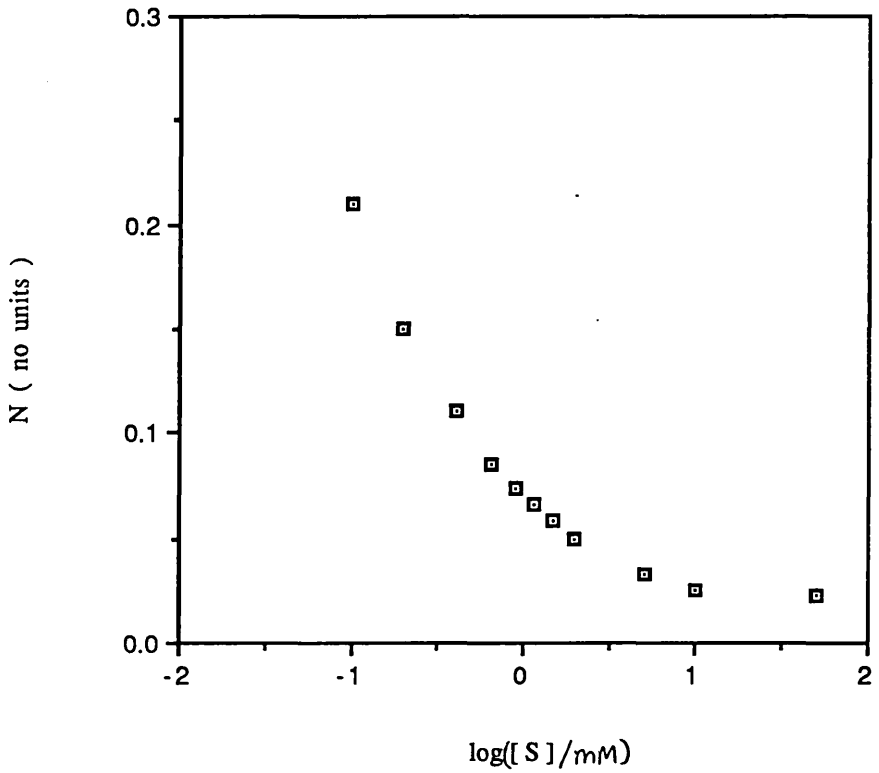
5.2.5 Analysis of the collection efficiency

The collection efficiency of the ring electrode is observed to decrease as [S] is increased. The variation of N with [S] is shown in fig(5.13). To analyse these data in terms of the homogeneous theory, we must understand what each case of interest predicts for the variation of N with [S].

In case V, M' has a parabolic concentration profile, as seen in fig(A.6). The height of the parabola is given by $\beta \kappa_E/4$, and is thus dependent on both [E] and [S]. On increasing [S], the parabola will increase in height, and thus the flux of M' being lost to the bulk will be increased and an increase in the ring current should be observed. The parabolic concentration profile will increase until on the case V - VI boundary, the height of the parabola i.e. the concentration of M', is quite significant compared to M. In case VI, the parabola becomes distorted towards the electrode on further increasing [S] and continues to grow in height until a linear concentration gradient of M' from very close to the electrode surface to the outside edge of the diffusion layer is obtained (seen in fig(A.7)). This linear concentration profile will not alter on further increasing [S], and so the flux of M' into the bulk becomes constant. Thus the ring current is expected to become constant; however the disc current will continue to increase because the concentration gradient of M' to the electrode becomes steadily steeper. Thus as [S] is increased, N should decrease and approach zero.

The same pattern of behaviour is predicted for the case V - II transition, On moving into case II, the concentration profile for M' is a distorted parabola, biased towards the electrode. However the height of this profile is given by $\kappa_M/20$ which is independent of [S].

Fig(5.13) The variation of N with [S]
at 9 Hz



Thus the flux of M' into the bulk is constant and the ring current will be constant while the disc current increases, once more resulting in N falling to zero.

This predicted pattern of behaviour is indeed observed experimentally, as seen in fig(5.13). Thus the homogeneous theory is supported. However this does not allow us to distinguish between the two possible transitions through the case diagram on increasing [S].

Now the magnitude of the experimentally observed collection efficiency shall be considered. The standard geometric collection efficiency cannot be applied to the homogeneous mechanism. The equation for the geometric collection efficiency in reference [133] applies to the case where there is a linear concentration profile of the electroactive species from the bulk solution to the disc electrode. In the homogeneous theory, the situation is more complicated. The bulk concentrations of both M and M' are zero, and there are a number of different concentration profiles that can occur.

Firstly, we shall consider case V. We can see from fig(A.6) that in this case, M' has a parabolic concentration profile. We need not concern ourselves with the concentration profile for M, since the ring electrode is always held at an oxidizing potential. The parabolic concentration profile gives rise to a special case for the collection efficiency which has been solved without using the thin gap thin ring (TGTR) approximation [142]. The collection efficiency for case V is given by [143]:

$$N_{case\ V} = 2 [(r_3 - r_1)/ r_1] [1 + (r_3 - r_1)/ r_1] [1 - (r_3 - r_1)/ r_1]$$

where r_1 is the disc radius, and r_3 is the outer ring radius. The inner ring radius does not feature in the expression, since the TGTR approximation assumes the gap between the disc and the ring to be so small that it effectively does not exist, and the ring electrode can be treated as an extension of the disc electrode. $N_{case\ V}$ can be calculated using the electrode dimensions given in section 2.4.4. It is found that $N_{case\ V} \approx 0.35$. This is clearly greater than the observed collection efficiency, shown in fig(5.13) for increasing [S]. Thus case V is a poor explanation of the observed collection efficiency.

It is interesting that $N_{case\ V}$ is much greater than the geometric collection efficiency of 0.23 (calculated in section 5.2.1). This is because the parabolic concentration profile in M' results in a greater flux of M' being swept onto the ring electrode than would occur for a linear concentration profile. Also, any M' oxidized on the ring electrode will produce M, which may be reduced on reaction with E' and be oxidized once more at the ring electrode. Thus there is an extra catalytic current on the ring electrode. The size of this catalytic current will be dependent on the mediator reaction layer thickness. If the reaction layer thickness is very small, then any M produced by the oxidation of M' at the ring electrode will rapidly regenerate M' which in turn can be oxidized. If the reaction layer thickness is much greater i.e. it approaches the diffusion layer thickness, any M produced by the oxidation of M' will be swept away from the ring unreacted. In case V, the size of the catalytic current will be minimal because $\kappa_M << 1$, which corresponds to the mediated reaction layer thickness being very small.

Now supposing the ring-disc electrode data starts close to the case V - II boundary and moves into case II. We can see from fig(A.2) that the concentation profile of M' is like a lopsided parabola biased

towards the electrode. Then the collection efficiency will be greater than the geometric collection efficiency once more, although it will be slightly lower than in case V since the electrode has a greater flux compared to the bulk. Thus a transition across the case V - II boundary is a poor explanation of the data since it requires N ≈ 0.35 initially, and N > 0.23 throughout.

Suppose the data shift from case V to case VI. In fig(A.7) we can see that on the case V - VI boundary, M' has a parabolic concentration profile, so that N ≈ 0.35. On moving into case VI, we obtain another situation for M' that cannot be explained by the geometric N. In case VI, M is quickly consumed next to the electrode in a very small reaction layer. As [S] is increased, the size of this reaction layer decreases. Similarly, the linear profile in M' is drawn closer into the electrode. Thus the concentration gradient of M' to the electrode becomes steadily steeper, while the concentration gradient of M' to the bulk remains constant. This implies that on increasing [S], the ring current will approach a limiting value while the disc current continually rises. Thus it would appear that the collection efficiency should decrease towards zero. However this does not take into account the catalytic current on the ring electrode mentioned above. In case VI, the mediator reaction layer is very small and so the regeneration of M' from M next to the ring electrode will be significant and will supply M' back to the ring.

The mathematical treatment of N for case VI, using the TGTR approximation, gives $N_{case\ VI}$ as [143]:

$$N_{case\ VI} \approx (8/3\pi^{1/2}) \{ 1/3 [(r_3 / r_1)^3 - (r_2 / r_1)^3] \}^{3/2} .$$

Using the values given in section 2.4.4, $N_{case\ VI} \approx 0.084$. Thus for a case V - VI transition, N varies from N ≈ 0.35 in case V and on the case V - VI boundary, to N ≈ 0.084 in case VI. Inspection of the data in fig(5.13) indicates that much lower values are obtained. Case I has not been considered in detail; however inspection of the concentration profile in fig (A.2) indicates that N will be approximately the same as for case VI. Thus the case V - VI - I transition is not a good explanation of the ring-disc electrode experiment.

5.2.6 Conclusion of the ring-disc electrode study

The potential dependence of the ring electrode indicated two oxidation reactions were occurring; at +300 mV giving a limiting current, and at +600 mV giving a peak which was ≈ 3 - 4 times larger than the first oxidation current. No reduction current was observed. The pattern of behaviour could be explained by either theory. The redox species was assigned as TTF^{o} since this can undergo both one and two electron oxidation to TTF^{+} and TTF^{2+} respectively, and the oxidation potentials coincide with the observed oxidation potentials. No other species that could be present in the stable potential range of the electrode could undergo both one and two electron oxidation reactions. Also, the anomalously large second oxidation current could be explained for TTF^{o}, and it was noted that TTF^{o} gave similar behaviour when acting as a mediator between reduced glucose oxidase and a platinum electrode [141]. It was concluded that the ring electrode should be held at +300 mV to observe the limiting flux of the redox species.

The effect of increasing [S] on the ring current was measured. The heterogeneous theory predicted that the ring current would be independent of [S] and would depend on $\omega^{1/2}$. However the ring current was observed to increase with [S] and to give negative rotation speed dependence. Thus it was concluded that the heterogeneous re dox catalysis theory totally failed to explain the ring current.

The homogeneous mediation theory predicted that the ring current would rise with [S], in good agreement with the experiment. The collection efficiency was also predicted for certain cases in the case diagram. For case V, $N \approx 0.35$, for case VI, $N \approx 0.084$ and in case II, $0.23 < N < 0.35$. These values were higher than the experimentally determined value of N. Thus it was concluded that the homogeneous theory was not an adequate explanation of the observed value of N. However, the increase in the ring current with [S] strongly suggests some mediated process is occurring. It may be possible that another mediated mechanism is occurring, which can give similar behaviour to the homogeneous mediation mechanism.

It should be noted that the concentration of mediator on the ring cannot be calculated since the profile for M', according to the homogeneous theory, is complicated and cannot be decribed by a simple relationship such as the Levich equation.

5.3 Conclusions

The potential dependence of the current of a rotating disc electrode in the presence of reduced glucose oxidase was explicable by the homogeneous mediation theory by a translation from case V

to case II. The heterogeneous redox catalysis theory totally failed to give an adequate explanation of the data.

The ring-disc electrode study indicated that TTF^{o} was detected on the ring electrode. It was found that increasing the concentration of substrate resulted in the ring current increasing. This, and the negative rotation speed dependence of the ring current, were in direct contradiction with the behaviour predicted by the heterogeneous redox catalysis theory. Thus it was concluded that it was highly unlikely that the heterogeneous mechanism was occurring.

The collection efficiency was observed to decrease on increasing [S], and this behaviour was explicable by the homogeneous theory. The observed collection efficiency was smaller than the predicted values given by the theory. It should be noted that the ring current has been observed to increase with time, and that after approximately one hour, the collection efficiency can double in value [141]. The reason for this is uncertain, and it suggests a more complicated type of mediated process is occurring than has previously been assumed.

Thus it is concluded that that homogeneous mediation theory is a better explanation of the ring-disc study than the heterogeneous theory, and that some type of mediated process is occurring although its exact nature is not known.

Chapter 6

Conclusions

The work in this thesis gives a good deal of insight into the mechanism of electron transfer between an oxidoreductase enzyme and a conducting organic salt electrode. In Chapter 3, it was seen that a number of oxidoreductase enzymes could be oxidized at electrodes composed of TTF TCNQ and/or NMP TCNQ. These enzymes exhibit a range of different cofactors, and so the general nature of the electron transfer is observed. Analysis of the steady state responses of membrane electrodes prepared with these enzymes allows calculation of k_S', the rate constant for the mass transport of substrate through the membrane. For four of the enzymes studied, k_S' is greater for an electrode composed of NMP TCNQ compared to TTF TCNQ. This is in contradiction with the membrane electrode theory since:

(1) The k_S' values are governed by the membrane characteristics and should be independent of the electrode material.

(2) The membrane electrode theory assumes the electron transfer between the enzyme and the conducting organic salt electrode is direct. However the only possible explanation of the k_S' values is for some type of mediated process to be occurring, which can influence the membrane kinetics.

Thus it is seen that the assumption of direct electron transfer is doubtful.

Electron micrographs presented in Chapter 3 lead to the conclusion that the intercrystallar spacing on a conducting organic

salt electrode can be greater than the mediator reaction layer thickness. This suggests that the roughness of the electrode, compared to a single crystal electrode, should result in a larger saturated electrode flux, as is indeed observed. Again, the possibility of a mediated electron transfer is supported.

The homogeneous mediation mechanism for the electron transfer is presented in Chapter 4, along with an alternative mechanism, heterogeneous redox catalysis. Analysis of the data from a rotating TTF TCNQ electrode in the presence of reduced glucose oxidase strongly supports the homogeneous mediation theory, while casting serious doubts on the heterogeneous theory. In particular, the heterogeneous theory cannot explain the first order dependence of the current on the concentration of substrate.

The two theories are further tested in Chapter 5. The potential dependence of the current of a rotating disc electrode in the presence of reduced glucose oxidase is explicable by the homogeneous theory but not by the heterogeneous theory. In view of all the experimental evidence in favour of the homogeneous mediation mechanism, a ring-disc electrode study was made, with TTF TCNQ as the disc material, to see if any mediator species could be measured on the platinum ring. The ring electrode gives a measurable current in the presence of reduced glucose oxidase. The potential dependence of this current indicates that TTF^{o} is being detected; this is explicable by both theories. The ring current is observed to increases with substrate concentration, and also to have negative rotation speed dependence. This is in direct contradiction with the behaviour predicted by the heterogeneous redox catalysis theory, and it can be concluded that it is extremely unlikely for this mechanism to be occurring.

The collection efficiency of the ring decreases with substrate concentration in a pattern explicable by the homogeneous theory. However the magnitude of the collection efficiency is approximately half the predicted value, and this casts some doubts on a mediated mechanism occurring as assumed in the homogeneous mediation theory.

Thus in conclusion, it is extremely probable that the electron transfer between a reduced enzyme and a conducting organic salt electrode occurs by a mediated mechanism. The precise nature of this mechanism is uncertain. Mediator species may dissolve off the electrode and shuttle between the enzyme and the electrode as assumed in the homogeneous mediation theory, although the reason for the low values for the collection efficiency is uncertain. Alternatively the mediator may bind to the enzyme to form an enzyme : mediator complex. This possibility is currently being investigated in the laboratories of P.N. Bartlett.

Further experiments must be carried out to confirm the nature of the species detected at the ring electrode. The use of TTF^{o} as a mediator between the reduced glucose oxidase and a platinum electrode has been confirmed [141]. A measure of the rate constant for the mediated process would enable comparison with the calculated values of k_M in Chapter 4. Also, mathematical treatment of the ring current would allow the concentration of mediator species detected at the ring electrode to be calculated. Again, comparison could be made with the calculated values of m_o in Chapter 4. The case diagram for the homogeneous mediation theory can be further investigated. Increasing enzyme concentration should enable data to cross from case V, through case VI, to case VII and possibly even case I. This would give a pattern of dependence on [E] of 1, 1/2, 1,

1/2. Similarly, using enzyme with a lower K_M/k_{cat} value than glucose oxidase may enable the case III - V boundary to be explored. Also using different enzymes would enable the general nature of the homogeneous mediation mechanism to be explored.

Appendix A

The homogeneous mediation theory

In section 4.3.2 the basic theory and assumptions made have been outlined, and the seven cases obtained presented in a case diagram. In this appendix the theory and the derivation of the cases are presented fully.

A.1 The basic theory

The theory proposes that electron transfer from the enzyme to the electrode occurs by a mediated mechanism in homogeneous solution, where the source of the mediator is the electrode itself. The mechanism is presented schematically in fig(A.1).

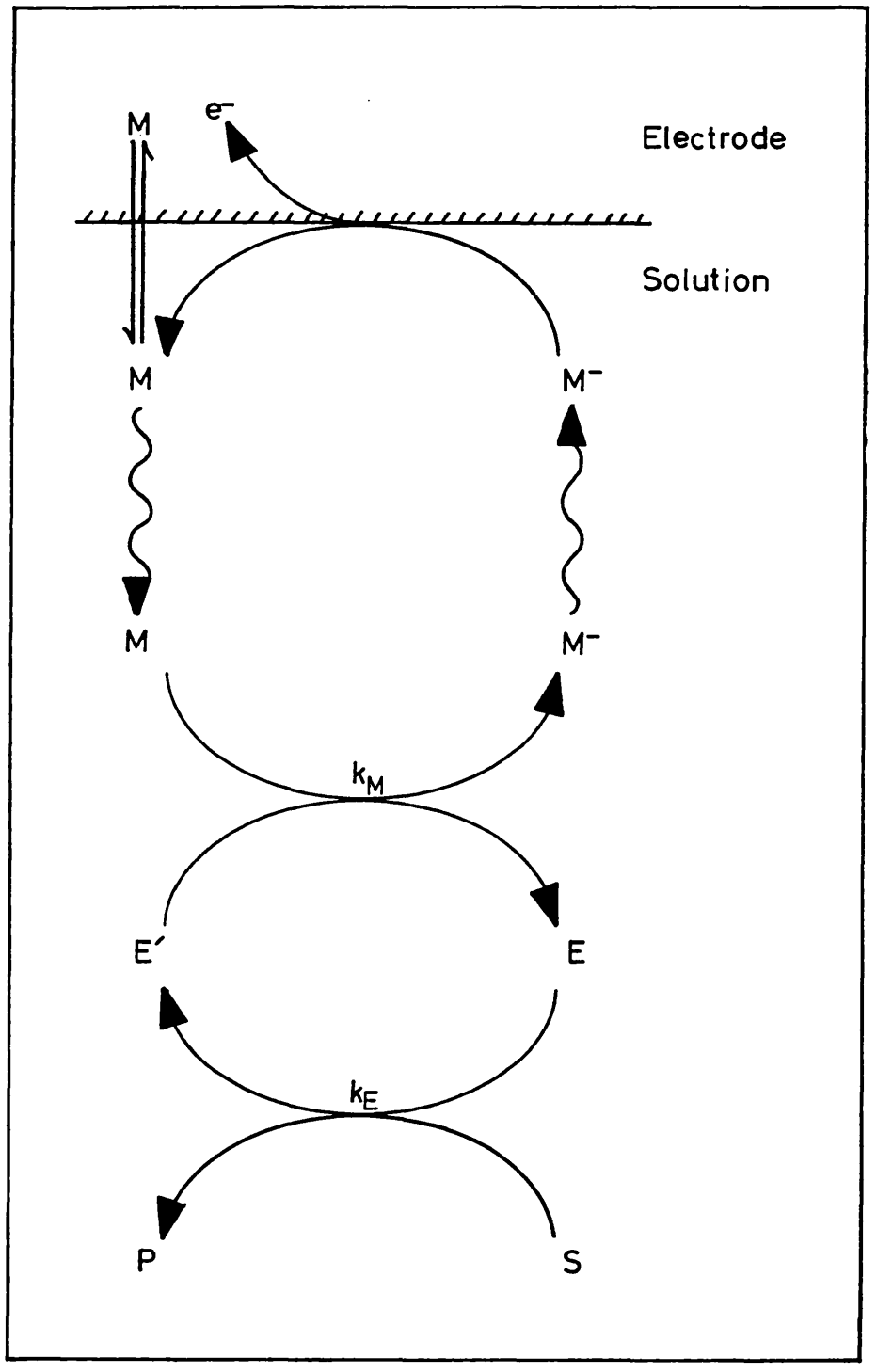
In homogeneous solution, the enzyme, E, reacts with its substrate, S, with the Michaelis Menten rate constant, k_E:

$$E + S \xrightarrow{k_E} E' + P$$

where for the unsaturated enzyme:

$$k_E = k_{cat} [S] / (K_M + [S]). \qquad (A.1)$$

For the saturated enzyme, $k_E = k_{cat}$. It is assumed that [S] is sufficiently large for there to be no concentration polarization of S within the diffusion layer. Confirmation of this assumption is made



Fig(A.1) The scheme for the homogeneous mediation mechanism.

in section 4.5.8.1 . [S] is also assumed to be sufficiently large for all enzyme in the bulk solution to be in the reduced form.

The reduced enzyme is then oxidized by mediator, M, with the second order rate constant k_M :

$$E' + M \xrightarrow{k_M} E + M'$$

It should be noted that more than one electron may be transferred for the oxidation of the enzyme. However it is assumed that the transfer of only the first electron is rate limiting.

The reduced mediator species M', on reaching the electrode, is then oxidized, regenerating M:

$$M' \longrightarrow M$$

n electrons may be transferred per each M' → M reaction. It is assumed that all M' reaching the electrode is oxidized and that this reaction is fast and not rate limiting.

A.2 Differential equations and boundary conditions

Initially Fick's second law [135] is applied to the four species M, M', E and E', describing their diffusion and kinetics within the diffusion layer, of thickness z_D:

$$D_M \delta^2 m/\delta z^2 - k_M\ e'\ m = 0 \qquad (A.2)$$

$$D_M \delta^2 m'/\delta z^2 + k_M\ e'\ m = 0 \qquad (A.3)$$

$$D_E \delta^2 e'/\delta z^2 - k_M\ e'\ m + k_E\ e = 0 \qquad (A.4)$$

$$D_E \delta^2 e/\delta z^2 + k_M\ e'\ m - k_E\ e = 0\ . \qquad (A.5)$$

Lower case letters have been used to denote the concentrations of species. The diffusion coefficient is assumed to be the same for both reduced and oxidized species.

The boundary conditions are given below:
on the electrode surface, i.e. at z=0,

$$m = m_o \qquad (A.6)$$

$$m' = 0 \qquad (A.7)$$

and $$(\delta e/\delta z)_o = (\delta e'/\delta z)_o = 0\ . \qquad (A.8)$$

From conditions (A.6) and (A.7) it is seen that all M' reaching the electrode is oxidized. Consequently the concentrations of enzyme species on the electrode surface are constant, as shown by the boundary condition (A.8).

On the outside edge of the diffusion layer, i.e. $z = z_D$,

$$m = m' = 0 \qquad (A.9)$$

$$e = 0 \qquad (A.10)$$

and $$e' = e_\Sigma\ , \qquad (A.11)$$

where e_Σ is the enzyme concentration in the bulk solution.

The flux of electrons at the electrode surface is described by Fick's first law [136], for the conversion of M' to M with the simultaneous transfer of n electrons:

$$j = n\, D_M\, (\delta m'/\delta z)_o \quad . \qquad (A.12)$$

An expression describing the relation between m and m' can be obtained by combining eqn.s (A.2) and (A.3), then integrating and applying the boundary conditions:

$$m + m' = m_o\, (1 - z/z_D) \quad . \qquad (A.13)$$

Similarly using eqn.s (A.4) and (A.5) an expression relating e and e' is obtained:

$$e + e' = e_\Sigma \quad . \qquad (A.14)$$

These equations are now expressed in terms of dimensionless variables. The following variables are defined: $u = m/m_o$, $u' = m'/m_o$, $v = e'/e_\Sigma$, $\chi = z/z_D$, $\kappa_M = k_M z_D^2 e_\Sigma / D_M$, $\kappa_E = k_E z_D^2 / D_E$ and $\gamma = k_M m_o / k_E$. The physical significance of the dimensionless parameters κ_E , κ_M and γ is discussed below in section A.3.

These dimensionless variables may now be substituted into eqn.s (A.2) - (A.5) which, together with eqn. (A.14), give the two differential equations:

$$\delta^2 u/\delta\chi^2 = \kappa_M\, u\, v \qquad (A.15)$$

and

$$\delta^2 v/\delta\chi^2 = \gamma\, \kappa_E\, u\, v - \kappa_E\, (1 - v) \quad . \qquad (A.16)$$

Eqn. (A.13) becomes:

$$u + u' = 1 - \chi \quad . \tag{A.17}$$

The boundary conditions are:

$$\text{at } \chi = 0 \text{ , } u = 1 \text{ , } u' = 0 \text{ and } \delta v/\delta\chi = 0 \text{ ,} \tag{A.18}$$

$$\text{at } \chi = 1 \text{ , } u = u' = 0 \text{ and } v = 1 \quad . \tag{A.19}$$

The flux of electrons is given by:

$$j = (nD_M m_o / z_D) (\delta u'/\delta\chi)_o \quad . \tag{A.20}$$

Then it is seen from eqn. (A.20) that the parameter $(\delta u'/\delta\chi)_o$ must be determined in order to obtain a solution for j . Two general relations for this parameter can be derived. Firstly, eqn. (A.17) is differentiated:

$$(\delta u'/\delta\chi)_o = - (\delta u/\delta\chi)_o - 1 \quad . \tag{A.21}$$

Secondly, the uv term is eliminated between eqn.s (A.15) and (A.16):

$$\beta \, \delta^2 v/\delta\chi^2 - \delta^2 u/\delta\chi^2 = - \beta \, \kappa_E (1 - v) \tag{A.22}$$

where

$$\beta = \kappa_M / \gamma \kappa_E = D_E e_\Sigma / D_M m_o \, .$$

Integration and application of the boundary conditions at $\chi = 0$ gives:

$$\beta (v - v_o) + 1 - u + (\delta u/\delta\chi)_o \chi = -\beta \, \kappa_E \int_o^\infty \int_o^\infty (1 - v) \, \delta\chi'' \delta\chi' . \tag{A.23}$$

Applying the boundary conditions at $\chi = 1$ and using eqn. (A.21) gives:

$$(\delta u'/\delta \chi)_0 = \beta (1 - v_0) + \beta \kappa_E \int_0^\infty \int_0^\infty (1-v) \delta \chi'' \delta \chi' \quad . \qquad (A.24)$$

A general analytical solution is not possible. However, the sizes of the parameters κ_E , κ_M and γ relative to unity allow derivation of expressions for u and v and hence $(\delta u'/\delta \chi)_0$ can be determined for particular cases. A three dimensional case diagram can be constructed for the cases using the parameters $\log \kappa_E$, $\log \kappa_M$ and $\log \gamma$ as axes.

A.3 The physical significance of the dimensionless variables

In order to fully comprehend the physical significance of each case, the dimensionless parameters from which they are derived must be understood. The three dimensionless variables each describe the probability of a certain event happening, the probability being dependent on the magnitude of the variable relative to unity. Both κ_M and κ_E compare the diffusion layer thickness, z_D , to a reaction layer thickness. For κ_M , this is the reaction layer thickness for M, $(D_M / k_M e_\Sigma)^{1/2}$ and for κ_E , it is the reaction layer thickness for E, $(D_E / k_E)^{1/2}$. The reaction layer thickness is the distance a species can diffuse before being consumed by reaction.

Thus κ_M describes the likelihood of mediator, M, escaping from the diffusion layer before reacting with reduced enzyme: if $\kappa_M > 1$, then the diffusion layer thickness is greater than the reaction layer thickness for M, and it is more probable that M will react with E'

within the diffusion layer than escape from it unreacted. If $\kappa_M < 1$, then the converse is true; some M will escape to the bulk before reacting.

The parameter κ_E describes the probability of E being converted to E' before escaping from the diffusion layer unreacted. If $\kappa_E > 1$, then the diffusion layer thickness is greater than the reaction layer thickness for E, and most E will be converted back to E' within the diffusion layer. If $\kappa_E < 1$, then most E will escape from the diffusion layer before being regenerated back to E' .

The parameter γ describes the local steady state between reduced and oxidized forms of the enzyme at the electrode surface. It should be remembered that at the electrode surface the concentrations of M and M' are fixed and consequently the concentrations of E and E' are fixed. Diffusion of enzyme to the electrode is unimportant and the relative concentrations of E and E' are governed by steady state kinetics. If $\gamma > 1$, then the rate constant for the destruction of E' ($k_M m_o$) is faster than the rate constant for the destruction of E (k_E); E will predominate at the electrode surface. Somewhere within the diffusion layer the predominant form of the enzyme will switch from E to E', since E' is predominant throughout the bulk solution. If $\gamma < 1$, then E' will be predominant at the electrode surface and hence throughout the whole diffusion layer and the bulk.

A.4 Derivation of the cases

The three dimensionless parameters describe a 3-dimensional case diagram where the x, y and z axes are represented by κ_E , κ_M and γ respectively. Initially only the $\gamma >> 1$ plane is considered. This condition implies that the predominant form of enzyme at the

electrode is E , the oxidized form. Then a switch over somewhere within the diffusion layer to E' being the predominant species will occur.

A.4.1 Cases I and II

Consider the situation where $\gamma \kappa_E << 1$. Since $\gamma >> 1$, $\kappa_E <<<< 1$. Then in eqn. (A.16), the $\gamma \kappa_E$ and κ_E terms can be neglected since both u and v are equal to or less than unity. The differential equation for v can be solved and the boundary conditions satisfied with v=1. This implies that the predominant form of enzyme at the electrode and throughout the whole diffusion layer is in fact E' . This is in direct contradiction with the initial condition $\gamma >> 1$, and will be explained below.

Substituting v=1 into eqn. (A.15) reduces it to a simple first order differential equation, allowing a solution for u to be found:

$$u = \cosh(\kappa_M^{1/2}\chi) - \sinh(\kappa_M^{1/2}\chi)\coth(\kappa_M^{1/2}) \quad . \qquad (A.25)$$

From eqn.s (A.21) and (A.25), we obtain:

$$(\delta u'/ \delta \chi)_o = \kappa_M^{1/2} \coth(\kappa_M^{1/2}) - 1 \quad . \qquad (A.26)$$

Now if $\kappa_M >> 1$, $(\delta u'/ \delta \chi)_o \approx \kappa_M^{1/2}$ and from eqn. (A.20) we obtain:

$$j = n (D_M k_M e_\Sigma)^{1/2} m_o \quad . \qquad (A.27)$$

This is case I. Since $\kappa_M >> 1$, M diffuses only a very small distance from the electrode surface before being consumed. Then the rate

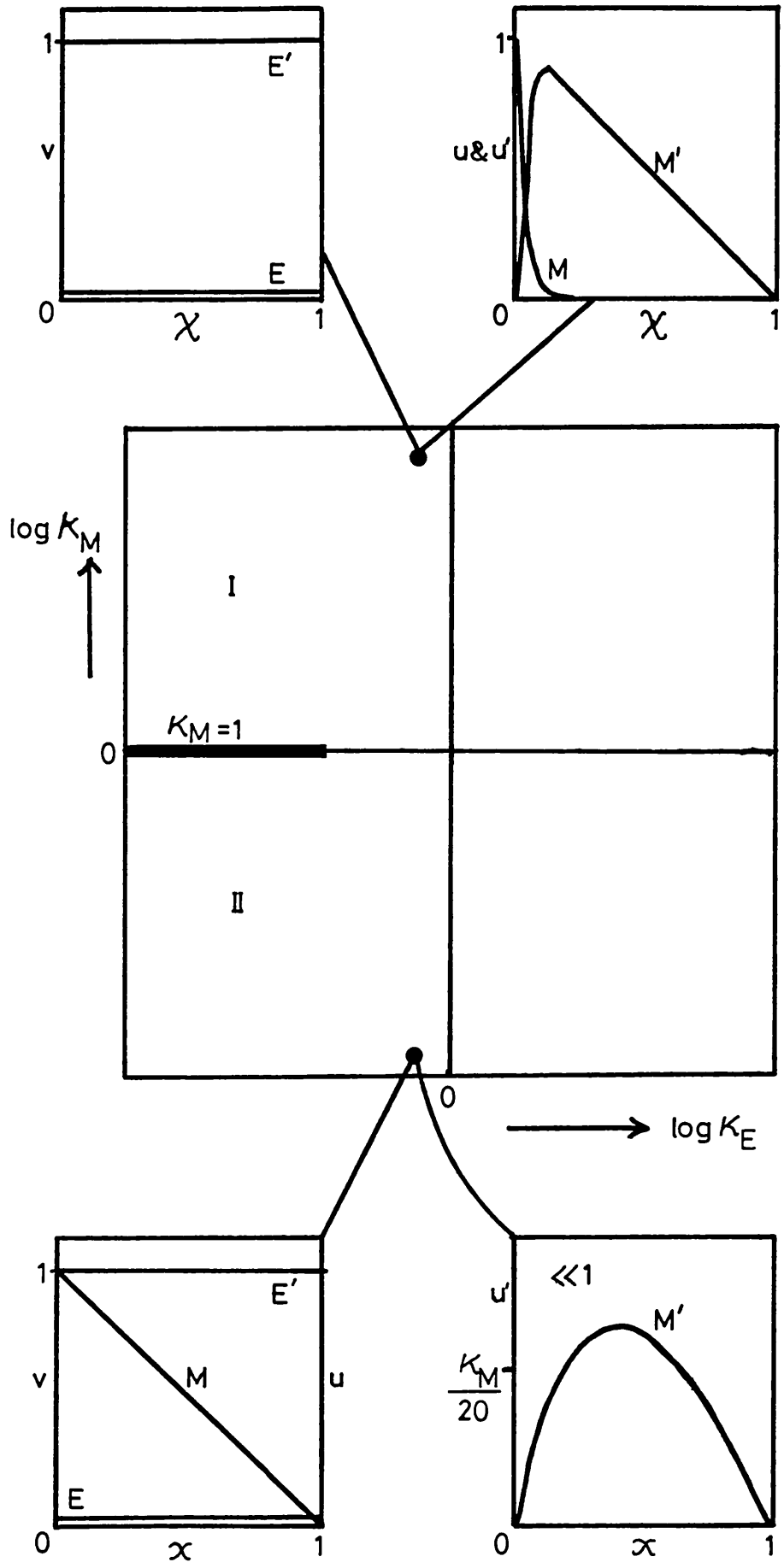
limiting step is the mediator being consumed by E' present at its bulk concentration in a small reaction layer next to the electrode surface. The predominant form of enzyme throughout the diffusion layer is E', since the kinetics of the E' + M reaction are too slow to perturb the E' concentration i.e. any E formed is present at a much lower concentration than E'.

If $\kappa_M << 1$, the coth function in eqn. (A.26) can be expanded to give $(\delta u'/ \delta \chi)_0 = \kappa_M / 3$, and thus:

$$j = (1/3)\, nk_M m_0 e_\Sigma z_D \quad . \tag{A.28}$$

This is case II. In this situation, M diffuses away from the electrode to the bulk since $\kappa_M << 1$. There is a linear concentration profile in M from m_0 at the electrode to zero at z_D . Then E' can react slowly with M throughout the diffusion layer. Again the kinetics of the E' + M reaction are too slow to perturb the E' concentration in the diffusion layer from its bulk concentration. Thus the rate limiting process in case II is the reaction between E' and M within z_D .

The factor of 1/3 in eqn. (A.28) can be understood by considering the concentration profiles for M and M' in case II. The rate of making M' within the diffusion layer is $1/2\ k_M m_0 e_\Sigma z_D$. However the concentration profile of M' is such that 2/3 of the M' made is recovered at the electrode and 1/3 is lost to the bulk. The electrode does better since the concentration of M is greater at the electrode compared to the edge of the diffusion layer, and so more M' is generated close to the electrode. Hence the flux of M' at the electrode is 2/3 of $1/2\ k_M m_0 e_\Sigma z_D$, and the flux of electrons at the electrode is $1/3\ nk_M m_0 e_\Sigma z_D$. Case II should be contrasted with case I, where because M' is produced in a thin reaction layer close to the electrode



Fig(A.2) Constructing the $\gamma > 1$ plane: cases I and II. The concentration profiles for E, E', M and M' within the diffusion layer are shown.

surface, almost all M' is recovered at the electrode and hardly any is lost to bulk.

In fig(A.2), cases I and II are placed on the $\gamma >> 1$ plane; the boundary between cases I and II is given by $\kappa_M = 1$. The concentration profiles for both enzyme and mediator species are also shown. The mediator concentration profiles are derived from eqn. (A.25) and eqn. (A.17), applying the boundary conditions appropriate for each case. In case II, the mediator kinetics are not sufficiently fast to build up the concentration of M', hence it is present at much lower concentrations than M.

Note that the mediator and enzyme concentration profiles can be derived for each case and each case boundary from the appropriate expression for u, u' and v and using eqn.s (A.14) and (A.17).

A.4.2 Cases II and III

Now the case next to case II separated by the boundary $\gamma \kappa_E = 1$ is considered. This is in the bottom right hand corner of the case diagram. In this corner, $\kappa_M << 1$, so that the right hand side of eqn. (A.15) may be neglected and a simple second order differential equation for u is obtained. On applying the boundary conditions, this is solved with $u = 1 - \chi = \chi'$. In physical terms, M has a linear concentration gradient from unity at the electrode to zero at z_D.

Now $\kappa_E << 1$ and since $\gamma >> 1$, $\gamma \kappa_E \approx 1$. The relative sizes of κ_E and $\gamma \kappa_E$ means that the $\gamma \kappa_E$ term dominates eqn. (A.16) and the κ_E term may be neglected. Substituting for u and χ' into eqn. (A.16) then gives:

$$\delta^2 v/(\delta\chi')^2 = \gamma \kappa_E \chi' v \, . \qquad (A.29)$$

This equation is solved using Airy functions [137] to give:

$$v = [\, Bi'(\phi)\, Ai(\phi\chi') - Ai'(\phi)\, Bi(\phi\chi') \,] / [\, Ai(0)\, Bi'(\phi) - Bi(0)\, Ai'(\phi) \,] \qquad (A.30)$$

where

$$\phi = (\gamma \kappa_E)^{1/3} \quad . \qquad (A.31)$$

We now want to find v_o (the value of v at $\chi = 0$ or $\chi' = 1$) and substitute it into eqn. (A.24) to find $(\delta u'/ \delta \chi)_o$. In working out v_o we use the Wronskian relation for Airy functions and in eqn. (A.24) the integral term can be neglected because $\kappa_E << 1$. We then obtain:

$$(\delta u'/ \delta \chi)_o = \beta \{ 1 - \pi^{-1}/ [Ai(0)\, Bi'(\phi) - Bi(0)\, Ai'(\phi)] \} \quad . \qquad (A.32)$$

When $\phi << 1$, the Airy functions can be expanded as a series to obtain:

$$Ai(0)\, Bi'(\phi) - Bi(0)\, Ai'(\phi) = \pi^{-1} (1 + \phi^3/3 \ldots\ldots) \quad .$$

Substitution into eqn. (A.32) together with eqn. (A.31) gives:

$$(\delta u'/ \delta \chi)_o \approx \beta \gamma \kappa_E /3 = \kappa_M /3 \quad . \qquad (A.33)$$

This is the same result as obtained for case II. This is very satisfactory since if $\phi << 1$, $\gamma \kappa_E << 1$ which implies that $\kappa_E <<<< 1$ since $\gamma >> 1$ i.e. we are in the same position in the case diagram as before.

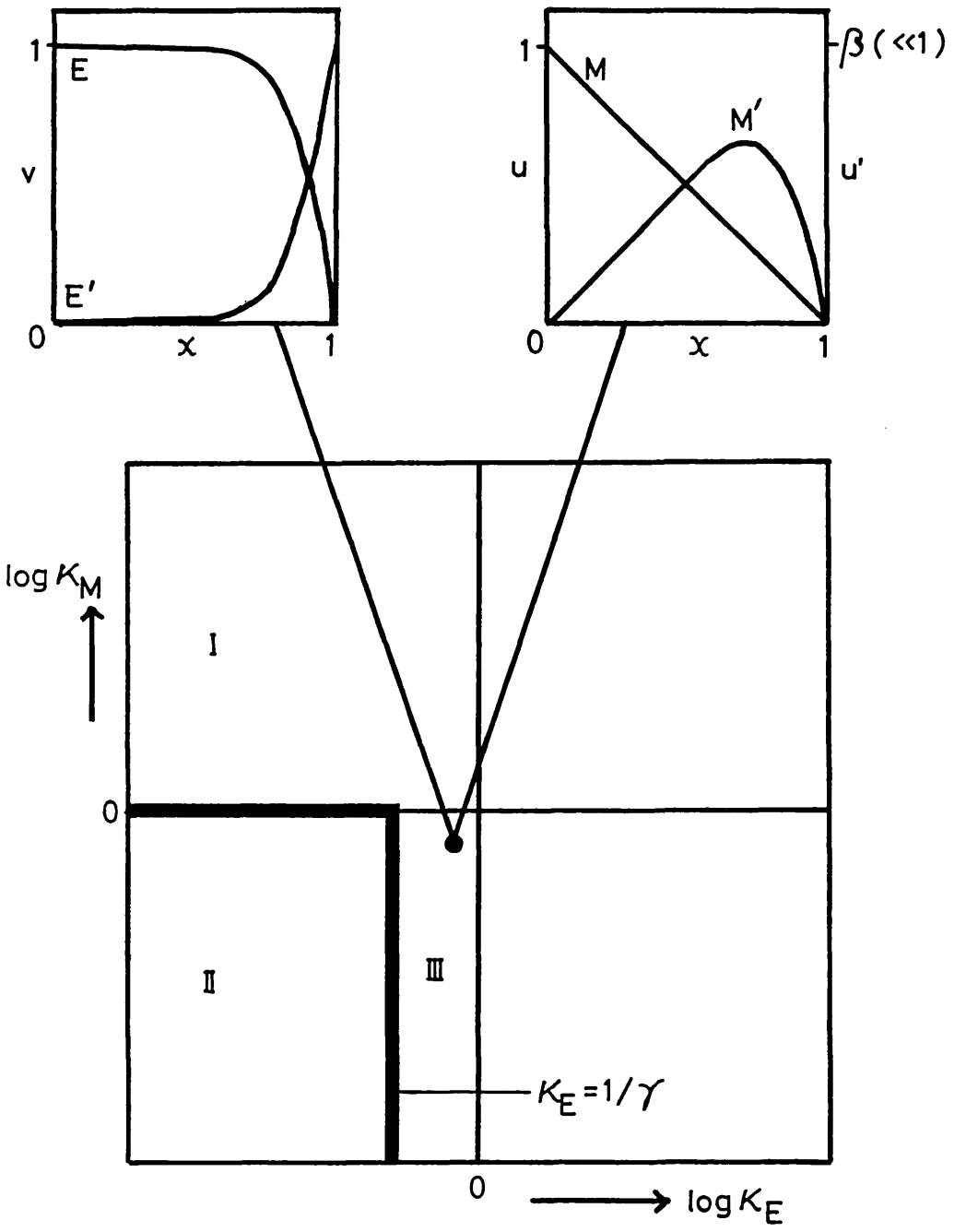
If $\phi >> 1$, the $Bi'(\phi)$ term in eqn. (A.32) is $>> 1$, and hence $(\delta u'/ \delta \chi)_o \approx \beta$. Substitution into (A.20) gives:

$$j = nD_E e_\Sigma / z_D \quad . \qquad (A.34)$$

This is case III. This expression suggests that the rate limiting step is the diffusion of enzyme across the diffusion layer. However the concentration profiles for E' suggest that it is reacting with M on the outside edge of the diffusion layer and is not itself penetrating far into the layer. Therefore most M' made is lost to the bulk rather than diffusing back and turning over at the electrode. Thus over a small distance into the diffusion layer, say z_* , the fluxes of M' diffusing out and E' diffusing in can be matched i.e. $D_M m'_* \approx D_E e_\Sigma$. The flux of m'_* reaching the electrode is given by $D_M m'_* / z_D$, which is equivalent to $D_E e_\Sigma / z_D$. Then although eqn. (A.34) appears to describe the situation where the rate limiting step is the diffusion of E' into the reaction layer, it is in fact the diffusion of M' , made in a small reaction zone on the outside edge of the diffusion layer, back to the electrode that is rate limiting.

Case III should be contrasted with case II, where because $\gamma \kappa_E \ll 1$, E' is predominant throughout the diffusion layer. Then the supply of E' for the E' + M reaction is good, and the rate of reaction between E' and M throughout the diffusion layer becomes rate limiting. In case III, where $\gamma \kappa_E \approx 1$, E' is no longer predominant, and so the diffusion of E' into the diffusion layer to react with M becomes rate limiting.

Cases II and III are shown in the case diagram (fig(A.3)). The boundary between cases II and III is given by $\gamma \kappa_E = 1$. The concentration profiles for all species involved are given.



Fig(A.3) Constructing the $\gamma > 1$ plane: cases II and III. The concentration profiles for E, E', M and M' within the diffusion layer are shown.

A.4.3 Cases I and IV

Now the boundary to the case I solution in the top left hand corner of the case diagram is explored. In this corner, $\kappa_M > 1$ and $\kappa_E < 1$. The fact that $\kappa_M > 1$ implies that there is a small reaction layer next to the electrode for the E' + M reaction. This situation has indeed been found for case I . It is assumed that in this thin reaction layer that $v = v_o$, so that in eqn. (A.15), we can obtain a solution for u:

$$u = \exp[\ -(\kappa_M v_o)^{1/2}\chi\ ] \quad . \tag{A.35}$$

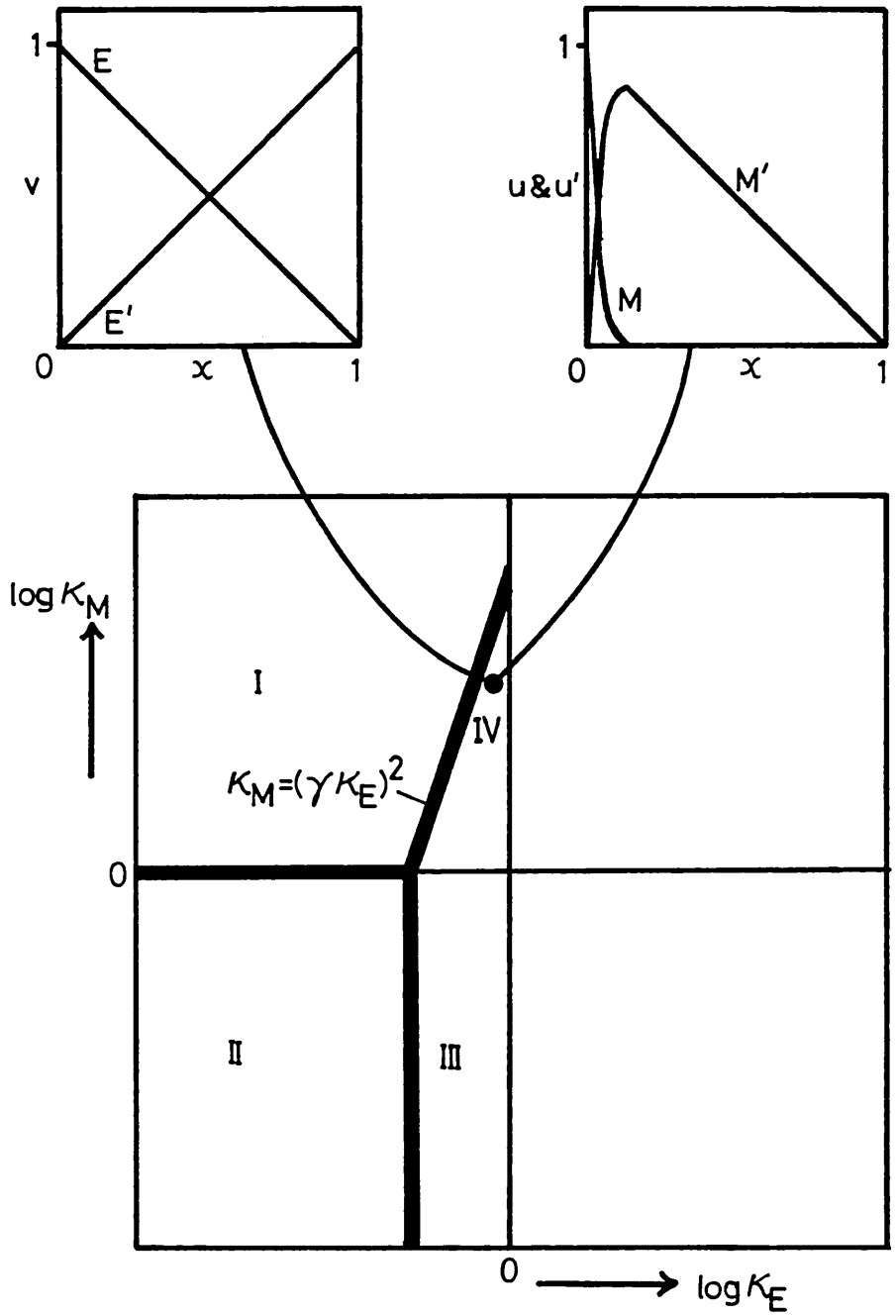
Now on the edge of this reaction layer, we can match the flux of M leaving the electrode surface with the flux of E' diffusing into the reaction layer across the diffusion layer:

$$-D_M(\ \delta m/\delta z\ )_o = D_E(\ e_\Sigma - e_o'\ )/\ z_D \quad . \tag{A.36}$$

Expressing eqn. (A.36) in dimensionless variables and differentiating eqn. (A.35) gives:

$$-(\ \delta u/\ \delta\chi\ )_o = (\kappa_M v_o)^{1/2} = \beta(1-v_o)\ .$$

We now have a quadratic equation which can be solved for v_o. We can assume that $(\ \delta u'/\ \delta\chi\ )_o \approx -(\ \delta u/\ \delta\chi\ )_o >> 1$ since M' is made in a thin reaction layer next to the electrode surface and so almost all M' formed will turn over at the electrode. Using this assumption and substituting for v_o in the expression for $-(\ \delta u/\ \delta\chi\ )_o$, we obtain:



Fig(A.4) Constructing the $\gamma > 1$ plane: cases I and IV. The concentration profiles for E, E', M and M' within the diffusion layer are shown.

$$(\delta u'/ \delta \chi)_o = \kappa_M^{1/2}[1 + \kappa_M/(4\beta^2)]^{1/2} - \kappa_M/2\beta \qquad (A.37)$$

This equation reduces to two simpler expressions depending on the size of the ratio κ_M/β^2 . If $\kappa_M/\beta^2 << 1$, then $(\delta u'/ \delta \chi)_o \approx \kappa_M^{1/2}$, and we have recovered case I. If $\kappa_M/\beta^2 >> 1$, then expanding the square root in eqn. (A.37) gives $(\delta u'/ \delta \chi)_o \approx \beta$ and:

$$j = nD_E e_\Sigma / z_D \quad . \qquad (A.38)$$

This is case IV. The rate limiting step is the diffusion of enzyme across the diffusion layer to the small E' + M reaction layer next to the electrode. Since E' reacts with M , the surface concentration of E' is much less than in the bulk. This case should be compared with case I, where because $\gamma \kappa_E << 1$, E' is predominant throughout the diffusion layer. Then the diffusion of E' to the E' + M reaction layer is no longer important and the reaction between E' and M becomes rate limiting.

Case IV is shown in fig(A.4). The boundary between cases I and IV is given by $\kappa_M/\beta^2 = 1$.

A.4.4 Cases III and IV

Eqns. (A.34) and (A.38) show that j is given by the same expression for cases III and IV. The current appears to be governed by the diffusion of E' across the diffusion layer. As has been discussed above, this is the true physical situation for case IV , but for case III, E' is in fact reacting on the outside edge of the diffusion layer and it is the diffusion of M' across the diffusion layer that is rate limiting.

Now in both cases III and IV , $\kappa_E << 1$ and since $\gamma >> 1$, $v_o << 1$. Then in eqn.(A.24) , the general result is obtained that $(\delta u' / \delta \chi)_0 = \beta$, giving the solutions in eqn.s (A.34) and (A.38) . The boundary between cases III and IV is found by considering eqn. (A.23) and ignoring terms in κ_E and v_o . Applying the boundary conditions at $\chi = 1$ gives:

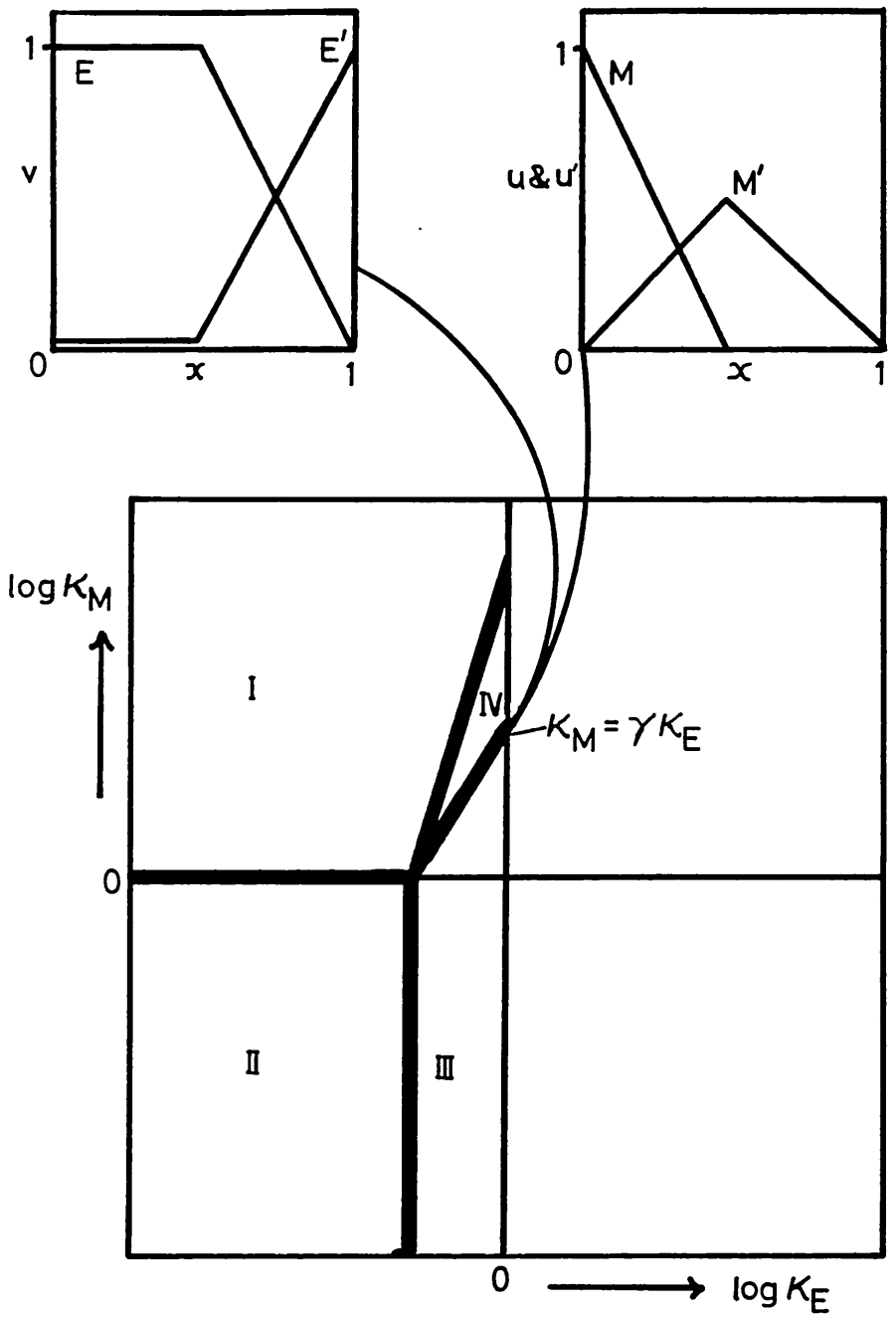
$$(\delta u / \delta \chi)_0 = - (1+\beta) \ . \qquad (A.39)$$

Then the magnitude of β determines whether we are in case III or IV. If $\beta = 1$ i.e. $\kappa_M = \gamma \kappa_E$, we are on the boundary between cases III and IV . If $\beta >> 1$, we are in case IV, and if $\beta << 1$, we are in case III.

Now in case III, the reaction zone is on the outside edge of the diffusion layer, while in case IV, it is very small and next to the electrode. Then it can be concluded that on the boundary between cases III and IV, the reaction zone lies somewhere between these limits, say at χ_* . Now in the reaction zone, $u \approx 0$ and $v \approx 0$ since they are consumed. Applying these conditions for χ_* to eqn. (A.23) gives:

$$\chi_* = 1/(1+\beta) \ . \qquad (A.40)$$

If $\beta << 1$, i.e. case III, $\chi_* \approx 1$ and the reaction zone is on the outside edge of the diffusion layer. If $\beta >> 1$, i.e. case IV , χ_* is very small and the reaction zone is next to the electrode. If $\beta = 1$, i.e. on the boundary between cases III and IV , $\chi_* = 1/2$ and the reaction zone is halfway across the diffusion layer. This is sensible because β compares the mediator and enzyme diffusional fluxes.



Fig(A.5) Constructing the $\gamma > 1$ plane: cases III and IV. The concentration profiles for E, E', M and M' within the diffusion layer are shown.

The case boundary between cases III and IV can now be added to the case diagram (fig(A.5)).

A.4.5 Cases III and V

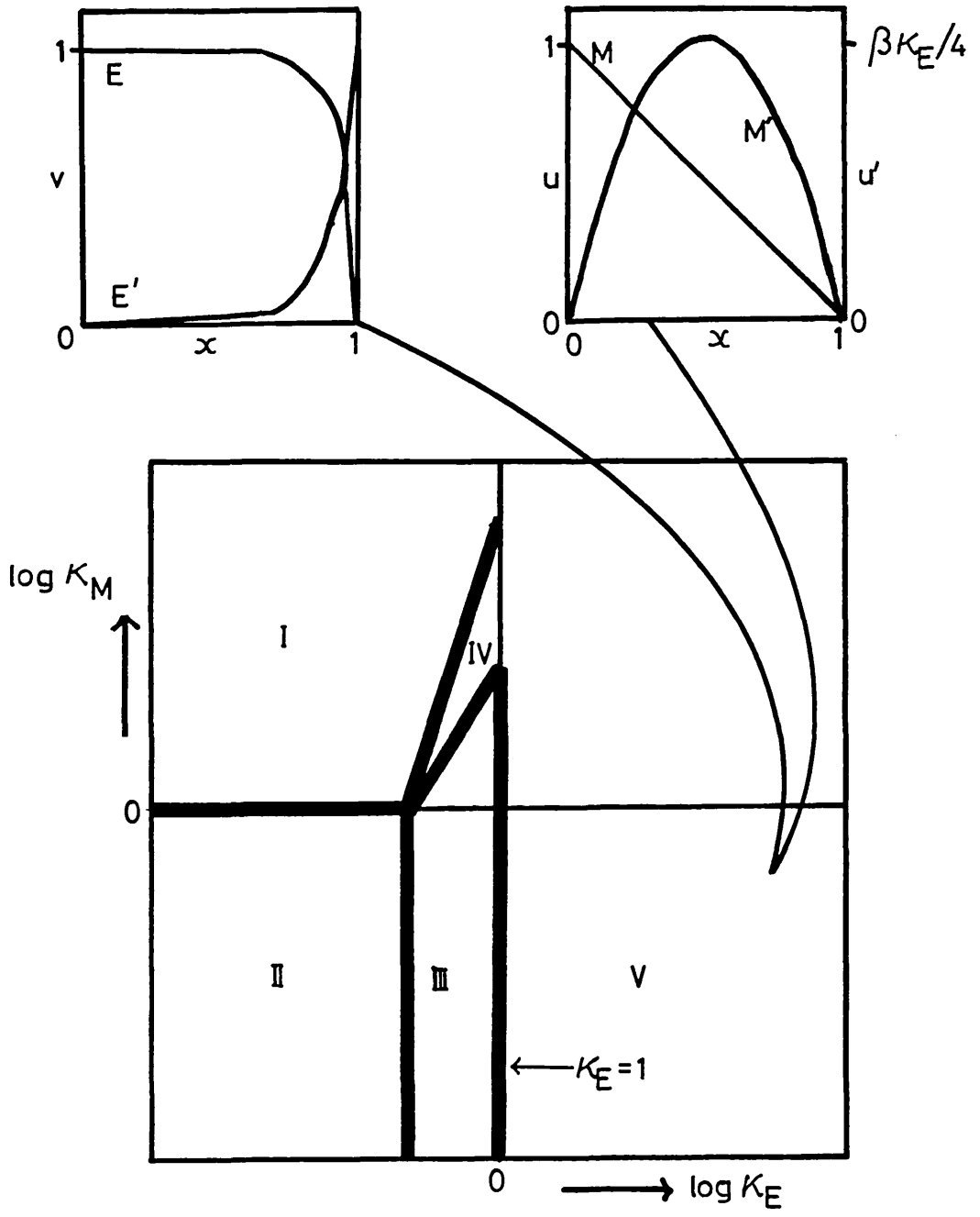
We now consider the case to the right hand side of case III i.e. $\kappa_E >> 1$ and the regeneration of E' from E is significant. In this part of the case diagram $\kappa_M < 1$ and $\gamma \kappa_E >> 1$ since we are to the right of the case II - III boundary. Now since $\kappa_M << 1$, the E' + M kinetics are sluggish and M penetrates to the outside edge of the diffusion layer. Thus the reaction zone is on the outside edge of the diffusion layer. This has already been shown above in section A.4.4 for case III and it can be concluded from this that v is very small throughout the diffusion layer. Then in eqn. (A.24) terms in v and v_0 can be neglected to give:

$$(\delta u'/ \delta \chi)_0 = \beta (1 + \kappa_E/2) \quad . \tag{A.41}$$

Now if $\kappa_E << 1$, case III is recovered. The regeneration of E' from E is slow and so E' must be supplied by diffusion from the bulk. If $\kappa_E >> 1$, $(\delta u'/ \delta \chi)_0 = \beta \kappa_E/2 = \kappa_M/2\gamma$, and we obtain:

$$j = (1/2)\, n k_E e_\Sigma z_D \quad . \tag{A.42}$$

This is case V. The rate limiting step is the regeneration of E' from E throughout the diffusion layer. Thus E' can react with M, generating M' throughout the diffusion layer. A parabolic profile in M' is obtained: half the M' reaches the electrode and half diffuses to the bulk and is lost. Thus the factor of 1/2 in eqn. (A.42) is understood.



Fig(A.6) Constructing the $\gamma > 1$ plane: cases III and V. The concentration profiles for E, E', M and M' within the diffusion layer are shown.

Case V is shown on the case diagram in fig(A.6). The boundary between cases III and V is $\kappa_E = 1$.

A.4.6 Cases V and VI

Now we consider the boundary next to case V where $\kappa_E >> 1$. Under this condition the regeneration of E' from E is very efficient and so it can be concluded that the diffusion of enzyme is unimportant compared to the steady state kinetics of the enzyme and the mediator. Then in eqn. (A.16), the $\delta^2 v/\delta\chi^2$ term can be ignored to give:

$$v \approx 1/(1+ \gamma u) \ . \qquad (A.43)$$

We are interested in u when $u \approx 1$ (i.e. at the electrode surface) and since $\gamma >> 1$, $v \approx 1/\gamma$. Substituting this into eqn. (A.15) gives:

$$\delta^2 u/ \delta\chi^2 \approx \kappa_M/ \gamma \ . \qquad (A.44)$$

This equation is equivalent to:

$$D_M \delta^2 m/ \delta z^2 = k_E e_\Sigma \ . \qquad (A.45)$$

It describes the diffusion of M in a reaction layer where the rate limiting step in the destruction of M is not the reaction of M and E' , but the regeneration of E' from E. The concentration of E' is much less than its bulk concentration, and so the concentration of E is close to e_Σ . This type of reaction layer is called a " zero order reaction layer " to distinguish it from the more usual first order case.

Integrating eqn. (A.44) and applying the boundary conditions at $\chi = 0$ gives:

$$u = 1 + \chi(\delta u/ \delta \chi)_o + \kappa_M \chi^2/ 2\gamma \quad . \tag{A.46}$$

Now we need to find $(\delta u/ \delta \chi)_o$. M will penetrate a certain distance, say χ_* , into the diffusion layer before being consumed (this is the reaction layer thickness of M). Then at $\chi = \chi_*$, both u and $\delta u/ \delta \chi$ equal zero. Application of these conditions to eqn. (A.46) gives:

$$\chi_* = (2\gamma /\kappa_M)^{1/2}$$

and

$$(\delta u/ \delta \chi)_o = - (2\kappa_M/\gamma)^{1/2} \quad . \tag{A.47}$$

Substituting eqn. (A.47) into eqn. (A.21) gives:

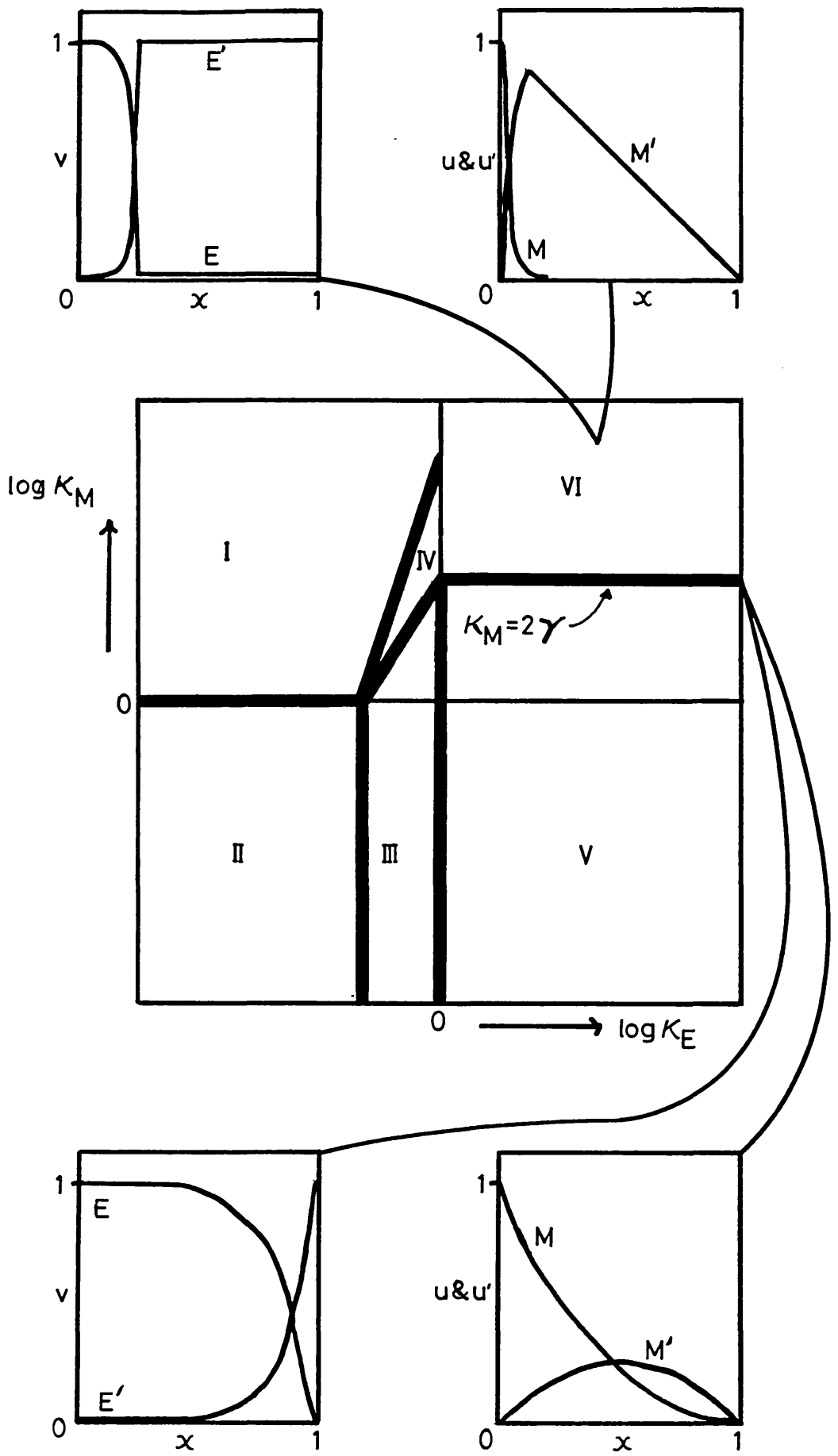
$$(\delta u'/ \delta \chi)_o = (2\kappa_M/\gamma)^{1/2} - 1 \quad . \tag{A.48}$$

Now if $\kappa_M << 2\gamma$, $\chi_* \approx 1$ and M penetrates to the outside edge of the diffusion layer. Then $u = 0$ at $\chi = 1$ and applying this condition to eqn. (A.46) gives:

$$(\delta u/ \delta \chi)_o = - (1 + \kappa_M/2\gamma)$$

which on substituting into eqn. (A.21) gives:

$$(\delta u'/ \delta \chi)_o = \kappa_M/2\gamma \quad . \tag{A.49}$$



Fig(A.7) Constructing the $\gamma > 1$ plane: cases V and VI. The concentration profiles for E, E', M and M' within the diffusion layer are shown for case VI and for the case V - VI boundary.

Substituting eqn. (A.49) into eqn. (A.20) recovers the expression for case V, given by eqn. (A.42). Since $\gamma >> 1$, and $\kappa_M << 2\gamma$, we can conclude $\kappa_M << 1$ i.e. the E' + M reaction is slow and M diffuses from the electrode to the bulk; thus the reaction zone is on the outside edge of the diffusion layer.

Now if $\kappa_M >> 2\gamma$, $\chi_* << 1$, and from eqn. (A.48):

$$(\delta u' / \delta \chi)_o = (2\kappa_M / \gamma)^{1/2} - 1 \quad . \tag{A.50}$$

Thus we obtain:

$$j = n(2D_M k_E e_\Sigma m_o)^{1/2} - nD_M m_o / z_D \quad . \tag{A.51}$$

This is case VI. Here $\kappa_M >> 1$ and so the E' + M reaction is fast and the reaction zone is close to the electrode surface (this is confirmed by $\chi_* << 1$). The rate limiting step is the regeneration of E' from E within the zeroth order reaction layer.

Thus the boundary between cases V and VI is given by $\kappa_M = 2\gamma$. The boundary is very sharp and no expression is obtained for both cases V and VI on crossing the boundary. The case diagram is amended for case VI in fig(A.7).

The zeroth order reaction layer can be understood by matching the regeneration of enzyme in the reaction layer of thickness z_* with the diffusion of M into that layer:

$$j/n = k_E e_\Sigma z_* = 2D_M m_o / z_* \quad . \tag{A.52}$$

The factor of 2 for the diffusional flux of m_o arises because the concentration profile of M is parabolic. Extrapolation of the

concentration gradient at $\chi = 0$ would intercept the χ axis at $\chi_*/2$. Eliminating for χ_* in eqn. (A.52) gives eqn. (A.51) .

A.4.7 Cases IV and VII

Now we look at the boundary between case IV and a new case, case VII. From inspection of the case diagram, this will be above the line $\kappa_M = 2\gamma$. Then from section (A.4.6) we know that $\chi_* << 1$ but there is still a titration reaction where for $\chi << \chi_*$ there is no E' and for $\chi >> \chi_*$ there is no M. For $\chi << \chi_*$, we take v and $v_o \approx 0$, and apply this to eqn. (A.23), which is then integrated and the condition that u=0 at $\chi = \chi_*$ applied, to obtain:

$$(\delta u/ \delta \chi)_o = 1/ \chi_* + \beta \kappa_E \chi_*/2 \quad . \tag{A.53}$$

Differentiation of eqn. (A.23) also gives:

$$\beta(\delta u/ \delta \chi)_* = - (\delta u/ \delta \chi)_o - \beta \kappa_E \chi_* \quad . \tag{A.54}$$

For $\chi >> \chi_*$, u=0 and so eqn. (A.16) becomes:

$$\delta^2 v/ \delta \chi^2 = - \kappa_E (1-v) \quad .$$

Integration with the boundary conditions that v=1 at $\chi = 1$ and v=0 at $\chi = \chi_* << 1$ gives:

$$v = 1 - \text{cosech}[(\kappa_E)^{1/2}] \sinh[(\kappa_E)^{1/2}(1-\chi)]$$

and

$$(\delta v/ \delta \chi)_* = (\kappa_E)^{1/2} \coth[(\kappa_E)^{1/2}] \tag{A.55}$$

Elimination between eqn.s (A.53) to (A.55) gives:

$$\beta\kappa_E \chi_*^2/2 + \beta\kappa_E^{1/2} \chi_* \coth[(\kappa_E)^{1/2}] - 1 = 0 \qquad (A.56)$$

and

$$-(\delta u/ \delta\chi)_0 = \beta\kappa_E^{1/2} \coth[(\kappa_E)^{1/2}] + \beta\kappa_E \chi_* \quad . \qquad (A.57)$$

Now for the cases we are considering, $\beta >> 1$ ($\kappa_M >> 2\gamma$). Under this condition, χ_* is very small, so that the first term in eqn. (A.56) and the last term in eqn. (A.57) can be neglected. These two terms describe the regeneration of E' within z_*. The layer is so thin that it is a reasonable assumption that there is negligible enzyme regeneration within this layer. We then obtain:

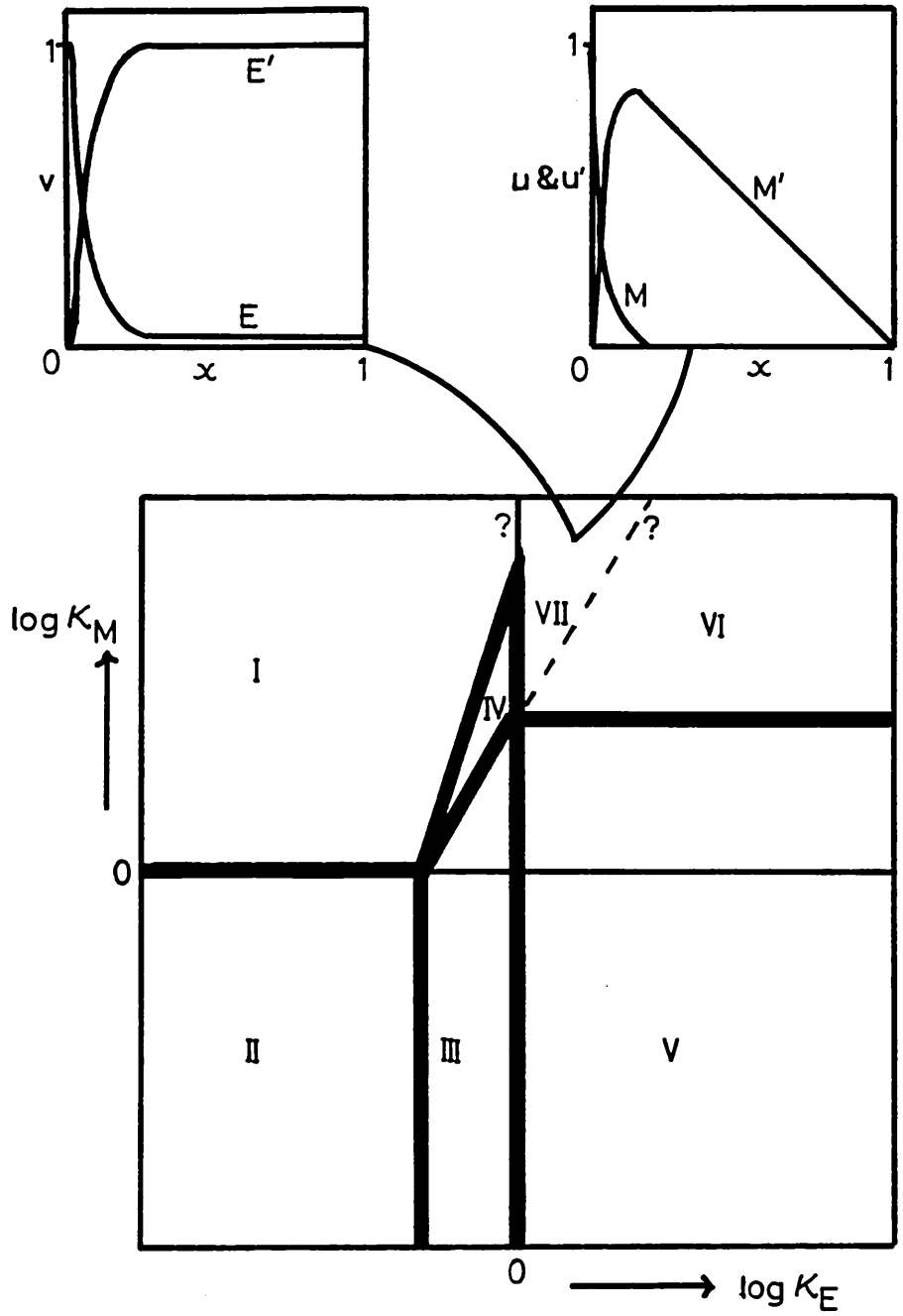
$$(\delta u'/ \delta\chi)_0 \approx -(\delta u/ \delta\chi)_0 = 1/ \chi_* = \beta\kappa_E^{1/2} \coth[(\kappa_E)^{1/2}] \qquad (A.58)$$

where it has been assumed in using eqn. (A.21) that the reaction layer is so close to the electrode surface that nearly all M' generated within z_* reaches the electrode.

Now if $\kappa_E << 1$, eqn. (A.58) becomes $(\delta u'/ \delta\chi)_0 \approx \beta$, and we have recovered case IV (eqn. (A.38)). Here the reaction zone is small and close to the electrode, agreeing with $z_* << 1$, and the diffusion of E' from the bulk to the reaction zone is rate limiting, agreeing with $\kappa_E << 1$ i.e. poor regeneration of E' from E.

When $\kappa_E >> 1$, $(\delta u'/ \delta\chi)_0 \approx \beta\kappa_E^{1/2}$, giving:

$$j = (D_E k_E)^{1/2} e_\Sigma \quad . \qquad (A.59)$$



Fig(A.8) Constructing the $\gamma > 1$ plane: cases IV and VII. The concentration profiles for E, E', M and M' within the diffusion layer are shown.

This is case VII. This describes the rate limiting step as the regeneration of E' from E in its own thin reaction layer $z_E = (D_E/k_E)^{1/2}$ close to the reaction zone.

Case VII is added to the case diagram in fig(A.8) and the boundary between cases IV and VII is seen to be $\kappa_E = 1$.

Now we have found all seven cases for the $\gamma >> 1$ plane. In order to complete the plane, the case boundaries between cases VI and VII and cases I and VII must be investigated.

A.4.8 Cases VI and VII

From inspection of the case diagram in fig(A.8), it is seen that we cross the $\kappa_M = 2\gamma$ line from case V to case VI, and the $\kappa_E = 1$ line from case IV to case VII. Thus the boundary between cases VI and VII must be in the top right hand quadrant defined by these lines i.e. $\kappa_M >> 2\gamma$ and $\kappa_E >> 1$. Since $\kappa_M >> 2\gamma$, the expressions derived for the IV - VII boundary still apply, and applying the condition $\kappa_E >> 1$ in eqn.s (A.56) and (A.57) reduces the $\coth[(\kappa_E)^{1/2}]$ terms to unity. We can then solve a quadratic in χ_* to obtain:

$$\chi_* = \kappa_E^{-1/2} [(1+2/\beta)^{1/2} - 1] \qquad (A.60)$$

and

$$(\delta u'/ \delta \chi)_o \approx - (\delta u/ \delta \chi)_o = \beta \kappa_E^{1/2} (1+2/\beta)^{1/2} . \qquad (A.61)$$

Now if $\beta << 1$, then:

$$(\delta u'/ \delta \chi)_o \approx (2\beta \kappa_E)^{1/2} = (2\kappa_M/\gamma)^{1/2} . \qquad (A.62)$$

This gives the same solution obtained for case VI which is given in eqn. (A.51).

If $\beta >>1$, the right hand side of eqn. (A.61) approximates to $\beta\kappa_E^{1/2}$, which is the same solution giving j in eqn. (A.59) for case VII.

Then the boundary between cases VI and VII is $\beta =1$ or $\kappa_M = \gamma \kappa_E$. In both cases the rate limiting step is the regeneration of E' from E within either the zeroth order reaction layer ($z_* = (2D_M m_o/ k_E e_\Sigma)^{1/2}$) or within the enzyme reaction layer ($z_E = (D_E/ k_E)^{1/2}$) for cases VI and VII respectively. If $\beta >>1$, then $z_E > z_*$, enzyme regeneration within the reaction layer is dominant and we have case VII. If $\beta <<1$, then $z_E < z_*$, and enzyme regeneration within the zeroth order reaction layer is dominant and we have case VI.

A.4.9 Cases I and VII

The remaining boundary to find is that between cases I and VII. From inspection of fig(A.8), it is seen that $\kappa_M >> 1$, $\kappa_E > 1$ and $\kappa_M >> \gamma \kappa_E$.

Now since $\kappa_M >> 1$, we can say M will diffuse from the electrode into a thin reaction layer in which it will be totally consumed. Eqn. (A.35) is obtained for u as before:

$$u = \exp[- (\kappa_M v_o)^{1/2} \chi] \quad . \tag{A.63}$$

Substituting eqn. (A.63) into eqn. (A.16) and applying the boundary conditions gives a solution for v:

$$v = 1 - (1-v_o)/[(\kappa_E)^{1/2} - (\kappa_M v_o)^{1/2}]\{ (\kappa_E)^{1/2} \exp[-(\kappa_M v_o)^{1/2} \chi] - (\kappa_M v_o)^{1/2} \exp[-(\kappa_E)^{1/2} \chi] \} . \tag{A.64}$$

Substituting this solution back into eqn. (A.16) and equating the $\exp[-(\kappa_M v_o)^{1/2}\,\chi]$ terms gives the following relation for v_o:

$$v_o + \gamma\, v_o/[\,1 + (\kappa_M v_o/\kappa_E)^{1/2}\,] = 1 \quad . \tag{A.65}$$

Now the case I - VII borderline is above the case V - VI border, given by $\kappa_M = \gamma\,\kappa_E$. Then on the case I - VII border, $\kappa_M >> \gamma\,\kappa_E$. Also $\kappa_E >> 1$ and from the case V - VI discussion it can be concluded that $v_o \approx 1/\gamma$. Then $\kappa_M v_o >> \kappa_E$, and applying this condition to eqn. (A.65) gives a quadratic equation for $v_o^{1/2}$ which can be solved:

$$v_o^{1/2} = [\,1 + \gamma^2\,\kappa_E/4\kappa_M\,]^{1/2} - (\,\gamma^2\,\kappa_E/4\kappa_M\,)^{1/2} \quad . \tag{A.66}$$

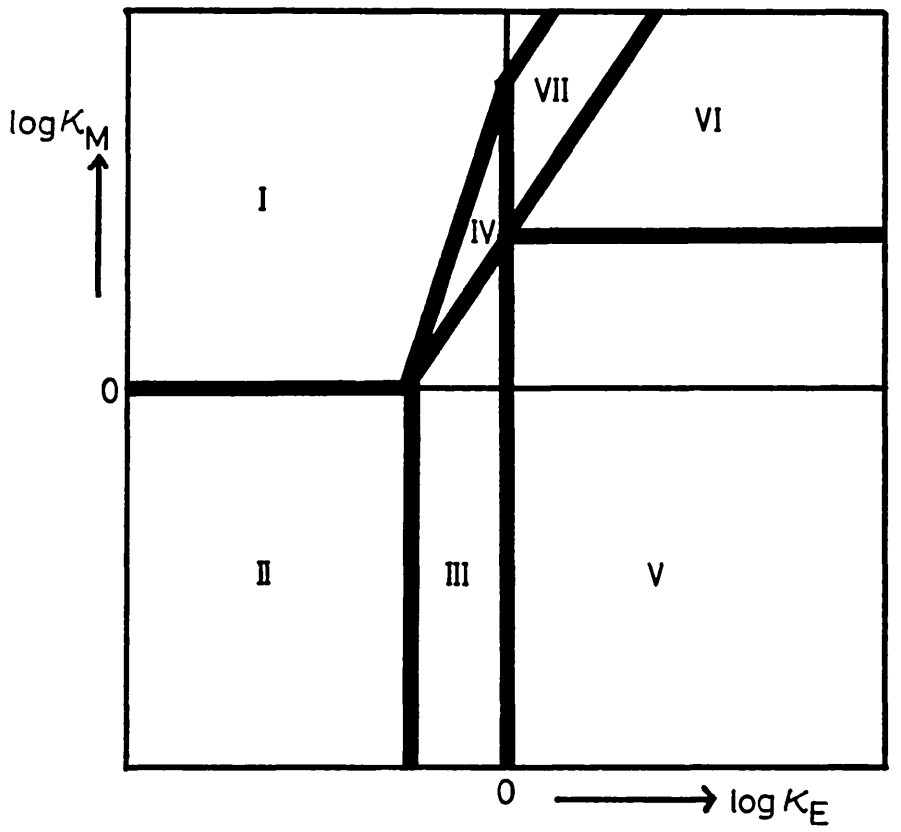
Since $\kappa_M >> 1$, it is assumed that M' is consumed in a small reaction layer next to the electrode, so that $(\,\delta u/\delta\chi\,)_o \approx -(\,\delta u'/\delta\chi\,)_o$. Now from eqn. (A.63), $(\,\delta u/\delta\chi\,)_o = -(\,\kappa_M\, v_o\,)^{1/2}$, and using eqn. (A.66) we find:

$$(\,\delta u'/\delta\chi\,)_o = (\,\kappa_M + \gamma^2\,\kappa_E/4\,)^{1/2} - \gamma/2(\,\kappa_E\,)^{1/2} \quad . \tag{A.67}$$

Now when $\kappa_M > \gamma^2\,\kappa_E$, then $(\,\delta u'/\delta\chi\,)_o \approx \kappa_M^{1/2}$. This is case I. If $\kappa_M < \gamma^2\,\kappa_E$, then $(\,\delta u'/\delta\chi\,)_o \approx [\,\kappa_M/\,\gamma\,(\kappa_E)^{1/2}\,] = \beta\,\kappa_E^{1/2}$. This is case VII. Thus the boundary between cases I and VII is $\kappa_M = \gamma^2\,\kappa_E$. The completed case diagram is shown in fig(A.9).

A.5 The complete case diagram

The completed case diagram is shown in fig(A.9). It is satisfactory that for each case boundary an expression for $(\,\delta u'/\delta\chi\,)_o$ can be



Fig(A.9) The complete case diagram for the $\gamma > 1$ plane.

Cases	Boundary equations	
I & II	$(\delta u'/\delta \chi)_o = \kappa_M^{1/2} \coth(\kappa_M^{1/2}) - 1$	(A.26)
I & IV	$(\delta u'/\delta \chi)_o = \kappa_M^{1/2} [1 + \kappa_M/(4\beta)^2]^{1/2} - \kappa_M/2\beta$	(A.37)
I & VI	$(\delta u'/\delta \chi)_o = \{ 2\kappa_M/ \gamma [1 - 1/ \gamma \ln(1 + \gamma)]\}^{1/2} - 1$	(A.82)
I & VII	$(\delta u'/\delta \chi)_o = (\kappa_M + \gamma^2 \kappa_E/ 4)^{1/2} - (\gamma / 2) \kappa_E^{1/2}$	(A.67)
II & III	$(\delta u'/\delta \chi)_o = \beta \{ 1 - \pi^{-1}/ [Ai(0) Bi'(\phi) - Bi(0)Ai'(\phi)]\}$	(A.32)
II &V	$(\delta u'/\delta \chi)_o = (\kappa_M/ \gamma)[1/2 - 1/ \gamma + 1/ \gamma^2 \ln(1 + \gamma)]$	(A.78)
III &V	$(\delta u'/\delta \chi)_o = \beta (1 + \kappa_E/2)$	(A.41)
IV & VII	$(\delta u'/\delta \chi)_o = \beta \kappa_E^{1/2} \coth(\kappa_M^{1/2})$	(A.58)
V & VI	$\kappa_M >> 2\gamma$ $\quad (\delta u'/\delta \chi)_o = (2\kappa_M/ \gamma)^{1/2} - 1$	(A.50)
	$\kappa_M << 2\gamma$ $\quad (\delta u'/\delta \chi)_o = (\kappa_M/ 2 \gamma) = \beta \kappa_E/2$	(A.49)
VI & VII	$(\delta u'/\delta \chi)_o = \beta (\kappa_E)^{1/2} (1 + 2/\beta)^{1/2}$	(A.61)

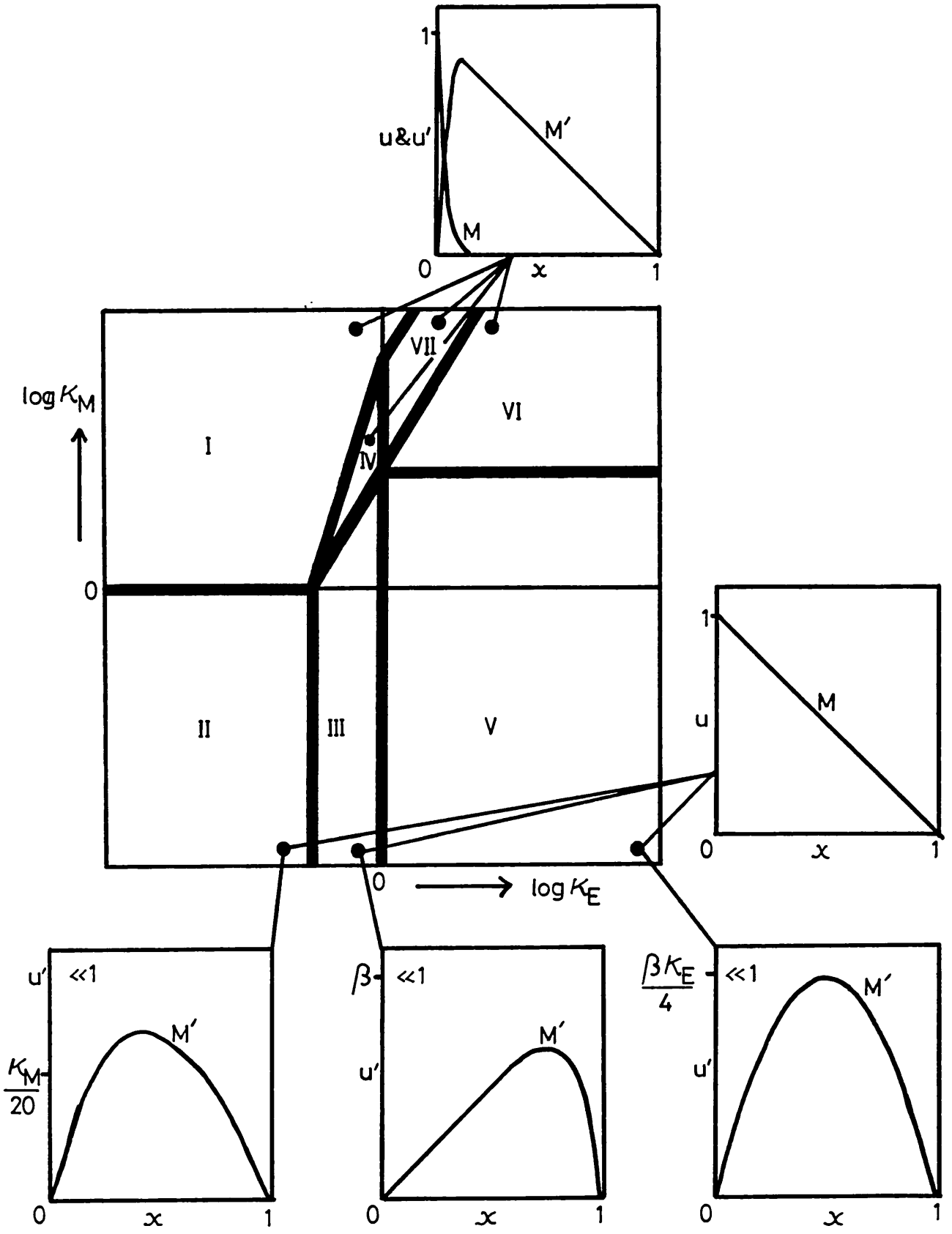
Table A.1 Summary of the equations describing the case boundaries.

found, which can be reduced to the two cases on either side of the boundary. The expressions for $(\delta u'/\delta \chi)_0$ on the case boundaries are given in table A.1.

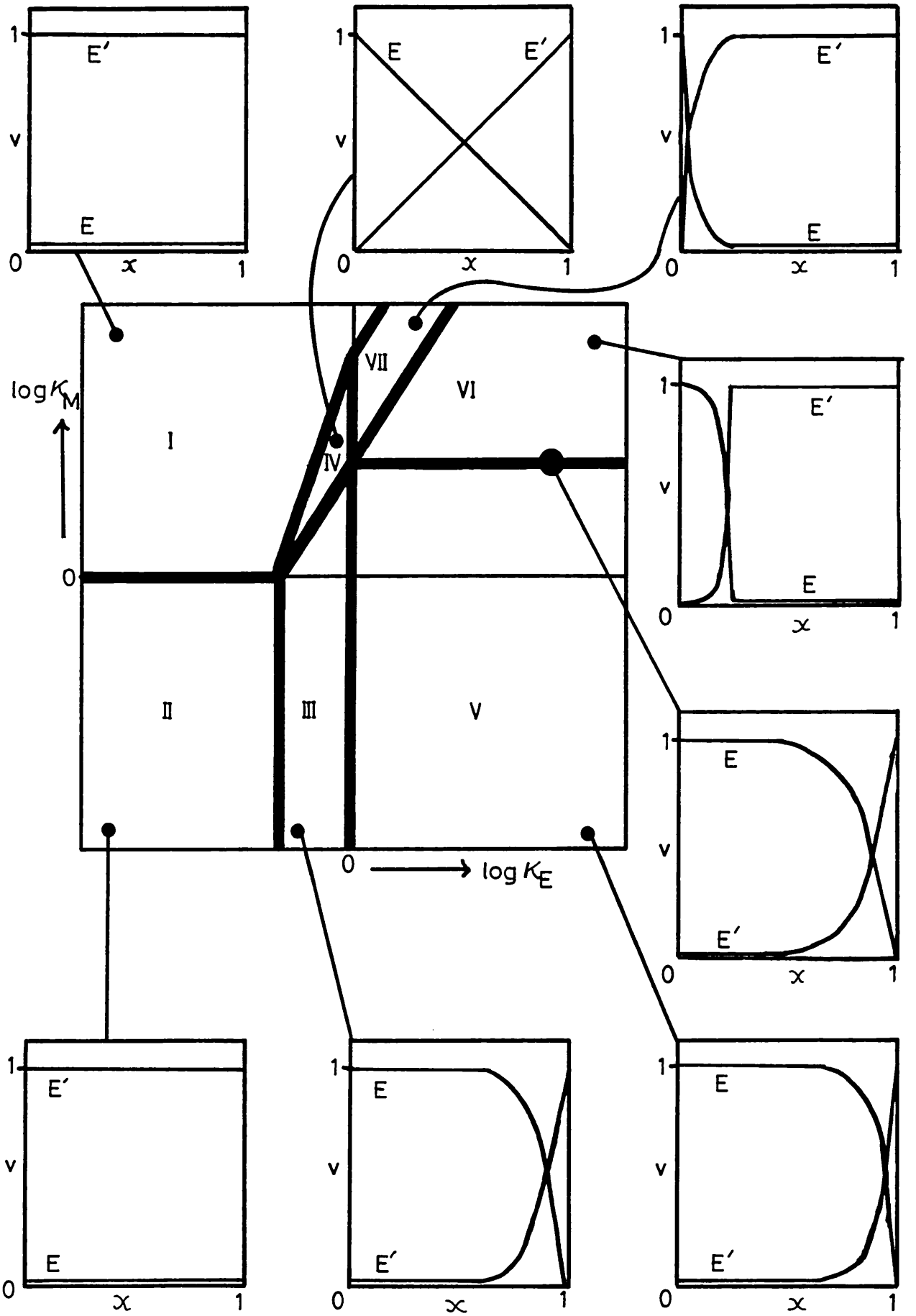
In all, seven cases have been found. In cases I and II, the rate limiting step is the reaction between E' and M either within the small mediator reaction layer next to the electrode or throughout the whole diffusion layer. In cases III and IV, the rate limiting step is the diffusion of either M' from the outside edge of the diffusion layer to the electrode, or E' from the bulk to the small mediator reaction layer next to the electrode. In cases V, VI and VII, the regeneration of E' from E is rate limiting either within the diffusion layer, the zeroth order reaction layer or in a small enzyme reaction layer close to the electrode. It is satisfactory that these last three cases occur in the region where $\kappa_E >> 1$ i.e. the regeneration of E' from E is fast.

The mediator concentration profiles are shown in fig(A.10). It is pleasing that for cases I, IV, VI and VII, where $\kappa_M >> 1$, the mediator reaction layer is very small and close to the electrode. Loss of M' to the bulk solution is negligible. For cases II, III and V, where $\kappa_M << 1$, the E' + M reaction is sluggish and so M has a linear concentration profile from the electrode to the solution. M' is made throughout the diffusion layer for cases II and V, and on the outside edge of the diffusion layer for case III. Thus some M' is lost to the bulk for each of these cases and the concentration of M' is always less than that for M.

The enzyme concentration profiles are shown in fig(A.11). As has been noted above in section A.3, on the $\gamma >> 1$ plane the predominant form of enzyme at the electrode should be E, and since only E' is present in the bulk, there should be a switch over from E to E' being the predominant species somewhere within the diffusion layer. This



Fig(A.10) The concentration profiles for M and M' for each case on the $\gamma > 1$ plane.



Fig(A.11) The concentration profiles for E and E' for each case on the $\gamma > 1$ plane.

is indeed observed for cases III, IV, V, VI and VII. For cases III and V, this switch occurs on the outside edge of the diffusion layer. For cases VI and VII, it occurs next to the electrode. For case IV, there is a linear profile in both E and E' throughout the whole diffusion layer, so that the switch over occurs at half way across the layer. Cases I and II do not obey the predicted behaviour. In both these cases, the rate determining step is the E' + M reaction, either close to the electrode or throughout the whole diffusion layer. The reaction is too slow to generate a sufficient quantity of E to perturb the E' concentration, and so E' is predominant throughout the whole diffusion layer.

A.6 New coordinates for the case diagram

So all seven cases for the $\gamma >> 1$ plane of the three dimensional case diagram have been derived. Further planes can be obtained for the $\gamma \approx 1$ and $\gamma << 1$ planes, however no new cases are introduced, and some of the present cases are eliminated. The three axes of the case diagram are κ_E , κ_M and γ which depend on the experimental variables [E], [S] and 1/[S] respectively. Thus for any change in [S], it is very complex to move through the case diagram in a sideways and vertical shift.

For this reason, the case diagram has been redrawn with respect to the new coordinates $1/\gamma$, β and ϕ where:

$$1/\gamma = k_E/k_M m_o \qquad (A.68)$$

$$\beta = D_E e_\Sigma / D_M m_o \qquad (A.69)$$

$$\phi = z_D^2 k_M m_o / D_E \quad . \tag{A.70}$$

$1/\gamma$ and β depend on [S] and [E] respectively, while ϕ is independent of both [E] or [S]. Thus if $1/\gamma$, β and ϕ are identified with the x, y and z axes, any experiment varying either [E] or [S] wiil be on a fixed ϕ plane, and only two dimensional transitions can occur. This is much easier to comprehend.

The new variables are related to the old variables by:

$$\gamma \kappa_E = \phi \tag{A.71}$$

and

$$\kappa_M = \phi \beta \quad . \tag{A.72}$$

These relationships will be used to convert the $\gamma >> 1$ plane into a $\phi >> 1$ plane.

Initially the case boundaries are considered. They must be converted into the new coordinates. These are shown in table A.2. With the exception of the case II - III boundary, these boundaries can be placed on the $\phi >> 1$ plane. The case II - III boundary is described by the plane $\phi = 1$, which is parallel to the $\phi >> 1$ plane. Thus it cannot exist on the $\phi >> 1$ plane. The $\phi = 1$ plane is considered below. Note that the case V - VI boundary is given by $\kappa_M = 2\gamma$ or $\phi\beta = 2\gamma$. However it should be remembered that the log of the line is plotted, and since $\kappa_M >> 1$ and $\gamma >> 1$, $\kappa_M \approx \gamma$ or $\phi\beta \approx \gamma$ i.e. the factor of 2 may be ignored.

The points of intersection of the case boundaries on the $\gamma >> 1$ plane must be converted into the new coordinates to check that the intersection points still exist. Firstly, take the intersection between cases I, II, III and IV. This is the intersection between the lines

Cases	Old boundary $\gamma >> 1$ plane	New boundary $\phi >> 1$ plane
I - II	$\kappa_M = 1$	$\beta = 1/\phi$
I - IV	$\kappa_M = (\gamma \kappa_E)^2$	$\beta = \phi$
I - VII	$\kappa_M = \gamma^2 \kappa_E$	$\beta = \gamma$
II - III	$\kappa_E = 1/\gamma$	$\phi = 1$
III - IV	$\kappa_M = \gamma \kappa_E$	$\beta = 1$
III - V	$\kappa_E = 1$	$1/\gamma = 1/\phi$
IV - VII	$\kappa_E = 1$	$1/\gamma = 1/\phi$
V - VI	$\kappa_M = 2\gamma$	$\phi\beta = 2\gamma$
VI - VII	$\kappa_M = \gamma \kappa_E$	$\beta = 1$

Table A.2 Summary of the case boundaries converted into the new coordinates for the $\phi >> 1$ plane.

$\kappa_M = 1$, $\kappa_E = 1/\gamma$, $\kappa_M = (\gamma \kappa_E)^2$ and $\kappa_M = \gamma \kappa_E$ and occurs when $\kappa_E = 1/\gamma$ and $\kappa_M = 1$ i.e. $\phi = 1$ and $\beta = 1/\phi$. Then this point of intersection is on the $\phi = 1$ plane and cannot exist on the $\phi >> 1$ plane. Thus cases I, II, III and IV will not all border in the same manner in the new case diagram. The second intersection point is that between cases I, IV and VII i.e. between the lines $\kappa_M = (\gamma \kappa_E)^2$, $\kappa_M = \gamma^2 \kappa_E$ and $\kappa_E = 1$. The intersection point is where $\kappa_E = 1$ and $\kappa_M = \gamma^2$ i.e. $1/\gamma = 1/\phi$ and $\beta = \phi$. The third intersection point is where cases III, IV, V, VI and VII intersect. This is where $\kappa_E = 1$ and $\kappa_M = 2\gamma$ i.e. $1/\gamma = 1/\phi$ and $\beta = 1$.

The $\phi >> 1$ plane can now begin to be constructed. This is shown in fig(A.12). It should be remembered that the case diagram is represented in logarithmic units. Thus the lines $\beta = \gamma$ and $\beta \phi = \gamma$ are linear since:

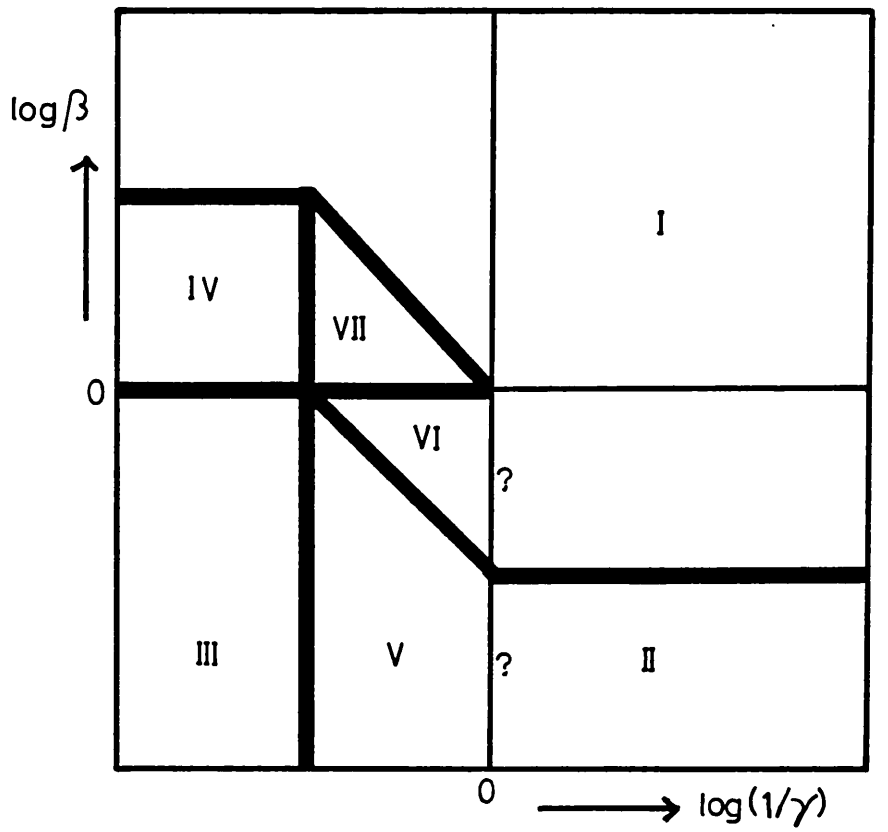
$$\log \beta = - \log(1/\gamma)$$

and

$$\log \beta = \log(1/\phi) - \log(1/\gamma) \quad .$$

respectively. Then the line $\beta = \gamma$ must pass through the point ($1/\gamma = 1$, $\beta = 1$) and this fixes the lower end of the case I - VII boundary. The line $\beta \phi = \gamma$ is parallel to the line $\beta = \gamma$, but will intersect the $1/\gamma = 1$ axis at $\beta = 1/\phi$. This fixes the bottom of the case V - VI boundary.

From the case diagram it is seen that two new case boundaries exist: the case V - II boundary and the case VI - I boundary. These did not exist on the case diagram described by the old coordinates and so must be shown to exist on the new case diagram. There are also two new intersection points, namely between cases I, VI and VII and cases I, II, V and VI which must also be found.



Fig(A.12) The incomplete $\phi > 1$ plane. The boundaries between cases V and II and cases VI and I are unknown.

A.6.1 Cases V and II

It is seen from fig (A.12) that the case boundaries between cases V and II and cases VI and I occur where $\beta < 1$ and $\gamma \approx 1$. Now to be in case II, we must be below the line $\beta = 1/\phi$ i.e. $\beta < 1/\phi$ or $\beta\,\phi < 1$, and it is thus seen from eqn. (A.72) that $\kappa_M < 1$. This means that most M will escape the diffusion layer before reacting with E', so that the concentration profile for M will be linear across the diffusion layer:

$$u = 1 - \chi = \chi' \quad . \tag{A.73}$$

Now the case V - II boundary is to the right of the case III - V boundary i.e. $1/\gamma > 1/\phi$, which from eqn. (A.71) implies $\kappa_E >> 1$. Then, as seen in section A.4.6, the $\delta^2 v/\delta\chi^2$ term in eqn. (A.16) is negligible compared to the κ_E terms and so:

$$v \approx 1/(1 + \gamma u) = 1/(1 + \gamma \chi') \quad . \tag{A.74}$$

From eqn. (A.17) it is seen that $-\delta^2 u/\delta\chi^2 = \delta^2 u'/\delta\chi^2$. Using this in eqn. (A.15), along with eqn.s (A.73) and (A.74), gives:

$$\delta^2 u'/\delta\chi^2 = \delta^2 u'/(\delta\chi')^2 = -\kappa_M uv = -\kappa_M \chi'/(1 + \gamma\chi') \tag{A.75}$$

Integrating and applying the boundary condition that $u'=0$ at $\chi'=0$ ($\chi = 1$) gives:

$$(\delta u'/\delta\chi') = (\delta u'/\delta\chi')_{\chi'=0} - \kappa_M \chi'/\gamma + \kappa_M \gamma^{-2} \ln(1 + \gamma\chi') \tag{A.76}$$

and

$$u' = (\delta u'/\delta \chi')_{\chi' = o} \chi' + \kappa_M \gamma^{-3} [(1 + \gamma \chi') \ln(1 + \gamma \chi') - \gamma \chi' - (\gamma \chi')^2/2] \ . \tag{A.77}$$

Applying the boundary condition that u'=0 at $\chi'=1$ ($\chi = 0$) to eqn. (A.77) gives $(\delta u'/\delta \chi')_{\chi' = o}$. Substituting this into eqn. (A.76) gives $(\delta u'/\delta \chi)_o$:

$$(\delta u'/\delta \chi)_o = - (\delta u'/\delta \chi')_{\chi' = 1} = \kappa_M/\gamma \, [\, 1/2 - 1/\gamma + 1/\gamma^2 \ln(1 + \gamma) \,] \ . \tag{A.78}$$

Now the size of γ will give two solutions for $(\delta u'/\delta \chi)_o$. If $\gamma >> 1$, then eqn. (A.74) simplifies to:

$$(\delta u'/\delta \chi)_o = \kappa_M/2\gamma = \beta \kappa_E/2 \ . \tag{A.79}$$

This is the same answer for case V given by eqn. (A.42).

If $\gamma << 1$, then expanding the ln term in eqn. (A.78) as a series gives $(\delta u'/\delta \chi)_o \approx \kappa_M/3$. This is the same answer for case II, given by eqn. (A.28). Thus on the new case diagram, the boundary between cases V and II is $\gamma = 1$. When $1/\gamma < 1$, we are in case V, and when $1/\gamma > 1$, we are in case II. This leaves the case VI - I boundary to be found.

A.6.2 Cases VI and I

To obtain case I we must be above the line $\beta = 1/\phi$ i.e. $\beta \phi > 1$ and from eqn. (A.72) it is seen that $\kappa_M >> 1$. We also know from the case V- II boundary discussion that $\kappa_E >> 1$. Now we can proceed as for cases VI - VII (section A.4.9) and substitute eqn. (A.43) into eqn. (A.15) to obtain:

$$\delta^2 u/\delta\chi^2 = \kappa_M u/(1 + \gamma u) \quad . \qquad (A.80)$$

Multiplication of both sides by ($\delta u/\delta\chi$) and integration gives:

$$(\delta u/\delta\chi)^2 = (2\kappa_M/\gamma)[u - \gamma^{-1}\ln(1 + \gamma u)] \quad . \qquad (A.81)$$

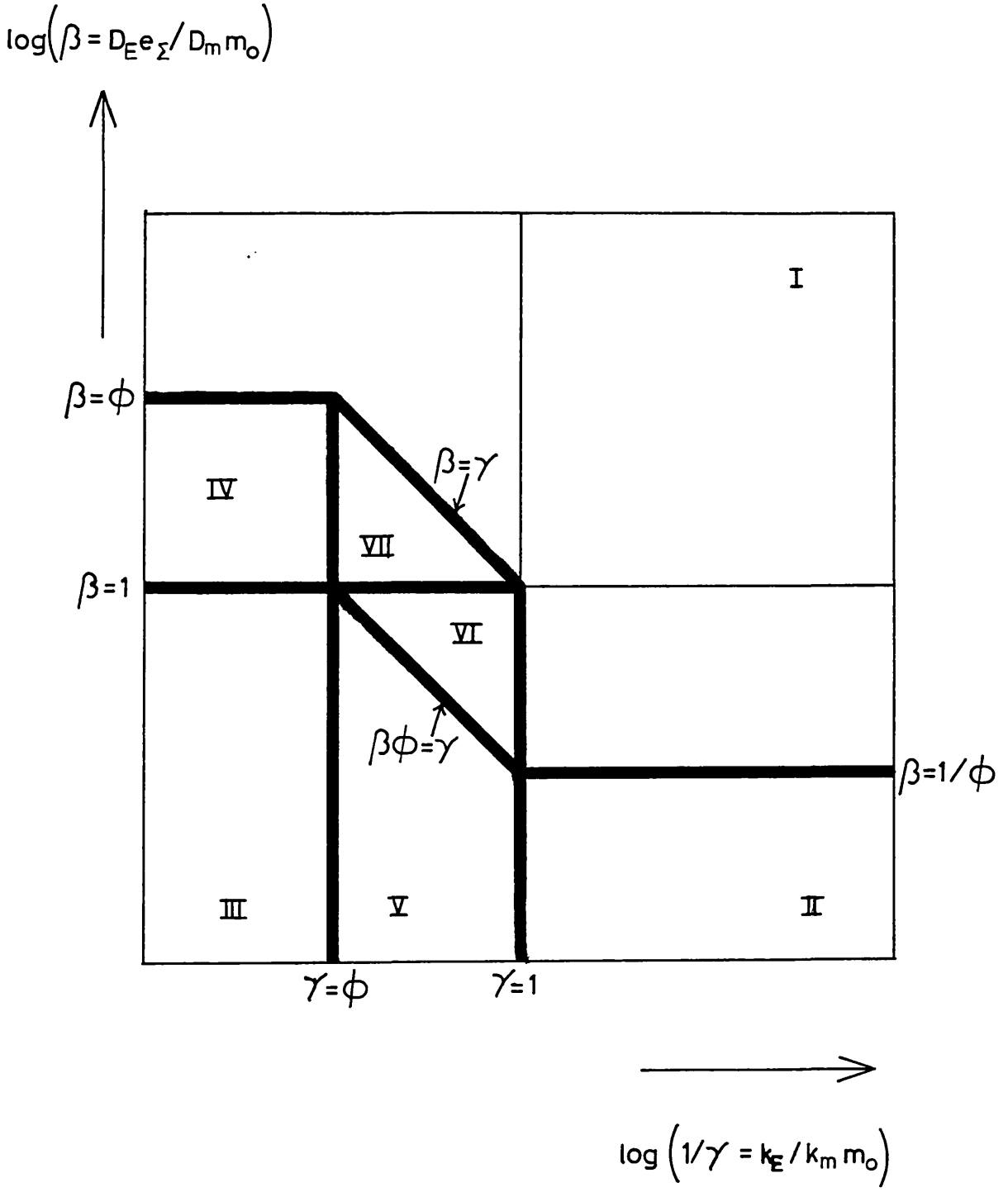
Applying the boundary condition that u=1 at $\chi = 0$, to eqn. (A.81) and then substituting into eqn. (A.21) gives:

$$(\delta u'/\delta\chi)_o = \{ (2\kappa_M/\gamma)[1 - \gamma^{-1}\ln(1 + \gamma)] \}^{1/2} - 1 \; . \quad (A.78)$$

Now when $\gamma >>1$, the ln term is negligible, and eqn. (A.82) reduces to $(2\kappa_M/\gamma)^{1/2} - 1$. We have recovered case VI, given by eqn. (A.51). This is case VI. When $\gamma <<1$, the ln term in eqn. (A.82) can be expanded as a series and since $\kappa_M >>1$, the second term on the right of the equation can be ignored to give $(\delta u'/\delta\chi)_o \approx \kappa_M^{1/2}$. This is the answer for case I, given in eqn. (A.27). Thus the boundary between cases VI and I is $\gamma =1$.

A.6.3 The complete case diagram with the new coordinates

Now we have obtained all the case boundaries for the $\phi >1$ plane, and can thus find the remaining points of intersection. For the intersection point between cases I, II, V and VI, the lines $1/\gamma =1$ and $\beta = 1/\phi$ intersect at ($1/\gamma =1, \beta = 1/\phi$). It is satisfactory that this point lies on the line $\beta \phi = \gamma$ (the case V-VI boundary). For the intersection point between cases I, VI and VII , the line $1/\gamma =1$ intersects $\beta = 1$, at ($1/\gamma =1, \beta = 1$). It is satisfactory that this point lies



Fig(A.13) The complete $\phi > 1$ plane.

on the line $\beta = \gamma$ (the case I - VII boundary). Thus the $\phi > 1$ plane is complete. This is shown in fig(A.13).

A.6.4 The $\phi \approx 1$ plane

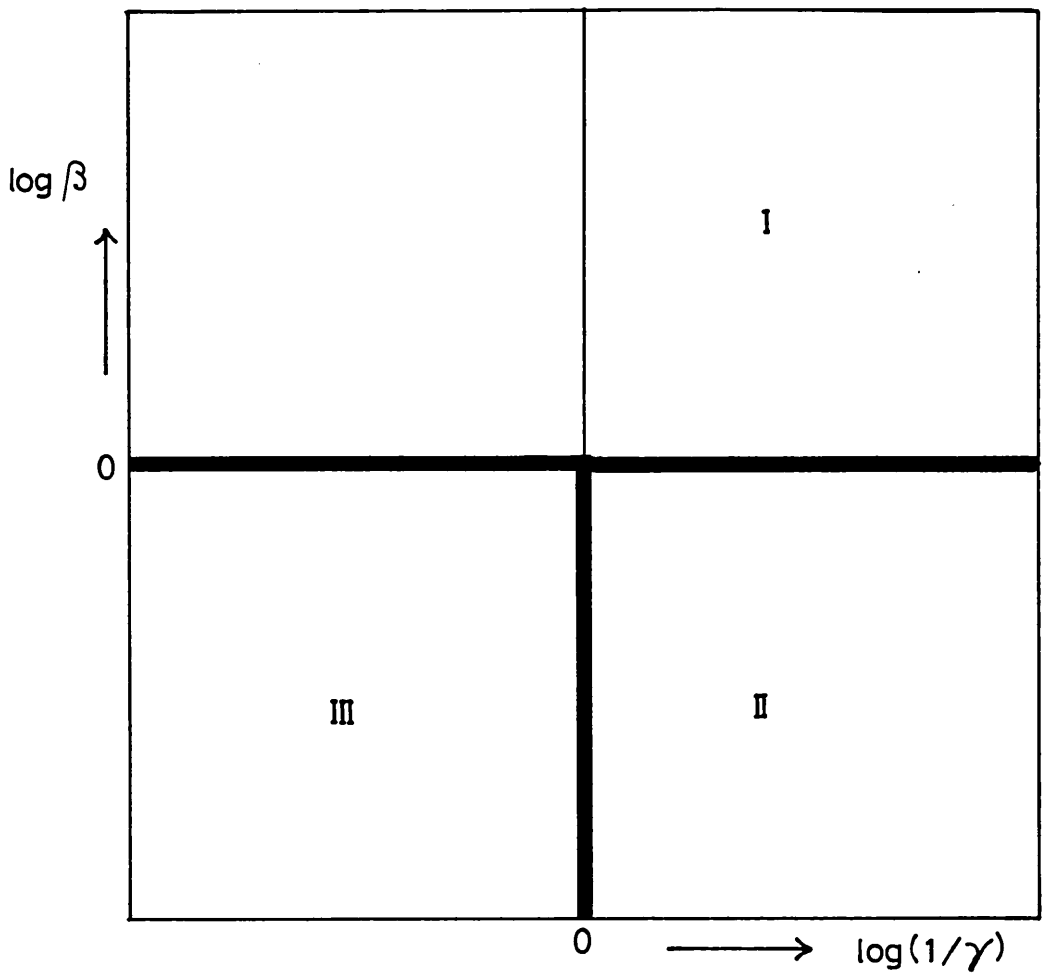
It is interesting to consider what happens when $\phi \approx 1$. We have seen that on this plane, there is a case boundary between cases I and III and now it is shown how this is obtained. Consider what happens to the $\phi > 1$ plane when ϕ is decreased towards unity. The line $1/\gamma = 1/\phi$ will shift towards the $1/\gamma = 1$ line, decreasing the areas of cases V, VI and VII. The $\beta = \phi$ line will shift towards the $\beta = 1$ line, decreasing the areas of cases IV and VII. The line $\beta = 1/\phi$ will move vertically up the case diagram towards the line $\beta = 1$, increasing the area of case II and decreasing the area of case VI since the point of intersection between the case V - VI boundary and the case VI - I boundary is given by the value of $\beta = 1/\phi$ on the line $1/\gamma = 1$.

When $\phi \approx 1$, then cases IV, V, VI and VII will become infinitesimally small and only cases I, II and III will remain on the case diagram. This is shown in fig(A.14). The boundary between cases I and II and cases I and III becomes $\beta = 1$ and between cases II and III becomes $1/\gamma = 1$.

This plane is unimportant in terms of the experimental work of this thesis and is presented for the sake of completion. Thus it need not be investigated in any further detail.

A.7 Experimental variables

The electrode current, i, is related to the flux of electrons, j, by $j = i/AF$, where A is the area of the electrode. The change in



Fig(A.14) The $\phi \approx 1$ plane.

electrode current with the experimental variables enables the position in the case diagram for a particular set of experimental conditions to be found. Thus the dimensionless variables must be related to the experimental variables.

In the new case diagram the three axes are described by $1/\gamma$, β and ϕ respectively. There are four experimental variables, namely [S] , e_Σ , ω (the rotation speed of the electrode) and the potential of the electrode relative to a saturated calomel electrode.

Only $1/\gamma$ is dependent on [S] (given by the k_E term) and hence an increase in [S] will result in an increase in k_E , equivalent to a translation to the right hand side of the diagram, parallel to the $1/\gamma$ axis.

Only β is dependent on e_Σ , and hence an increase in e_Σ will result in a linear translation towards the top of the case diagram, parallel to the β axis.

The rotation speed of the electrode, ω (in Hz), is described by z_D , the diffusion layer thickness of the electrode. z_D is given by [126]:

$$z_D = 0.643\ \nu^{1/6}\ D^{1/3}\ \omega^{-1/2} \qquad (A.83)$$

where ν is a constant called the kinematic viscosity of the solution, and D is the diffusion coefficient for the species in the bulk solution. Only ϕ is dependent on z_D ; $\phi\ \alpha\ z_D^2\ \alpha\ \omega^{-1}$. Then an increase in rotation speed will result in a decrease in ϕ . Then to investigate the effect of a change of ω on the case diagram, it is best to look at a ϕ vs. β or $1/\gamma$ plane, although this would require further manipulation of the mathematics. Alternatively, a change in ω could be followed on a γ plane, since γ is independent of ω i.e. fig(A.9) for the $\gamma >> 1$ plane. However the experimental range of ω values is between 1 - 36 Hz,

and on a logarithmic scale this is quite small. Only small transitions in the case diagram can be made and it is doubtful whether any case boundaries could be crossed. Thus it is not expected that any change in dependence of current on ω at fixed [E] and [S] would be observed.

The experimental variable ω is best used as a support for the analysis of data according to [E] or [S]. There are a number of cases which give identical order of dependence on either [E] or [S]. For instance, if the current is found to depend on $[S]^0$, then the data could be in cases I, II, III or IV. However the ω dependence in these cases is 0, -1/2, +1/2 and +1/2 respectively. Thus the ω dependence can be used to distinguish between the cases.

The dependence on potential is given by m_o , and is discussed in more detail in chapter 5.

Appendix B

The heterogeneous redox catalysis theory

The basic mechanisms and assumptions made have been outlined in section 4.3.3, and the three of the six cases obtained have been presented in a case diagram. In this appendix the complete mathematical treatment of the theory and the derivation of the cases are given.

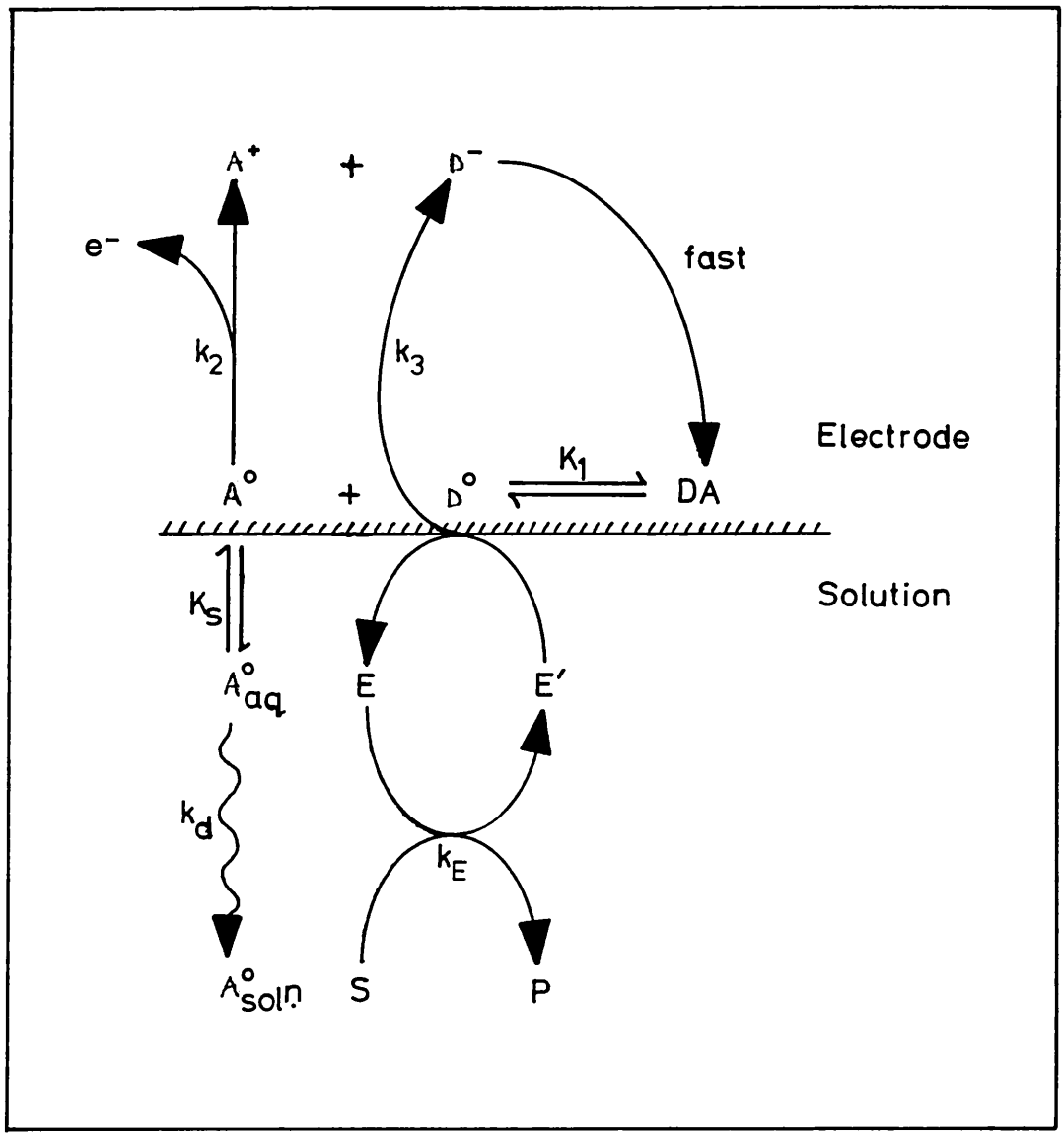
B.1 Theoretical description of the theory

The reaction scheme for the heterogeneous redox catalysis theory is shown in fig(B.1). The theory proposes that because of the limited solubility of the electrode species A^+ and D^- , reactions involving these species take place on the electrode surface itself. It is assumed that on the surface of a conducting organic salt electrode A^+D^- there is a labile equilibrium involving the energetic species A^o and D^o, described by K_1:

$$A^+D^- \overset{K_1}{\rightleftharpoons} A^o + D^o$$

It is assumed that A^o can be oxidized to A^+ , with the first order rate constant k_2 :

$$A^o \xrightarrow{k_2} A^+$$



Fig(B.1) The scheme for the heterogeneous redox catalysis mechanism.

It is also assumed that the reduced enzyme, E' , can be oxidized by the species D^0 with the second order rate constant k_3 :

$$D^0 + E' \xrightarrow{k_3} D^- + E$$

In the case of glucose oxidase, E' may require two molecules of D^0 for its oxidation. Thus n, the number of D^0 equivalents required, is introduced into the expression describing the flux of electrons i.e. for each D^0 reduced by reaction with E', an A^0 species must be oxidized at the electrode. It is assumed that the removal of only the first electron from the enzyme is rate limiting.

The A^+ and D^- formed on the electrode surface by the k_2 and k_3 reactions are assumed to recombine readily to give the original salt:

$$A^+ + D^- \xrightarrow{\text{fast}} A^+ D^-$$

This process is assumed to be fast and therefore not rate limiting.

So far, all the reactions have been assumed to take place on the electrode surface. This implies the reaction layer is so small that it is confined to the electrode surface. Thus it would be unaffected by the thickness of the diffusion layer, which is governed by the rotation speed of the electrode. Then in order to introduce the possibility of rotation speed dependence, it is assumed that A^0 can become solvated and diffuse away from the electrode surface to the bulk:

$$A^0 \overset{K_S}{\rightleftharpoons} A^0(aq) \xrightarrow{k_D} A^0(soln.)$$

K_S (cm^{-1}) describes the solubility of A^o and k_D (cm s^{-1}) is the mass transfer rate constant for A^o :

$$k_D = D_A / z_D \qquad (B.1)$$

where D_A is the diffusion coefficient of A^o and z_D is the thickness of the diffusion layer. In the steady state, the flux of A^o dissolving into the bulk solution is balanced by an equal flux of D^- leaving the electrode surface. This is necessary to achieve mass balance.

In the solution, enzyme, E, is reacting with its substrate, S, with the Michaelis-Menten rate constant, k_E :

$$E + S \xrightarrow{k_E} E' + P$$

where P denotes product, and E' reduced enzyme, and k_E is given by:

$$k_E = k_{cat}[S] / \{ K_M + [S] \} \quad . \qquad (B.2)$$

The concentration of S is assumed to be sufficiently large for there to be no concentration polarization of the substrate within the diffusion layer. This assumption is confirmed in section 4.5.8.1 . [S] is also assumed to be sufficiently large for all enzyme in the bulk solution to be in the reduced form.

B.2.1 Kinetics at the electrode surface

Initially the surface kinetics are considered. At steady state:

$$K_1 = a\,d \qquad (B.3)$$

$$j_e = k_2\,a \qquad (B.4)$$

$$j_E = k_3\,e'_o\,d \qquad (B.5)$$

where a, d, and e' denote the concentrations of A^o , D^o and E' , and o denotes at the electrode surface. a and d are surface concentrations, measured in mol cm^{-2} . Note that the theory distinguishes j_e , the flux of electrons, from j_E , the flux of enzyme.

In the steady state, the fluxes of A^o and D^o must also be matched:

$$(k_2 + K_S k_D)\,a = n\,k_3\,e'_o\,d \quad . \qquad (B.6)$$

From eqn.s (B.3) - (B.6), a simple relation between j_e and j_E is found:

$$j_e = n\,j_E\,(1+\theta) \qquad (B.7)$$

where θ is a dimensionless variable given by:

$$\theta = K_S k_D / k_2 \quad . \qquad (B.8)$$

The physical significance of θ is described in section B.3 .

Eliminating a between eqn.s (B.3) and (B.6), followed by substitution for d in eqn. (B.5) gives:

$$j_E = (K_1 k_2 k_3 (1+\theta)\,e'_o / n)^{1/2} \quad . \qquad (B.9)$$

Since e'_o is unknown, it is now necessary to solve Fick's second law for the enzyme.

B.2.2 Enzyme kinetics

Fick's second law for the enzyme in the direction z normal to the electrode is:

$$D_E \, \delta^2 e/\delta z^2 = - k_E \, e \qquad (B.10)$$

where e is the concentration of E, and it is assumed that E and E' have the same diffusion coefficient. It is also known that:

$$e + e' = e_\Sigma \qquad (B.11)$$

where e_Σ is the total concentration of enzyme species.

The boundary conditions are as follows:

$$\text{at } z = z_D \text{ , } e = 0 \text{ and } e' = e_\Sigma \qquad (B.12)$$

and

$$\text{at } z = 0 \text{ , } \quad j_E = D_E(\delta e/\delta z)_o \quad . \qquad (B.13)$$

We now rewrite the above equations in terms of the dimensionless variables $v = e'/e_\Sigma$, $\kappa_E = k_E \, z_D{}^2 / D_E$ and $\chi = z/z_D$. These variables are identical to those in Appendix A.

Substituting eqn. (B.11) into eqn. (B.10) then gives:

$$\delta^2 v/\delta \chi^2 = - \kappa_E \, (1-v) \qquad (B.14)$$

with the boundary conditions that at $\chi = 1$, $v = 1$ and at $\chi = 0$,

$$j_E = (D_E e_\Sigma / z_D) (\delta v / \delta \chi)_o \quad . \tag{B.15}$$

Integrating eqn. (B.14) gives:

$$(1-v) = (1-v_o) [\cosh(\kappa_E^{1/2} \chi) - \sinh(\kappa_E^{1/2} \chi) \coth(\kappa_E^{1/2})]. \tag{B.16}$$

Differentiation then gives:

$$(\delta v / \delta \chi)_o = (1-v_o) \kappa_E^{1/2} \coth(\kappa_E^{1/2}) \quad . \tag{B.17}$$

v_o is an unknown variable and must be determined.

B.2.3 Flux of electrons

Now f, a dimensionless variable, is defined to describe j_e :

$$j_e = n f D_E e_\Sigma / z_D \quad . \tag{B.18}$$

From eqn.s (B.7), (B.15) and (B.18) it is found that:

$$(\delta v / \delta \chi)_o = f(1+\theta) \quad . \tag{B.19}$$

Using eqn.s (B.9), (B.15) and (B.19):

$$v_o = (1+\theta) \rho f^2 \tag{B.20}$$

where ρ is a dimensionless variable given by:

$$\rho = (ne_{\Sigma}/ K_1k_2k_3) (D_E/ z_D)^2 \quad . \tag{B.21}$$

Now that v_o is known, substitution of eqn.s (B.19) and (B.20) into eqn. (B.17). This gives a quadratic in f:

$$\rho f^2 + f \tanh(\kappa_E{}^{1/2})/\kappa_E{}^{1/2} - 1/(1+\theta) = 0 \quad . \tag{B.22}$$

The solution for f is then:

$$f = (1/2\rho){ [\tanh^2(\kappa_E{}^{1/2})/\kappa_E + 4\rho/(1+\theta)]^{1/2} - \tanh(\kappa_E{}^{1/2})/\kappa_E{}^{1/2} } \tag{B.23}$$

By considering the relative sizes of the variables κ_E , ρ and θ , functions of f are found which, on substituting into eqn. (B.18), give particular cases for j_e .

B.3 Physical significance of the dimensionless variables

In order to understand how the cases relate to the actual physical situation occuring, the significance of the three dimensionless variables, κ_E , ρ and θ, must be understood. The three dimensionless variables describe the probability of a certain event happening, that probability being dependent on the magnitude of the variable relative to unity.

κ_E is identical to the variable κ_E in the homogeneous mediation theory (Appendix A) and compares the diffusion layer thickness, z_D , to the enzyme reaction layer thickness, $(D_E/ k_E)^{1/2}$. Thus κ_E

describes the probability of E being converted to E' before escaping from the diffusion layer unreacted. If $\kappa_E > 1$, then the diffusion layer thickness is greater than the reaction layer thickness for E, and so most E will be converted back to E' within the diffusion layer. If $\kappa_E < 1$, the converse is true and most E will escape from the diffusion layer before being regenerated to E'.

ρ describes the balance between surface kinetics, $(ne_\Sigma K_1 k_2 k_3)^{1/2}$, and mass transport of the reduced enzyme, $(n D_E e_\Sigma / z_D)$. If $\rho > 1$, then the surface kinetics are slow, and the flux , j_e , will be controlled by the flux of the surface reactions. If $\rho < 1$, then the surface kinetics are fast, and the flux will be controlled by the mass transport of the reduced enzyme to the electrode.

θ describes the partitioning of A^o between diffusion into the bulk solution $(K_S k_d)$ and oxidation to A^+ (k_2). θ is defined by eqn. (B.8) which together with eqn. (A.83), gives:

$$\theta = K_S D_A / k_2 z_D = K_S D_A \omega^{1/2} / k_2 (z_D)_{\omega = 1\ Hz} \ . \qquad (B.24)$$

Thus θ depends on the square root of the rotation speed of the electrode. If $\theta > 1$, then most A^o is lost to the bulk and rotation speed dependence of j_e will be observed. If $\theta < 1$, then most A^o will be oxidized at the electrode and j_e will not depend on the rotation speed of the electrode.

B.4 Derivation of the cases

The three dimensionless variables describe a 3-dimensional case diagram where the x, y and z axes are represented by κ_E , ρ and θ

respectively. Initially only the $\theta >> 1$ plane is considered. On this plane, the rotation speed dependence of j_e is at a maximum.

B.4.1 The $\theta >> 1$ plane

Consider the condition:

$$\rho/(1+\theta) >> \tanh^2(\kappa_E^{1/2})/\kappa_E \quad . \tag{B.25}$$

The ρ term then dominates the right hand side of eqn. (B.23) and f becomes:

$$f = \{ \rho(1+\theta) \}^{-1/2} \quad . \tag{B.26}$$

Using eqn. (B.18), the flux of electrons, j_e , is given by:

$$j_e = [nK_1k_2k_3e_\Sigma/ (1+\theta)]^{1/2} \quad . \tag{B.27}$$

This is the case where surface kinetics are rate limiting, denoted Sθ.

Now we consider the situation where $\rho/(1+\theta) << \tanh^2(\kappa_E^{1/2})/\kappa_E$. The square root term in eqn. (B.23) can be expanded to give:

$$f \approx \kappa_E^{1/2} \coth(\kappa_E^{1/2})/ (1+\theta) \quad . \tag{B.28}$$

Now particular solutions for f can be found depending on the size of κ_E. If $\kappa_E << 1$, then:

$$f \approx 1/ (1+\theta) \tag{B.29}$$

and substituting eqn. (B.29) into eqn. (B.18) gives:

$$j_e = n D_E e_\Sigma / [z_D(1+\theta)] \quad . \tag{B.30}$$

This is the case where surface kinetics are fast and the transport of E' across the diffusion layer is rate limiting. This case is denoted Tθ.

If $\kappa_E >> 1$, then:

$$f \approx \kappa_E^{1/2} / (1+\theta) \tag{B.31}$$

and using eqn. (B.18), j_e is given by:

$$j_e = n (D_E k_E)^{1/2} e_\Sigma / (1+\theta) \quad . \tag{B.32}$$

In this case the surface kinetics are fast and the regeneration of the reduced form of the enzyme is rate limiting. This case is denoted Eθ. Thus the boundary between the enzyme kinetics case (Eθ) and the enzyme transport case (Tθ) is given by $\kappa_E = 1$.

Thus the three cases for the $\theta >> 1$ plane have been found. The boundary between case Sθ and cases Eθ and Tθ is given by:

$$\rho/(1+\theta) = \tanh^2(\kappa_E^{1/2})/\kappa_E \quad . \tag{B.33}$$

Now in Tθ, $\kappa_E << 1$, and eqn. (B.33) reduces to:

$$\rho = (1+\theta) \quad . \tag{B.34}$$

This is the equation describing the boundary between cases Tθ and Sθ.

Now in Eθ, $\kappa_E >> 1$, and eqn. (B.33) reduces to:

$$\rho \kappa_E = (1+\theta) \ . \qquad (B.34)$$

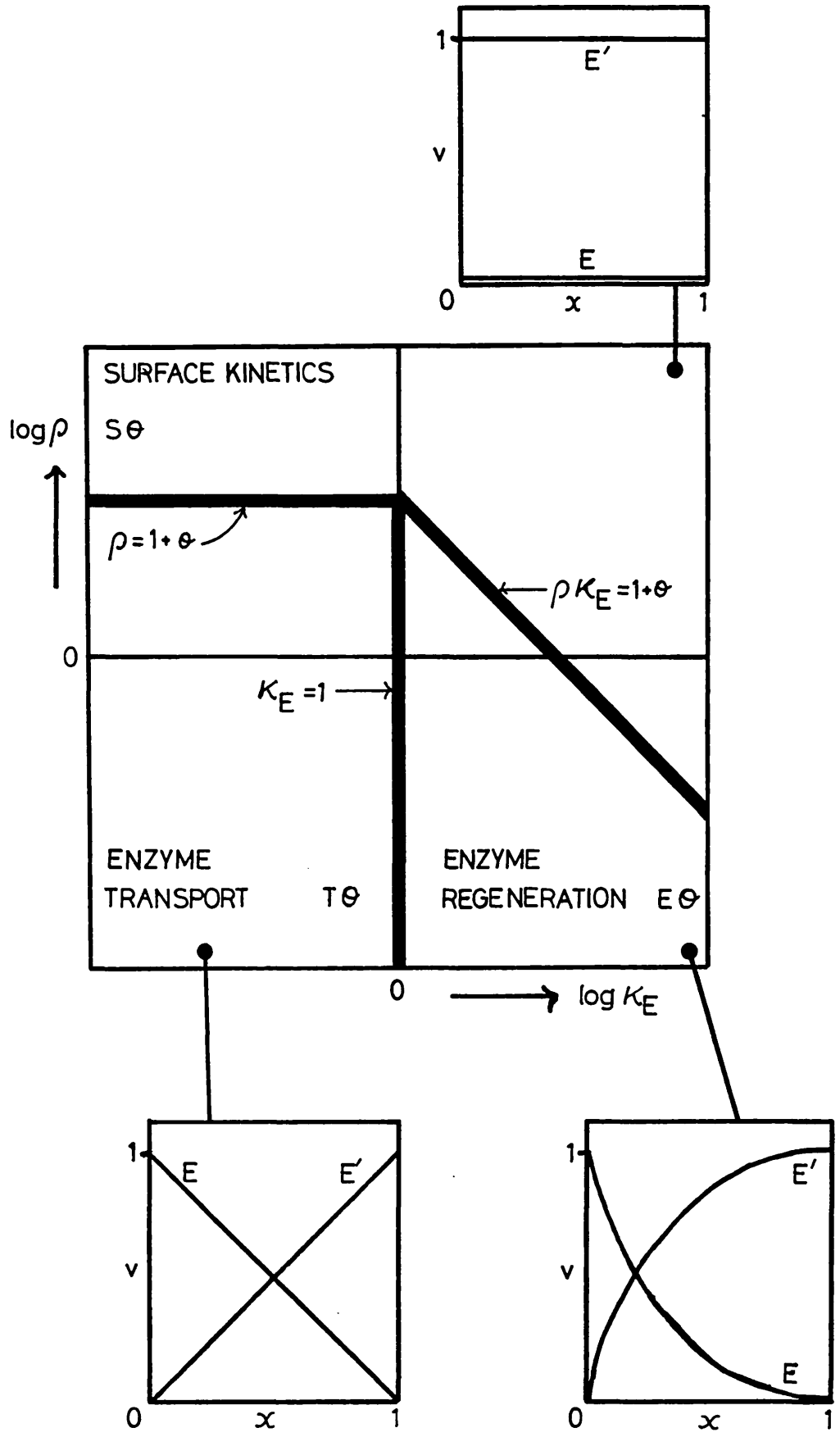
This is the boundary between cases Eθ and Sθ.

B.4.2 The complete case diagram

The case diagram for the $\theta >> 1$ plane is shown in fig(B.2). There are three cases on the $\theta >> 1$ plane. Note that each case contains the term $1/(1+\theta)$. This is to be expected since on the $\theta >> 1$ plane, diffusion of A^o and D^- away from the electrode should occur whatever the rate controlling process for the flux of the electrons. As observed above (section B.3), $\theta \ \alpha \ \omega^{1/2}$. Thus if $\theta >> 1$, $1/(1+\theta) \approx 1/\theta$ and j_e will depend on $\omega^{-1/2}$ in case Eθ and $\omega^{-1/4}$ in case Sθ. In case Tθ, there is also a $1/ z_D$ term, so that if $\theta >> 1$, no ω dependence is observed.

Also shown in fig(B.2) are the concentration profiles for E and E' within the diffusion layer. These profiles are derived by substituting the expression for f for each case into eqn. (B.20) for v_o , and then substituting this into eqn. (B.16) and applying the appropriate condition for κ_E.

There are some similarities betweeen the homogeneous and heterogeneous theories. Case Tθ describes the rate limiting step as the transport of E' from the bulk to the electrode and in this respect is identical to case IV in the homogeneous theory. Case Eθ describes the rate limiting step as the regeneration of E' from E within the small enzyme reaction layer, $(D_E / k_E)^{1/2}$, next to the electrode. In this respect this case is identical to case VII in the homogeneous



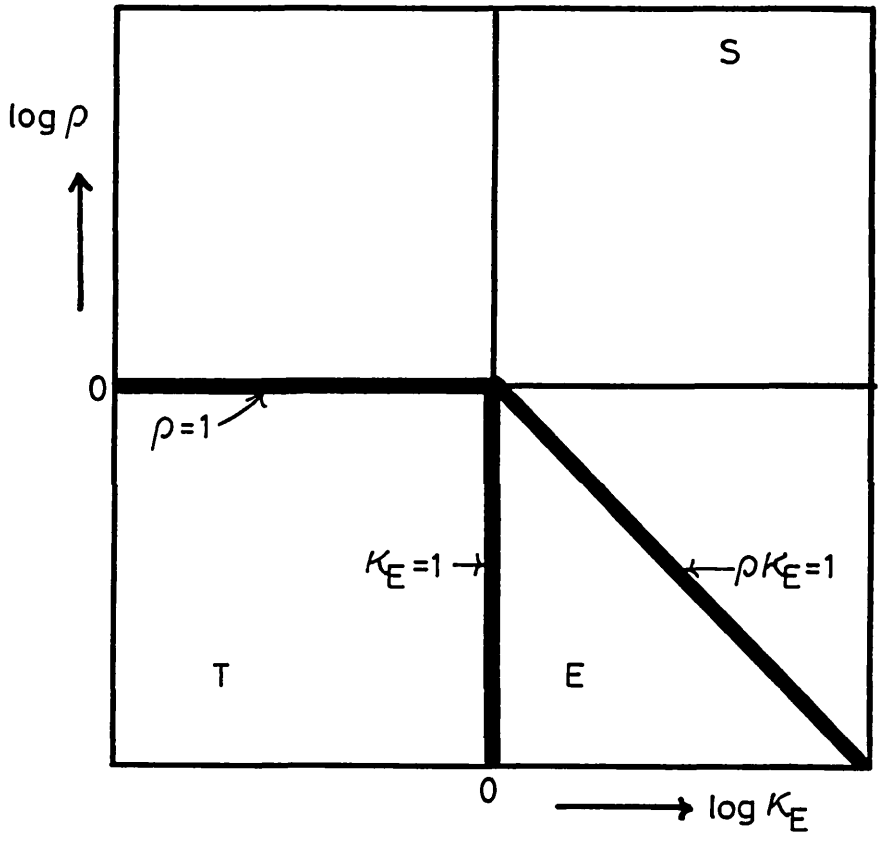
Fig(B.2) The θ > 1 plane. The concentration profiles for E and E' are shown for each case.

theory. The boundary between cases Tθ and Eθ is $\kappa_E = 1$, and this agrees with the homogeneous theory for the $\gamma >> 1$ plane, where the boundary between cases IV and VII is also $\kappa_E = 1$ (see fig(A.8)).

In the heterogeneous theory, case Sθ borders cases Tθ and Eθ on increasing ρ. In the homogeneous theory, case I borders cases IV and VII on increasing κ_M. The concentration profiles for E and E' in case Sθ and case I are identical, although in case Sθ, the rate limiting step is the surface kinetics while in case I, it is the reaction between E' and M in a small reaction layer next to the electrode. Thus there are certain similarities between the two theories, although in the heterogeneous theory, each case has a (1+θ) term.

B.4.3 The θ << 1 plane

If θ << 1, then (1+θ) ≈ 1, and this term may be ignored in the expressions for j_e for cases Tθ, Eθ and Sθ. Then three new cases are found, denoted T, E and S. In these three cases, the diffusion of A^o and D^- away from the electrode surface is no longer important. The θ << 1 plane is shown in fig(B.3). In cases E and S, no ω dependence is observed. In case T, the z_D term remains, so j_e depends on $\omega^{1/2}$. The case boundaries between cases T and S , and cases T and E , become ρ = 1 and $\rho\ \kappa_E = 1$ respectively. The boundary between cases Tθ, Eθ and Sθ and cases T, E and S is given by the plane θ = 1. For values of θ close to unity, intermediate orders of rotation speed can be observed i.e. in Eθ between -1/2 and 0, in Sθ between -1/4 and 0, and in Tθ between 0 and +1/2.



Fig(B.3) The $\theta << 1$ plane.

B.5 The experimental variables

The flux of electrons, j_e , is related to the electrode current by $j_e = i/AF$ as before (section A.7). Relating the dependence of the current on the experimental variables allows the position of a particular set of experimental conditions in the case diagram to be determined. The x, y and z axes of the case diagram are represented by κ_E , ρ and θ respectively. There are four experimental variables: [S], e_Σ , ω and the potential of the electrode relative to the saturated calomel electrode.

κ_E is the only theoretical variable dependent on [S]. Increasing [S] will result in a horizontal shift across the case diagram parallel to the κ_E axis. ρ is the only theoretical variable dependent on e_Σ. Increasing e_Σ will result in a vertical shift up the case diagram parallel to the ρ axis.

The dependence on ω is complex. All three theoretical variables depend on z_D , which is related to ω by eqn. (A.83). Any change in ω would correspond to a 3-dimensional translation in the case diagram. However as observed before (section A.7), the experimental variable ω is best used as a support for the analysis of data according to [E] or [S].

The dependence on potential is given by the $K_1k_2k_3$ and the k_2 terms. Increasing potential should result in an increase in k_2 , corresponding to a decrease in both θ and ρ . The dependence on potential is discussed in greater depth in chapter 5.

REFERENCES

1. Biosensors, Fundamentals and Applications, Ed. by A.P.F. Turner, I. Karube and G.S. Wilson, Oxford University Press (1987)
2. Biosensors, Ed. by M. Akhatar, C.R. Lowe and I.J. Higgins, Royal Society London (1987)
3. F.W. Scheller, F. Schubert, R Renneberg and H-G. Muller, Biosensors, **1**, 135 (1985)
4. C.R. Lowe, Biosensors, **1**, 3 (1985)
5. G.A. Rechnitz, C. & E.N., Sept. 5th, 24 (1989)
6. J.R. Wilson, Trends in Anal. Chem., **3**(9), 223 (1984)
7. G. Davis, Biosensors, **1**, 161 (1985)
8. J.C. Crawhall and W.C. Purdy, Trends in Anal. Chem., **1**(8), 184 (1987)
9. V.M. Owen and A.P.F. Turner, Endeavour, New Series, **11**(2), 100 (1987)
10. A.P.F Turner and J.C. Pickup, Biosensors, **1**, 85 (1985)
11. D.J. Claremount, J. Med Eng. Technol., **11**(2), 51 (1987)
12. I.J. Higgins and H.A.O. Hill, Essays in Biochem., **21**, 119 (1985)
13. p.456 - 466 in Biological Electrochemistry, Ed. by G. Dryhurst et al, **1** (1982), published by Academic Press
14. Y. Degani and A. Heller, J. Phys. Chem., **91**(6), 1285 (1987)
15. p.80 in Instrumental Methods in Electrochemistry, by the Southampton Electrochemistry Group, Published by Ellis Horwood (1985)
16. L.C. Clark, Ann. N. Y. Acad. Sci., **102**, 29 (1962)

17. M. Mascini and G.G. Guilbault, Biosensors, **2**, 147 (1986)
18. I. Karube, T. Okada and S. Suzuki, Anal. Chem, **53**, 1852 (1981)
19. M. Hikuma, H. Obana, T. Yasuda, I. Karube and S. Suzuki, Anal. Chim. Acta, **116**, 61 (1980)
20. R.K. Kobos and H.y. Pyon, Biotechnol. Bioeng., **23**, 627 (1981)
21. I. Satoh, I. Karube and S. Suzuki, Biotechnol. Bioeng., **18**, 269 (1976)
22. G.S. Sittampalam and G.S. Wilson, Trends in Anal. Chem., **3**(4), 96 (1984)
23. M. Aizawa, A. Morioka, S. Suzuki and Y. Nagamura, Anal. Biochem., **94**, 22 (1979)
24. K. Di Gleria, M.J. Green, H.A.O. Hill and C.J. McNeil, Anal. Chem., **58**, 1203 (1986)
25. G.S. Sittampalam and G.S. Wilson, Anal. Chem., **55**, 1608 (1983)
26. M.Y.K. Ho and G.A. Rechnitz, Anal. Chem., **59**, 536 (1987)
27. G.G. Guilbault and J. Montalvo, J.A.C.S., **91**, 2164 (1969)
28. Immobilized Enzymes, Ed. by I. Chibata, Halsted Press (1978)
29. M. Mascini and G. Palleschi, Anal. Chim. Acta, **145**, 213 (1983)
30. M. Mascini, M. Iannello and G. Palleschi, Anal. Chim. Acta, **146**, 135 (1983)
31. P. Vadgama, Trends in Anal. Chem., **3**(1), 13 (1984)
32. P.N. Bartlett and R.G. Whittaker, J. Electroanal. Chem.,**224**, 37 (1987)
33. P.C. Pandey, J. Chem. Soc. Faraday Trans. 1, **84**(7), 2259 (1988)
34. M. Umana and J. Waller, Anal. Chem., **58**, 2979 (1986)

35. R. Szentrimay, P. Yeh and T. Kuwana, in p.43 of Electrochemical Studies of Biological Systems, Ed. by D. Sawyer, A.C.S. Washington D.C. (1977)

36. R.C. Prince, S.J.G. Linkletter and P.L. Dutton, Biochim. et Biophys. Acta, **635**, 132 (1981)

37. G.D. Watt, Anal. Biochem., **99**, 399 (1979)

38. M.L. Fultz and R.A. Durst, Anal. Chim. Acta, **140**, 1 (1982)

39. P.L. Dutton and M. Baltscheffsky, Biochim. Biophys. Acta, **267**, 172 (1972)

40. M.T. Stankovich, Anal. Biochem., **109**, 295 (1980)

41. M.T. Stankovich, L.M. Schopfer and V. Massey, J. Biol. Chem., **253**(14), 4971 (1978)

42. J.J. Kulys and N.K. Cenas, Biochim. Biophys. Acta, **744**, 57 (1983)

43. A.E.G. Cass, G. Davis, G.D. Francis, H.A.O. Hill, W.J. Aston, I.J. Higgins, E.V. Plotkin, L.D.L. Scott and A.P.F. Turner, Anal. Chem., **56**, 667 (1984)

44. A.E.G. Cass, G. Davis, M.J. Green and H.A.O. Hill, J. Electroanal. Chem., **190**, 117 (1985)

45. A.P.F. Turner, W.J. Aston, I.J. Higgins, J.M. Bell, J. Colby, G. Davis and H.A.O. Hill, Anal. Chim. Acta, **163**, 161 (1984)

46. E.J. D'Costa, I.J. Higgins and A.P.F. Turner, Biosensors, **2**, 71 (1986)

47. J.A. Duine and J. Frank, TIBS, Oct. 1981, 278.

48. R.M. Ianniello, T.J. Lindsay and A.M. Yacynych, Anal. Chem., **54**, 1098 (1982)

49. R.M. Ianniello, T.J. Lindsay and A.M. Yacynych, Anal. Chim. Acta, **141**, 23 (1982)

50. K. Narsimhan and L.B. Wingard, Anal. Chem., **58**, 2984 (1986)

51. M.J. Eddowes and H.A.O. Hill, J.A.C.S., **101**, 4461 (1979)

52. P.M. Allen, H.A.O. Hill and N.J. Walton, J. Electroanal. Chem., **178**, 69 (1984)

53. A. Torstensson and L. Gorton, J. Electroanal. Chem., **130**, 199 (1981)

54. D.C.-S. Tse and T. Kuwana, Anal. Chem., **50**(9), 1315 (1978)

55. M.A. Harmer and H.A.O. Hill, J. Electroanal. Chem., **189**, 229 (1985)

56. H. Durliat and M. Comtat, Anal. Chem., **56**, 148 (1984)

57. H. Durliat and M. Comtat, Anal. Chem., **54**, 856 (1982)

58. F.A. Armstrong, H.A.O. Hill and N.J. Walton, FEBS Lett., **145**(2), 241 (1982)

59. Y. Degani and A. Heller, J. Phys. Chem., **91**(6), 1285 (1987)

60. P.N. Bartlett, R.G. Whittaker, M.J. Green and J. Frew, J. Chem. Soc. Chem. Commun., 1603 (1987)

61. J.J. Kulys, A.S. Samalius and G.J.S. Svirmickas, FEBS Lett., **114**(1), 7 (1980)

62. W.J. Albery, P.N. Bartlett and D.H. Craston, J. Electroanal. Chem., **194**, 223 (1985)

63. W.J. Albery, P.N. Bartlett, M. Bycroft, D.H. Craston and B.J. Driscoll, J. Electroanal. Chem., **218**, 119 (1987)

64. K. McKenna and A. Brajter-Toth, Anal. Chem., **59**, 954 (1987)

65. W.J. Albery, P.N. Bartlett, A.E.G. Cass and K.W. Sim, J. Electroanal. Chem., **218**, 127 (1987)

66. K.W. Sim, PhD Thesis, Univ. Lond. (1985)

67. p.199 in ref. [1]

68. M.G. Boutelle, C. Stanford, M. Fillenz, W.J. Albery and P.N. Bartlett, Neurosci. Lett., **72**, 283 (1986)

69. B.S. Hill, C.A. Scolari and G.S. Wilson, J. Electroanal. Chem., **252**, 125 (1988)

70. N.K. Cenas and J.J. Kulys, J. Electroanal. Chem., **128**, 103 (1981)

71. W.J. Albery, P.N. Bartlett, B.J. Driscoll and R.B. Lennox, to be submitted

72. W.J. Albery, P.N. Bartlett and A.E.G. Cass, Phil. Trans. R. Soc., Lond., **B 316**, 107 (1987)

73. S. Venitt and C. Crofton-Sleigh, Mutation. Res., **68**, 107 (1979)

74. L.R. Melby, R.J. Harder, W.R. Hertler, W. Mahler, R.E. Benson and W.E. Mochel, J.A.C.S., **84**, 3374 (1962)

75. L.R. Melby, Can. J. Chem., **43**, 1448 (1965)

76. J. Ferraris, D.O. Cowan, V. Walatka and J.H. Perlstein, J.A.C.S., **95**(3), 948 (1973)

77. R.C. Wheland and J.L. Gillson, J.A.C.S., **98**(13), 3916 (1976)

78. M.R. Bryce and L.C. Murphy, Nature, **309**, 10th May, 119 (1984)

79. B.J. Driscoll, PhD Thesis, Univ. Lond. (1988)

80. D.O. Cowan and F.M. Wiygul, C. & E.N., July 21st, 28 (1986)

81. C.J. Fritchie,. Acta Cryst., **20**, 892, (1966)

82. T.J. Kistenmacher, T.E. Phillips and D.O. Cowan, Acta Cryst., **B 30**, 763 (1974)

83. J.B. Torrance, Acc. Chem. Res., **12**(3), 79 (1979)

84. J.H. Perlstein, Angew. Chem. Int. Ed. Engl., **16**, 519 (1977)

85. C.D. Jaeger and A.J. Bard, J.A.C.S., **101**(7), 1690 (1979)

86. C.D. Jaeger and A.J. Bard, J.A.C.S., **102**(17), 5435 (1980)

87. K. El Kacemi and M. Lamache, Electrochim. Acta, **31**(9), 1197 (1986)

88. B. Janik and P.J. Elving, Chem. Rev., **68**, 312 (1968)

89. H.J. Bright and D.J.T. Porter, p. 421 of The Enzymes, 3rd ed., vol. XII, Oxidation-reduction Part B: electron transfer (1975), Academic Press

90. p. 456 in Biological Electrochemistry, Ed by G. Dryhurst et al, **1**, (1982), Academic Press

91. G. Tollin, T.E. Meyer and M.A. Cusanovich, Biochim. Biophys. Acta, **853**, 29 (1986)

92. H. Durliat and M. Comtat, J.B.C., **262**(24), 11497 (1987)

93. W.J. Albery and P.N. Bartlett, J. Electroanal. Chem., **194**, 211 (1985)

94. C.S. Hanes, Biochem. J., **26**, 1406 (1932)

95. M. Suzuki, J. Biochem., **89**, 599 (1981)

96. S. Hayashi, S. Nakamura and M. Suzuki, Biochem. Biophys. Res. Commun., **96**(2), 924 (1980)

97. I. Zelitch and S. Ochoa, J.B.C., **201**, 707 (1953)

98. Y. Lindqvist and C.-I. Branden, J. Mol. Biol., **143**, 201 (1980)

99. W.B. Sutton, J.B.C., **226**, 395 (1957)

100. W.B. Sutton, J.B.C., **216**, 749 (1955)

101. W.B. Sutton, J.B.C., **210**, 309 (1954)

102. F.R. Williams and L.P. Hager, Arch. Biochem. Biophys., **116**, 168 (1966)

103. J. Chiriboga, Arch. Biochem. Biophys., **116**, 516 (1966)

104. M. Sugiura, H. Yamamura, K. Hirano, M. Sasaki, M. Morikawa and M. Tsuboi, Chem Pharm. Bull., **27**(9), 2003 (1979)

105. A. Lavin, C. Sung, A.M. Klibanov and R. Langer, Science, **230**, Nov. 1st, 543 (1985)

106. N. Tanaka and S. Murao, Agric. Biol. Chem., **46**(10), 2499 (1982)

107. C. Sung, A. Lavin, A.M. Klibanov and R. Langer, Biotechnol. Bioeng., **28**(10), 1531 (1986)

108. M.S. Jorns, Biochem., **24**, 3189 (1985)

109. O. Folin and H. Wu, J.B.C., **38**(1), 81 (1919)

110. Z. Dvorak, Anal. Chim. Acta, **208**, 307 (1988)

111. B.J. Driscoll, private communication

112. R.A. Kamin and G.S. Wilson, Anal. Chem., **52**, 1198 (1980)

113. Y. Lindqvist and C.-I. Branden, Proc. Natl. Acad. Sci. USA, **82**, 6855 (1985)

114. S.L.T. Durrant, PhD Thesis, Univ. Lond. (1987)

115. L.P. Hager, J.B.C., **229**, 251 (1957)

116. J. Chiriboga, Biochem. Biophys. Res. Commun., **11**(4), 277 (1963)

117. M.A. Nabi Rahni, G.G. Guilbault and N.G. Olivera, Anal. Chem., **58**, 523 (1986)

118. T. Fonong, Anal. Chim. Acta, **186**, 301 (1986)

119. J. Fevery, p.11 in Bile in Health and Disease, Proc. 6th BSG-SKF Int. Workshop (1985)

120. S. Murao and N. Tanaka, Agric. Biol. Chem., **45**, 2383 (1981)

121. S. Murao and N. Tanaka, Agric. Biol. Chem., **46**, 2031 (1982)

122. Eqn. (1.32) in Instrumental Methods in Electrochemistry, Southampton Electrochemistry Group, Ellis Horwood (1985)

123. Q.H. Gibson, B.E.P. Swoboda and V. Massey, J.B.C., **239**(11), 3927 (1964)

124. C.P. Wilde, private communication

125. M. Bycroft, private communication

126. Eqn. (3.6) in Electrode Kinetics, W.J. Albery, Oxford University Press (1975)

127. Handbook of Chemistry and Physics, 59th Ed., CRC Press, Florida

128. B.E.P. Swoboda and V. Massey, J.B.C., **240**(5), 2209 (1965)

129. M.J. Eddowes and M. Gratzel, J. Electroanal. Chem., **152**, 143 (1983)

130. M.F. Cardosi and A.P.F. Turner, Chapter 15 in ref. [1]

131. H.J. Bright and M. Appleby, J.B.C., **244**(13), 3625 (1969)

132. P.F. Greenfield, J.R. Kittrel and R.L. Laurence, Anal. Biochem., **65**, 109 (1975)

133. Eqn. (2.16) in Ring-disc Electrodes, W.J. Albery and M.L. Hitchman, Oxford University Press (1971)

134. p. 898 in Introduction to Organic Chemistry (2nd Ed.), A. Streitweiser and C.H. Heathcock, Macmillan (1981)

135. Eqn. (4.3.8) in Electrochemical Methods: Fundamentals and Applications, A.J. Bard and L.R. Faulkner, Wiley (1980)

136. Eqn. (4.3.5) in ref. [135]

137. p.446 in Handbook of Mathematical Functions, Ed. M. Abramowitz and I.A. Stegun, Dover Press (1965)

138. D.H. Craston, PhD Thesis, Univ. Lond. (1986)

139. Eqn. (4.39) in ref. [122]

140. K. El Kacemi and M. Lamache, Electrochim. Acta, **31**(7), 845 (1986)

141. Y. Kalia, private communication

142. p.123 in ref. [133]

143. W.J. Albery, unpublished work

144. The Electronic Structure and Chemistry of Solids, P.A. Cox, Oxford University Press (1987)